Robust multivariable control for vehicle dynamics

Soheib Fergani

UNIVERSITÉ DE GRENOBLE

THÈSE

pour obtenir le grade de

DOCTEUR DE L'UNIVERSITÉ DE GRENOBLE

Spécialité : **AUTOMATIQUE-PRODUCTIQUE**

Arrêté ministériel : 7 août 2006

Présentée par
Fergani Soheib

Thèse dirigée par **Sename Olivier** et
codirigée par **Dugard Luc**
préparée au sein du
au Département Automatique du GIPSA-lab
dans **Electronique, Electrotechnique, Automatique, Traitement du Signal (EEATS)**

Commande Robuste LPV/H_∞ Multivariable pour la dynamique véhicule

Thèse soutenue publiquement le **23/10/2014**,
devant le jury composé de :

Michel Basset
Professeur, Université de Haute Alsace, Président du jury
Daniel Alazard
Professeur, Institut Supérieur de l'Aéronautique et de l'Espace, Toulouse, France, Rapporteur
Massimo Canale
Professeur, Politecnico di Torino, Italie, Rapporteur
Brigitte d'Andréa-Novel
Professeur, Mines ParisTech, Paris, France, Examinateur
Olivier Sename
Professeur, Grenoble INP, Directeur de thèse
Luc Dugard
Directeur de Recherche, CNRS, Co-directeur de thèse

UNIVERSITÉ DE GRENOBLE

ÉCOLE DOCTORALE EEATS

Electronique, Electrotechnique, Automatique, Traitement du Signal

T H È S E

pour obtenir le titre de

docteur en sciences

de l'Université de Grenoble

Mention : AUTOMATIQUE-PRODUCTIQUE

Présentée et soutenue par

Fergani Soheib

Commande Robuste LPV/H_∞ Multivariable pour la dynamique véhicule

Thèse dirigée par Olivier Sename et Luc Dugard

préparée au Département Automatique du GIPSA-lab (sigle labo)

soutenue le 23/10/2014

Jury :

Rapporteurs :	Daniel Alazard	-	Institut Supérieur de l'Aéronautique et de l'Espace, Toulouse, France
	Massimo Canale	-	Politecnico di Torino, Italie
Directeur :	Olivier Sename	-	Grenoble INP, Gipsa-lab, Grenoble, France
Co-directeur :	Luc Dugard	-	CNRS, Gipsa-lab, Grenoble, France
Président :	Michel Basset	-	Université de Haute Alsace, Mulhouse, France
Examinateur :	Brigitte d'Andréa-Novel	-	Mines ParisTech, Paris, France

Remerciements

Je ne peux commencer mes remerciements autrement que par m'incliner devant la personne qui compte le plus dans ma vie, qui m'a tout donné sans jamais rien attendre, qui a toujours été là pour moi, celle qui a fait de moi ce que je suis aujourd'hui (que le bon côté de ma personne), celle a qui je dois tout et que je ne pourrais lui exprimer ma gratitude même avec un livre entier de remerciements : à ma mère. Je tiens en particulier à exprimer mon éternelle reconnaissance à Olivier Sename et Luc Dugard qui m'ont accueilli dans leur équipe et qui m'ont pris sous leur responsabilité pendant ces trois ans de thèse. Ils m'ont tout a pris de ce monde de la recherche scientifique, ils ont toujours été présent pour répondre à mes questions scientifiques et cela dans la bonne humeur et (voir même dans la dérision. . .). Leurs qualité scientifique et leur côté pointilleux sur nombre de détails m'a toujours fasciné. Je les remercie aussi de m'avoir toujours permis de m'exprimer et de m'avoir soutenu à chaque fois que j'avais de nouvelles idées (même des délires parfois). Je remercie Olivier et Luc de m'avoir fait aimer la recherche académique à travers leurs qualités humaines, ils m'ont toujours fait sentir qu'ils étaient plus une famille pour moi que des supérieurs. Je ne les remercierai jamais assez d'avoir fait de mes trois années de thèse un réel plaisir. Je remercie également Pr. Daniel Alazard et Pr. Massimo Canale les rapporteurs de ce mémoire de thèse qui ont accepté de me consacrer une partie de leur temps précieux pour examiner mon travail et pour me faire part de leurs remarques et questions. Je remercie également Pr. Michel Basset et Pr. Brigitte d'Andréa-Novel, les examinateurs de mon jury de thèse, pour avoir participé à ce jury et pour l'intérêt qu'ils ont porté à mon travail tout au long de ces trois ans. Je les remercie tous de m'avoir honoré par leurs participation à la soutenance et d'avoir contribué à faire de ce jour un grand moment pour moi. Je remercie également Jozsef Bokor, Peter Gáspár et Zoltan Szabó, qui se sont occupés de moi lors de mes multiples séjours à Budapest, et qui ont contribué à ce que ces déplacements me soient extrêmement bénéfiques (Köszönöm !), j'espère avoir d'autres occasions de travaillez avec vous. Aussi, je remercie Pr. Ricardo Ramirez, Pr. Ruben Morales-Mendes, J.C Tudon, C. Vivas and D. Hernandez pour leurs contributions dans la collaboration Mexicaine et pour m'avoir accueilli Tecnologico De Monterrey pour un magnifique séjour (de super moment à manger des tacos à la cafète et regarder la coupe du monde de foot).

Je remercie aussi mon père qui m'a appris comment devenir un homme, j'espère qu'il est fier de ce que je suis devenu. Je remercie aussi mon grand frère "seif", mon idole de toujours et qui ne pourra plus me taquiner de ne pas être docteur comme lui. Mes soeurs aussi, les diamants de notre maison : Fifi, Mohdja et Rahil, vous m'avez toujours apporté de la joie et du réconfort (enfin presque toujours), j'espère avoir été un bon frère jusqu'à maintenant.
J remercier un frère (peut être pas de sang, mais qui m'est très cher), Ignacio Rubio Scola (allias Nacho) que je baptise Ignacio Fergani. Je suis plus heureux de faire ta connaissance d'avoir eu ce grade de docteur. Je te remercie d'avoir été un si bon ami et frère, des personnes comme toi sont rares.
Je remercie aussi sa femme Marilina, ma belle soeur et la femme la plus gentille que j'ai

jamais rencontré, merci pour tout ce que tu as fait pour moi, merci pour tout les tartes salées et sucrées que tu nous a préparé et d'avoir toléré les parties dégénérées de PES que nous faisions.
Je remercie aussi Madeleine, une personne exceptionnelle qui m'a surpris par sa gentillesse et bonté (mais d'abord et avant tout par ses phrases qu'elle ne finissait jamais). Je la remercie d'avoir pris de son temps (et ratée ses cours surtout) pour m'aider un à acheter mes habilles de soutenance, et tout préparé pour mon pot de thèse (très grand chef la Madeleine). Je ne te remercierai jamais assez, c'est des personnes comme toi qu'on veut garder toujours près de soi.
Je remercie aussi Cyrielle qui a fait le déplacement de Toulouse pour assister à ma présentation. Sa disponibilité depuis que j'ai commencé à rédiger la thèse m'a beaucoup réconforté (vu son expérience). Je te remercie beaucoup d'être une aussi bonne amie. Je remercie aussi Caroline, la première personne à qui j'ai parlé à Gipsa, on a travaillé pour le même maitre (Oliver biensûre), merci d'avoir fait le déplacement depuis Paris rien que pour mes 45 minutes de thèse, ça m'a fait énoremément plaisir de te connaitre (et partager des pizzas Arthur à parc Mistral avec toi).
Je remercie aussi une autre personne exceptionnelle, Jessica, elle m'a beaucoup appris à travers sa personnalité, sa manière inédite de voir les choses de la vie et surtout de m'avoir fait aimé la montagne (pour un gars qui a toujours vécu sur une plage). Je la remercie aussi pour sa grande tolérance et d'avoir supporté ma mauvaise humeur durant les moments difficile de la thèse.
Je remercie Faty la personne qui ne m'a jamais laissé tomber dans le meilleurs et dans le pire depuis toujours, je n'ai pas les mots pour décrire ce que je lui dois mais je sais qu'elle le sais déjà, merci infiniment.

Je souhaite remercier tous les gens que j'ai connu à Gipsa-lab. Je remercie le Grand Mazen Alamir pour sa gentillesse et ses conseils (aussi les matchs de foot), Emanuel Witrant pour sa bonne humeur et chalenges sportifs (j'attends de voir ton saut), Damien Koenig pour être absolument une personne exceptionnelle (scientifiquement et humainement mais aussi un chercheur avec une Benz CLK...), John pour les préparations sympathiques des cours GI (Produit Futurs), Nicolas qui m'a piqué mon bureau, Ahmad et Nassim pour leurs soutient et conseils. Je remercie tous les profs de Gipsa-lab d'avoir été si gentil avec moi et d'avoir fait de mon séjour dans ce laboratoire un agréable souvenir.

Je remercie aussi et infiniment mes frères d'armes, mais camarades de "galère" doctorale, avec qui j'ai partagé les meilleurs moments de ces dernières années : Oumayma, Sonia, Valentina, Mihaly, Lam, Rachid, Humberto, Abraham, Marouane, Mustapha, Tahar, Sébastien, Diana, Sylvain, Jonhatan, Juan, Jorge, Raouia, Maelle, Sarah, John, Peter, Bojan, Quan (ma version V.02). Je vous remercie pour tous les bons moments (barbecue, soirée poker,... bon n'exposons pas tous ces plans débauches).
Aussi, je souhaite laisser une trace par rapport aux poses café, j'espère que Nicolas va

baptiser la cafète à mon nom, ces moments de détente et d'échange ont vraiment enrichie mon quotidien et ma vie, ce n'était pas du temps perdu et ça n'influe pas sur la productivité si ce n'est d'une bonne manière, donc un message aux bosses, encouragez vos esclaves (oups doctorants) à s'intégrer dans la vie du laboratoire, c'est une opportunité unique surtout dans un magnifique endroit comme Gipsa.

Je remercie toute l'équipe administrative, en particulier Elsa, Marielle, Cécilia, et Patricia

qui m'ont bien aidé à affronter les lourdeurs administratives, à préparer les missions, toujours dans la bonne humeur. Je remercie également l'équipe technique, notamment Gabriel, Pascal , Olivier, Jonathan, Thierry, m'ont aidé à passer trois années assez sereines.

Je remercie l'équipe de foot Gipsa (encore et toujours) pour tout les bons moments que nous avons partagé : Xavier, Lee, Farouk, aladine, Bilal, Rodrigo. J'espère que vous allez gagné le trophée cette année.

Je remercie mes amis d'enfance, mon vieil amis Seifou mon magistrat adoré, Rachid mon ami

de toujours et la personne sur laquelle je me suis toujours appuyé, Mohamed le plus gentil de mes amis, Brahim, Djallal, Zaki, Issam, Hamza, je ne vous oublie pas, vous avez toujours été là pour moi.

je remercie mes profs de l'Ecole Nationale Polytechnique d'Alger pour m'avoir formé et fait

aimer l'ingénierie et surtout l'automatique (et m'avoir évité de sombrer dans le dark side du management). Je remercie mes profs de collège Yemmouna Guemouh et de mon primaire que je croise souvent et qui me font rappelr le petit garçon (agaçant) que j'étais avant, je ne pourrais jamais assez vous remercier mais je n'oublierai jamais ce que vous avez fait pour moi.

Et pour finir, je dédie ce manuscrit à l'âme de la personne qui m'a marqué le plus dans ce

monde et qui j'admire plus que tout, Mon grand père Bachir tu resteras toujours dans mon coeur.

Soheib Fergani

(Passage au royaume Gipsa 2011−2014)

Résumé des travaux

Les systèmes automobiles sont constitués de composants de plusieurs sous-systèmes complexes. Ces éléments sont soumis à des demandes du conducteur (angle du volant,pression sur les pédales de freinage, et pédale d'accélérateur) et contraintes de l'environnement (profil de la route, adhérence, vent ...). L'ensemble de ces sous-systèmes comportent aujourd'hui de plus en plus d' actionneurs et de capteurs afin d'améliorer constamment le confort et la sécurité de conduite.

Pour atteindre les objectifs de performance de haut niveau en ce qui concerne le confort de la sécurité des véhicules et des passagers, plusieurs compétences techniques sont nécessaires. En effet, pour améliorer la dynamique du véhicule, à la fois des stratégies d'observation efficaces et de surveillance ainsi que de contrôle sont indispensables en complément de connaissances en mécanique de l'automobile. Il est très important que la communauté de la recherche prouve que les stratégies théoriques proposés peuvent conduire à de véritables solutions réalisables qui répondent aux besoins de l'industrie. Ceci peut être réalisé par des simulations sur des modèles validés expérimentalement et par la mise en oeuvre expérimentale réelle (sur banc d'essai et sur des voitures commerciales réelles) des solutions académiques développées. Pour cela, le projet INOVE a été mis en place par l'Agence Nationale de la Recherche française (ANR), qui rassemble plusieurs laboratoires travaillant dans différents domaines de la dynamique du véhicule et un partenaire industriel pour la procédure de validation. Cette thèse a été soutenue par le projet ANR BLAN Inove.

0.1 Présentation du projet

INOVE (INtegrated Observation and Control for Vehicle dynamics) est un projet national français soutenu par l'ANR, lancé en Octobre 2010 à Janvier 2015. Les principaux objectifs de ce projet sont de développer de nouvelles méthodologies et des solutions innovantes, dans un cadre unifié, pour la la modélisation et l'identification du comportement des véhicules, en vue de l'observation de situations critiques, la détection et le contrôle de la contrôle robuste tolérante aux fautes pour la dynamique du véhicule. En outre, l'un des principaux objectifs des solutions développées dans ce projet est d'améliorer la sécurité des véhicules et la le confort des passagers.
Pour montrer l'efficacité des stratégies développées pour gérer le compromis entre les deux objectifs de performances par rapport à la situation de conduite critique, certains scénarios exigeants, difficiles ont été considérés comme :

– Conduire sur les routes irrégulières, avec différentes conditions de route (sec, humide

...), avec / sans freinage.
- Freinage en courbe (en dévers ou pas).
- Conduire dans une courbe à haute vitesse, près du risque de renversement.

L'originalité de cette étude, proposée dans le projet Inove, est l'intégration de diffèrentes stratégies de commande et d'observation de la dynamique véhicule dans des approches unifiées pour réaliser les performances désirées. Certains des derniers développements de la théorie du contrôle automatique ont été appliqués aux systèmes automobiles au sein de ce projet :
- Les méthodes algébriques pour l'estimation / observation.
- L'approche LPV pour l'observation et le contrôle robuste : généricité et robustesse de la commande de H_∞, les objectifs de performance adaptables et les contrôleurs multi-sorties multi-entrées.
- La commande Tolérante aux défauts utilisant des stratégies de commutations.

Ce projet vise à apporter des solutions innovantes et des percées scientifiques intéressantes pour des problématiques majeures dans les domaines de l'automatique et les systèmes automobiles :

- **Modélisation/Identification** : Dans cette partie deux objectifs principaux ont été pris en compte :
  - Développement d'un modèle de bibliothèque (Matlab / Simulink) permettant de simuler de nombreuses situations de conduite, à partager entre les partenaires, puis ouverte à la communauté scientifique.
  - De proposer des lignes directrices pour l'identification des paramètres des modèles de véhicules qui ont une forte influence sur la dynamique du véhicule.
- **Observation et supervision** : Plusieurs approches sont développées pour assurer la supervision et l'observation des situations de conduite, afin d'éviter l'utilisation de beaucoup de capteurs et caméras embarquées (des restrictions de coûts).
  - Classification des situations de conduite / de la route.
  - Développement de nouveaux observateurs (robuste, fiable, facilement réalisable) pour détecter certaines situations critiques telles que : perte d'adhérence, trop forte d'accélération latérale / de lacet, de renversement, inter-distance, capteurs / actionneurs défaillance.
  - Développement d'estimateurs algébriques, tant pour l'estimation et la compensation de dynamiques inconnus dans les algorithmes de contrôle.
- **Synthèse des lois de commande** : Cette partie concerne la conception de contrôleurs en utilisant des techniques de contrôle linéaire et / ou non linéaire. L'objectif est d'améliorer les performances de stabilité et de sécurité des véhicules.
  - Synthèse de lois de commande intégrées pour les différents actionneurs véhicule (freinage, suspension, direction) pour garantir la sécurité ainsi que le confort des passagers.
  - Adaptation en ligne des contrôleurs à diverses situations dangereuses détectées par les observateurs / estimateurs. Cela permet une réaction rapide de la voiture face aux situations de conduites critiques.

Les grandes ambitions de ce projet ont révélé des obstacles et des difficultés, car il est difficile de gérer un grand nombre de compétences et de les utiliser dans un but commun. Pour faire face à ce problème, de nombreuses collaborations entre plusieurs laboratoires de

recherche au niveau national et international ont été établis ainsi qu'un partenariat industriel. Les principaux partenaires de ce projet sont les suivants :

- **Gipsa-Lab** :

  Le projet INOVE est dirigé par le Pr. Olivier Sename, qui est aussi directeur de l'équipe de recherche Systèmes Linéaires et Robustesse au laboratoire Gipsa-Lab. Dernièrement, ses activités de recherches se sont concentrées sur la modélisation, l'observation et la commande des systèmes automobiles.
  Aussi, au sein de l' equipe de recherche de Gipsa-Lab "Systèmes Linéaires et Robustesse" pluisieurs activitées de recherche concernant les observateurs/commandes robustes ont été effectuées. Ainsi, la modélisation et la commande de véhicules (commande globale *châssis*, suspension, freinage, braquage) ont été abordées utilisant les approches robustes comme ($\mathcal{H}_\infty$, H_2, Multi-objective), et plus récemment en utilisnt le context LPV (Linéare à Paramètres Variants).

- **MIPS, Mulhouse** :

  L'équipe de recherche MIPS-MIAM est l'une des six équipes de recherche du laboratoire Modélisation, Intéligence dans les Processus Systèmes (MIPS) de l'Université de Haute Alsace (UHA). Le groupe MIPS-MIAM est localisé à l'école d'ingénieurs ENSISA. Depuis les années 80, cette équipe de recherche a été impliquée dans plusieurs études intéressantes concernant la modélisation et l'identification des systèmes complexes à dynamique rapide stable et pseudostable (en particulier, l'estimation des paramètres physiques) pour developper des stratégies de diagnostic et d'estimation de défauts ainsi que des lois de commande. Les applications les plus importantes effectuées au sein de cette équipe concernent l'automobile et l'aéronautique. Le savoir faire de cette équipe investie dans le projet INOVE concerne les sujets suivant :
  - Commande multivariable des systèmes complexes.
  - Etude des architectures embarquées pour l'acquisition de données et pour la commande.
  - Commande latérale et longitudinale des véhicules automobiles.

- **Mines Paris-Tech (ARMINES-CAOR)** :

  ARMINES-CAOR (centre de recherche de la robotique "Ecole des Mines de Paris") est bien reconnu dans le domaine de la vision et de la commande pour les systèmes de transports intelligents.
  En particulier, Brigitte d'Andrea-Novel a une forte activité de recherche dans le contrôle des systèmes automobiles : commande longitudinale des véhicules, de la suspension et des systèmes de freinage .... Sa participation à ce projet permet de renforcer la collaboration entre nous sur le régulateur de vitesse et de profiter de son expérience dans ce domaine de recherche. Les questions les plus importantes traitées par ARMINES CAOR sont :

- Le développement de nouvelles stratégies pour la commande longitudinale.
- L'approche intégrée pour le commande latérale et de suspension en vue d'une commande globale du châssis.
- Les nouveaux observateurs de variables dynamiques non mesurées en utilisant des méthodes algébriques avancées.

- **SOBEN** :

  SOBEN est un fabricant français d'amortisseurs, avec une capacité de production de 500000 amortisseurs/an. Il est également le premier fabricant de semi-amortisseurs actifs du monde. L'approche industrielle et pratique de SOBEN complète les différentes études des laboratoires de recherche, et les met en avant.
  Les tâches principales du partenaire industriel SOBEN sont :
  - De fournir un banc d'essai d'un véhicule entièrement équipée de 4 amortisseurs semi-actifs électro-rhéologiques pour les tests de la dynamique verticale.
  - D'aider à définir une procédure de test pour les contrôleurs multivariables développés sur de vraies voitures et pistes réelles.

En outre, ce projet tire parti de certaines collaborations internationales existantes. Certains objectifs du projet se basent sur les résultats obtenus dans le cadre de ces collaborations, ce qui donne plus de visibilité et d'influence de la solution développée à l'échelle internationale :

- PICS-CNRS CROTALE 2010 – 2012 : avec des collègues hongrois de MTA SZTAKI (Académie des sciences Budapest) sur la modélisation et le controle de l'automobile. Dans ce contexte, les travaux conjoints ont été développés en collaboration avec les Pr. Peter Gaspar et Josef Bokor pendant mon séjour de recherche leur qui ont conduit à plusieurs publications (voir la liste de publication).
- PCP 2007 – 2010 et 2010 – 2013 : un projet franco-mexicain avec des collègues de Technilogico di Monterrey, au Mexique, et de deux entreprises industrielles (Metalsa Mx, Soben Fr), sur des stratégies de contrôle tolérantes aux défauts pour les systèmes automobiles a été mis en place. Plusieurs travaux communs ont été développés au cours de la collaboration que se soit à Grenoble ou Monterrey (voir la liste de publication).

Pour rendre plus claire la contribution de cette thèse dans le projet, rappelons les diverses tâches du projet INOVE répartis entre les partenaires.

0.2 Résumé des contributions

Cette thèse présente le travail de trois ans (octobre 2008 septembre 2011), réalisé dans l'équipe SLR (Systèmes Linéaires et Robustesse), département Automatique, GIPSALab, sur "la commande LPV robuste multivariable pour la dynamique du véhicule", sous la direction de Mr. Olivier Sename (Professeur, Grenoble INP) et de Mr. Luc Dugard (Directeur de Recherche, CNRS). Ce travail a été financé par le projet INOVE ANR 2010 – 2014.

La thèse est la continuité de travaux antérieurs effectués dans l' équipe de recherche SLR :

- Ricardo Ramirez-Mendoza (voir [Ramirez-Mendoza, 1997])„ "Sur la Modélisation et la Commande de Véhicules automobiles" a été la première étude dans le domaine de l'automobile. Le travail a été axé sur la description et la modélisation des véhicules, ainsi que sur les premières tentatives sur les méthodologies de commande des suspensions actives.
- Damien Sammier (voir [Sammier, 2001])„ "Sur la Modélisation et la Commande de la Suspension de Véhicules automobiles" a présenté la modélisation et la conception de régulateur d'une suspension active (utilisant les techniques H_∞ pour les systèmes LTI). La modélisation et la commande de suspension semi active ont également été étudiées pour un amortisseur semi-actif de PSA Peugeot Citroen.
- Alessandro Zin (voir [Zin, 2005]), "Sur la Commande Robuste de suspensions automobiles en vue du Contrôle global de châssis", a étendu les travaux antérieurs avec une attention particulière sur la commande LPV/H_∞ d'une suspension active afin d'améliorer les propriétés de robustesse. Un schéma de commande globale de châssis, grâce à l'utilisation des quatre suspensions, a également été obtenu à l'aide une distribution anti-roulis.
- Charles Poussot-Vassal (voir [Poussot-Vassal, 2008]), "Commande Robuste LPV Multivariable de Châssis Automobile", a fourni des outils et des méthodologies de conception de contrôleur afin d'améliorer le confort et la sécurité dans les véhicules automobiles. Deux principales contributions sont la commande des suspensions semi-actives (en utilisant l'approche LPV pour garantir le caractère semi-actif de la suspension) et la commande globale de châssis (concernant la commande des actionneurs de freinage et de virage pour l'amélioration de la sécurité des véhicules).
- Sébastien Aubouet (voir [Aubouet, 2010]), "Modélisation et Commande dúne Suspension semi-active SOBEN", a présenté une méthodologie de conception d'observateur permettant au concepteur de suspension de construire et de régler un observateur qui estime des variables non mesurées. Ensuite, les résultats précédents de Charles Poussot-Vassal, pour la commande de la suspension semi-active, ont été étendus au modèle vertical complet de véhicule, et complétés avec une méthode de placement de pôles, une stratégie de séquencement basée sur un modèle d'amortissement et une commande d'amortisseur locale.
- Anh Lam Do (voir [DO, 2011])„ "Approche LPV pour la commande robuste de la dynamique des véhicules : amélioration conjointe du confort et de la sécurité", a fourni de nouvelles solutions à de nombreuses problèmatiques de développement de méthodes de commandes avancées pour les suspensions automobiles afin d'améliorer la tenue de route des véhicules et le confort des passagers, tout en respectant les contraintes technologiques liées aux actionneurs de suspension (passivité, non-linéarités, limites structurelles).

Durant ma thèse, j'ai eu la chance de collaborer avec des nombreux collègues dans des laboratoires nationaux et internationaux. J'ai eu le privilège d'effectuer deux séjours (2011-2012 et $2012-2013$) de recherche dans l'université technologique de Budapest Hongrie (MTA SZTAKI). J'ai eu l'opportunité de travailler avec le professeur Peter Gaspar sur la commande LPV multivatiable du châssis véhicule, ce qui a donné lieu plusieurs publications (voir liste de publication).

Dans le cadre des collaborations intérnationales, j'ai eu aussi l'ocassion d'effectuer un séjour de recherche au Tecnologico De Monterrey. De nombreuses publications communes ont été faites sur diverses thématiques notemment la commande LPV tolérante aux défauts et l'adaptation du comportement des véhicules aux profils de routes sur lesquelles elles roulent (voir liste de publication).

Aussi, pendant mes trois années de thèse j'ai eu l'occasion de travailler avec des chercheurs de très haut niveau dans les laboratoire de Mines ParisTech notammment Pr. Brigitte d'Andréa-Novel et le laboratoire du MIPS de Mulhouse avec Pr. Michel Basset. Ces collaboration ont donné lieu à de nombreuses publications et à des travaux expérimentaux. En effet, les travaux effectués avec les collègues de Mines ParisTech se sont focalisés sur l'intégration des approches de commandes robuste à paramètres variants et les approches algébriques de commande par platitude (voir liste de publication). Tandis qu'avec nos collègues du MIPS, nous avons réussi à valider un modèle non linéaire d'une voiture réelle. Enfin, la mise en oeuvre expérimentale des contrôleurs et des observateurs développés dans le cadre du projet INOVE a été réalisée sur la "Renault Mégane Coupé".

Dans ce manuscrits, les contributions apportées ont été présentées dans plusieurs chapitres classés dans 3 parties comme suits :

- La première partie donne des outils généraux qui facilitent la lecture du manuscrit. elle contient les chapitres suivants :
  - D'abord dans le premier, une présentation du projet dans lequel la thèse a été développée est fournie. En outre, certains faits historiques concernant l'étude de la dynamique des véhicules sont cités. Ensuite, le cadre général de la thèse, à savoir, le contrôle global du châssis pour l'amélioration du comportement dynamique du véhicule est introduit .
  - Après dans le deuxième chapitre de la thèse, un rappel théorique des différents éléments de la théorie du contrôle : définition des sytstèmes dynamique linéaires /non linéaires, LTI/LPV. Aussi, un rapelle sur différents concepts de robustesse et stabilité puis la méthodologie de synthèse et développement de commande robuste. Après, la commande LPV/H_∞ est présentée en vue de la commande du véhicule
  - Ensuite dans le troisième chapitre, un chapitre modélisation, incluant les différents modèles des systèmes automobiles developpés et validés, notamment le modèle vertical, bicyclette pour des objectifs de simulations et le modèle non linéare du véhicule complet validé par des testes expérimentaux sur la "Renault Mégane Coupé" pour la validation des méthodes développées.

- La deuxième partie comporte une des contributions majeurs de cette thèse qui est commande adaptative des véhicules sur divers profils de route :
  - Dans cette partie, les premiers travaux se sont orientés vers l'estimation du profile

de route en utilisant diverses approches (voir le quatrième chapitre de la thèse), notamment :

1. Estimation du profile de route utilisant un observateur robuste H_∞.
2. Estimation du profile de route utilisant des méthododes d'estimation algébrique.
3. Estimation du profile de route utilisant un algorithme d'identification paramètrique.
4. Algorithme d'identification du type de route se basant sur la norme ISO8608.

- Ensuite, et en se basant sur l'estimation du profile de route, une commande innovante robuste LPV/H_∞ qui adapte le comportement du véhicule aux irrégularités de la route (voir le cinquème chapitre du manuscrit). Cela permet d'orienter les objectifs de performance pour améliorer soit le confort des passagers soit la tenue de route.

– La dernière partie est dédiée à la commande globale multivariable du châssis de véhicule. Cette partie comprend plusieurs contributions majeures dans le domaine de la commande du châssis de véhicule comme suit :
- Le sixième chapitre de la thèse est dédié à la présentation d'un contrôleur LPV/H_∞ intégré dans une structure de commande globale du châssis utilisant les actionneurs de freinage, braquage et suspensions semi-active. Une stratégie intéressante de collaboration et coordination entre ces différents actionneurs y est présentée grâce au contexte LPV.
- Le septième chapitre du manuscrit concerne la commande par allocation d'effort. C'est une nouvelle stratégie qui permet, en se basant sur la supervision de différentes dynamiques du véhicule, d'affecter les bons efforts de suspensions qui permettent de stabiliser le véhicule dans les situations de conduite dangereuses. Cette stratgie a permis de développer les travaux suivants :
  1. La commande globale miultivatiable LPV/H_∞ pour l'amélioration de la dynamique véhicule.
  2. La commande tolérante aux défauts pour gérer des défaillances actionneurs, plus particuloèrement des actionneurs de suspensions et du freinage, pour améliorer la sécurité de la conduite.
  3. La commande combinée LPV/H_∞ par allocation d'effort pour la dynamique verticale avec la commande algébrique par platitude pour les dynamiques latérale et longitudinale du véhicule.

Aussi, durant cette thèse deux bancs d'essais ont permis de valider certains travaux et stratégies qui ont été développées et utilisées :

– **La première plateforme** est le "INOVE CAR". Cette plateforme est un banc de test mis au point essentiellement pour l'étude de la dynamique verticale du véhicule.

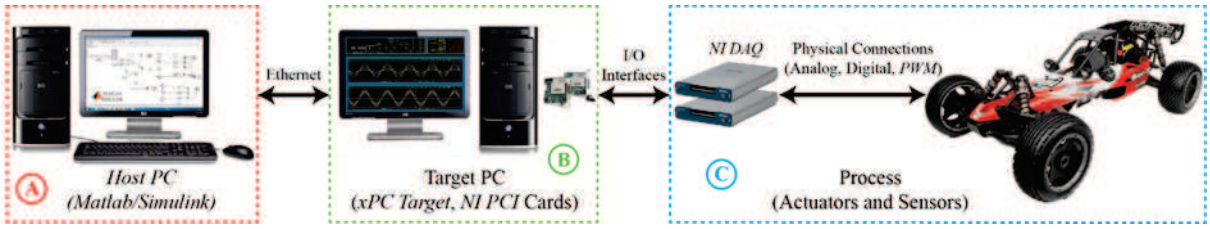

FIGURE 1 – Schema de la platforme expérimentale INOVE CAR.

Elle est composée de 3 parties principales :

1. PC hôte : L'interface de contrôle est hébergé dans cet ordinateur. Cette interface est l'endroit où l'utilisateur définit les paramètres d'initialisation, de configuration du profil de la route désirée, il met en œuvre les algorithmes de contrôle de suspension, et enregistre les données acquises. Cette interface est développé en utilisant $Matlab/Simulink^{TM}$.

2. PC cible : Dans cet ordinateur, un système d'exploitation RT (xPC Target $^{\text{TM}}$) est en marche. Dans ce PC l'algorithme de contrôle est compilé et exécuté avec une période d'échantillonnage de $200Hz$.

3. Processus : Le processus comprend des capteurs, des actionneurs, et le véhicule mis à l'échelle. Dans le processus, la pièce principale est une voiture de course type Baja ramenée à une échelle de 1/5 (adaptée à la taille de la platforme), ce qui représente un véhicule complet, y compris les roues, le moteur, la direction, le système de freinage, et l'élément clé : des suspensions Semi-Actives. En fait, cette plate-forme est dédiée à l'étude du comportement vertical de la voiture, c'est pourquoi ni la direction, ni les freins ne seront utilisés.

Le système de suspension semi-active contient 4 amortiseurs amortisseurs électro-rhéologiques de la firme $Fludicon^{TM}$ avec une plage de variation de force entre $[-50\ 50]N$. Ces amortisseurs sont ajustés à l'aide d'une tension de manipulation entre 0 et 5 kV, obtenus par des modules amplificateurs.

– **La deuxième plateforme** est le véhicule d'essai du MIAM, la "Renault Scenic (NADINE)" présenté dans Fig. 2.

Ce véhicule est un modèle de première génération, équipé d'une motorisation 2.0L 115ch et avec une boîte de vitesses automatique. il contient plusieurs capteurs (**RT3002, Xsens MTI, Magellan Aquarius 5002MK and Scorpio 6002SK, Capteurs GPS** et actionneurs (**Régulateur de vitesse, Booster actif,Actionneur de braquage**)qui sont présentés dans Fig. 2 et décrits comme suit :

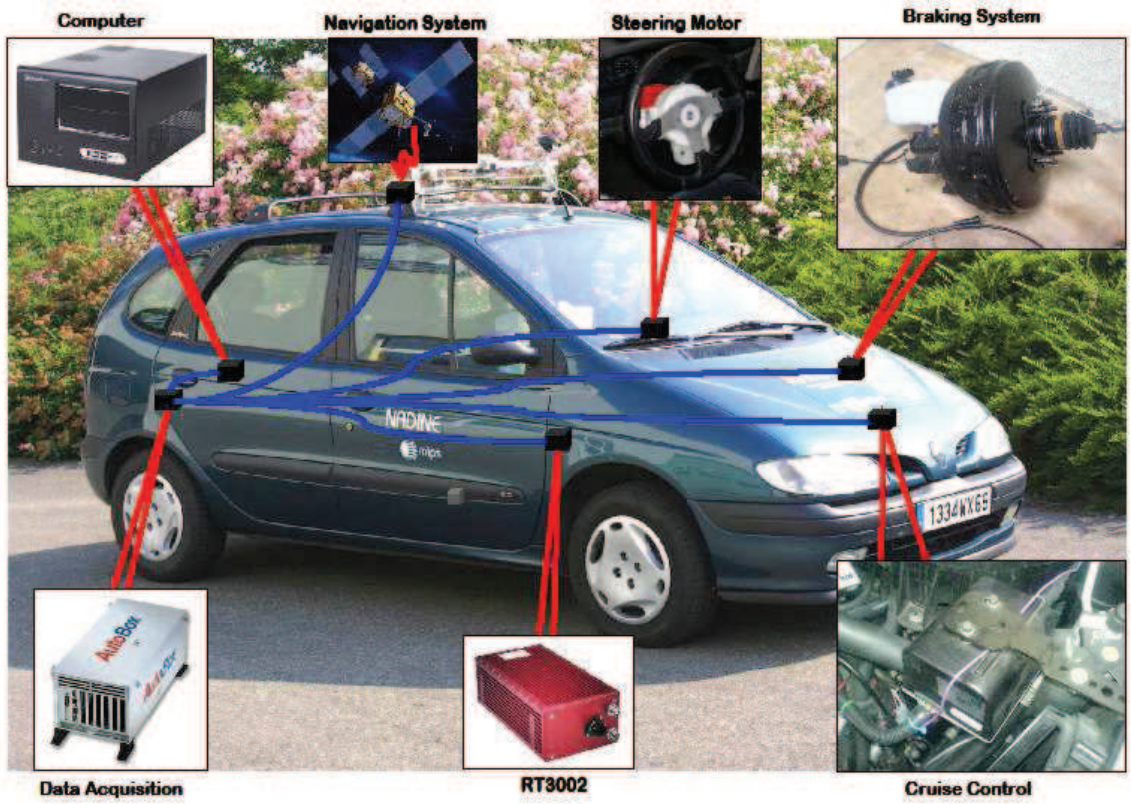

FIGURE 2 – Véhicule expérimentale : Mégane Scénic (Nadine).

Outre, pour faciliter la mise en oeuvre, un ordinateur embarqué basé sur Windows permet de surveiller et de contrôler les actionneurs en temps réel par le biais du logiciel ContolDesk (dSpace) et des différents écrans installés sur le véhicule.
Dans le cadre de cette thèse, une implementation d'un contrôleur LPV/H_∞ pour la dynamique latérale du véhicule a été réalisée sur la voiture précédemment définie (très récemment le 04/07/2014). Les testes ont été réalisés par un conducteur professionel sur une piste de course (piste spécialement aménagé pour tester les performances des véhicules sous différentes conditions de route).

Ainsi, le détail de ces différentes contributions réalisées au cours de ces trois dernières années de thèse est présenté dans ce manuscrit et les publications jointes. Cette thèse a été orientée vers l'étude et l'analyse de la commande globale du châssis grâce à l'utilisation des outils de commande robuste LPV/H_∞ . Le problème principal est de développer de nouveaux contrôleurs MIMO pour le Châssis qui améliorent la dynamique d'ensemble du véhicule tout en préservant la stabilité du véhicule dans les situations de conduite critiques. Le travail est présenté dans 3 parties différentes regroupant 9 chapitres.

Notations

$\mathbb{R}$	Real values set
$\mathbb{C}$	Complex values set
M^*	Conjugate of $M \in \mathbb{C}$
M^T	Transpose of $M \in \mathbb{R}$
$(*)^T$	Defines the conjugate (or transpose) element of a matrix $\in \mathbb{C}$ ($\in \mathbb{R}$)
σ	Singular value ($\sigma(T)$ defines the eigenvalues of the operator T s.t. $(T^*T)^{1/2}$)
j	Complex value
$Re(.)$	Real part of a complex number
$Im(.)$	Imaginary part of a complex number (j is the imaginary unit)
$M \prec (\preceq) 0$	Matrix M is symmetric and negative (semi)definite
$M \succ (\succeq) 0$	Matrix M is symmetric and positive (semi)definite
$\mathbf{Tr}(M)$	Trace of M matrix (sum of the diagonal elements)
$\mathbf{Co}(X)$	Convex hull of set X
$A = A^T$	Matrix A is real symmetric
$A = A^*$	Matrix A is hermitian
$AA^* = A^*A = I$	Matrix A is unitary
s	Laplace variable $s = j\omega$, where ω is the pulsation

GCC	Global Chassis Control
ABS	Anti-locking Braking System
ESC(P)	Electronic Stability Control (Program)
ABC	Active Body Control
LTI	Linear Time Invariant
LPV	Linear Parameter Varying
LMI	Linear Matrix Inequality
SDP	Semi-Definite Programming
EMB	Electro-Mechanical Braking
MRD	Magneto-Rheological Damper
DOF	degree of freedom
COG	center of gravity
iff.	if and only if
w.r.t.	with respect to
s.t.	such that / so that
resp.	respectively

Contents

List of Figures

List of Tables

CHAPTER 1

Introduction

1.1 Introduction

Automotive systems are made up of components of several complex subsystems. These elements are subject to requests from the driver (steering wheel angle, pressure on the braking pedals) and constraints from the environment (road profile, adhesion, wind ...). All these subsystems incorporate today more and more actuators and sensors in order to constantly improve comfort and safety driving. To achieve high-level performance objectives regarding the vehicle safety and passengers comfort, several engineering skills are needed. Indeed, to enhance vehicle dynamics, both efficient observation, monitoring and control strategies are essential in addition to mechanical engineering knowledge. It is very important that the research community proves that proposed theoretical strategies can lead to real implementable solutions that meet the industrial requirements. This can be achieved by simulations on experimentally validated models and by real experimental implementation (on test-bench and on real car) of the academically developed solutions.
For this sake, the INOVE project was set up by the French national research agency (**ANR**), gathering several laboratories working in different fields of the vehicle dynamics and an industrial partner for the validation procedure.
This thesis has been supported by the ANR BLAN INOVE project.

1.2 Project presentation

INOVE (**IN**tegrated **O**bservation and Control for **Ve**hicle dynamics) is a French national project supported by the ANR, initiated in October 2010 up to January 2015. The main objectives of this project are to develop new methodologies and innovative solutions, in a unified framework, for the modeling and identification of the vehicles behavior, the observation in view of critical situations detection and for the robust fault tolerant control of the vehicle dynamics. Also, one of the main objectives of the developed solutions within this project is to improve the safety of vehicles and the passengers comfort.
To show the efficiency of the given strategies to handle the trade off between the two performance objectives during critical driving situation, some rough scenarios have been considered such as :

- Driving on uneven roads, with different road conditions (dry, wet...), with/without braking. Extension to the case of inter-distance control.
- Braking in a (banked or not) curve.
- Driving in a curve at high speed, close to roll-over.

The originality of this study, proposed in INOVE project, is the collaborative integration between very recent advanced control and observation approaches in unified strategies to enhance the desired performance objectives. Some of the latest developments in the automatic control theory have been applied to the automotive systems within this project :

- Algebraic methods for estimation/observation.
- LPV approach for observation and robust control : genericity and robustness of the $\mathcal{H}_\infty$ control approach, varying performance objectives, Multi-Input Multi-Output controllers.
- Fault-tolerant control using switching strategies.

This project intends to bring innovative solutions and interesting scientific breakthrough for key issues in the fields of automatic control and automotive systems:

- **Modelling/Identification**: In this part two main objectives have been considered.
  - Development of a model library (Matlab/Simulink) allowing to simulate many driving tests, to be shared between the partners, and then open to the scientific community.
  - To propose some guidelines for identification of the vehicle model parameters that have a strong influence on vehicle dynamics.
- **Observation and monitoring**: Several approaches are developed to ensure the monitoring and observation of the driving situations, in order to avoid the over use of the sensors and to avoid the use of embedded cameras (for cost restrictions).
  - Classification of driving/road situations.
  - Development of new observers (robust, reliable, easily implementable) to detect some critical situations such as: loss of adhesion, too large lateral acceleration/yaw rate, roll-over, too small vehicle inter-distance, sensors/actuators failures.
  - Development of algebraic estimators both for the estimation and compensation of unknown dynamics in the control algorithms.
- **Control design**: This part concerns the design of controllers using linear and/or non linear control technics. The objective is to enhance stability, safety and vehicle performances.
  - Synthesis of integrated control laws for different subsystems (braking, suspension, steering) to guarantee the passenger safety and comfort as well.
  - On-line adaptation of the controllers to various dangerous situations detected by the observers/estimators. This permits a fast reaction of the car face to undesired phenomena.

The large scale ambitions of this project have brought some obstacles and difficulties since it is hard to manage a lot of skills and use them towards a common goal. To face this problem, collaborations between several research laboratories at the national and international level have been established as well as an industrial partnership. The main partners in this project are:

- **Gipsa-Lab**:
  First let us recall that Pr. Olivier Sename is the INOVE project leader. He is the team leader of ”Robustness and Linear Systems” team at GIPSA-lab. His research activities concern observation and control of dynamical systems, specifically, in modelling and control of automotive vehicles, in the last decade.
  The ”Robustness and Linear Systems” team of the Control Systems department from GIPSAlab Grenoble has been developing, among other, various research activities on analysis and design

of robust observers/controllers. Modelling and control of automotive vehicles (chassis, suspension, steering, braking) is one of the main tackled topics using robust control approaches such as ($\mathcal{H}_\infty$, H_2, Multi-objective), and, more recently, control methods for Linear Parameter Varying (LPV) systems.

- **MIPS, Mulhouse**:

The MIPS-MIAM research team is one of the six research groups of the Modelling, Intelligence in Processes and Systems (MIPS) Laboratory of the UHA in the engineering sciences research centre. The MIPS-MIAM group is hosted by the ENSISA, an engineering school where the research activity will take place. Since the middle of eighties, it has carried out a number of studies in the field of modelling and identification of stable or pseudostable fast complex systems (in particular, physical parameters estimation) in order to develop fault diagnosis and control applications. Application fields are both the automotive and aeronautic domains. The research activities of the MIAM that are involved in the project area are:

  - Modelling and identification of stable or pseudostable fast complex systems.
  - Multivariable control of systems.
  - Embedded architecture study for acquisition and control.
  - Longitudinal and lateral dynamic control.

- **Mines Paris-Tech (ARMINES-CAOR)**:

ARMINES-CAOR (Robotic research center of the "Ecole de Mines de Paris") is well recognized in the field of vision and control for intelligent transports systems.
In particular Brigitte d'Andrea-Novel has a strong research activity in automotive control: longitudinal control, suspension, braking systems.... Her participation in this project allows to strengthen the collaboration between us on cruise control and to get benefits from her experience in that research field. The most important issues that ARMINES-CAOR deals with are:

  - Development of new strategies for longitudinal control, such as "Adaptive Cruise Control" and "Stop & Go".
  - Integrated approach for lateral and suspension control in view of global chassis control.
  - New observers of non measured dynamical variables using advanced algebraic methods.

- **SOBEN**:

SOBEN a French dampers manufacturer, with a production capacity of 500000 dampers/year. It is also the world's leading semi active dampers manufacturer. The industrial and practical SOBEN approach completes the different studies of the research laboratories, and puts them to advantage.
The main tasks of the industrial partner SOBEN are:

  - To provide a test-bed of a full vehicle equipped by 4 semi-active Electro-Rheological dampers for vertical dynamics testing.

– To help to define a test procedure for the developed multivariable controllers on real cars and real tracks.

Also, this project takes advantage of some existing international collaborations. Parts of the project works lie on results obtained in the framework of these collaborations, which gives more visibility and influence to the developed solution on the international scale:

- PICS-CNRS CROTALE $2010-2012$: with Hungarian colleagues from MTA SZTAKI (Academy of sciences - Budapest) on automotive modeling and control. In this context, joint works have been developed in collaboration with Pr. Peter Gaspár and Josef Bokor during my research stay their that have led to the following publication (, n.d.).

- PCP $2007 - 2010$ and $2010 - 2013$: a French-Mexican project with colleagues from Technilogico di Monterrey, Mexico, and 2 industrial companies (Metalsa Mx, Soben Fr), on fault tolerant control strategies for automotive systems. Several joint works have been developed during the research stays either in Grenoble or Monterrey (see (Tudon-Martinez *et al.*, 2013*b*), (Tudon-Martinez *et al.*, 2014) and (Martinez *et al.*, 2014)).

To make clearer my contribution in this thesis, let recall various tasks of the INOVE project distributed among the partners.

1.3 Project tasks management

The main goal of the INOVE project is to propose innovative global integrated control and observation approaches to enhance the overall dynamics of the vehicle.
This will allow to adapt the vehicle control to the driving situation conditions. The results of this project may bring feasible solutions to the existing problems faced by the automotive industry and some perspective for the future driving technologies solution. To better tackle the various problems raised in this project, a good management of tasks distributions is mandatory.

Then, this project is organised as shown in Fig. 1.1 and includes the following tasks:

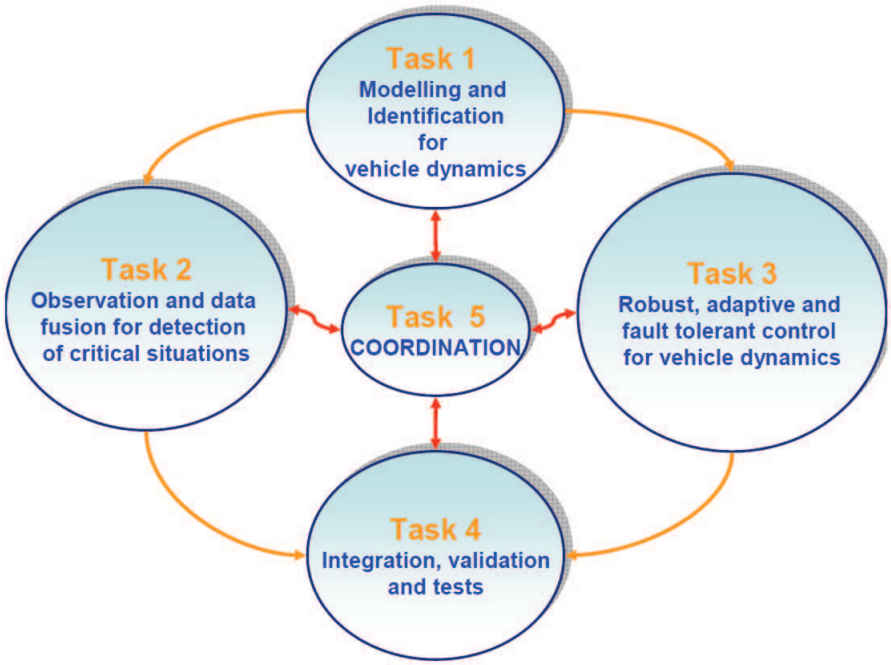

Figure 1.1: Project INOVE Tasks.

- **Task 1:Modelling and Identification for vehicle dynamics**: Gipsa-Lab and MIPS collaborates to achieve this part. This task will focus on the following objectives 1.2:

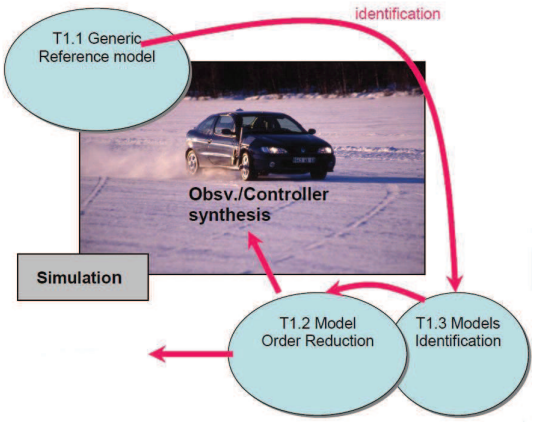

Figure 1.2: Scheme of the task 1.

  - Developing vehicle models and simplifying (order reduction).
  - Fixing the final models in Matlab code framework.
  - Identifying and validating the model by experimental procedures.

- **Task 2:Observation and data fusion for detection of critical situations** (see Fig. 1.3): This task is a collaborative work between Gipsa-Lab and Mines Paris-Tech (ARMINES-CAOR). It

focuses on:

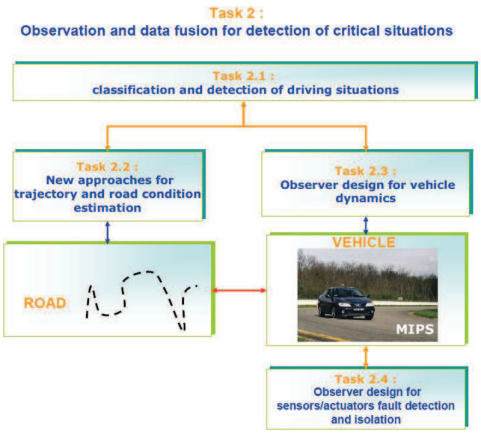

Figure 1.3: Scheme of the task 2.

- Development of new observers to detect critical situations
- Development of algebraic estimators both for estimation and compensation of unknown dynamics.
- Classification of driving situations.

- **Task 3: Robust, adaptive and fault-tolerant control for vehicle dynamics** (see Fig. 1.4: Gipsa-lab is the leader of this task, the main objectives are:

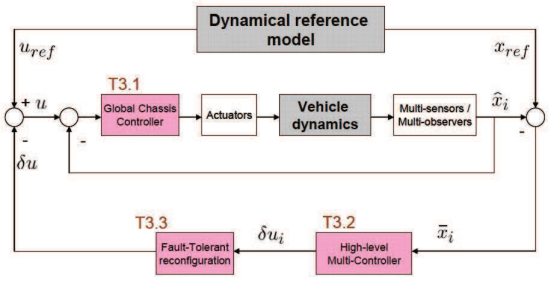

Figure 1.4: Scheme of the task 3.

- Design of innovative integrated multivariable robust control strategies to enhance the overall dynamics of the vehicle.
- Development of fault tolerant control strategies to overcome dangerous situations due, mainly, to actuators failures.

- **Task 4: Integration, validation and tests** (see Fig. 1.5): Soben and MIPS are the main leaders of this task which aims at:

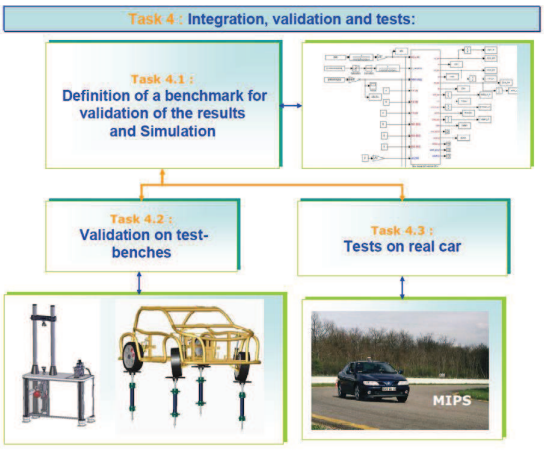

Figure 1.5: Scheme of the task 4.

– Validation of the developed strategies for control, observation and estimation.

– Proof of the industrial interest of these strategies, and that academic community can bring excellent and feasible solutions to the automotive industrial issues.

Hence, all these tasks are complementary and allow to achieve the project objectives in terms of providing the adequate solutions to overcome the real world automotive issues.

1.4 Historical development of vehicle dynamics

The history of the automotive vehicles development starts when the first steam engine was used in personal automobile transportation. Afterwards, other types of engines were used in the 19^{th} and 20^{th} centuries such as combustion engine and electric engines.
In fact, the automotive ground vehicles market was first developed in Europe, specifically, in France in 1890 then in the United States at the beginning of the 20^{th} century.

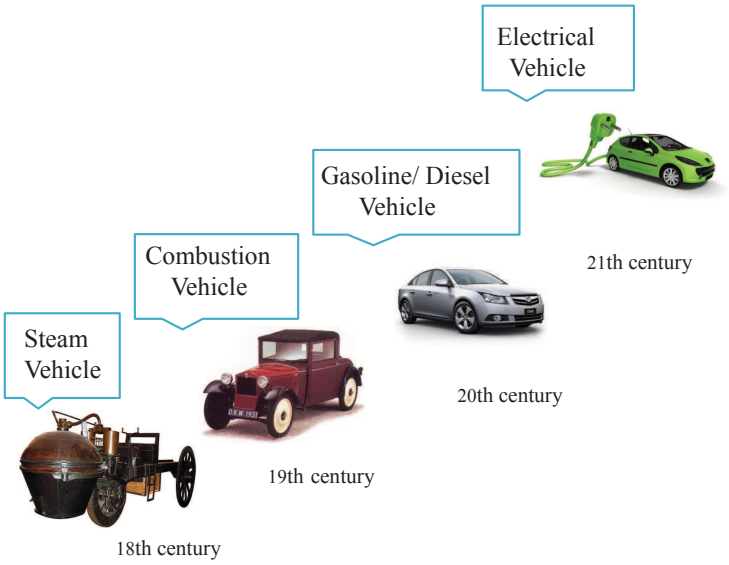

Figure 1.6: Historical development of automobile.

First the automobile was an exclusive mean of transportation for rich people. Then, it became more popular and more accessible to the middle class since automotive vehicles became cheaper thanks to Henry Ford who was the first to price his car to be as affordable as possible. Traveling using personal vehicles became increasingly popular as they simplified the transportation and give more freedom on the time and the destinations of the travels.
Nowadays, the number of the cars used in the wold, that exceeds 1.015 billion in 2010, has araised a lot of issues on the automotive systems dynamical behaviour. Indeed, vehicles have a very complex and non linear dynamical behaviour, strongly related to the driving situation. A lot of studies have treated these complex dynamics as in (Kiencke and Nielsen, 2000) and (Milliken and Milliken, 1995).

Since the main dynamics of the car are influenced by the suspension, steering and braking subsystems, a brief presentation of those subsystems of the vehicle will make it clear to the reader that the control of these elements is very important in view of improving the performance objectives. Indeed as shown later, a lot of woks have treated these subsystems as in (Zin *et al.*, 2008) where only the suspensions are designed to improve either comfort or roadholding, according to the kind of vehicle, the braking control was used separately to improve lateral and yaw behaviour of the vehicle and to tackle critical driving situations (Denny, 2005), (Tanelli *et al.*, 2007). Also, in (S.Mammar and D.Koenig, 2002) a strategy using active steering for vehicle handling improvement was presented. Then, in this thesis, we develop an innovative global chassis control, coordinating the use of these 3 actuators to achieve the performance objectives.

1.4.1 Suspension systems

The suspension systems are very important components of the ground vehicles. They consist of a connecting device between the chassis and the wheels (called by the automotive expert community ”sprung mass” , resp, ”unsprung”). Indeed, the suspensions play a key road in defining the vertical

vehicle dynamical performances of the vehicle. The suspension systems are usually composed of (see Fig. 1.7):

- A **spring** used to support the weight of the car.
- A **damper** whose goal is to slow down the spring movements to avoid harmful rebond.

Historically, the suspensions and their components have evolved to meet the automotive industry demands. Various types of springs were used through the vehicle evolution technologies, as follows:

- Leaf springs: multi-blade or single blade, working in bending (the first types of springs to be used).
- Cylindrical spiral springs (coil springs): almost always manufactured with the log steel with high mechanical characteristics and manufactured to combined bending and torsion.
- Torsion springs manufactured by means of a straight element of circular cross section or made up of several square section combined blades.

More recently, new types of springs have been used in the automotive industry (see 1.7):

- Air springs: constituted by a flexible rubber membrane canvas with metal jigs.
- Gas springs: supplemented by a hydraulic complex device.
- Rubber springs working in compression.

Figure 1.7: Various types of springs in automobile.

Concerning the dampers, the evolution was based on the mechanics, hydraulics and electrical technological advances. A damper is used to limit the oscillations on a system or to isolate a system

from the vibrations by dissipating energy.
Several kinds of dampers based on different technologies were used in the vehicular industry. Indeed, the technological advances have allowed to provide various solutions depending on criteria involving size, cost for the components. Some examples of the most used dampers in the suspension systems are (see Fig. 7.27):

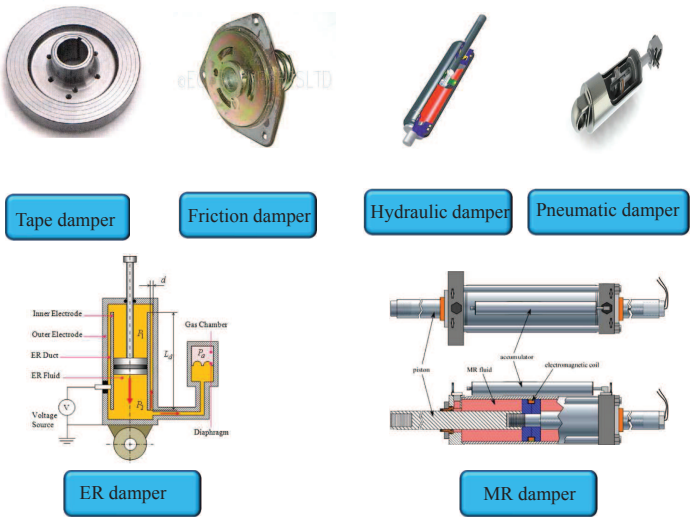

Figure 1.8: Types of dampers in automobile.

- **Tape damper**: which was made up of a ribbon (leather or rubber) wound and connected to the leaf spring of the suspension. Most of these dampers available in the market are passive.
- **Friction damper**: the effect was due to the friction of two or more disks, braked in their rotational movement by a powerful spring mounted on its fixation axis with, in most cases, adjustability of the damping by means of a nut. Most of these dampers available in the market are passive.
- **Hydraulic damper**: one of the most used dampers. It is typically a double acting damper, and slows the oscillations in both directions with a greater energy in the expansion phase of the suspension springs. There are a lot of hydraulic dampers types, depending on the mechanical assembly. Most of these dampers available in the market are passive.
- **Pneumatic damper**: similar to the hydraulic one, but the damper is filled with air. There are two common types of hydraulic and pneumatic dampers: Mono Tube Shock Absorber and Twin Tube Shock Absorber. Most of these dampers available in the market are passive.
- **Magneto-Rheological damper**:uses a magnetic field to change the damping coefficient of the suspension system.

  Indeed, rather than the conventional oil, the MR dampers incorporate a magneto rheological fluid with magnetic particles whose characteristics can be continuously controlled by an **elec-**

tric current through a coil generating the magnetic field. This kind of dampers allows to use different control strategies to adapt them to the desired performance objectives. It is already used in some luxury and sport cars as (*eg: Audi TT, R8, Farrari...*).

- **Electro-Rheological damper**: it presents some similarities as the previous damper. The electro-rheological damper is a kind of damper filled by an electro-rheological fluid that changes its characteristics under varying **electric field intensity**. Indeed, as the electric field changes the volume of the ER fluid change and thus the damping coefficient of these dampers changes. This kind of damper is used in the test-bench that we have developed in Gipsa-Lab (with Soben) for the vehicle vertical dynamics study and analysis.

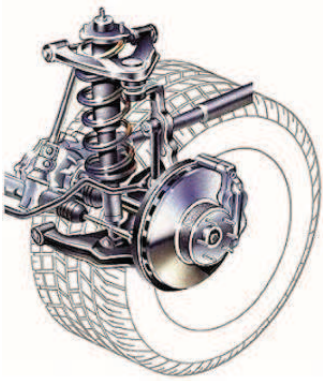

Figure 1.9: Suspension system in automobile.

Also, the suspension systems (see Fig. 1.9) job is to carry the static weight of the vehicle, to preserve manoeuvrability and handling of the car and to ensure a good behaviour of the vehicle subject to tire forces due to braking actions.
The use of different kinds of springs, dampers, assembly geometries and fluid technologies has led to develop several general types of suspensions, namely, passive, semi-active and active suspensions. The main objectives of any suspension system are:

- to improve the passengers comfort by ensuring a good insulation of the chassis from the road irregularities.

- to ensure a permanent contact between the tire and the road and to maximise the friction between them to enhance vehicle safety.

1.4.1.1 Passive suspension:

Passive suspensions (see Fig. 1.10) are systems which always dissipate energy, with components (spring and damper) characteristics that are **fixed**. These characteristics are chosen by the engineering designers, depending on the desired objectives for the intended application.

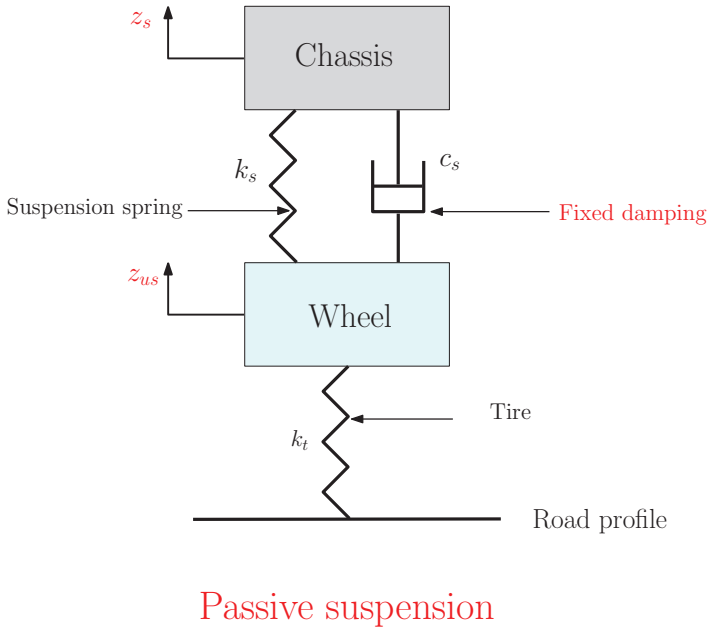

Figure 1.10: Passive suspension.

Remark: Fig. 1.10 illustrates the passive suspension where z_s is the chassis displacement, z_{us} the wheels displacement, k_s the spring stiffness, k_t the tire stiffness and c_s the damping coefficient.

Indeed, a highly damped suspension will yield good handling, but may not isolate the chassis from the road irregularities. On the other hand, when the suspension damping is low, the passengers comfort is improved but it may reduce the vehicle stability in some driving situations. The most commonly used passive dampers are hydraulic, Pneumatic and friction ones (see 1.4.1).
To illustrate the characteristics of each type of suspensions, the Speed/Effort Rule (SER) is helpful to analyse the differences between them. For the suspension, the considered speed is the suspension deflection (difference between the chassis and the wheel speeds), and the effort is the damping force.

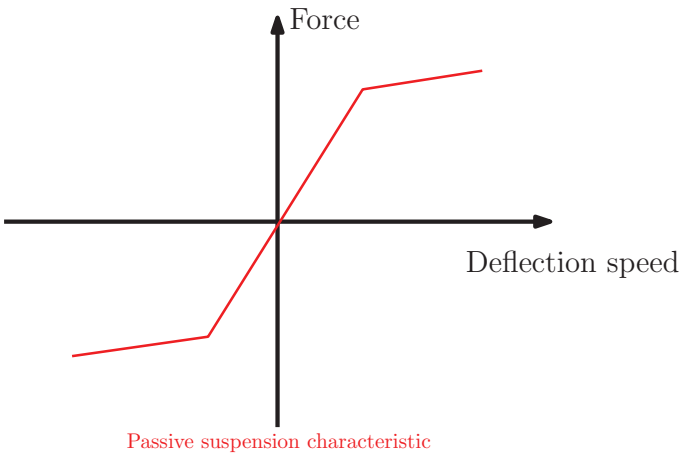

Figure 1.11: SER of Passive suspension.

Let us discuss now the mathematical model of this type of suspension.
First, since the suspension system is composed of a spring and a damper, the suspension force is :

$$F_s = F_k(.) + F_d(.) \tag{1.1}$$

where $F_k(.)$ is the force provided by the spring, and $F_d(.)$, the force provided by the considered damping element, depending on the type of suspension. (i.e. passive, semi-active or active).
The spring force can be either linear: $F_k = kz_{def}$, where k is the linear spring stiffness and $z_{def} = z_s - z_{us}$, the spring deflection, or non linear: $F_k = k\big(z_{def}\big)$ where the spring stiffness is a non linear function of the deflection. For the passive damper, $F_d(.)$ can be:

- Linear: the damping coefficient is constant c_s and the damping force is linear and changes depending on the deflection speed $\dot{z}_{def} = \dot{z}_s - \dot{z}_{us}$ as follows:

$$F_d(.) = c_s \dot{z}_{def} \tag{1.2}$$

- Non linear: the damping coefficient is a non linear function (F_d) of the suspension deflection speed as follows:

$$F_d(.) = F_d(\dot{z}_{def}) \tag{1.3}$$

1.4.1.2 Active suspension:

Active suspensions (see Fig. 1.12) are systems that can both generate and dissipate energy. Indeed, they can be seen as active actuators providing the adequate force to meet the required objectives without consideration to the suspension deflection and speed.

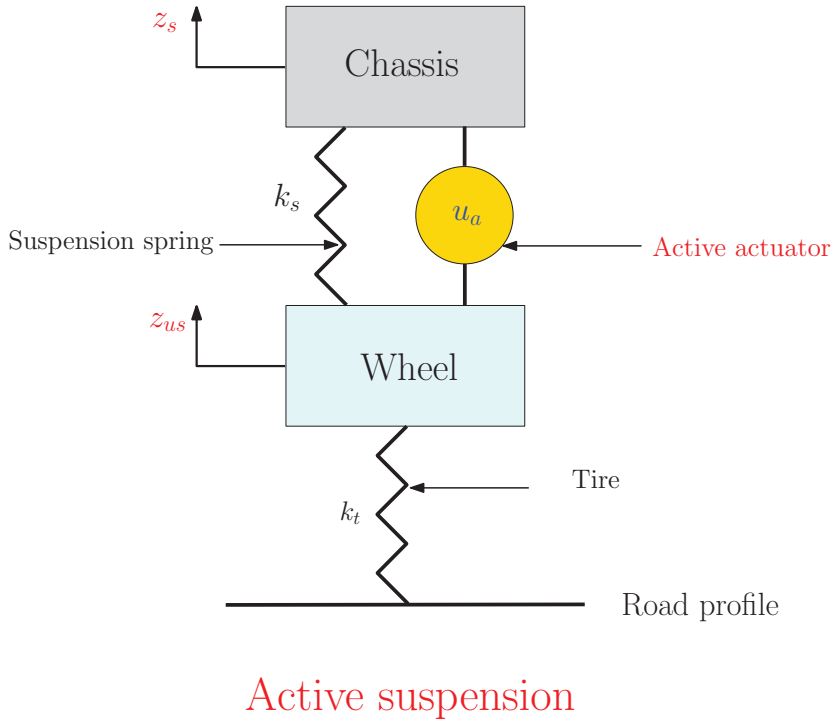

Figure 1.12: Active suspension.

This type of suspensions allows to improve the ride safety and comfort in the same time since it can dissipate and generate the energy (see Fig. 1.13). In the SER scheme, it can be clearly seen that the active suspension can provide and dissipate energy whatever the suspension deflection is.

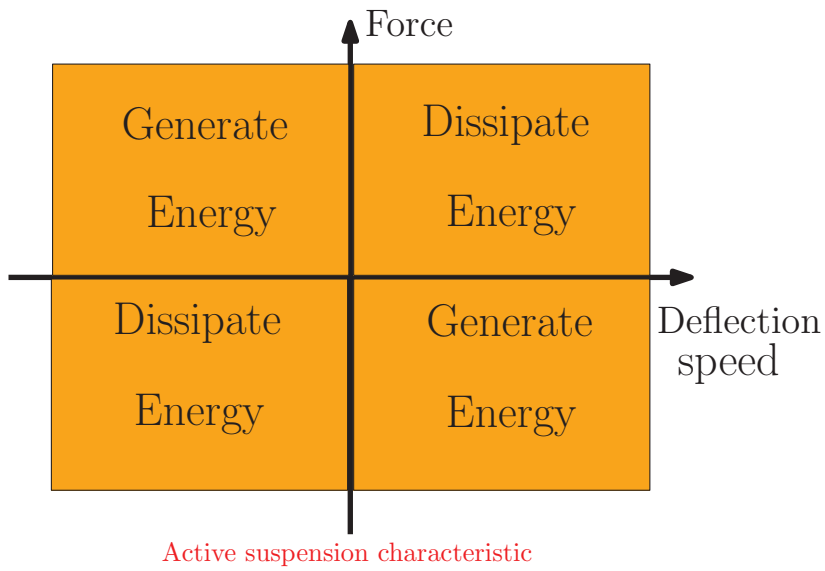

Figure 1.13: SER of Active suspension.

Based on equation Eq. 1.1, the active part of the suspension force can be modeled as follows:

$$\dot{u} = \varpi(u^0 - u) \tag{1.4}$$

where u is the effective force provided by the actuator, u^0 the required force, and ϖ the cut-off frequency of the actuator.

Remark: According to Eq. 1.1, in this case the damper force depends on the controlled input ($F_d = u_a$).

1.4.1.3 Semi-active suspension:

Semi-active suspension subsystems can only dissipate energy through the variation of the damping property (varying dissipation flow rate). Whereas the active suspension system requires an external energy source to power an actuator that generate and dissipate energy and then controls the vertical dynamics of the car, the semi-active suspension system uses the external energy sources to adjust the damping level of the damper to only dissipate energy and achieve the required performance objectives.

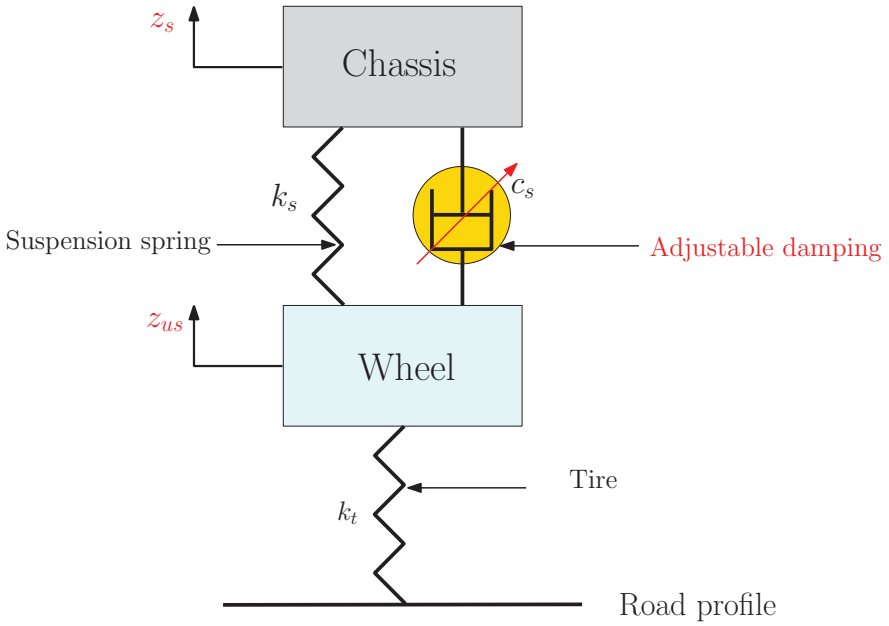

Figure 1.14: Semi-active suspension.

Then, a simple definition of the semi-active suspension system is a suspension with a controlled damping coefficient. This damping coefficient is given by:

$$F_d = F_d(., \Omega) \tag{1.5}$$

where $F_d(.)$ is the damping function that allows to dissipate energy and Ω is the control input (depending on the damper type) that allows to tune the damping coefficient. Values of $F_d(.)$ that tune the damping characteristics of the vehicle are limited as in Fig. 1.15 and allows only to dissipate energy in order to meet the tradeoff between the vehicle safety and the passengers comfort.

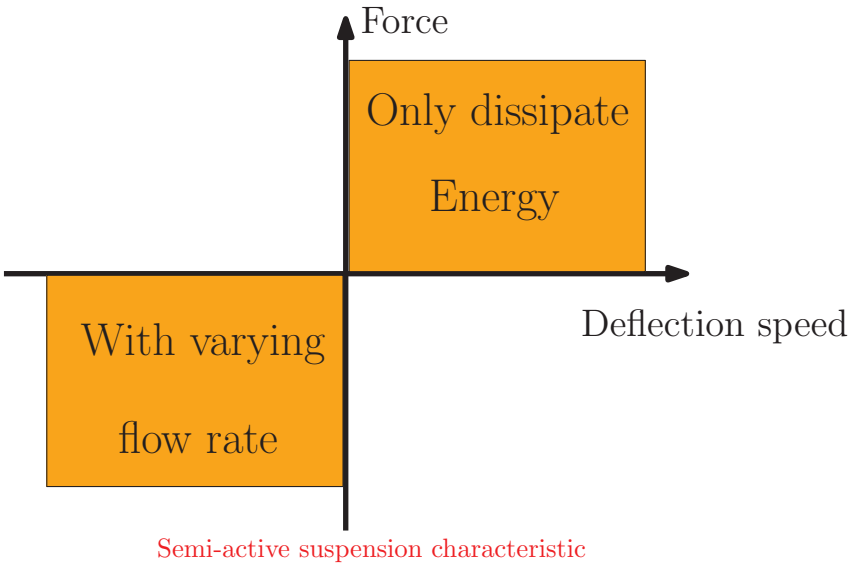

Figure 1.15: SER of Semiactive suspension.

Several types of semi-active suspension exist such as the Hydraulic (Soben), Magneto-Rheologic (DELPHI) and Electro-Rheologic semi-active suspensions. Each type uses a different technology to dissipate the energy and to vary the flow rate.
The mathematical model of these types of suspension is usually non linear (to meet the dissipation requirements) but could be linear in some case for simplicity reasons:

- Linear: this model expresses the damping force as a linear function of the suspension deflection speed, with the damping coefficient $c_s(\Omega)$ which depends on the considered control input Ω (w.r.t the technology used for each type of semi-active suspension system):

$$F_d(., \Omega) = c_s(\Omega)\dot{z}_{def} \tag{1.6}$$

- Non Linear: a lot of non linear dampers models have been used for several applications. One of the interesting non linear dampers model can be established as follows:

  - Non linear static models: one of the most used models is the one introduced in (Shuqui *et al.*, 2006):

$$F_d(., \Omega) = A_1(\Omega)\tanh\left(A_2(\Omega)\dot{z}_{def}\right) + A_3(\Omega)\dot{z}_{def} \tag{1.7}$$

    where $\{A_1, A_2, A_3\}$ are model parameters that are dependent on the input (Ω parameter). Other models where introduced, mainly, by making the damping force dependent on the suspension deflection, deflection speed and acceleration to better model the non linear behaviours.

1.4.2 Braking system

In this study, Electro-Mechanical Braking (EMB) actuators are considered since they are widely used in the automotive industry. Indeed, the challenging issues regarding more environmentally friendly systems, fuel economy, simplified system assembly, and improvement of the vehicle manoeuvrability and safety have led to develop the braking systems from the old hydraulic one to the EMB actuators.

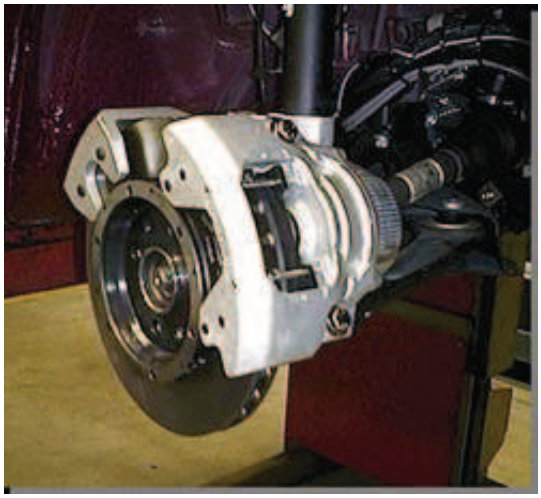

Figure 1.16: Electro-Mechanical Braking actuator.

The Electro-Mechanical Braking systems have evolved, compared to the previous hydraulic and electro-hydraulic braking systems. The braking force is directly generated by high performance electric motors on the wheels, depending on the signals sent from the braking pedal module. This kind of braking system has a lot of advantages as:

- Environmentally friendly (no brake fluid).
- Shorter stopping distances and optimized stability. Electromechanical brakes also include complicated communication networks since each caliper has to receive multiple data inputs in order to generate the proper amount of braking force. Due to the safety-critical nature of these systems, there should be redundant, using a secondary bus to deliver raw data to the calipers.
- Saves space and uses fewer parts which reduces considerably the cost of maintenance. Unlike electro-hydraulic brakes, all of the components in an electro-mechanical system are electronic. The calipers have electronic actuators instead of hydraulic slave cylinders, and everything is governed directly by a control unit instead of a high pressure master cylinder. These systems also require a number of additional hardware, including temperature, clamp force, and actuator position sensors in each caliper.

Remark: It is worth noting that the Electro-Mechanical Braking systems can be easily networked with future traffic management systems for more efficient automotive control and dynamical improvement global strategies (see (Savaresi and Tanelli, 2010)).

1.4.3 Steering system

In this study, the Active Steering (AS) has been considered. The active steering describes the driver assistance by correcting the driver steering input through the corrective steering control of an actuator that may alter continuously and smartly the steered wheel angle.

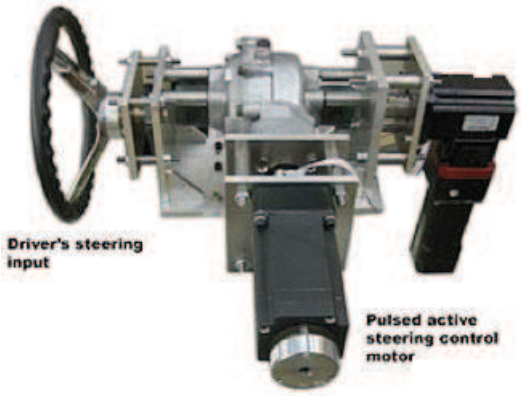

Figure 1.17: Active steering actuator.

Indeed, the active steering reacts faster than the driver does to unexpected yaw disturbances. The active steering allows to correct the steering input needed to achieve different driving performances.

Also, the driving safety, comfort, and handling can be significantly improved by using the steering input as vehicle dynamics control. The yaw motion has been widely studied and investigated through several works and strategies (i.e. yaw disturbance rejection and skidding avoidance). By developing controllers for active steering, the driver assistance system can ensure the vehicle yaw stabilization subject to rough driving situations. The active steering is important since it has a direct impact on the yaw behaviour of the car and then helps to avoid roll over in case of critical situations. Indeed, the lateral stability of the car can be greatly influenced by the active steering control design. Also, active steering allows to improve the low speed maneuverability and the high speed stability of the vehicle. It is worth noting that there are several types of active steering as: the direction column, steer by wire and other types that act as a torque on the steering wheel or as a corrective steering angle.

1.5 Introduction to the thesis framework

The main issue of this thesis is to work out new Global Chassis MIMO controllers that enhance the overall dynamics of the vehicle while preserving the vehicle stability in critical driving situations. Many innovative strategies have been explored and finalized to deal with these problematics. Various solutions have been given to deal with the vehicle stability and performance objectives. Indeed, many works based on the $LPV/\mathcal{H}_\infty$ approach have been developed to control simultaneously the braking, steering and suspension actuators. On the other hand, innovative road profile estimation strategies have been introduced and validated via experimental procedures, providing new cheap and easily implementable techniques to estimate the road profile characteristics. Then, the vehicle control is adapted, depending on the road roughness (since it influences greatly the behaviour and the stability

of the car). Several fault tolerant control strategies have been also considered to handle the actuators failures while keeping the vehicle stability, safety and enhancing the dynamical behaviour of the car in dangerous and critical driving situations.

The general content of this thesis is as follows :

- **PART I** : Theoretical backgrounds and vehicle modeling.
- **PART II** : Road adaptive control vehicle dynamics.
- **PART III** : Global chassis control using several actuators.

Also, during this thesis and using the previous works of the advisors and the thesis results, a Matlab ToolBox "Automotive" has been developed to provide a bench test for the different automotive control studies.

1.6 Publication List

Throughout this thesis, several publications in various control conferences and journals have been achieved and others are on progress.

- **Books chapters** :

1. Charles Poussot-Vassal, Olivier Sename, Soheib Fergani, Moustapha Doumiati and Luc Dugard. Global chassis control using coordinated control of braking/steering actuators. Springer book chapter: Robust Control and Linear Parameter Varying approaches: application to vehicle dynamics, 2013, 237-266.

- **International conference papers with proceedings** :

1. soheib Fergani, Olivier Sename and Luc Dugard. LPV/$\mathcal{H}_\infty$ Fault Tolerant control for automotive semi-active suspensions using roll and pitch monitoring. Accepted in Vehicle System Dynamics, Identification and Anomalies (VSDIA 2014), Hungary, 2014.
2. Soheib Fergani, Menhour Lghani, Olivier Sename, Luc Dugard and Brigitte D' Andréa-Novel. Full vehicle dynamics control based on LPV/$\mathcal{H}_\infty$ and flatness approaches. Proceeding of ECC 2014 - 13th European Control Conference (ECC 2014), France, 2014.
3. Juan Carlos Tudon-Martinez, Soheib Fergani, Olivier Sename, Ruben Morales-Menendez, Luc Dugard. Online Road Profile Estimation in Automotive Vehicles. Proceeding of ECC 2014 - 13th European Control Conference (ECC 2014), France, 2014.
4. Fergani Soheib, Olivier Sename and Luc Dugard. A LPV/$\mathcal{H}_\infty$ fault tolerant control of vehicle roll dynamics under semi-active damper malfunction. Proceedings - 2014 American Control Conference (ACC 2014), United-States, 2014.
5. Soheib Fergani, Lghani Menhour, Olivier Sename, Luc Dugard and Brigitte D' Andréa-Novel. A new LPV/$\mathcal{H}_\infty$ semi-active suspension control strategy with performance adaptation to roll behavior based on non linear algebraic road profile estimation. Proceedings of 52nd IEEE CDC - 52nd IEEE Conference on Decision and Control (CDC 2013), Italy, 2013.

6. Soheib Fergani, Olivier Sename and Luc Dugard. A LPV suspension control with performance adaptation to roll behavior, integrated in a global vehicle dynamic control strategy. Proceedings of the ECC 2013 - 12th biannual European Control Conference (ECC 2013), Switzerland, 2013.
7. Soheib Fergani, Olivier Sename and Luc Dugard. A new LPV/$\mathcal{H}_\infty$ Global Chassis Control through load transfer distribution and vehicle stability monitoring. Proceedings 5th IFAC Symposium on System Structure and Control - IFAC Joint conference SSSC - 5th Symposium on System Structure and Control, France, 2013.
8. Juan-Carlos Tudon-Martinez, Soheib Fergani, Sebastien Varrier, Olivier Sename, Luc Dugard, Ruben Morales-Menendez and Ricardo Ramirez-Mendoza. Road Adaptive Semi-active Suspension in a Pick-up Truck using an LPV Controller. Proceedings of IFAC Advances in Automotive Control (AAC 2013), Japan, 2013.
9. Soheib Fergani, Menhour Lghani, Olivier Sename, Luc Dugard and Brigitte D' Andréa-Novel. Study and comparison of non-linear and LPV control approaches for vehicle stability control. Proceeding in 21st Mediterranean Conference on Control and Automation - 21st Mediterranean Conference on Control and Automation, Greece, 2013.
10. Olivier Sename, Juan-Carlos Tudon-Martinez and Soheib Fergani. LPV methods for fault-tolerant vehicle dynamic control. Proceedings of Conference on Control and Fault-Tolerant Systems (SysTol), France, 2013.
11. Soheib Fergani, Olivier Sename and Luc Dugard. Performances improvement through an LPV/$\mathcal{H}_\infty$ control coordination strategy involving braking, semi-active suspension and steering Systems. Proceedings of CDC 2012 - 51st IEEE Conference on Decision and Control (CDC 2012), United-States, 2012.
12. Soheib Fergani, Olivier Sename and Luc Dugard. A LPV/$\mathcal{H}_\infty$ Global Chassis Controller for performances Improvement Involving Braking, Suspension and Steering Systems. Proceedings 7th IFAC Symposium on Robust Control Design (ROCOND 2012), Denmark, 2012.
13. Soheib Fergani, Olivier Sename, Luc Dugard, Peter Gaspar, Zoltan Szabó and Jozsef Bokor . A combined suspension/ four steering control, integrated in a global vehicle dynamics control strategy. Proceeding 13th Mini Conference on Vehicle System Dynamics, Identification and Anomalies (VSDIA 2012), Hungary, 2012.
14. Soheib Fergani, Olivier Sename and Luc Dugard. Commande coordonnée des actionneurs de freinage et de suspension semi-active pour la dynamique des véhicules automobile. Proceedings of Septiéme Conférence Internationale Francophone d'Automatique (CIFA 2012), France, 2012.

- **National conference papers with proceedings** :

1. Soheib Fergani, Olivier Sename and Luc Dugard. Commande LPV/$\mathcal{H}_\infty$ du braquage 4 roues et des suspensions avec adaptation aux dynamiques roulis dans une stratÃ©gie globale de commande de châssis de véhicule. Proceedings of JD/JN MACS 2013 - 5émes Journées Doctorales / Journées Nationales MACS2013, France, 2013.
2. Soheib Fergani, Olivier Sename and Luc Dugard. Approches LPV pour la coordination des actionneurs en vue du contrôle global de la dynamique véhicule. Proceedings of Journées Automatique et Automobile, Octobre (JAA 2013), France, 2013.

- **Journals under revision** :

1. Soheib Fergani, Olivier Sename and Luc Dugard. An LPV/$\mathcal{H}_\infty$ integrated VDC. Submitted to IEEE Transaction on Vehicular Technology Journal, 2014.

- **Submitted journal and conference papers** :

1. Juan .C. Tudon Martinez, soheib Fergani, Olivier Sename, John J.Martinez, Ruben Morales-Menendez, and Luc Dugard. Adaptive Road Profile Estimation in Semi-Active Car Suspensions. Submitted to Transactions on Control Systems Technology, 2014.
2. Manh-Quan Nguyen, Olivier Sename, Luc Dugard and Soheib Fergani. An LPV/$\mathcal{H}_\infty$ motion adaptive suspension control of a full car model. Submitted to the 53rd IEEE Conference on Decision and Control, United-States, 2015.

1.7 Conclusion

This chapter was dedicated to present the thesis framework. First, the National French Research agency supporting the thesis studies was introduced. The context of the research and the collaboration established within this work were then highlighted. After that, the organisation of the project tasks and the collaborative works are presented. Then, a historical recall on the automobile evolution based on the technological advances through the last century. Finally, a short introduction to the global chassis control of automotive ground vehicle has been given, emphasizing the advantages of the integrated global MIMO control compared to the separately SISO designed controllers.
It is worth noting that this work is a continuation of the previous studies carried out in the Linear Systems and Robustness team, is particular the Phd thesis of (Ramirez-Mendoza, 1997), (Sammier, 2001), (Zin, 2005), (Poussot-Vassal, 2008), (Aubouet, 2010) and (Anh lam, 2011).

Part I

Background on control theory and vehicle modeling

CHAPTER 2

Background on Control Theory

2.1 Introduction

This chapiter presents some theoretical backgrounds on the mathematical tools and notions used in this dissertation for advanced control design and analysis. This will help non-expert readers to better understand the various developments presented in this study. For this sake, we will first start by a brief presentation of the linear and non linear systems to introduce the readers to the physical systems modeling and state space representations. Also, some tools that help to understand the major control design problem formulation are presented such as Linear Matrix Inequalities, convexity and dissipativity concepts. Then, $\mathcal{H}_\infty$ control design problem formulation is introduced with the LMI's formulation of this design problem and the detailed LTI/$\mathcal{H}_\infty$ solution. Then, the LPV/$\mathcal{H}_\infty$ control approach based on the LMI convex optimisation is presented briefly.
It is worth noting that theoretical developments are not the core contribution of the thesis. The problems of dissipativity, robust control, LMI, have been extensively developed in a lot of previous works of C.W. Scherer, F. Doyle, L. El-Ghaoui, P. Apkarian, P. Gahinet, D. Arzelier, J. Bokor and othrs(see (Boyd *et al.*, 1994), (Alazard, 2003), (El-Ghaoui, 1997), (Scherer *et al.*, 1997), (Apkarian and Adams, 1998)). It is also worth noticing that all the theoretical backgrounds are given for the continuous time problems.
This chapter is structured as follows: Section 1 introduces some definitions of the linear and the non linear systems. Then, Section 2 presents the LTI and the LPV systems definitions as well as some mathematical backgrounds to understand the control approach. In Section 3, the notions of robustness together with the dissipativity theory are given and a solution to the classical quadratic performance objectives for LTI systems controllers based on the LMI resolution is provided. Section 4 gives the LMI's based solution of the LPV/$\mathcal{H}_\infty$ controller synthesis for the polytopic systems. Finally, Section 5 recalls the non linear algebraic estimation, and the flatness based control is presented to better apprehend further development given in the next chapters.

2.2 Dynamical system, norm and LMI definitions

In this section, fundamental mathematical notations and definitions concerning dynamical systems are introduced. Then definitions of mathematical tools such as LMIs and convexity are provided.

2.2.1 Definitions

Dynamics is directly linked to the notion of change, and a Dynamical System defines how a system of variables interacts and changes with time. Furthermore, very few physical dynamical systems are truly linear. Indeed, most of the real systems are fundamentally non linear. To study the linear and non linear systems in control theory, dynamical systems are mostly modeled using a set of linear or non linear Ordinary Differential Equations (ODE) (PDE are not in the scope of this work). The most

generic models are non linear models obtained from physical equations, but the most common method to design controllers is to start by linearizing these models around some operating conditions, which yields linear models, and then to use linear control techniques. Also, there are systems for which the nonlinearities are important and cannot be ignored. For these systems, nonlinear analysis and design techniques exist and still can be used.

2.2.2 Continuous time Nonlinear dynamical systems

From the physical equations, the non linear models of real physical systems are derived thanks to the ODEs to describe the system dynamical behavior as well as possible.

Definition 2.2.1 (*Nonlinear dynamical system*)

For given functions $f : \mathbb{R}^n \times \mathbb{R}^{n_w} \mapsto \mathbb{R}^n$ and $g : \mathbb{R}^n \times \mathbb{R}^{n_w} \mapsto \mathbb{R}^{n_z}$, a nonlinear dynamical system ($\Sigma_{\mathcal{NL}}$) can be described as:

$$\Sigma_{\mathcal{NL}} : \begin{cases} \dot{x}(t) &= f(x(t), w(t)) \\ z(t) &= g(x(t), w(t)) \end{cases} \tag{2.1}$$

where $x(t)$ is the state which takes values in a state space $X \subset \mathbb{R}^n$, $w(t)$ is the input taking values in the input space $W \subset \mathbb{R}^{n_w}$ and $z(t)$ is the output that belongs to the output space $Z \subset \mathbb{R}^{n_z}$.

Most of the physical phenomena of the systems can be handled by the introduced non linear model (Eq. 2.2.1). The complexity of the non linear models induces several difficulties while trying to study them as they are, especially to find the adequate mathematical and methodological tools for identification, observation, control synthesis and analysis. One can notice that the study of a complex non linear model is very difficult and sometimes almost impossible without introducing some simplifications or making linearization.
In lot of physical systems studies, non linear models are more suitable for simulation and performance analysis but quite difficult to use for the synthesis objectives.

2.2.3 Continuous time LTI dynamical systems

The linear approach starts with the transformation of the previous non linear system into a linear one: this is referred to as the linearization, which is to be done at a selected operating point of the system.

Definition 2.2.2 (*LTI dynamical system*)

Given matrices $A \in \mathbb{R}^{n \times n}$, $B \in \mathbb{R}^{n \times n_w}$, $C \in \mathbb{R}^{n_z \times n}$ and $D \in \mathbb{R}^{n_z \times n_w}$, a Linear Time Invariant (LTI) dynamical system (Σ_{LTI}) can be described as:

$$\Sigma_{LTI} : \begin{cases} \dot{x}(t) &= Ax(t) + Bw(t) \\ z(t) &= Cx(t) + Dw(t) \end{cases} \tag{2.2}$$

where $x(t)$ is the state which takes values in a state space $X \subset \mathbb{R}^n$, $w(t)$ is the input taking values in the input space $W \subset \mathbb{R}^{n_w}$ and $z(t)$ is the output that belongs to the output space $Z \subset \mathbb{R}^{n_z}$.

A good start for the study of a nonlinear system is to find its equilibrium points. This, in itself, might be a formidable task. The system may have more than one equilibrium point. Linearization is often performed about the equilibrium points of the system. It allows to characterize the behavior of

the solutions in the neighborhood of the equilibrium point.
The LTI models are more frequently used for the control and observation tasks. Many theoretical tools are available both for SISO and MIMO systems and are easy to handle unlike the non linear models. Thus, the main problem of the use of the LTI systems is that they are only valid around the linearization points and describe locally the real physical system behavior. The following scheme summarizes the use of the linearization to simplify the non linear problems: where x is the state vector,

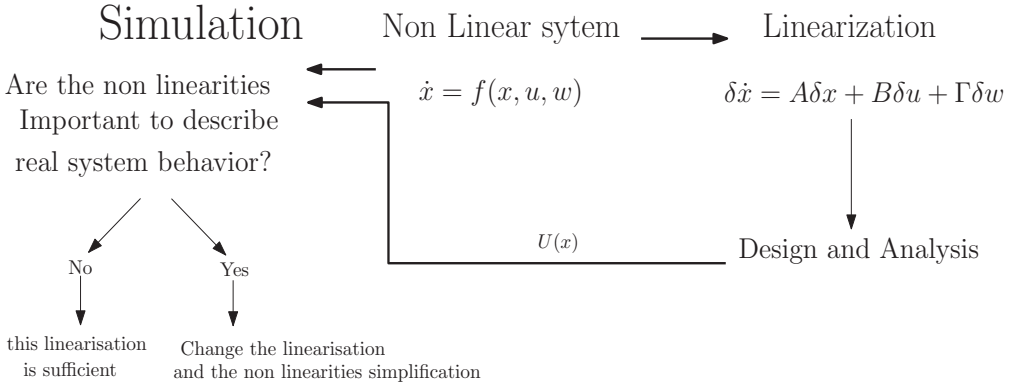

Figure 2.1: Linearization procedure

u the control input, ω the disturbances and $U(x)$ is the designed control input, As presented, if the simulation does not yield the expected results, then, two possibilities arise: higher order non linear terms that were neglected must have been significant, or a change of the linearization points is needed since the considered one doesn't ensure global stability.

2.2.4 Continuous time LPV dynamical systems

Linear Parameters Varying (LPV) system can be represented as linear systems where the matrices A, B, C and D are functions of some vector of varying, measurable parameters. In the sequel, the focus will be on the state space representation of LPV systems as follows:

Definition 2.2.3 (*LPV dynamical system*)

Given the linear matrix functions $A \subset \mathbb{R}^{n\times n}$, $B \subset \mathbb{R}^{n\times n_w}$, $C \subset \mathbb{R}^{n_z\times n}$ and $D \subset \mathbb{R}^{n_z\times n_w}$, a Linear Parameter Varying (LPV) dynamical system (Σ_{LPV}) can be described as:

$$\Sigma_{LPV} : \left\{ \begin{array}{rcl} \dot{x}(t) & = & A(\rho(.))x(t) + B(\rho(.))w(t) \\ z(t) & = & C(\rho(.))x(t) + D(\rho(.))w(t) \end{array} \right. \tag{2.3}$$

where $x(t)$ is the state which takes values in a state space $X \subset \mathbb{R}^n$, $w(t)$ is the input taking values in the input space $W \subset \mathbb{R}^{n_w}$ and $z(t)$ is the output that belongs to the output space $Z \subset \mathbb{R}^{n_z}$. In 2.3, $\rho(.)$ is a varying parameter vector that takes values in the parameter space $\mathcal{P}_\rho$ (assumed a convex set) such that,

$$\mathcal{P}_\rho := \{\rho(.) := \left[\begin{array}{ccc} \rho_1(.) & \dots & \rho_l(.) \end{array} \right]^T \in \mathbb{R}^l \text{ and } \rho_i \in \left[\begin{array}{cc} \underline{\rho}_i & \overline{\rho}_i \end{array} \right] \forall i = 1, \dots, l\} \tag{2.4}$$

where l is the number of varying parameters. For sake of readability, $\rho(.)$ will be denoted as ρ. Then, from a general viewpoint, if:

- *$\rho(.) = \rho$, a constant value, (2.3) is a Linear Time Invariant (LTI) system.*
- *$\rho(.) = \rho(t)$ where the mathematical description of $\rho(t)$, (2.3) is a Linear Time Varying (LTV) system.*
- *$\rho(.) = \rho(x(t))$, (2.3) is a quasi-Linear Parameter Varying (qLPV) system.*
- *$\rho(.) = \rho(t)$ an external parameter, (2.3) is an LPV system.*

The LPV systems can be seen as a combination of several LTI systems each time the varying parameters takes values in the set of variations (depending on the used varying parameters it can be affine, polynomial,...ect).
An LPV system ensures a good approximation of a non linear model by using a state space varying parameters representation that is close to the real dynamical behaviour of the non linear model The advantage of the LPV system is that it keeps a linear structure which allows to use several synthesis and analysis mathematical tools for linear systems.
Several representations of the LPV systems are available. The one used all over this work is the the LPV polytopic approach (see Zin (2005) PhD Thesis).

Since $\mathcal{P}_\rho$, the parameter space, is assumed to be bounded, a usual way to represent the Eq. 2.3 is to rewrite it into a polytopic description.

Definition 2.2.4 (*Polytopic LPV dynamical system*)

An LPV system is said to be polytopic if it can be expressed as:

$$\left[\begin{array}{c|c} A(\rho) & B(\rho) \\ \hline C(\rho) & D(\rho) \end{array}\right] = \sum_{i=1}^{N} \alpha_i(\rho) \left[\begin{array}{c|c} A(\omega_i) & B(\omega_i) \\ \hline C(\omega_i) & D(\omega_i) \end{array}\right] \in \mathbf{Co}\left\{ \left[\begin{array}{c|c} A_1 & B_1 \\ \hline C_1 & D_1 \end{array}\right], \ldots, \left[\begin{array}{c|c} A_N & B_N \\ \hline C_N & D_N \end{array}\right] \right\} \tag{2.5}$$

where ω_i are the vertices of the polytope formed by all the extremities of each varying parameter $\rho \in \mathcal{P}_\rho$, and where $\alpha_i(\rho)$ are defined as,

$$\alpha_i(\rho) := \frac{\prod_{k=1}^{l} |\rho_k - \mathcal{C}(\omega_i)_k|}{\prod_{k=1}^{l} (\overline{\rho}_k - \underline{\rho}_k)} \, , i = 1, \ldots, N \tag{2.6}$$

$$\alpha_i(\rho) \geq 0 \text{ and } \sum_{i=1}^{N} \alpha_i(\rho) = 1 \tag{2.7}$$

where $\mathcal{C}(\omega_i)_k$ is the k^{th} component of the vector $\mathcal{C}(\omega_i)$ defined as,

$$\mathcal{C}(\omega_i)_k := \{\rho_k | \rho_k = \overline{\rho}_k \text{ if } (\omega_i)_k = \underline{\rho}_k \text{ or } \rho_k = \underline{\rho}_k \text{ otherwise}\} \tag{2.8}$$

Then, $N = 2^l$ is the number of vertices of the polytope formed by the extremum values of each varying parameter ρ_i and A_i, B_i, C_i and D_i are constant known matrices (that represent the system evaluated at each vertex).

The polytopic LPV system is defined as a convex combination of the systems defined at the upper and lower bounds of each parameter set of variation as seen later. This convexity allows to simplify the stabilization procedure while synthesizing the global LPV controller.

To have the appropriate polytopic representation of the LPV systems, a state space representation affinely dependent on the parameters is required (more precisely when the varying parameter is a state of the model).

Example: LPV modeling with 2 parameters. Let consider a 2 parameter affinely dependent LPV system (parameters $\rho_1(.)$ and $\rho_2(.)$, $l = 2$). Then,

$$\rho = [\rho_1(.), \rho_2(.)] \in \mathcal{P}_\rho = \mathbf{Co}\{(\underline{\rho_1}, \underline{\rho_2}), (\overline{\rho_1}, \underline{\rho_2}), (\underline{\rho_1}, \overline{\rho_2}), (\overline{\rho_1}, \overline{\rho_2})\} = \mathbf{Co}\{\omega_1, \omega_2, \omega_3, \omega_4\} \tag{2.9}$$

The polytope $\mathcal{P}_\rho$ is formed of $N = 4$ vertices and

$$\Sigma_{LPV} \in \mathbf{Co}\{\Sigma(\omega_1), \Sigma(\omega_2), \Sigma(\omega_3), \Sigma(\omega_4)\} \tag{2.10}$$

The polytopic coordinates are given by :

$$\omega = \begin{bmatrix} \omega_1 \\ \omega_2 \\ \omega_3 \\ \omega_4 \end{bmatrix} = \begin{bmatrix} \underline{\rho}_1 & \underline{\rho}_2 \\ \underline{\rho}_1 & \overline{\rho}_2 \\ \overline{\rho}_1 & \underline{\rho}_2 \\ \overline{\rho}_1 & \overline{\rho}_2 \end{bmatrix} \text{ and } \mathcal{C}(\omega) := \begin{bmatrix} \overline{\rho}_1 & \overline{\rho}_2 \\ \overline{\rho}_1 & \underline{\rho}_2 \\ \underline{\rho}_1 & \overline{\rho}_2 \\ \underline{\rho}_1 & \underline{\rho}_2 \end{bmatrix} \tag{2.11}$$

As an illustration, by applying (2.8), to

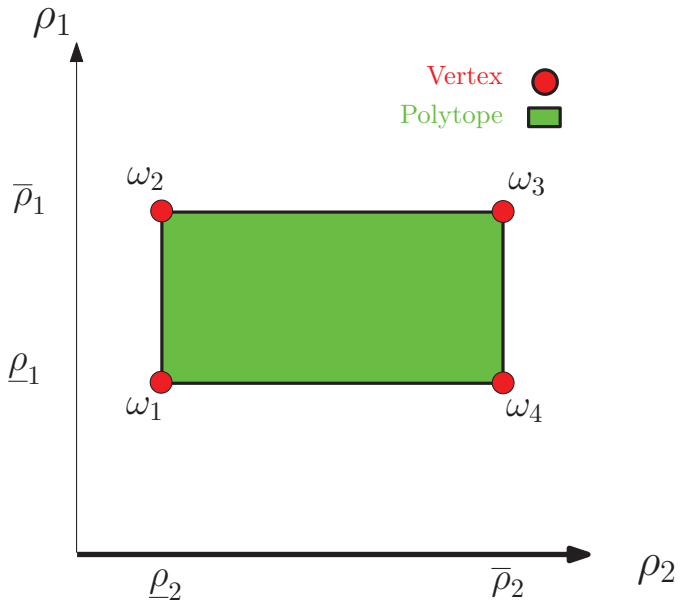

Figure 2.2: LPV polytopic system with 2 varying parameters.

- $i = 1$ and $k = 2$, i.e.,

$$\mathcal{C}(\omega_1)_2 := \{\rho_2 | \rho_2 = \overline{\rho}_2 \text{ if } (\omega_1)_2 = \underline{\rho}_2 \text{ or } \rho_2 = \underline{\rho}_2 \text{ otherwise}\} \tag{2.12}$$

  we obtain, $\mathcal{C}(\omega_1)_2 = \overline{\rho}_2$

- $i = 3$ and $k = 1$, i.e.,

$$\mathcal{C}(\omega_3)_1 := \{\rho_1 | \rho_1 = \overline{\rho}_1 \text{ if } (\omega_3)_1 = \underline{\rho}_1 \text{ or } \rho_1 = \underline{\rho}_1 \text{ otherwise}\} \tag{2.13}$$

  we obtain, $\mathcal{C}(\omega_3)_1 = \overline{\rho}_1$

Then we have,

$$\begin{aligned}
\omega_1 &= [\underline{\rho}_1, \underline{\rho}_2] \quad \alpha_1(\rho) = \frac{|\rho_1 - \overline{\rho}_1||\rho_2 - \overline{\rho}_2|}{(\overline{\rho}_1 - \underline{\rho}_1)(\overline{\rho}_2 - \underline{\rho}_2)} \\
\omega_2 &= [\overline{\rho}_1, \underline{\rho}_2] \quad \alpha_2(\rho) = \frac{|\rho_1 - \underline{\rho}_1||\rho_2 - \overline{\rho}_2|}{(\overline{\rho}_1 - \underline{\rho}_1)(\overline{\rho}_2 - \underline{\rho}_2)} \\
\omega_3 &= [\underline{\rho}_1, \overline{\rho}_2] \quad \alpha_3(\rho) = \frac{|\rho_1 - \overline{\rho}_1||\rho_2 - \underline{\rho}_2|}{(\overline{\rho}_1 - \underline{\rho}_1)(\overline{\rho}_2 - \underline{\rho}_2)} \\
\omega_4 &= [\overline{\rho}_1, \overline{\rho}_2] \quad \alpha_4(\rho) = \frac{|\rho_1 - \underline{\rho}_1||\rho_2 - \underline{\rho}_2|}{(\overline{\rho}_1 - \underline{\rho}_1)(\overline{\rho}_2 - \underline{\rho}_2)}
\end{aligned} \tag{2.14}$$

The polytopic system is defined as:

$$\begin{aligned}
\left[\begin{array}{c|c} A(\rho) & B(\rho) \\ \hline C(\rho) & D(\rho) \end{array}\right] &= \alpha_1(\rho) \left[\begin{array}{c|c} A(\omega_1) & B(\omega_1) \\ \hline C(\omega_1) & D(\omega_1) \end{array}\right] + \alpha_2(\rho) \left[\begin{array}{c|c} A(\omega_2) & B(\omega_2) \\ \hline C(\omega_2) & D(\omega_2) \end{array}\right] \\
&+ \alpha_3(\rho) \left[\begin{array}{c|c} A(\omega_3) & B(\omega_3) \\ \hline C(\omega_3) & D(\omega_3) \end{array}\right] + \alpha_4(\rho) \left[\begin{array}{c|c} A(\omega_4) & B(\omega_4) \\ \hline C(\omega_4) & D(\omega_4) \end{array}\right]
\end{aligned} \tag{2.15}$$

$\Diamond$

2.3 Robustness of dynamical systems analysis

Any mathematical model of a physical system suffers from inaccuracies. Both linear and even non linear models are not able to capture all the physical phenomena involved in the dynamics of the considered system. This could be the result of non-exact measurements or the complexity of the system. Then, a choice has to be made between considering a complex model or using a simplified one that takes into account some errors referred to as modeling uncertainties.

Therefore, the concept of uncertainties is introduced. It is a key describing the mismatch between the model and the physical system.

The notion of robustness is very large and often misused since it is often related to the $\mathcal{H}_\infty$ control design. However, if this approach has some interesting properties concerning robustness, it is not the only one and other control strategies can be robust. The main goal of robust control techniques is to take these uncertainties into account when analyzing or designing a controller for the considered system.

Let us recall that uncertainties may have several mathematical representations:

- Parametric uncertainties (ex: sensors errors, measurements errors,..etc).
- Dynamic uncertainties (ex: unmodeled dynamics).
- Unstructured uncertainties and structured uncertainties.

The robustness analysis after uses the control scheme given in Fig. 2.3, which defines a linear fractional transformation, where:

- $\Sigma(s)$ is the system model, that can be either LTI, LPV, switched ... Usually $\Sigma(s)$ includes both actuators and sensors models.
- $C(s)$ is the controller (it could be LTI, LPV, nonlinear...)
- $w(t)$ represents the exogenous system inputs (reference, disturbances, noise, etc.).
- $\Delta(s)$ represents the considered modelling uncertainties.
- $y(t)$ is the output (or measured) signal provided by set of sensors on the system; it is used by the controller.
- $u(t)$ is the control signal provided by the controller $C(s)$ that feeds the system $\Sigma(s)$.
- $z(t)$ is the controlled output.

2.4 Dissipativity concept for dynamical systems

For theoretical considerations and practical applications, the notion of dissipativity is a very important concept.

In engineering applications, the dissipativity is the rate at which palpable energy is dissipated away into other forms of energy. Indeed, for a dissipative system, at any time, the amount of energy

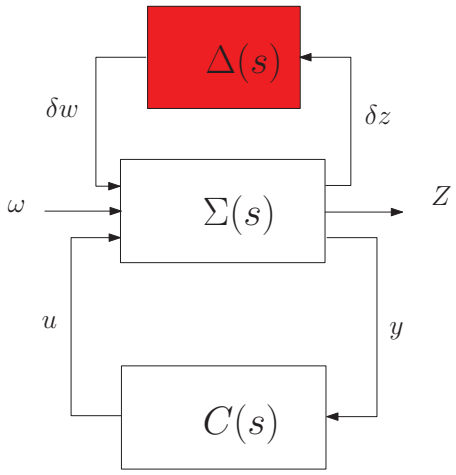

Figure 2.3: Standard Problem.

that the system can supply to its environment can not exceed the amount of energy that has been supplied to it. As the dissipative system evolves, it absorbs a part of the supplied energy and transforms it for example into heat, an increase of entropy, mass, electro-magnetic radiation, or other kinds of energy "losses". By observing the physical interaction between the system and its environment, the dissipativity property of the system can be proven. The dissipativity notion will help to understand some physical and control notions that will be introduced later.

To formulate this concept in the control theory, the following notions must be introduced:

- the storage function "$V(x(t))$" defined as follows:

$$V : X \to \mathbb{R} \tag{2.16}$$

  This function is tightly linked to the Lyapunov function.

- The supply rate "$s(w(t), z(t))$" is the rate at which the energy flows into the system, and is defined as:

$$s : W \times Z \to \mathbb{R} \tag{2.17}$$

  where $w \in W$ and $z \in Z$. Then, assume that for all $t_0 < t_1 \in \mathbb{R}$, the supply function $s(w(t), z(t))$ (or supply rate) which represents the supply delivered to the system, is locally absolutely integrable.

Now, let us introduce the dissipativity concept as follows:

Definition 2.4.1 (*Dissipativity*)

The nonlinear system defined by

$$\Sigma_{\mathcal{NL}} : \begin{cases} \dot{x}(t) &= f(x(t), w(t)) \\ z(t) &= g(x(t), w(t)) \end{cases} \tag{2.18}$$

with the supply function $s(w(t), z(t))$, or simply $s(w, z)$, is said to be dissipative if there exists a storage function $V(x(t))$ such that for all $t_0 \leq t_1$,

$$\begin{aligned} & V(x(t_0)) + \int_{t_0}^{t_1} s(w(t), z(t))dt \geq V(x(t_1)) \\ \Leftrightarrow \quad & V(x(t_1)) - V(x(t_0)) - \int_{t_0}^{t_1} s(w(t), z(t))dt \leq 0 \\ \Leftrightarrow \quad & \int_{t_0}^{t_1} \big[\frac{\partial V(x(t))}{\partial t} - s(w(t), z(t))\big]dt \leq 0 \end{aligned} \tag{2.19}$$

where all signals ($w(t) \in W$, $x(t) \in X$ and $z(t) \in Z$) satisfy the nonlinear system dynamical equations (Eq. 2.18). The pair $(\Sigma_{\mathcal{NL}}, s(w, z))$ is said to be

- *Conservative, if the equality holds for all $t_0 \leq t_1$ in Eq. 2.19.*
- *Strictly dissipative, if the strict inequality holds in (2.19).*

"s(.,.)" should be interpreted as the supply delivered to the system. In the time interval $[0\ T]$, energy is supplied "to" the system whenever $\int_0^T s(w(t), z(t))dt$ is positive, and the system is losing (dissipating) energy whenever $\int_0^T s(w(t), z(t))dt$ is negative.
Then, a dissapative system stores a part of the the supplied energy and looses the remaining part. In other words, the change of the internal storage of a dissipative system $V(x(t_1)) - V(x(t_0)$, at any moment in the bounded interval $[t_0\ t_1]$, will never exceed the supplied energy to the system.

2.5 Linear Matrix Inequalities in control theory

Linear Matrix Inequalities (LMI) are a very important tool in control theory. Indeed, this mathematical tool have been proven to be very efficient to reduce a very wide variety of problems arising in system and control theory to a few standard convex or quasi convex optimization problems (see (Bergounioux, 2001; Scorletti, 2004; Ciarlet, 1998; Bonnans, 2006)). LMis have brought new solutions to some control optimization problems. A brief historical of the LMIs in control theory shows the importance of the LMIs as a mathematical tool in the control theory:

- 1890: The first LMI appears; analytic solution of the Lyapunov LMI via Lyapunov equation.
- $1940's$: Application of Lyapunov's methods to real control engineering problems. Simple LMIs solved "by hand".
- Early $1960's$: Positive Real lemma gives graphical techniques to solve another family of LMIs.
- Late $1960's$: It has been noticed that the same family of LMIs can be solved by solving an ARE.

- Early $1980's$: Recognition that many LMIs can be solved by computer via convex programming.
- Late $1980's$: Development of interior-point algorithms for LMIs.
- $1990's$: development of Matlab® robust control toolbox including LMIs.
- Now: Development of several toolboxes and softwares for the LMIs resolution: MILAB, Yalmip..., and the use of LMI optimisation in several control approaches: fuzzy control, $\mathcal{H}_\infty$, predictive control,....

The use of the LMIs for the optimization problems resolution have led to introduce the notion of convexity since the LMIs that arise in system and control theory can be formulated as convex optimization problems that are amenable to computer solution.

Definition 2.5.1 (*Convex function*)

A function $f : \mathbb{R}^m \to \mathbb{R}$ is convex if and only if for all $x, y \in \mathbb{R}^m$ and $\lambda \in [0\ 1]$,

$$f(\lambda x + (1-\lambda)y) \leq \lambda f(x) + (1-\lambda)f(y) \tag{2.20}$$

Equivalently, f is convex if and only if its epigraph,

$$\textbf{\textit{epi}}(f) = \{(x, \lambda) | f(x) \leq \lambda\} \tag{2.21}$$

is convex.

Ensuring the convexity allows to use several efficient mathematical tools for optimization. Some of the most common convex sets that can be found are:

- The empty set $\emptyset$, any single point x_0, and the whole space $\mathbb{R}$ are affine (hence convex) subsets of $\mathbb{R}$.
- Any line is affine. If it passes through zero, it is a subspace, hence also a convex cone.
- A line segment is convex, but not affine (unless it reduces to a point).
- Any subspace is affine, and a convex cone (hence convex).

Here, a particular category of convex functions is concerned by the Linear Matrix Inequalities (LMIs) which are defined as follows.

Definition 2.5.2 (*(Strict) LMI constraint*)

A Linear Matrix Inequality constraint on a vector $x \in \mathbb{R}^n$ is defined as,

$$F(x) = F_0 + \sum_{i=1}^{m} F_i x_i \succeq 0 (\succ 0) \tag{2.22}$$

where $F_0 = F_0^T$ and $F_i = F_i^T \in \mathbb{R}^{n \times n}$ are given, and the symbol $F \succeq 0 (\succ 0)$ means that F is symmetric and positive semi-definite ($\succeq 0$) or positive definite ($\succ 0$), i.e. $\{\forall u \mid u^T F u \geq (>) 0\}$.

Example: Lyapunov equation. A very famous LMI constraint is the Lyapunov inequality lined to an autonomous system $\dot{x} = Ax$. The stability LMI associated to the autonomous system is given by,

$$\begin{array}{rcl} x^T K x & > & 0 \\ x^T (A^T K + KA) x & < & 0 \end{array} \tag{2.23}$$

which is equivalent to

$$F(K) = \left[\begin{array}{cc} -K & 0 \\ 0 & A^T K + KA \end{array} \right] \prec 0 \tag{2.24}$$

where $K = K^T$ is the decision variable. Then, the inequality $F(K) \prec 0$ is linear in K.
$\Diamond$

If the LMI constraints $F(x) \succeq 0$ are convex in x, the optimization problem is convex, and the global optimization result x^* can be efficiently found.
Let us recall some important lemmas in the LMIs based optimization in control theory. These lemmas are used latter for the LMI constraint establishment and relaxation.

Lemma 2.5.1 (*Schur lemma*)

Let $Q = Q^T$ and $R = R^T$ be affine matrices of compatible size, then the condition

$$\left[\begin{array}{cc} Q & S \\ S^T & R \end{array} \right] \succeq 0 \tag{2.25}$$

is equivalent to

$$\begin{array}{rcl} R & \succ & 0 \\ Q - SR^{-1}S^T & \succeq & 0 \end{array} \tag{2.26}$$

Thanks to he Schur lemma, the conversion from a quadratic constraint into an LMI constraint is possible.

Lemma 2.5.2 (*Kalman-Yakubovich-Popov lemma*)

For any triple of matrices $A \in \mathbb{R}^{n\times n}$, $B \in \mathbb{R}^{n\times m}$, $M \in \mathbb{R}^{(n+m)\times(n+m)} = \begin{bmatrix} M_{11} & M_{12} \\ M_{21} & M_{22} \end{bmatrix}$, the following assessments are equivalent:

1. *There exists a symmetric $K = K^T \succ 0$ s.t.*

$$\begin{bmatrix} I & 0 \\ A & B \end{bmatrix}^T \begin{bmatrix} 0 & K \\ K & 0 \end{bmatrix} \begin{bmatrix} I & 0 \\ A & B \end{bmatrix} + M < 0$$

2. *$M_{22} < 0$ and for all $\omega \in \mathbb{R}$ and complex vectors $col(x, w) \neq 0$*

$$\begin{bmatrix} A - j\omega I & B \end{bmatrix} \begin{bmatrix} x \\ w \end{bmatrix} = 0 \Rightarrow \begin{bmatrix} x \\ w \end{bmatrix}^T M \begin{bmatrix} x \\ w \end{bmatrix} < 0$$

3. *If $M = -\begin{bmatrix} I & 0 \\ A & B \end{bmatrix}^T \begin{bmatrix} 0 & K \\ K & 0 \end{bmatrix} \begin{bmatrix} I & 0 \\ A & B \end{bmatrix}$ then the second statement is equivalent to the condition that, for all $\omega \in \mathbb{R}$ with $\det(j\omega I - A) \neq 0$,*

$$\begin{bmatrix} I \\ C(j\omega I - A)^{-1}B + D \end{bmatrix}^* \begin{bmatrix} Q & S \\ S^T & R \end{bmatrix} \begin{bmatrix} I \\ C(j\omega I - A)^{-1}B + D \end{bmatrix} > 0$$

Thanks to this lemma, the quadratic performances can be illustrated through the conversion of frequency inequalities into Linear Matrix Inequalities.

Lemma 2.5.3 (*Completion Lemma*)

Let $X = X^T, Y = Y^T \in \mathbb{R}^{n\times n}$ such that $X > 0$ and $Y > 0$. The three following statements are equivalent:

1. *There exist matrices $X_2, Y_2 \in \mathbb{R}^{n\times r}$ and $X_3, Y_3 \in \mathbb{R}^{r\times r}$ such that,*

$$\begin{bmatrix} X & X_2 \\ X_2^T & X_3 \end{bmatrix} \succ 0 \text{ and } \begin{bmatrix} X & X_2 \\ X_2^T & X_3 \end{bmatrix}^{-1} = \begin{bmatrix} Y & Y_2 \\ Y_2^T & Y_3 \end{bmatrix} \tag{2.27}$$

2. $\begin{bmatrix} X & I \\ I & Y \end{bmatrix} \succeq 0$ *and* **rank** $\begin{bmatrix} X & I \\ I & Y \end{bmatrix} \leq n + r$

3. $\begin{bmatrix} X & I \\ I & Y \end{bmatrix} \succeq 0$ *and* **rank** $[XY - I] \leq r$

This lemma is useful for solving LMIs. It allows to simplify the number of variables when a matrix and its inverse are used to solve a LMI.

2.6 $\mathcal{H}_\infty$ control theory

In the last decades, the $\mathcal{H}_\infty$ robust control theory for physical systems has remarkably grown and spread in several areas. Both industrial and academical communities have been interested by the use of the analysis and the synthesis tools that this control theory provides. Indeed, the $\mathcal{H}_\infty$ control design is expressed as a mathematical optimization problem and it has the advantage of being applicable to the problems involving multivariable systems with cross-coupling between channels.
The $\mathcal{H}_\infty$ problem statement (see Fig. 2.6) can be expressed as follows:
where Σ is a linear time-invariant system. The input ω is an exogenous input representing the

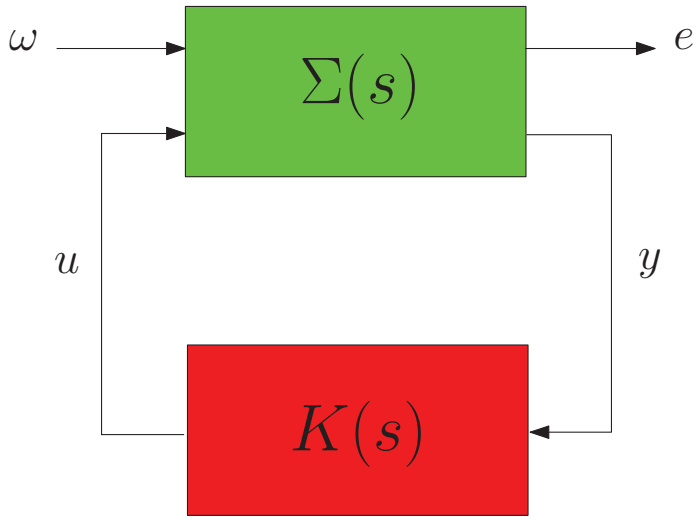

Figure 2.4: $\mathcal{H}_\infty$ control problem scheme

disturbance acting on the system. e is the controlled output, whose dependence on the exogenous input ω is to be minimized. The output y is a measurement, used to design the control input u, which is the tool to minimize the effect of ω on e. Let us keep in mind that, while trying to regulate the performance, the internal stability has to be maintained. The effect of ω on e after closing the loop is measured in terms of the energy and the worst disturbance w. This can be described by the $\mathcal{H}_\infty$ norm which is the supremum over all disturbances different from zero of the quotient of the energy flowing out of the system and the energy flowing into the system. Note that, in this scheme, no robust property is included. Then, this generalized LTI system can be described mathematically as follows:

$$\begin{bmatrix} \dot{x} \\ \hline z \\ y \end{bmatrix} = \left[\begin{array}{c|cc} A & B_1 & B_2 \\ \hline C_1 & D_{11} & D_{12} \\ C_2 & D_{21} & D_{22} \end{array}\right] \begin{bmatrix} x \\ \hline w \\ u \end{bmatrix} \tag{2.28}$$

This formulation will be used to solve the optimization problem in the control theory framework for LTI Σ.

Here, we will recall shortly some topological and mathematical facts on $\mathcal{H}_\infty$ control problem.

To better understand the following recalls, let us assume that for $x(t) \in \mathbb{C}$, its conjugate is denoted as $x^*(t)$, and real signals (i.e. $x(t) \in \mathbb{R}$), $x^*(t) = x^T(t)$.

Definition 2.6.1 ($\mathcal{L}_\infty$ *space*)

$\mathcal{L}_\infty$ is a Banach space of matrix-valued (or scalar-valued) functions on $\mathbb{C}$ and consists of all complex bounded matrix functions $f(j\omega)$, $\forall\omega \in \mathbb{R}$, such that,

$$\sup_{\omega\in\mathbb{R}} \overline{\sigma}[f(j\omega)] < \infty \tag{2.29}$$

$\overline{\sigma}$ is the biggest eigenvalue of the system.

Definition 2.6.2 ($\mathcal{L}_1$, $\mathcal{L}_2$, $\mathcal{L}_\infty$ *norms*)

- *The 1-Norm of a function $x(t)$ is given by,*

$$\|x(t)\|_1 = \int_0^{+\infty} |x(t)|dt \tag{2.30}$$

- *The 2-Norm (that introduces the energy norm) is given by,*

$$\begin{aligned} \|x(t)\|_2 &= \sqrt{\int_0^{+\infty} x^*(t)x(t)dt} \\ &= \sqrt{\frac{1}{2\pi}\int_{-\infty}^{+\infty} X^*(j\omega)X(j\omega)d\omega} \end{aligned} \tag{2.31}$$

  The second equality is obtained by using the Parseval identity.

- *The ∞-Norm is given by,*

$$\|x(t)\|_\infty = \sup_t |x(t)| \tag{2.32}$$

$$\|X\|_\infty = \sup_{Re(s)\geq 0} \|X(s)\| = \sup_\omega \|X(j\omega)\| \tag{2.33}$$

  if the signals that admit the Laplace transform, analytic in $Re(s) \geq 0$ (i.e. $\in \mathcal{H}_\infty$).

Definition 2.6.3 ($\mathcal{H}_\infty$ *and* $\mathcal{RH}_\infty$ *spaces*)

$\mathcal{H}_\infty$ is a (closed) subspace in $\mathcal{L}_\infty$ with matrix functions $f(j\omega)$, $\forall\omega \in \mathbb{R}$, analytic in $Re(s) > 0$ (open right-half plane). The real rational subspace of $\mathcal{H}_\infty$ which consists of all proper and real rational stable transfer matrices, is denoted by $\mathcal{RH}_\infty$.

Definition 2.6.4 ($\mathcal{H}_\infty$ *norm*)

The $\mathcal{H}_\infty$ norm of a proper LTI system defined as in definition (2.2.2) from input $w(t)$ to output $z(t)$ and which belongs to $\mathcal{RH}_\infty$, is the induced energy-to-energy gain ($\mathcal{L}_2$ to $\mathcal{L}_2$ norm) defined as,

$$\begin{aligned} \|G(j\omega)\|_\infty &= \sup_{\omega\in\mathbb{R}} \overline{\sigma}\left(G(j\omega)\right) \\ &= \sup_{w(s)\in\mathcal{H}_2} \frac{\|z(s)\|_2}{\|w(s)\|_2} \\ &= \max_{w(t)\in\mathcal{L}_2} \frac{\|z\|_2}{\|w\|_2} \end{aligned} \tag{2.34}$$

The $\mathcal{H}_\infty$ norm measures the maximum amplification that the system can deliver over the whole frequency set and then evaluates the worse case attenuation.
To link the notions of the $\mathcal{H}_\infty$ norm and spaces to the control theory, one may use the famous small gain theorem. Indeed, the small-gain theorem is an important tool to study the stability of interconnected systems since the gain of a system is directly related to how the norm of a signal increases or decreases as it passes through it. It also provides a sufficient condition for finite-gain stability of the feedback connection. The small-gain theorem can be described in two ways:

Theorem: Small gain 1. (Zhou *et al.*, 1996), Let consider the control loop given on Figure 2.5 where Σ is a BIBO stable system (Bounded Input Bounded Output). The loop is internally stable iff.

$$\forall x(t), y(t) \in \mathcal{L}_2, ||\Sigma(x(t)) - \Sigma(y(t))||_2 \leq \alpha||x(t) - y(t)||_2 \tag{2.35}$$

where $0 < \alpha < 1$. For a linear system Σ, this condition is equivalent to,

$$||\Sigma||_\infty < 1 \tag{2.36}$$

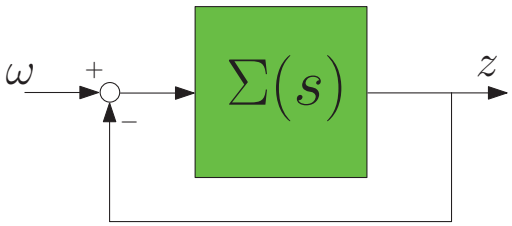

Figure 2.5: Small gain theorem 1.

△

Theorem: Small gain 2. (Zhou *et al.*, 1996), Let consider the control loop given in Figure 2.6 where Σ is a LTI nominally stable system (i.e. $\in \mathcal{RH}_\infty$), $\gamma > 0$. The interconnected system in Figure 2.6 is well-posed and internally stable for all $\Delta \in \mathcal{RH}_\infty$ with,

$$||\Delta||_\infty \leq \frac{1}{\gamma} \text{ iff. } ||M||_\infty \leq \frac{1}{\gamma} \tag{2.37}$$

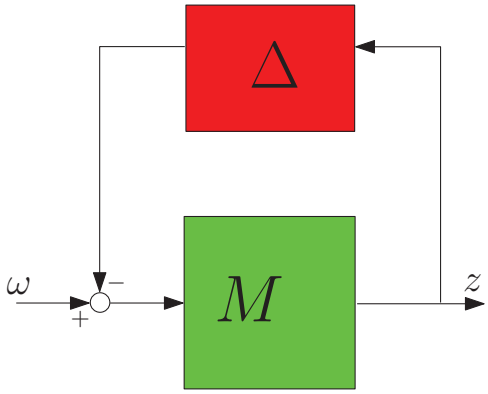

Figure 2.6: Small gain theorem 2.

△ It can be noticed that the small-gain theorem can be seen as a generalization of the Nyquist criterion to non-linear time varying MIMO systems (systems with multiple inputs and multiple outputs).

2.6.1 $\mathcal{H}_\infty$ performances

The$\mathcal{H}_\infty$ control problem: Find a controller $K(s)$ which based on the information in y, generates a control signal u which counteracts the influence of ω on e, thereby minimizing the closed-loop norm from ω to e.

Proposition 2.6.1 ($\mathcal{H}_\infty$ *as LMIs*)

Suppose that the system Σ_{LTI} defined in (Eq. 2.2) is controllable. Let us consider the quadratic supply function $s(w,z) = \gamma_\infty^2 w^T w - z^T z$, then the following statements are equivalent:

- *(Σ_{LTI}, s) is dissipative.*
- *There exists $K = K^T \succ 0$ such that the following LMI is feasible,*

$$\left[\begin{array}{cc|cc} I & 0 & & \\ A & B & & \\ \hline 0 & I & & \\ C & D & & \end{array}\right]^T \left[\begin{array}{cc|cc} 0 & K & 0 & 0 \\ K & 0 & 0 & 0 \\ \hline 0 & 0 & -\gamma_\infty^2 I & 0 \\ 0 & 0 & 0 & I \end{array}\right] \left[\begin{array}{cc|cc} I & 0 & & \\ A & B & & \\ \hline 0 & I & & \\ C & D & & \end{array}\right] \prec 0 \tag{2.38}$$

- *$\forall \omega \in \mathbb{R}$ with $\det(j\omega I - A) \neq 0$, the transfer function $T(i\omega) = C(j\omega I - A)^{-1}B + D$ satisfies (Kalman-Yakubovich-Popov lemma),*

$$T^*(j\omega) \times T(j\omega) < \gamma_\infty^2 I \tag{2.39}$$

Then, it follows

$$\begin{array}{rl} & \dfrac{z^*(j\omega)z(j\omega)}{w(j\omega)^* w(j\omega)} < \gamma_\infty^2 \\ \Leftrightarrow & \dfrac{||z||_2^2}{||w||_2^2} < \gamma_\infty^2 \\ \Leftrightarrow & ||T(j\omega)||_\infty = \sup\limits_{\omega \in \mathbb{R}} \overline{\sigma}(T(j\omega)) < \gamma_\infty^2 \end{array} \tag{2.40}$$

The corresponding dissipativity function is given by

$$x^T(t)Kx(t) - \int_0^t \left(\gamma_\infty^2 w^T(\tau)w(\tau) - z^T(\tau)z(\tau)\right)d\tau \tag{2.41}$$

and the quadratic form is:

$$P = \left[\begin{array}{cc} \gamma_\infty^2 I & 0 \\ 0 & -I \end{array}\right] \tag{2.42}$$

The $\mathcal{L}_2$-norm of the output z of a system Σ_{LTI} is uniformly bounded by γ_∞^2 times the $\mathcal{L}_2$-norm of the input w (initial condition $x(0) = 0$). This property is the basis of the $\mathcal{H}_\infty$ control, later used in this thesis. Then, the well known Bounded Real Lemma (BRL) that leads to the LMI approach of the

$\mathcal{H}_\infty$ control is derived as follows:

$$
\begin{aligned}
& \left[\begin{array}{cc} I & 0 \\ A & B \\ \hline 0 & I \\ C & D \end{array}\right]^T \left[\begin{array}{cc|cc} 0 & K & 0 & 0 \\ K & 0 & 0 & 0 \\ \hline 0 & 0 & -\gamma_\infty^2 I & 0 \\ 0 & 0 & 0 & I \end{array}\right] \left[\begin{array}{cc} I & 0 \\ A & B \\ \hline 0 & I \\ C & D \end{array}\right] \prec 0 \\
\Leftrightarrow \quad & \left[\begin{array}{cc} A^TK + KA + C^TC & KB + C^TD \\ B^TK + D^TC & D^TD - \gamma_\infty^2 I \end{array}\right] \prec 0 \\
\Leftrightarrow \quad & \left[\begin{array}{cc} A^TK + KA & KB \\ B^TK & -\gamma_\infty^2 I \end{array}\right] + \left[\begin{array}{cc} C^TC & C^TD \\ D^TC & D^TD \end{array}\right] \prec 0 \\
\Leftrightarrow \quad & \left[\begin{array}{cc} A^TK + KA & KB \\ B^TK & -\gamma_\infty^2 I \end{array}\right] + \left[\begin{array}{c} C^T \\ D^T \end{array}\right] I \left[\begin{array}{cc} C & D \end{array}\right] \prec 0 \\
\Leftrightarrow \quad & \left[\begin{array}{ccc} A^TK + KA & KB & C^T \\ B^TK & -\gamma_\infty^2 I & D^T \\ C & D & -I \end{array}\right] \prec 0
\end{aligned}
\tag{2.43}
$$

The transformation from the Bounded Real Lemma (BRL) to the LMI is possible if K and γ_∞ are the only unknowns. More details can be found in (Scherer *et al.*, 1997), (Iwasaki and Skelton, 1994).

2.6.2 $\mathcal{H}_\infty$ controller design

The $\mathcal{H}_\infty$ generalized scheme is shown in Fig. 2.7 where $W_i(s)$ and $W_o(s)$ are the weighting functions that shapes the disturbances and the outputs. The main idea of the $\mathcal{H}_\infty$ control synthesis is to minimize the impact of the input disturbances $\tilde{w}(t)$ on the controlled output $\tilde{z}(t)$.

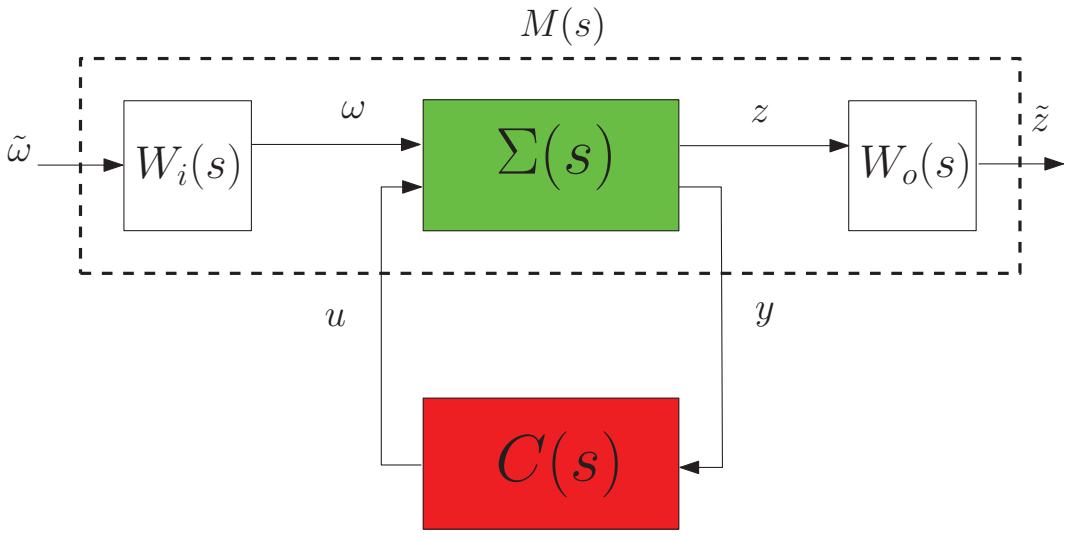

Figure 2.7: Generalized $\mathcal{H}_\infty$ problem.

More precisely, the aim is to find a stable controller so that the $\mathcal{H}_\infty$ norm of the transfer function

$T_{zw}(s)$, from input $\tilde{w}$ to output $\tilde{z}$ satisfies,

$$\begin{array}{rcl} ||T_{zw}(s)||_\infty & = & ||\mathcal{C}(sI-\mathcal{A})^{-1}\mathcal{B}+\mathcal{D}||_\infty < \gamma_\infty \\ & = & ||\mathcal{F}_l(M,C)||_\infty < \gamma_\infty \end{array} \tag{2.44}$$

The $\mathcal{H}_\infty$ problem is resolved to find a controller C for system M such that, given γ_∞,

$$||\mathcal{F}_l(M,C)||_\infty < \gamma_\infty \tag{2.45}$$

The minimum of this norm, denoted as γ_∞^*, is called the optimal $\mathcal{H}_\infty$ gain. Hence, it comes that:

$$\gamma_\infty^* = \min_{(A_c,B_c,C_c,D_c) s.t. \sigma\mathcal{A} \subset \mathbb{C}^-} \|T_{zw}(s)\|_\infty \tag{2.46}$$

This condition can be checked thanks to the BRL and the internal stability is ensured iff. $\exists\ K = K^T \succ 0$ such that (see Proposition 2.6.1),

$$\begin{bmatrix} \mathcal{A}^T K + K\mathcal{A} & K\mathcal{B} & \mathcal{C}^T \\ \mathcal{B}^T K & -\gamma_2^2 I & \mathcal{D}^T \\ \mathcal{C} & \mathcal{D} & -I \end{bmatrix} \prec 0 \tag{2.47}$$

where $\mathcal{A}$, $\mathcal{B}$, $\mathcal{C}$, $\mathcal{D}$ are the generalized plant state space matrices. Then, as an illustration,

Result 2.6.1 (*LTI/$\mathcal{H}_\infty$ solution (Scherer* et al., *1997)*)

The dynamical output feedback $\mathcal{H}_\infty$ controller of the form $C(s) = \left[\begin{array}{c|c} A_c & B_c \\ \hline C_c & D_c \end{array}\right]$ that solves the $\mathcal{H}_\infty$ control problem, is obtained by solving the following LMIs in ($\boldsymbol{X}$, $\boldsymbol{Y}$, $\widetilde{\boldsymbol{A}}$, $\widetilde{\boldsymbol{B}}$, $\widetilde{\boldsymbol{C}}$ and $\widetilde{\boldsymbol{D}}$), while minimizing γ_∞,

$$\begin{array}{l} \left[\begin{array}{cccc} M_{11} & (*)^T & (*)^T & (*)^T \\ M_{21} & M_{22} & (*)^T & (*)^T \\ M_{31} & M_{32} & M_{33} & (*)^T \\ M_{41} & M_{42} & M_{43} & M_{44} \end{array}\right] \prec 0 \\ \left[\begin{array}{cc} \boldsymbol{X} & I_n \\ I_n & \boldsymbol{Y} \end{array}\right] \succ 0 \end{array} \tag{2.48}$$

where,

$$\begin{array}{rcl} M_{11} & = & A\boldsymbol{X} + \boldsymbol{X}A^T + B_2\widetilde{\boldsymbol{C}} + \widetilde{\boldsymbol{C}}^T B_2^T \\ M_{21} & = & \widetilde{\boldsymbol{A}} + A^T + C_2^T\widetilde{\boldsymbol{D}}^T B_2^T \\ M_{22} & = & \boldsymbol{Y}A + A^T\boldsymbol{Y} + \widetilde{\boldsymbol{B}}C_2 + C_2^T\widetilde{\boldsymbol{B}}^T \\ M_{31} & = & B_1^T + D_{21}^T\widetilde{\boldsymbol{D}}^T B_2^T \\ M_{32} & = & B_1^T\boldsymbol{Y} + D_{21}^T\widetilde{\boldsymbol{B}}^T \\ M_{33} & = & -\gamma_\infty I_{n_u} \\ M_{41} & = & C_1\boldsymbol{X} + D_{12}\widetilde{\boldsymbol{C}} \\ M_{42} & = & C_1 + D_{12}\widetilde{\boldsymbol{D}}C_2 \\ M_{43} & = & D_{11} + D_{12}\widetilde{\boldsymbol{D}}D_{21} \\ M_{44} & = & -\gamma_\infty I_{n_y} \end{array} \tag{2.49}$$

Then, the reconstruction of the controller C is obtained by the following equivalent transformation,

$$\left\{\begin{array}{rcl} D_c & = & \widetilde{\boldsymbol{D}} \\ C_c & = & (\widetilde{\boldsymbol{C}} - D_cC_2\boldsymbol{X})M^{-T} \\ B_c & = & N^{-1}(\widetilde{\boldsymbol{B}} - \boldsymbol{Y}B_2D_c) \\ A_c & = & N^{-1}(\widetilde{\boldsymbol{A}} - \boldsymbol{Y}A\boldsymbol{X} - \boldsymbol{Y}B_2D_cC_2\boldsymbol{X} - NB_cC_2\boldsymbol{X} - \boldsymbol{Y}B_2C_cM^T)M^{-T} \end{array}\right. \tag{2.50}$$

where M and N are defined such that $MN^T = I_n - XY$ (that can be solved through a singular value decomposition plus a Cholesky factorization).

To avoid numerical issues, the set of LMIs is solved step by step as follows:

1. Problem solution: minimize γ_∞ subject to LMIs (2.48) and find γ_∞^*, the optimal $\mathcal{H}_\infty$ bound (optimization step).
2. Conditioning improvement: set $\gamma_\infty > \gamma_\infty^*$, and solve LMIs (2.48) for this fixed γ_∞ value (feasibility step).
3. Find the appropriate M and N (e.g. by singular values decomposition plus Cholesky factorization).
4. Controller reconstruction: reconstruct the controller according to (2.50).

2.7 An Overview of the LPV/$\mathcal{H}_\infty$ control

The framework of Linear Parameter Varying (LPV) systems (Eq. 2.3) concerns linear dynamical systems whose state-space representations depend on exogenous non-stationary parameters. The generalized state space representation corresponding to the LPV systems $\Sigma(\rho)$ can be described as follows:

$$\left[\begin{array}{c} \dot{x} \\ \hline z \\ y \end{array}\right] = \left[\begin{array}{c|cc} A(\rho) & B_1(\rho) & B_2(\rho) \\ \hline C_1(\rho) & D_{11}(\rho) & D_{12}(\rho) \\ C_2(\rho) & D_{21}(\rho) & 0 \end{array}\right] \left[\begin{array}{c} x \\ \hline w \\ u \end{array}\right] \tag{2.51}$$

This representation (see Fig. 2.8) is identical to the LTI generalized plant description with the performances shaping weighting functions, but where the state matrices are parameter dependent. Then, x is the state vector of the system together with the state of the considered weighting functions, z denotes the controlled output, y are the measured outputs, and u the control input.
Also, the corresponding LPV controller $C(\rho)$ for the previously presented systems is given as follows:

$$\left[\begin{array}{c} \dot{x_c} \\ u \end{array}\right] = \left[\begin{array}{cc} A_c(\rho) & B_c(\rho) \\ C_c(\rho) & D_c(\rho) \end{array}\right] \left[\begin{array}{c} x \\ y \end{array}\right] \tag{2.52}$$

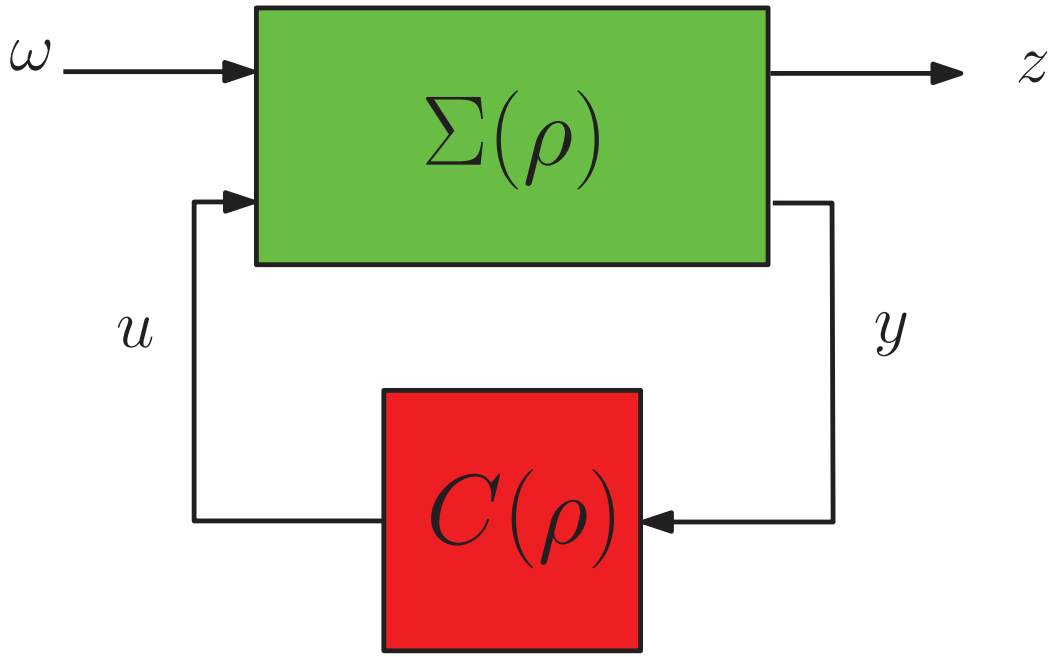

Figure 2.8: Generalized LPV/$\mathcal{H}_\infty$ control problem.

Let us recall that the varying parameters are considered to be bounded s.t:

$$\rho_i \in \left[\begin{array}{cc} \underline{\rho}_i & \overline{\rho}_i \end{array}\right], \forall i = 1, \ldots, p \tag{2.53}$$

The resulting controlled closed loop system is then given by:

$$\left[\begin{array}{c} \dot{\xi} \\ z \end{array}\right] = \left[\begin{array}{cc} \mathcal{A}(\rho) & \mathcal{B}(\rho) \\ \mathcal{C}(\rho) & \mathcal{D}(\rho) \end{array}\right] \left[\begin{array}{c} \xi \\ w \end{array}\right] \tag{2.54}$$

with,

$$\begin{array}{rcl} \mathcal{A} & = & \left[\begin{array}{cc} A(\rho)+B_2(\rho)D_c(\rho)C_2(\rho) & B_2(\rho)C_c(\rho) \\ B_c(\rho)C_2(\rho) & A_c(\rho) \end{array} \right] \\ \mathcal{B} & = & \left[\begin{array}{c} B_1(\rho)+B_2(\rho)D_c(\rho)D_{21}(\rho) \\ B_c(\rho)D_{21}(\rho) \end{array} \right] \\ \mathcal{C} & = & \left[\begin{array}{cc} C_1(\rho)+D_{12}(\rho)D_c(\rho)C_2(\rho) & D_{12}(\rho)C_c(\rho) \end{array} \right] \\ \mathcal{D} & = & D_{11}(\rho)+D_{12}(\rho)D_c(\rho)D_{21}(\rho) \end{array} \tag{2.55}$$

where $\xi = [x^T \; x_c^T]^T \in \mathbb{R}^{2n}$, $z \in \mathbb{R}^{n_z}$, $w \in \mathbb{R}^{n_w}$.
Now, with this representation, one can look for an LMI based solution to the LPV/$\mathcal{H}_\infty$ control problem defined later.
Indeed, Linear Matrix Inequalities (LMI's) have emerged as a powerful tool for approaching control problems that appear difficult if not impossible to solve in an analytic fashion.

2.7.1 LPV/$\mathcal{H}_\infty$ control

The LMIs are used to provide a solution to the robust control problem based on the previously introduced LPV closed loop system (Eq. 2.55).
In this study we will focus on the LMI-based designs for the robust control problems for polytopic linear parameter varying (LPV) systems.
Rewritting the LPV/$\mathcal{H}_\infty$ control problem (see Fig. 2.8) using structured LMIs allows to use new advanced solvers. Numerical methods for solving LMI, such as the ellipsoid algorithm and interior point methods (method of centers, primar-dual methods, projective methods of Nemirovsky), are methods of convex optimization but with very important improvements. These solvers give quick and reliable results, and since no analytical solutions can be obtained, they simplify the resolution of the introduced problem. Some of the most commonly used software for solving LMIs are: Yalmip, LMI Lab,...

Result 2.7.1 (*LMI-based LPV/$\mathcal{H}_\infty$ solution*)

The dynamical output feedback LPV/$\mathcal{H}_\infty$ controller of the form $C(s,\rho) = \left[\begin{array}{c|c} A_c(\rho) & B_c(\rho) \\ \hline C_c(\rho) & D_c(\rho) \end{array}\right]$ *is obtained by solving the following LMIs in* ($\boldsymbol{X}(\rho)$, $\boldsymbol{Y}(\rho)$, $\widetilde{\boldsymbol{A}}(\rho)$, $\widetilde{\boldsymbol{B}}(\rho)$, $\widetilde{\boldsymbol{C}}(\rho)$ *and* $\widetilde{\boldsymbol{D}}(\rho)$) *while minimizing* γ_∞,

$$\begin{array}{c} \left[\begin{array}{cccc} M_{11} & (*)^T & (*)^T & (*)^T \\ M_{21} & M_{22} & (*)^T & (*)^T \\ M_{31} & M_{32} & M_{33} & (*)^T \\ M_{41} & M_{42} & M_{43} & M_{44} \end{array}\right] \prec 0 \\ \left[\begin{array}{cc} \boldsymbol{X}(\rho) & I_n \\ I_n & \boldsymbol{Y}(\rho) \end{array}\right] \succ 0 \end{array} \tag{2.56}$$

where,

$$\begin{array}{rcl} M_{11} & = & A(\rho)\boldsymbol{X}(\rho) + \boldsymbol{X}(\rho)A(\rho)^T + \dfrac{\partial X(\rho)}{\partial \rho}\dot{\rho} + B_2\widetilde{\boldsymbol{C}}(\rho) + \widetilde{\boldsymbol{C}}(\rho)^T B_2^T \\ M_{21} & = & \widetilde{\boldsymbol{A}}(\rho) + A(\rho)^T + C_2^T\widetilde{\boldsymbol{D}}(\rho)^T B_2^T \\ M_{22} & = & \boldsymbol{Y}(\rho)A(\rho) + A(\rho)^T\boldsymbol{Y}(\rho) + \dfrac{\partial Y(\rho)}{\partial \rho}\dot{\rho} + \widetilde{\boldsymbol{B}}(\rho)C_2 + C_2^T\widetilde{\boldsymbol{B}}(\rho)^T \\ M_{31} & = & B_1(\rho)^T + D_{21}(\rho)^T\widetilde{\boldsymbol{D}}(\rho)^T B_2^T \\ M_{32} & = & B_1(\rho)^T\boldsymbol{Y}(\rho) + D_{21}(\rho)^T\widetilde{\boldsymbol{B}}(\rho)^T \\ M_{33} & = & -\gamma I_{n_u} \\ M_{41} & = & C_1(\rho)\boldsymbol{X}(\rho) + D_{12}(\rho)\widetilde{\boldsymbol{C}}(\rho) \\ M_{42} & = & C_1(\rho) + D_{12}(\rho)\widetilde{\boldsymbol{D}}(\rho)C_2 \\ M_{43} & = & D_{11}(\rho) + D_{12}(\rho)\widetilde{\boldsymbol{D}}(\rho)D_{21}(\rho) \\ M_{44} & = & -\gamma I_{n_y} \end{array} \tag{2.57}$$

Then, the reconstruction of the controller C *is obtained by the following equivalent transformation (for* $\dfrac{\partial X(\rho)}{\partial \rho}\dot{\rho} = 0$*),*

$$\left\{\begin{array}{rcl} D_c(\rho) & = & \widetilde{\boldsymbol{D}}(\rho) \\ C_c(\rho) & = & (\widetilde{\boldsymbol{C}}(\rho) - D_c(\rho)C_2(\rho)\boldsymbol{X}(\rho))M(\rho)^{-T} \\ B_c(\rho) & = & N(\rho)^{-1}(\widetilde{\boldsymbol{B}}(\rho) - \boldsymbol{Y}(\rho)B_2(\rho)D_c(\rho)) \\ A_c(\rho) & = & N(\rho)^{-1}(\widetilde{\boldsymbol{A}}(\rho) - \boldsymbol{Y}(\rho)A(\rho)\boldsymbol{X}(\rho) - \boldsymbol{Y}(\rho)B_2(\rho)D_c(\rho)C_2(\rho)\boldsymbol{X}(\rho) \\ & - & N(\rho)B_c(\rho)C_2(\rho)\boldsymbol{X}(\rho) - \boldsymbol{Y}(\rho)B_2(\rho)C_c(\rho)M(\rho)^T)M(\rho)^{-T} \end{array}\right. \tag{2.58}$$

where $M(\rho)$ *and* $N(\rho)$ *are defined such that* $M(\rho)N(\rho)^T = I_n - X(\rho)Y(\rho)$ *(that can be solved through a singular value decomposition plus a Cholesky factorization).*

Remark: Clearly a parameter-dependent Lyapunov function gives more design freedom. However, in the literature, the parameter- dependent Lyapunov function is applied only when it is really essential for the problem resolution. The difficulty of using a parameter-dependent Lyapunov function is that, if the parameter is time-varying, the rate of variation needs to be taken into account.

One can notice that since the varying parameters are taking infinite values in the bounded set of variations, the resulting LMIs problem to be solved is of infinite dimension. To avoid that, and to bring back this problem to a finite dimension, several approaches are proposed in the literature, as:

- The gridding approach.
- The Linear Fractional Representation (LFR) approach.
- The polytopic approach.

The simplest approach consists in looking for a common quadratic Lyapunov function that proves stability of the polytope of the dynamical matrices. Indeed, since the control synthesis is achieved through LMIs optimization, the use of the polytopic approach is quite appealing from a computational point of view. This approach can be summarized as follows:

- The first step consists in defining the parameter varying set, according to the nonlinear model, i.e. $\mathcal{P}_\rho$. This description can be simple but may introduce some conservatism in the solution of the controller, and so it has to be done carefully. The aim is to end with:

$$\mathcal{P}_\rho := \mathbf{Co}\{\omega_1, \ldots, \omega_N\} \tag{2.59}$$

  where N is the number of vertices of the parameter set ($N = 2^l$, with l the number of varying parameters). ω_i, which denotes the i^{th} vertex is a vector composed of a combination of the upper and lower bounds of the varying parameters (see Definition 2.2.4).

- Then, to construct the polytope for the control design synthesis, one needs to satisfy the following conditions:

  I- The generalized plant must be strictly proper. $D_{22}(\rho) = 0$.

$$M(\rho) = \left[\begin{array}{c} \dot{x} \\ \hline z \\ y \end{array}\right] = \left[\begin{array}{c|cc} A(\rho) & B_1(\rho) & B_2(\rho) \\ \hline C_1(\rho) & D_{11}(\rho) & D_{12}(\rho) \\ C_2(\rho) & D_{21}(\rho) & 0 \end{array}\right] \left[\begin{array}{c} x \\ \hline w \\ u \end{array}\right] \tag{2.60}$$

  II- - The varying parameters must not appear the input and the output matrices Indeed, the matrices $\left[\begin{array}{cc} B_2(\rho) & D_{12}(\rho) \end{array}\right]^T$ and $\left[\begin{array}{cc} C_2(\rho) & D_{21}(\rho) \end{array}\right]$ must be constant (i.e. independent of ρ). Then the polytopic systems under consideration must have the following form:

$$M(\rho) = \left[\begin{array}{c} \dot{x} \\ \hline z \\ y \end{array}\right] = \left[\begin{array}{c|cc} A(\rho) & B_1(\rho) & B_2 \\ \hline C_1(\rho) & D_{11}(\rho) & D_{12} \\ C_2 & D_{21} & 0 \end{array}\right] \left[\begin{array}{c} x \\ \hline w \\ u \end{array}\right] \tag{2.61}$$

  Usually, if this requirement is not respected, a simple strictly proper filter on the input (see (Do *et al.*, 2011) (or the output) matrices allows to achieve it.

- A local controller at each vertex of the polytope is obtained by solving the LPV/$\mathcal{H}_\infty$ problem for the upper and lower bounds of the varying parameters:

$$\left\{ \left[\begin{array}{c|c} A_{c_1} & B_{c_1} \\ \hline C_{c_1} & D_{c_1} \end{array}\right], \ldots, \left[\begin{array}{c|c} A_{c_N} & B_{c_N} \\ \hline C_{c_N} & D_{c_N} \end{array}\right] \right\} \tag{2.62}$$

  where ω_i defines each vertex of the parameter polytope.

- Finally, the global LPV controller ensuring the system stability is a convex combination of the previously obtained controllers at each vertex:

$$C(\rho) = \sum_{i=1}^{N} \alpha_i \begin{bmatrix} A_{c_i} & B_{c_i} \\ C_{c_i} & D_{c_i} \end{bmatrix} \tag{2.63}$$

where,

$$\alpha_i(\rho) := \frac{\prod_{k=1}^{l} |\rho_k - \mathcal{C}(\omega_i)_k|}{\prod_{k=1}^{l} (\overline{\rho}_k - \underline{\rho}_k)} \, , i = 1, \ldots, N \tag{2.64}$$

$$\alpha_i(\rho) \geq 0 \text{ and } \sum_{i=1}^{N} \alpha_i(\rho) = 1 \tag{2.65}$$

Remark: In the proposed application, there is no problem with the conservatism of this approach since the number of the varying parameters is reduced. This is the major reason of considering a constant Lyapunov function. In other complex cases where the conservatism might be a problem, finding a varying parameter Lyapunov function is essential.

2.8 Conclusion

In this chapter, some backgrounds on mathematical and control theory were summarized to help unfamiliar readers understand the following sections. The linear/nonlinear and LTI/LPV systems definitions were introduced. Then, some notions of passivity, dissipativity and robustness were provided. Linear matrix inequalities are, then, given as a tool for synthesizing the $\mathcal{H}_\infty$ robust controllers (since no analytical solution is possible) and simplifying the problem resolution.

CHAPTER 3

Vehicle Modeling

3.1 Introduction

Due to the increasing competition between automotive manufacturers in the last few years, an accurate knowledge of the vehicle's behaviour is mandatory to design the adequate strategies to enhance the several car dynamics. Having a good model is indeed important for simulation purpose but also for control design.

This chapter is concerned with the vehicle modeling issues. Several methods exist for the vehicle modeling, dedicated softwares (CarSim, SolidWorks,..) or home made model based on physical equations. Indeed, a lot of nicely explained models have been introduced in these works (Gillespie, 1992), (Milliken and Milliken, 1995), (Kiencke and Nielsen, 2000).

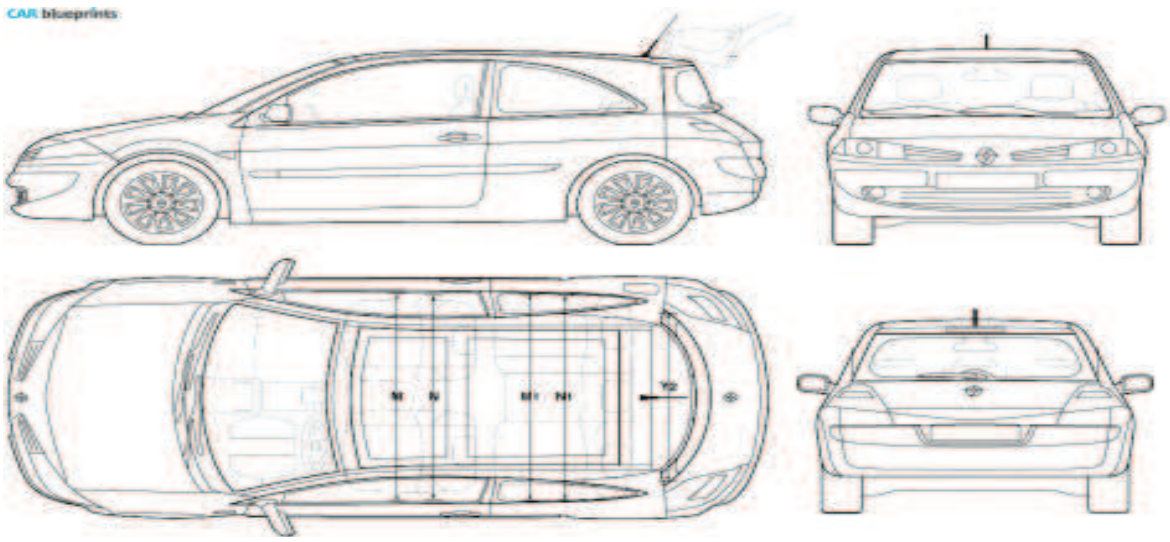

Figure 3.1: automotive vehicles modeling.

In this chapter, several models are defined. Most of the defined equations have been already given in the previous studies (see (Poussot-Vassal, 2008)). Here, the emphasize is put on correcting and enhancing some of the provided dynamical equations and we bring new results about the experimental validation of these equations.

The main contribution indeed concerns enhancing the full vehicle dynamics modeling by adding more precisely described dynamics and then performing several tests on a real car to validate the considered non linear model.
Section. 3.2 gives the parameters identified for the considered vehicle. In section. 3.3 presents the

models used for the control design objectives. The quarter vertical and 7DOF full vehicle model are used to study the vertical behaviour of the car. In section. 3.4 the bicycle model which allows to study the lateral (and longitudinal) dynamics of the vehicle is presented. Then, ,the mathematical equations in section. 3.5 that describe the full non linear vehicle dynamical behaviour are addressed with the experimental validation procedure of this model performed on a real car. This work was achieved within a collaboration with our colleagues from MIPS laboratory. [1]

Remark: In this chapter, we stress that the provided models are used for control purposes and to simulate and describe the main vehicle dynamical behaviors.
It has to be clear that all the simulations are performed on the non linear full vehicle model which has been experimentally validated as it is detailed in the following.

[1] Acknowledgements to G.L. Gissinger, M. Basset, C. Lamy, G. Pouly and J. Daniel for the validation (MIPS in Mulhouse).

3.2 Vehicle parameters and notations

Symbol	Unit	Signification
z_s		Vertical displacement of the center of gravity of the suspended mass (chassis) .
$z_{us_{ij}}$		Vertical displacement of each wheel.
$z_{s_{ij}}$		Vertical displacement of each corner of the car.
$z_{r_{ij}}$		Vertical road profil.
θ (resp. ϕ,ψ)		Roll (resp. pich, yaw) of the suspended mass (chassis) fot the full vehicle model.
m_s		Suspended mass (chassis)
$m_{us_{ij}}$:		Unsuspended mass.
k_t		Tire stifness.
I_x		Roll inertial moment of the chassis.
I_y		Pitch inertial moment of the chassis.
I_z		Yaw inertial moment of the chassis.
l_f		COG-front distance .
l_r		COG-rear distance
t_f		Front axle of the vehicle.
t_r		Rear axle of the vehicle.
H:		Chassis height.
$F_{ty_{ij}}$		Lateral tire force.
$F_{tx_{ij}}$		Longitudinal tire force.
$F_{s_{ij}}$		Suspension froce.
β		Sideslip of the vehicle.
λ_{ij}		Longitudinal slip ratio of each wheel.
v_{CoG}		Speed of the vehicle at COG.
ω_{ij}		Angular velocity of each wheel.
$z_{def_{ij}}$		Suspension deflection at each corner.
δ		Steering angle.
v_x		Longitudinal speed of the vehicle.
v_y		Lateral speed of the vehicle..
a_x		Longitudinal acceleration of the vehicle.
a_x		Lateral speed of the vehicle..
$C_{\lambda_{ij}}$		Longitudinal tire stiffness.
$C_{\alpha_{ij}}$		Lateral tire stiffness.
R		Tir radius.
$i = \{f, l\}$		front, rear.
$j = \{r, l\}$		right, left.

Table 3.1: Renault Mégane Coupé parameters

* All displacements are calculated w.r.t static equilibrium positions.

3.2.1 Modeling assumptions

Since the automotive vehicles are very complex systems, the modelling step requires some assumptions to get simplified models for simulation and control of the vehicle dynamics. In this chapter,

the following modeling assumptions have been done:

- An angle δ applied to the steering wheel results in the same angle δ on the front wheels.
- The gyroscopic effects of the sprung masses are neglected (i.e. wheels only generate longitudinal, lateral and vertical forces).
- Anti-roll bars are not considered.
- The auto-aligning moments are neglected.
- The vehicle chassis plane is considered parallel to the road.
- The aerodynamical and wheel resistive effects are neglected.
- The tire cambering is neglected.

3.3 Vertical dynamics and model of the vehicle for control design

In this section, the vertical model describes the vertical behaviour of the car. These models are mainly developed for control purposes.

3.3.1 LTI control oriented Quarter vehicle model

This model allows to study the vertical behavior of a vehicle according to the suspension characteristic (passive or controlled). The quarter vehicle model uses only one suspension system, as in Fig. 3.2, where:

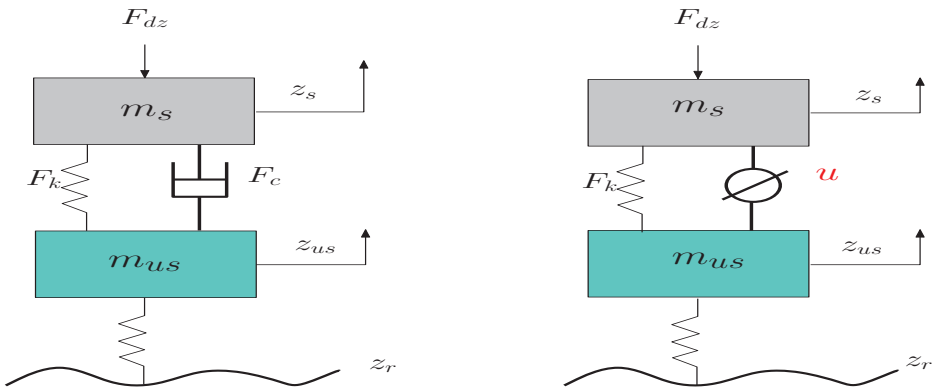

Figure 3.2: Passive (left) and Controlled (right) quarter car model.

- The sprung mass m_s represents the vehicle chassis and z_s is the corresponding relative vertical displacement.
- The unsprung mass m_{us} which represents the vehicle wheel and z_{us} is the corresponding relative vertical displacement

The car is subject to road disturbance z_r which acts on the wheels modeled here by a spring through the stiffness coefficient k_t.

The general equations that describe the vertical dynamical behaviour of the quarter vehicle are :

$$\begin{cases} m_s\ddot{z}_s &= -(F_{sz} + F_{dz}) \\ m_{us}\ddot{z}_{us} &= F_{sz} - F_{tz} \end{cases} \tag{3.1}$$

where F_{tz} represents the tire force and is considered as a linear function:

$$F_{tz} = k_t(z_{us} - z_r) + c_t(\dot{z}_{us} - \dot{z}_r) \tag{3.2}$$

F_{sz} represents the suspension force that can take 2 forms, considering passive and controlled suspension, as follows:

$$\begin{cases} F_{sz} &= F_k(z_s - z_{us}) + F_c(\dot{z}_s - \dot{z}_{us}) \quad \text{(passive suspension case)} \\ F_{sz} &= F_k(z_s - z_{us}) + u \quad \text{(controlled suspension case)} \end{cases} \tag{3.3}$$

where $F_k(.)$ can be a linear or a nonlinear function of the suspension deflection $z_{def} = (z_s - z_{us})$, $F_c(.)$ can be a linear or a nonlinear function of the deflection velocity, Then, F_{dz} describes a vertical disturbance force (that can be represented by a load transfer, e.g. steering situation). And where k_t and c_t are the linear tire stiffness and damping factors.
Also, the control input u characterize the kind of the suspension used int the quarter vehicle :

- If $u = F_c(\dot{z}_s - \dot{z}_{us})$, the suspension is passive.
- If $u = F_c(\dot{z}_s - \dot{z}_{us}, \Omega)$, the suspension is semi-active, where Ω is an input parameter that modifies the damping factor.
- If u is an independent function, the quarter car is said to be active.

When the suspension characteristics are considered as linear i.e. $F_k = k(z_s - z_{us})$ and $F_c = c(\dot{z}_s - \dot{z}_{us})$ where k and c are the linear stiffness and damping coefficients, the control oriented suspension linear model is given as follows:

$$\begin{cases} m_s\ddot{z}_s &= -k(z_s - z_{us}) - c(\dot{z}_s - \dot{z}_{us}) - u - F_{dz} \\ m_{us}\ddot{z}_{us} &= k(z_s - z_{us}) + c(\dot{z}_s - \dot{z}_{us}) + u - k_t(z_{us} - z_r) \end{cases} \tag{3.4}$$

and as an illustration, the associated state space representation:

$$\begin{bmatrix} \dot{z}_s \\ \ddot{z}_s \\ \dot{z}_{us} \\ \ddot{z}_{us} \end{bmatrix} = \begin{bmatrix} 0 & 1 & 0 & 0 \\ \frac{-k}{m_s} & \frac{-c}{m_s} & \frac{k}{m_s} & \frac{c}{m_s} \\ 0 & 0 & 0 & 1 \\ \frac{k}{m_{us}} & \frac{c}{m_{us}} & \frac{-k-k_t}{m_{us}} & \frac{-c}{m_{us}} \end{bmatrix} \begin{bmatrix} z_s \\ \dot{z}_s \\ z_{us} \\ \dot{z}_{us} \end{bmatrix} + \begin{bmatrix} 0 \\ \frac{-1}{m_s} \\ 0 \\ \frac{1}{m_{us}} \end{bmatrix} u + \begin{bmatrix} 0 \\ 0 \\ 0 \\ \frac{k_t}{m_{us}} \end{bmatrix} z_r + \begin{bmatrix} 0 \\ \frac{-1}{m_s} \\ 0 \\ 0 \end{bmatrix} F_{dz} \tag{3.5}$$

3.3.2 7 DOF control oriented full vehicle vertical model

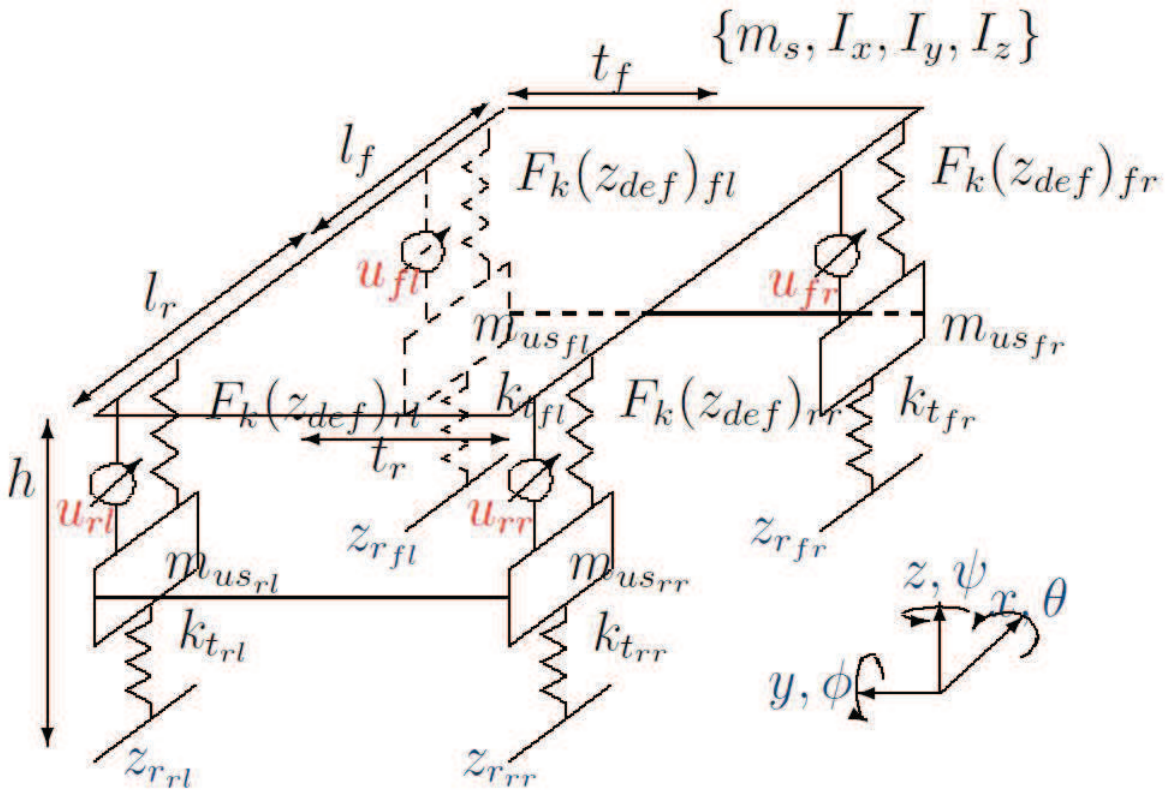

Figure 3.3: Full vertical vehicle model

This model includes the vertical dynamics of the chassis, the vertical motions of the wheels and the pitch and roll, respectively, z_s, $z_{us_{ij}}$, θ,and ϕ. The dynamical equations are:

$$\begin{cases} \ddot{z}_s &= -\big(F_{sz_f} + F_{sz_r} + F_{dz}\big)/m_s \\ \ddot{z}_{us_{ij}} &= \big(F_{sz_{ij}} - F_{tz_{ij}}\big)/m_{us_{ij}} \\ \ddot{\theta} &= \big((F_{sz_{rl}} - F_{sz_{rr}})t_r + (F_{sz_{fl}} - F_{sz_{fr}})t_f + mh\dot{v}_y\big)/I_x \\ \ddot{\phi} &= \big(F_{sz_f} l_f - F_{sz_r} l_r - mh\dot{v}_x\big)/I_y \end{cases} \tag{3.6}$$

where $F_{tz_i} = F_{tz_{il}} + F_{tz_{ir}}$ and $F_{sz_i} = F_{sz_{il}} + F_{sz_{ir}}$, stand for the vertical tire forces and the suspension forces respectively. Index $i = \{f, r\}$ and $j = \{l, r\}$ are used to identify vehicle front, rear and left, right positions respectively. **This model is mainly used for control design purposes**. it provides information on the vertical dynamics of the car.

Also, the vehicle is considered equipped with semi-active suspensions special dampers : the "Magneto-Rheological Dampers". The semi-active damping force (FMR) depends on an electric current value and is highly nonlinear with respect to the suspension motion. In the parametric model

of (Guo *et al.*, 2006*a*), the hysteresis loop force-velocity is well modeled with an hyperbolic tangent function. The *MR* damping force is given by:

$$F_{MR} = I f_c \tanh\left(a_1 \dot{z}_{def} + a_2 z_{def}\right) + b_1 \dot{z}_{def} + b_2 z_{def} \tag{3.7}$$

where, the electric current is bounded between $0 \leq I_{min} \leq I \leq I_{max} \leq 2.5$. I_{min} and I_{max} depend on the *MR* damper specifications. Experimental data obtained from a commercial *MR* damper are used to model the nonlinearities of this actuator by using (3.7). Figure 3.4 shows the performance of the *MR* damper model used in this analysis, whose parameters are: $fc = 600.9$, $a_1 = 37.8$, $a_2 = 22.1$, $b_1 = 2830.8$ and $b_2 = -7897.2$.

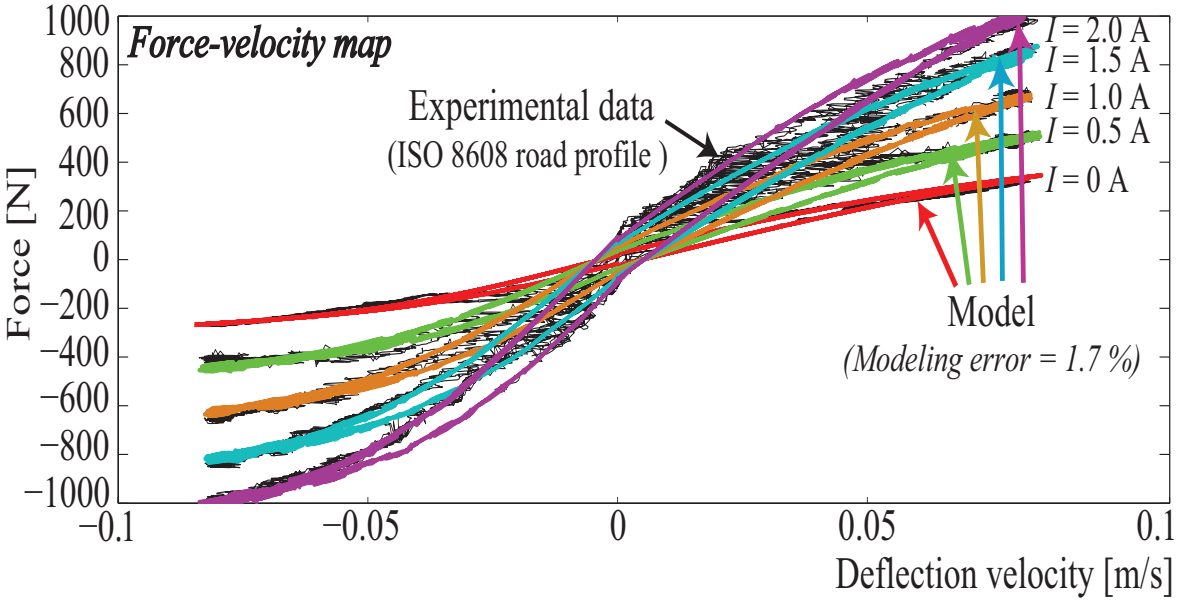

Figure 3.4: Model of the *MR* damper for different I values.

Remark:

- It is worth recalling that the Mulhouse car on which the validation was achieved is not equipped with controlled suspension. For the control design purposed (see chapter. 5), we consider $u = F_{MR}$ to develop the suspension semi-active control strategies.

- In the simulation, "k" depends in a non linear way of the suspension deflection (see (Savaresi *et al.*, 2010*b*)), while in the design step, it is a constant.

As the full vertical model is simply a simplified version of the complete one, the full non linear vehicle model will be presented in the following.

3.4 Extended control oriented lateral bicycle vehicle model

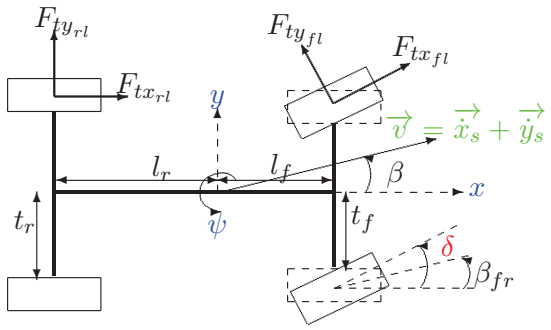

Figure 3.5: Extended bicycle vehicle model

This model emphasises the lateral dynamics of the vehicle. It is used especially for the design of the steering and braking controllers. The corresponding dynamical equations are:

$$\begin{bmatrix} \dot{v}_y \\ \dot{\psi} \\ \dot{\beta} \end{bmatrix} = \begin{bmatrix} \frac{-C_f - C_r}{mv} & v - \frac{-C_f l_f + C_r l_r}{mv} & 0 \\ \frac{-C_f l_f + C_r l_r}{I_z v} & \frac{-C_f l_f^2 - C_r l_r^2}{I_z v} & 0 \\ 0 & 1 + \frac{l_r C_r - l_f C_f}{mv^2} & -\frac{C_f + C_r}{mv} \end{bmatrix} \begin{bmatrix} v_y \\ \psi \\ \beta \end{bmatrix} + \begin{bmatrix} \frac{C_f}{m} & -\frac{1}{m} & 0 \\ \frac{C_f l_f}{I_z} & 0 & \frac{t_r}{RI_z} \\ \frac{C_f}{mv} & 0 & \frac{1}{mv} \end{bmatrix} \begin{bmatrix} \delta \\ F_{dy} \\ T_{b_{rj}} \end{bmatrix} \tag{3.8}$$

This model is used mainly for controller design purposes. It is largely used in the literature for the automotive studies and applications. Also, many industrial solutions for the vehicle dynamics enhancement are based on the bicycle model (eg: EPS...).

Remark: A non linear longitudinal/lateral bicycle model is provided for some control strategies development (see chapter. 8). This model can be found in literature for control design purposes (see (Hedrick *et al.*, 1991) and (Lim and Hedrick, 1999)).

3.5 Full vehicle simulation oriented non linear model: mathematical modeling and experimental validation

In some sense, the full non linear model is the concatenation of the previously introduced models. Indeed, this model gathers the vertical, lateral and longitudinal dynamics of the car. Then, the previously introduced bicycle and vertical model can be easily deduced from it. Also, this model is used mainly for simulation objectives, to test the efficiency of the developed control strategies.

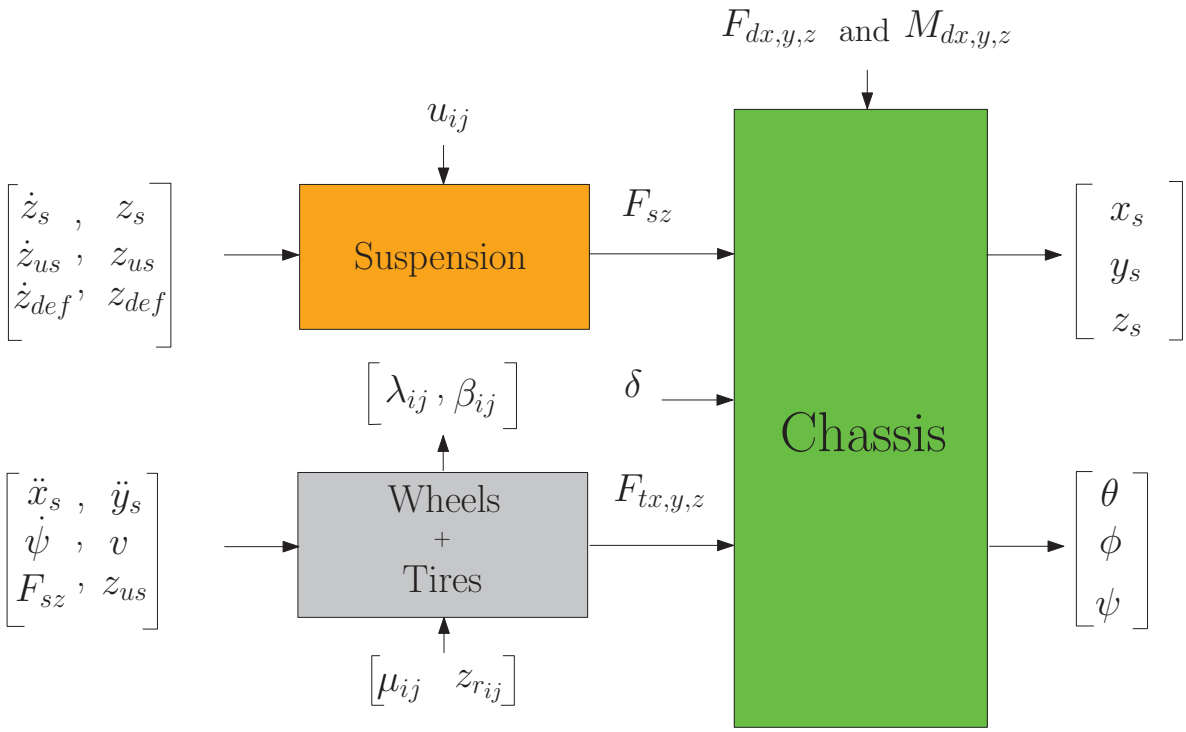

Figure 3.6: Full vehicle model synopsis

This model was validated on a real Renault Megane Coupé by experimental procedure within the national french agency project, INOVE Blan 0308 (see variables Table. 3.1).

3.5.1 The tire

First, we introduce a detailed modeling of various forces and dynamics linked to the tire. It is very important to have a good knowledge of the tire dynamics to understand well the behaviour of the car subject to different road irregularities and conditions.

3.5.1.1 Longitudinal tire slip

$$\lambda_{ij} = \frac{v_x - R\omega_{ij}\cos\beta}{\max(v_x, R\omega_{ij}\cos\beta)} \tag{3.9}$$

3.5.1.2 Sideslip of the tire

$$\beta_f = \delta - \tan^{-1}\left(\frac{l_f\dot{\psi} + v_{CoG}\sin\beta}{v_{CoG}\cos\beta}\right) \quad [rad] \tag{3.10}$$

$$\beta_r = \tan^{-1}\left(\frac{l_r\dot{\psi} - v_{CoG}\sin\beta}{v_{CoG}\cos\beta}\right) \quad [rad] \tag{3.11}$$

3.5.1.3 longitudinal tire Forces

$$F_{tx_{ij}} = \lambda_{ij}C_{\lambda_{ij}} \quad [N] \tag{3.12}$$

Coefficient	Value $[N]$
$C_{\lambda_{fl}}$	66100
$C_{\lambda_{fr}}$	66100
$C_{\lambda_{rl}}$	32144
$C_{\lambda_{rr}}$	32144

3.5.1.4 Lateral tire Forces

$$F_{ty_{ij}} = D\sin\Big(C\text{atan}\big[B(1-E)\beta + E\text{atan}\left(B\beta\right)\big]\Big)\mathrm{e}^{(-6(|(\lambda)|^5)} \quad [N] \tag{3.13}$$

The detailed non linear model of the tire can be found in Pacejka works (see (Pacejka, 2005)).

3.5.1.5 Vertical tire Forces

$$z_{def_{t_{ij}}} = z_{us_{ij}} - z_{r_{ij}} \tag{3.14}$$

$$F_{tz_{ij}} = k_t z_{def_{t_{ij}}} \tag{3.15}$$

3.5.1.6 Wheels dynamics

$$\ddot{z}_{us_{ij}} = \frac{F_{sz_{ij}} - F_{tz_{ij}}}{m_{us_{ij}}} \quad [m.s^{-2}] \tag{3.16}$$

$$\dot{\omega}_{ij} = \frac{R_{ij}F_{tx_{ij}} - T_{b_{ij}}}{I_z} \quad [m.s^{-1}] \tag{3.17}$$

3.5.2 Suspension system

The suspension systems influence mainly the vertical dynamics and ensure the link between the wheels(and then road irregularities) and the chassis. Then, it is important to emphasize the different dynamics related to these systems in each corner i,j of the vehicle.

3.5.2.1 Suspensions deflection

$$\begin{array}{rrcl} \text{Front left :} & z_{def_{fl}} & = & z_s - l_f \sin\phi + t_f \sin\theta - z_{us_{fl}} \\ \text{Front right :} & z_{def_{fr}} & = & z_s - l_f \sin\phi - t_f \sin\theta - z_{us_{fr}} \\ \text{Rear left :} & z_{def_{rl}} & = & z_s + l_r \sin\phi + t_r \sin\theta - z_{us_{rl}} \\ \text{Rear right :} & z_{def_{rr}} & = & z_s + l_r \sin\phi - t_r \sin\theta - z_{us_{rr}} \end{array} \tag{3.18}$$

3.5.2.2 Deflection speed

$$\begin{array}{rrcl} \text{Front left :} & \dot{z}_{def_{fl}} & = & \dot{z}_s - l_f\dot{\phi}\cos\phi + t_f\dot{\theta}\cos\theta - \dot{z}_{us_{fl}} \\ \text{Front right :} & \dot{z}_{def_{fr}} & = & \dot{z}_s - l_f\dot{\phi}\cos\phi - t_f\dot{\theta}\cos\theta - \dot{z}_{us_{fr}} \\ \text{Rear left :} & \dot{z}_{def_{rl}} & = & \dot{z}_s + l_r\dot{\phi}\cos\phi + t_r\dot{\theta}\cos\theta - \dot{z}_{us_{rl}} \\ \text{Rear right :} & \dot{z}_{def_{rr}} & = & \dot{z}_s + l_r\dot{\phi}\cos\phi - t_r\dot{\theta}\cos\theta - \dot{z}_{us_{rr}} \end{array} \tag{3.19}$$

3.5.2.3 Springs and dampers

The springs and dampers are an the main part of the suspension systems, they ensure the link between the wheels and the chassis.

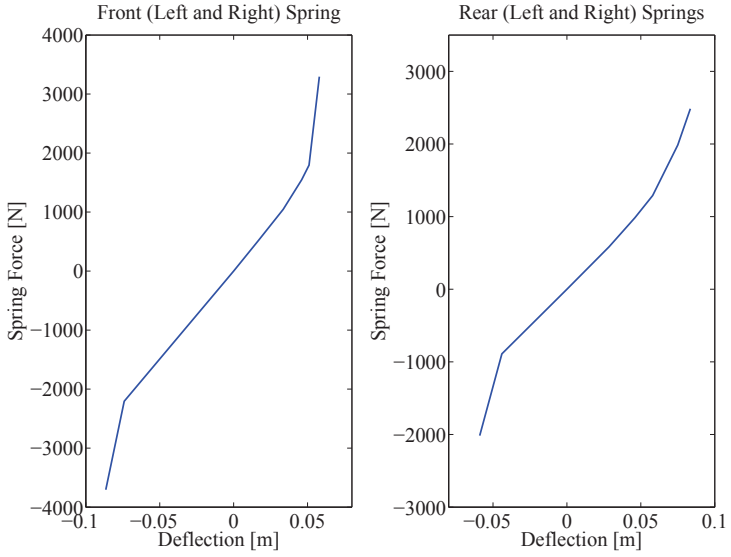

Figure 3.7: Spring force $F_k(.)$

Fig. 3.7 shows the characteristics of the suspensions springs. It represents the force specific to the stiffness of the spring.

Fig. 3.8 shows the characteristics of the passive dampers of the considered vehicle.

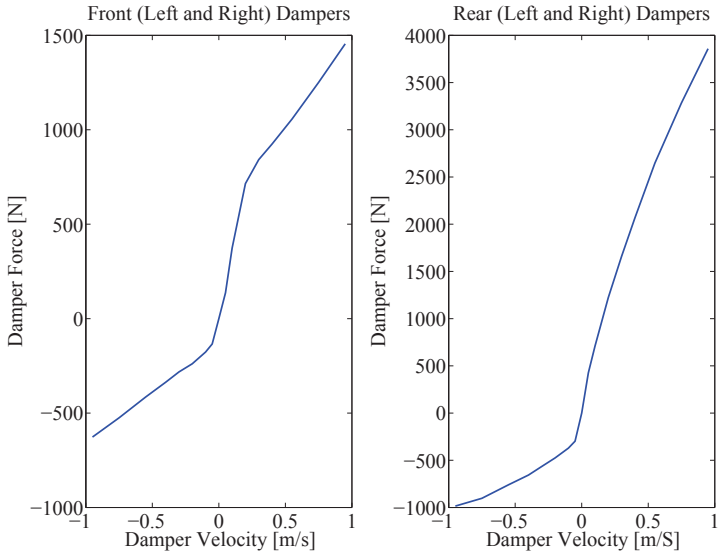

Figure 3.8: Passive damper force

3.5.3 Chassis dynamics

3.5.3.1 Sideslip angle in the gravity center

$$\dot{\beta}_{CoG} = \frac{F_{ty_f} + F_{ty_r} - m\dot{v}_{CoG}\sin(\beta_{CoG})}{mv_{CoG}\cos(\beta_{CoG})} - \dot{\psi} \tag{3.20}$$

3.5.3.2 Roll dynamical behaviour

$$\ddot{\theta} = \frac{-(F_{sz_{rl}} - F_{sz_{rr}})t_r - (F_{sz_{fl}} - F_{sz_{fr}})t_f + mh\dot{v}_y + M_{d_x}}{I_x} \tag{3.21}$$

3.5.3.3 Yaw dynamical behaviour

$$\ddot{\psi} = \frac{l_f(F_{tx_f}\sin\delta + F_{ty_f}\cos\delta) - l_r F_{ty_r} + (F_{tx_{fr}} - F_{tx_{fl}})t_f\cos\delta}{I_z} \\ \frac{(F_{tx_{rr}} - F_{tx_{rl}})t_r + (F_{ty_{fl}} - F_{ty_{fr}})\sin(\delta)t_f}{I_z} \tag{3.22}$$

3.5.3.4 Pitch dynamical behaviour

$$\ddot{\phi} = \frac{F_{sz_f}l_f - F_{sz_r}l_r + mha_x + M_{d_y}}{I_y} \tag{3.23}$$

3.5.3.5 Longitudinal dynamics

$$\dot{v}_x = \frac{(F_{tx_f}\cos\delta - F_{tx_r} + F_{ty_f}\sin\delta + F_{d_x})}{m} + \dot{\psi}v_y \tag{3.24}$$

$$a_x = \dot{v}_x - \dot{\psi}v_y \tag{3.25}$$

3.5.3.6 Lateral dynamics

$$\dot{v}_y = \frac{(F_{tx_f}\sin\delta + F_{ty_r} + F_{ty_f}\cos\delta + F_{d_y})}{m} - \dot{\psi}v_x \tag{3.26}$$

$$a_y = \dot{v}_y + \dot{\psi}v_x \tag{3.27}$$

3.5.3.7 Vertical acceleration of the chassis

$$\ddot{z}_s = -\frac{F_{sz_f} + F_{sz_r} + F_{d_z}}{m_s} \tag{3.28}$$

3.5.4 Experimental validation

The experimental validation was carried out on a real vehicle. Several tests were achieved to validate different car dynamics. The driving tests were performed on a real track in different road conditions.

3.5.5 The moose test

The moose test is performed on a circuit to determine how well a certain vehicle evades a suddenly appearing obstacle.This circuit is characterized a left bend who is followed by an obstacle avoidance in emergency situation (see Fig. 3.9).

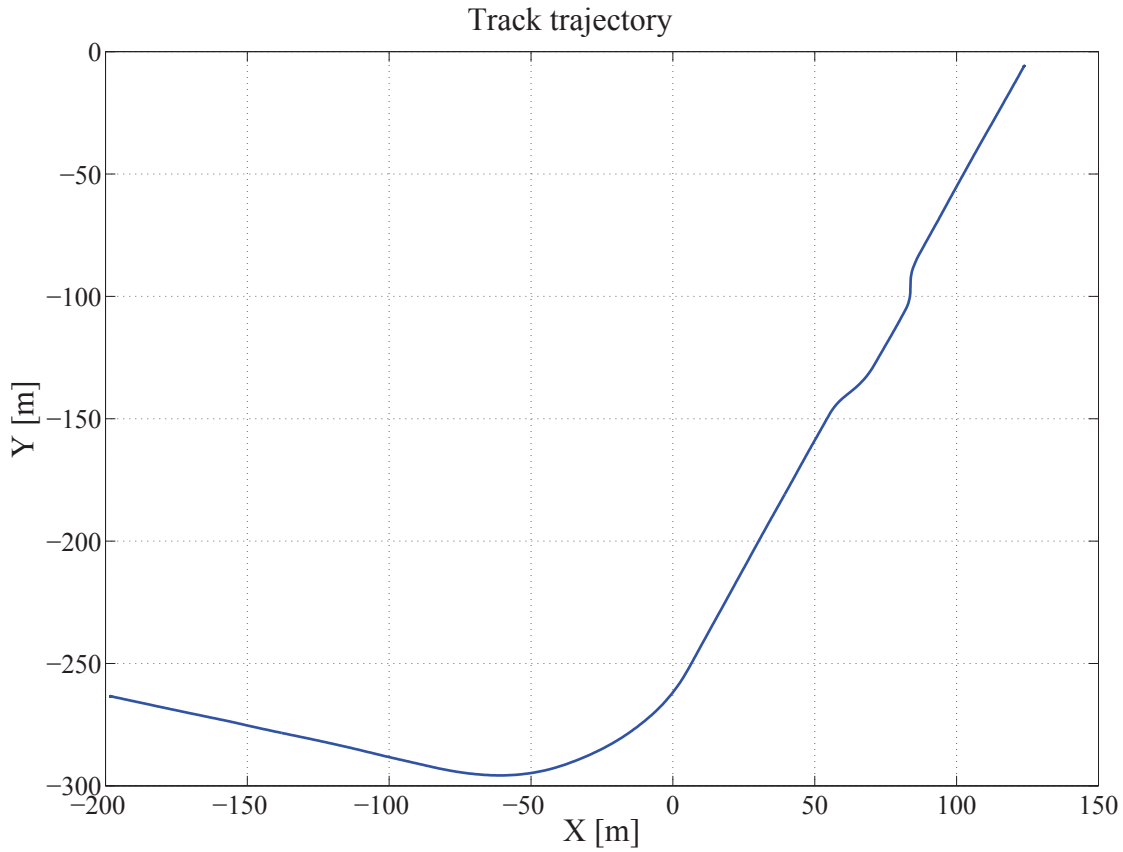

Figure 3.9: Track trajectory

3.5.5.1 Moose test for $V_x = 60km.h^{-1}$

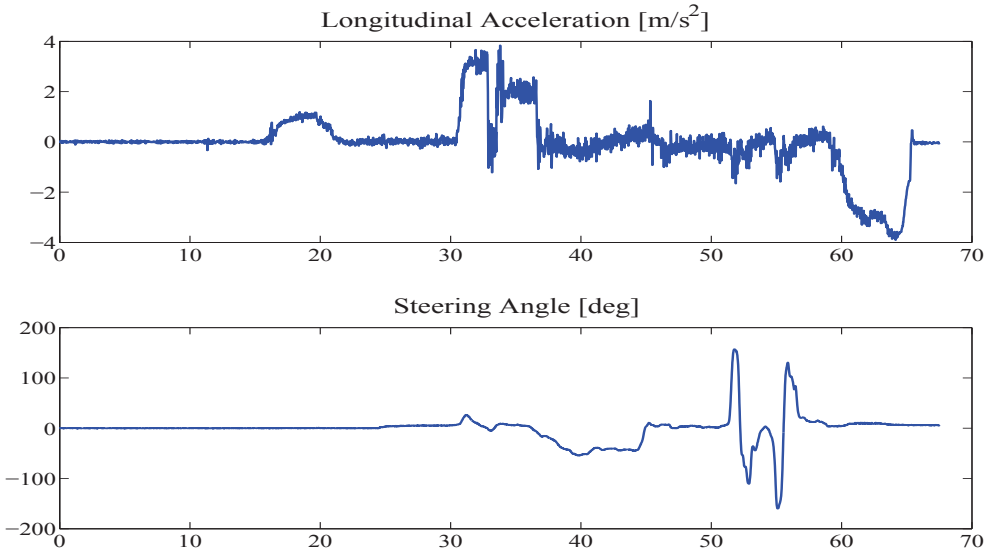

Figure 3.10: Model inputs.

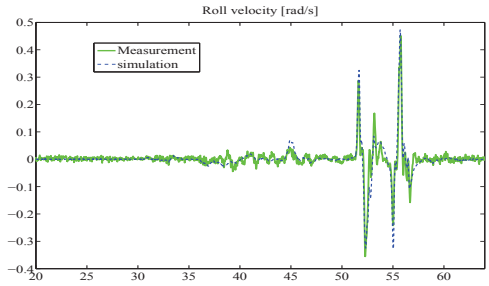

Figure 3.11: Roll velocity rad/s

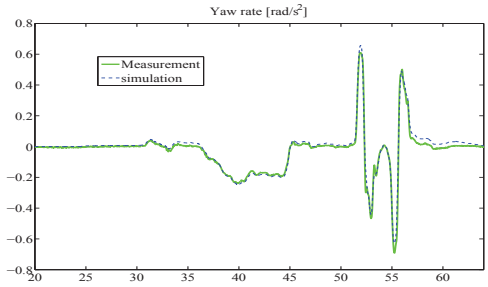

Figure 3.12: Yaw rate rad/s

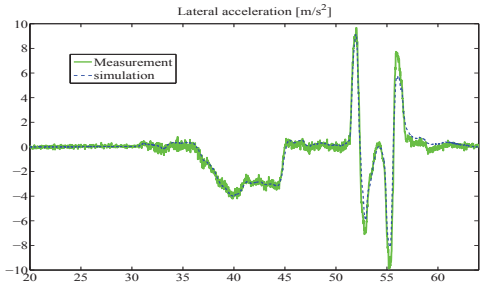

Figure 3.13: Lateral acceleration m/s^2

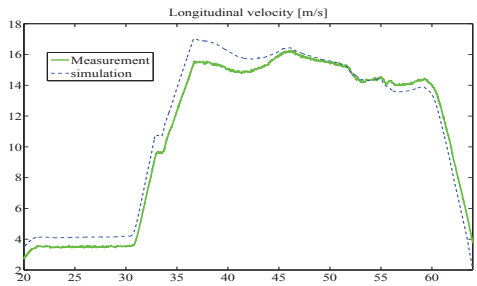

Figure 3.14: Longitudinal vehicle speed m/s

3.5.5.2 Moose test for $V_x = 90km.h^{-1}$

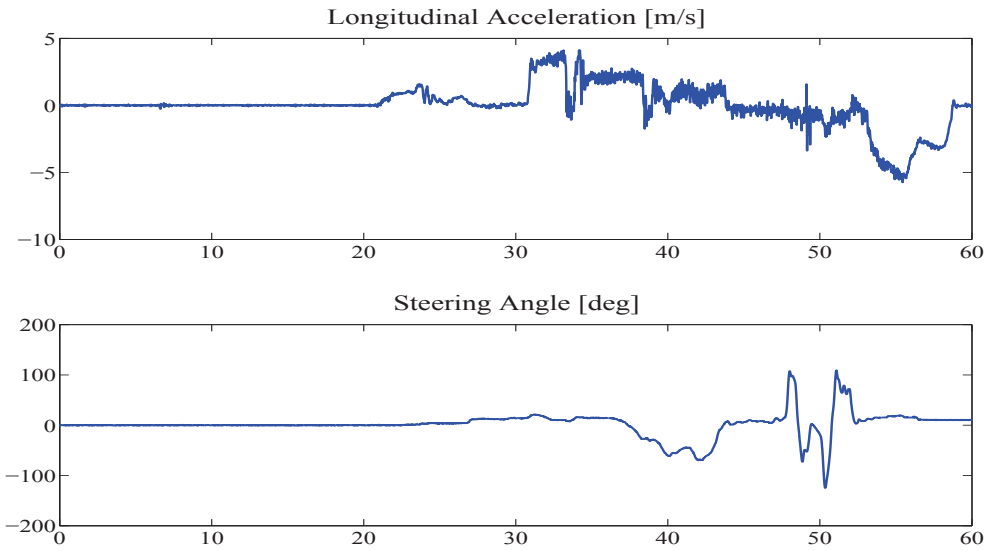

Figure 3.15: Model inputs.

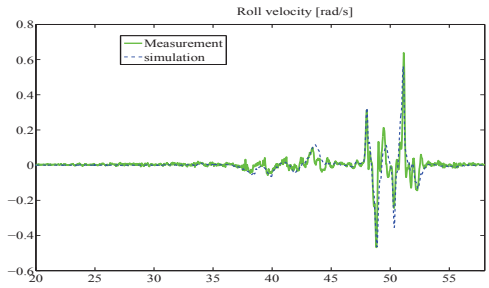

Figure 3.16: Roll velocity rad/s

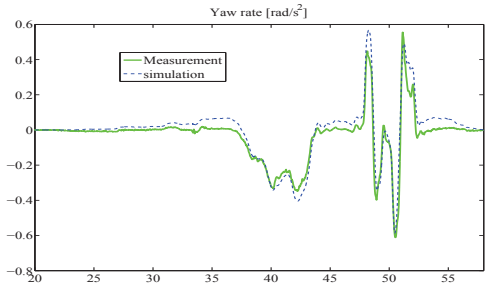

Figure 3.17: Yaw rate rad/s

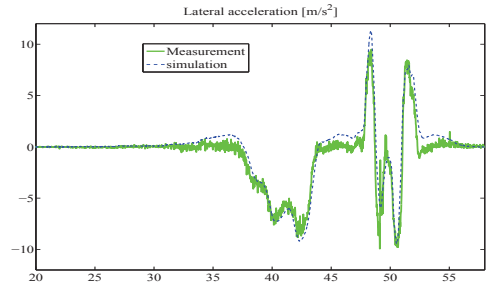

Figure 3.18: Lateral acceleration m/s^2

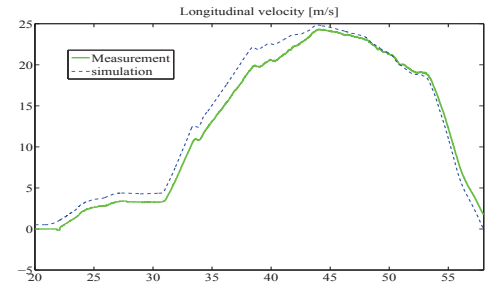

Figure 3.19: Longitudinal vehicle speed m/s

3.5.6 Sine Wave test

In this test scenario, a sine wave is applied on the steering wheel with a varying frequency between $[1-4]\ Hz$.

3.5.6.1 Sine Wave for $V_x = 40km.h^{-1}$

The first sine wave test is performed at the vehicle speed $V_x = 40km.h^{-1}$.

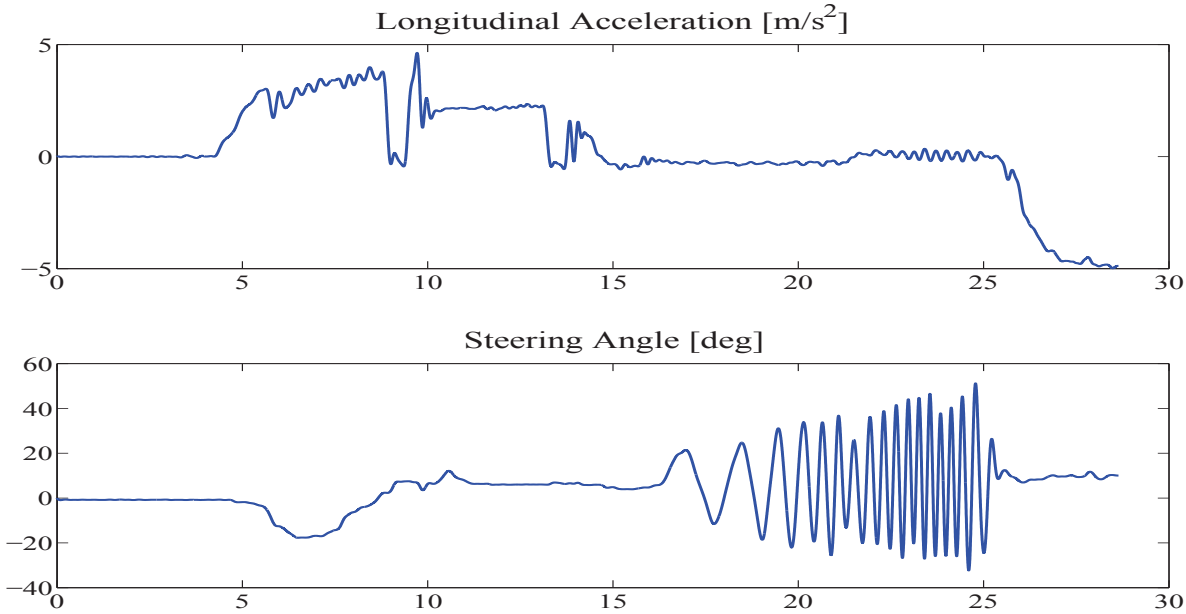

Figure 3.20: The model inputs

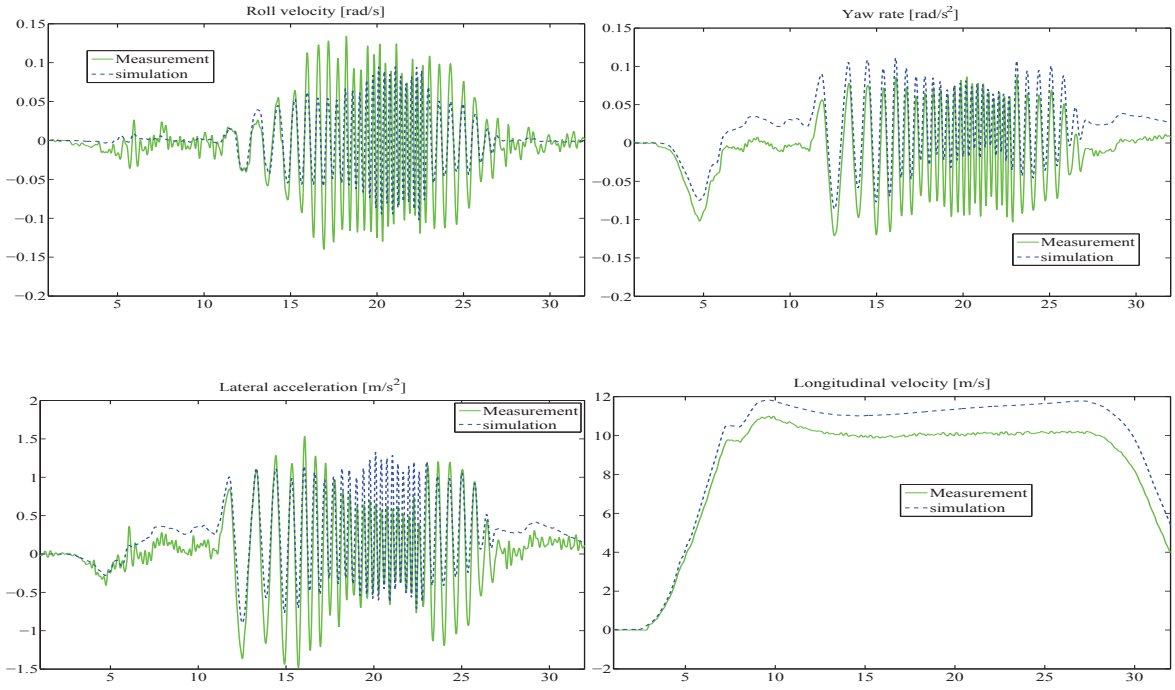

3.5.6.2 Sine Wave for $V_x = 60km.h^{-1}$

The second sine wave test is performed at the vehicle speed $V_x = 60km.h^{-1}$.

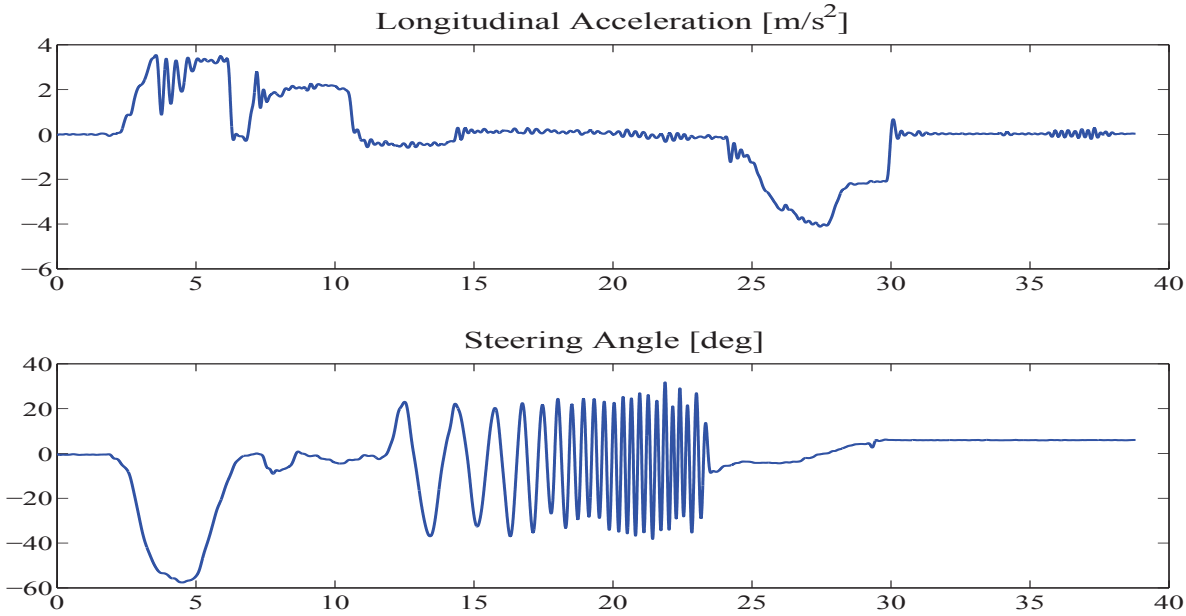

Figure 3.21: The model inputs

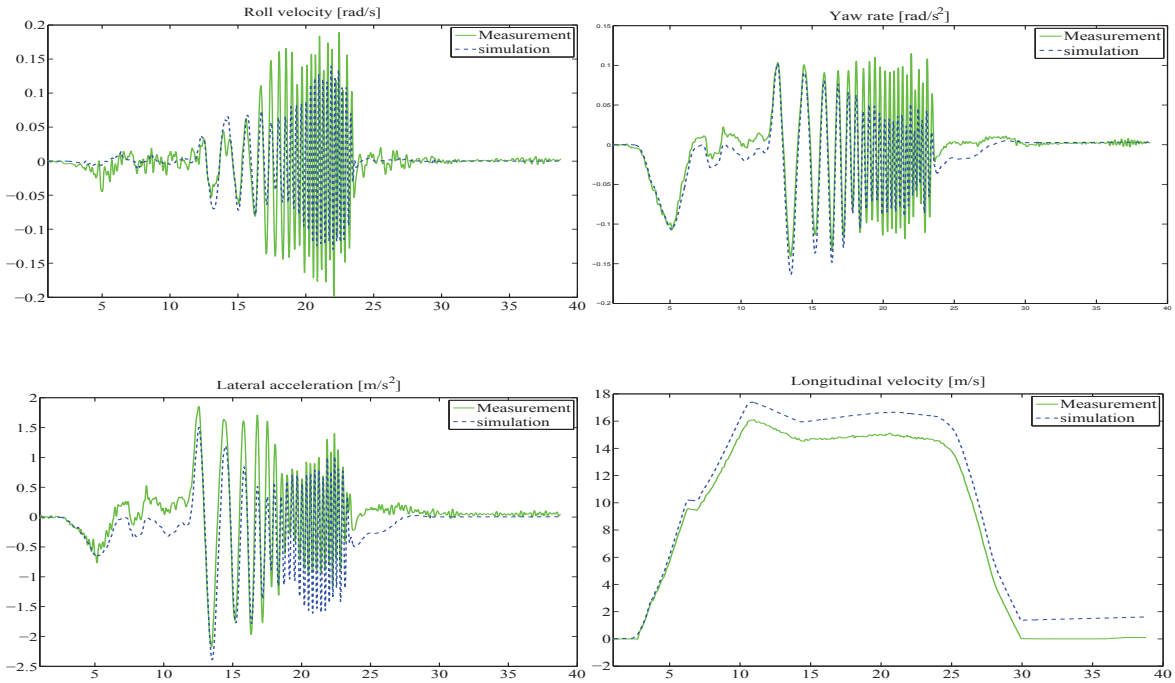

3.5.7 Conclusions and remarks

The experimental results obtained by the validation are close to the modeled ones. However, we notice some differences, especially in the frequency tests using sine waves. These differences are mainly due to the modeling errors of the tire (these tests could bring the tire dynamics to the non linear zone). Indeed, even if the non linear model is well defined, the parameters of the model are very difficult to identify exactly (they vary depending on temperature, road conditions...). However,

the over all dynamical behaviour is fairly well modeled. Then, for the moose test, simulated results on the defined modeled are very close to the measured ones.

3.6 Conclusion

In this chapter, several models have been introduced. These models are mainly used for the control synthesis. Indeed, the vertical models are mainly used for the suspension control design (see chapters. 5, 6, 7 and 8), while the extended bicycle one is used for the lateral dynamics control design purpose (see chapter. 6, 7 and 8). Moreover, a full non linear vehicle model has been validated through an experimental procedure on a real vehicle (”Renault Megane Coupé”).
The presented models are used in the following chapters to develop the new control strategies. [2]

[2]Thanks to Michel Basset, Jéremie Daniel and all automotive control team in Mulhouse for the experimental validation test.

Part II

Road profile estimation and road adaptive vehicle control dynamics

CHAPTER 4

Road Profile estimation strategies

4.1 Introduction

The vehicle performances enhancement has been always an important issue for both automotive industries and costumers. Then, since the vehicle dynamics depend on tire/road contact forces, the road profile is one of the most important factors that determine the vehicle performance. Thus, the knowledge of the road profile (estimation or measurement) can be used to adapt the damping coefficient on active or semi-active suspension control systems to improve the ride comfort and handling of a car (Hong *et al.*, 2002), (Kim *et al.*, 2002), (Fialho and Balas, 2002), such as the recent *magic body control* (look-ahead approach) in luxury cars of Mercedes-Benz™.

This has motivated a lot of works that look for an appropriate solution to handle the vehicle/road interactions. Existing methods for estimating the road roughness are based either on visual inspections (Kim *et al.*, 2002), (Stavens and Thrun, 2006) or on the use of a fully instrumented vehicle that can take direct measurements from road irregularities, e.g. profilographs (Yu *et al.*, 2013) or profilometers (Spangler and Kelly, 1966), (Healy *et al.*, 1977), which are commonly used for road serviceability and road maintenance, and are independent of the type of survey vehicle and of the profiling speed; the problem is that both methodologies are extremely expensive to be implemented and require a specialized operation, i.e. knowledge for sensors location, signal processing, etc. Moreover, during winter seasons with snowy environments, laser sensors cannot be used. To overcome these drawbacks, it is important to develop methods with low cost instrumentation easily implemented on a fleet of vehicles have gained importance, e.g. road estimators based on accelerometers that are rugged, easy to mount and process.

Recently, (González *et al.*, 2008) have proposed a road roughness estimator based on standard vehicle instrumentation (acceleration measurements) easy to implement; however, the road estimation algorithm depends on a specific frequency, i.e. the approach is designed for a constant vehicle velocity and the result is not ensured when the velocity changes. Similarly, a road estimator based on the Fourier transform, at constant vehicle velocity, is proposed in (Hong *et al.*, 2002). In (Ngwangwa *et al.*, 2010) the road roughness is estimated at variable velocity by using different standardized roads (ISO 8608), but the *ANN-NARX* estimator could demand many computational resources for an online estimation; similarly (Yousefzadeh *et al.*, 2010) proposed an *ANN* (Artificial Neural Network) for the road profile estimation by using 7 acceleration measurements as input vector, but to achieve a good classification, the vehicle behavior under each ISO road profile must be used in the learning phase.

A Kalman filter is used to estimate the road input of an augmented Quarter of Vehicle (*QoV*) state space model in (Yu *et al.*, 2013); however, the road inclusion in the state vector is assumed as a quadratic signal, indeed the ISO 8608 establishes that real roads follow a sum of sinusoidal waves.

Moreover, sophisticated road estimation methods have emerged; for instance, in (Heyns *et al.*, 2012) a road roughness monitoring system is proposed by using a Bayesian estimator that performs at

variable velocity but, a priori information of the road is required. A novel approach based on the cross-entropy method that employs Monte Carlo simulations is proposed in (Harris *et al.*, 2010) to obtain the optimal road profile estimation by using the sprung and unsprung mass accelerations; however this technique is practically impossible to implement for automotive suspension control purposes because the search of the optimum requires too much computing time, e.g. 5 hours to estimate 100 m of road roughness. The use of microphones to measure the tire noise, in addition with acceleration measurements, allows the road profile classification; however, a robustness study is needed because of the susceptibility of signal contaminations, the implementation of this strategy on a fleet of vehicles does not seem feasible.

This chapter 3 gives strategies of road profile estimation using the commonly used sensors available on most of the commercial cars, as follows:

- The first strategy is based on an $\mathcal{H}_\infty$ observer (work developed with colleagues from Tec Monterrey: J.C. Tudon and R. Morales).

- The second one is an algebraic observer with unknown input (work developed with colleagues from Mines Paristech-CAOR: L. Menhour and B. D'Adréa Novel).

- The third one is based on a parametric adaptive observation of the road profile (work developed with a colleague from Gipsa-Lab with J.J Martinez).

Experimental results on a 1:5 scale vehicle have been used to evaluate the proposed road profile estimation method; for simplicity, a *QoV* (Quarter of Vehicle) is used as survey case. Several ISO 8608 road profiles, at different vehicle velocities, with various Electro-Rheological (*ER*) damping coefficients validate the feasibility of the proposed road profile estimation method in view of its real time implementation.

These strategies allow to reconstruct the road profile; then, a **road roughness estimation and identification approach** will allow to classify the type of road by comparing it to the ISO 8608 norm of the road profiles. Indeed, these developed strategies have led to several publication in (Tudon-Martinez *et al.*, 2014) and (Martinez *et al.*, 2014).

Remark: All allong this chapter, all variables of this study are defined in the following Table 4.1:

Table 4.1: Definition of Variables.

Variable	Description	Units
α, β	Terms of the Fourier series	-
δ	Dirac impulse function, disturbance model input	-
ϵ	Adaptation error in the Q-parametrization	m
θ	Adaptive parameters	
λ	Forgetting factor in the adaptive algorithm	
A_{z_r}	Road profile amplitude	m
c_r	Roughness coefficient according to the ISO 8608	$\frac{\mathrm{m}^2 \cdot \mathrm{m}}{\mathrm{cycles}}$
d	Integer time delay of the internal model	-
e	Estimation error	m
F	Adaptation gain	-
F_{ER}	Electro-Rheological damping force	N
f_0	Critical spatial frequency	$\frac{\mathrm{cycles}}{\mathrm{m}}$
f_s	Sampling frequency	Hz
f_{z_r}	Road profile frequency	Hz
G_y	Discrete transfer function of y vs u	-
J	Error function cost	-
P	Characteristic polynomial of the closed loop	-
P_c	Probability of correct classification	-
P_{fa}	Probability of false alarms	-
S_y	Output sensitivity function	-
S_{z_r}	Power spectral density of the road roughness	$\frac{\mathrm{m}^2}{\mathrm{Hz}}$
T_f	Time window in the frequency estimation module	s
T_s	Sampling time	s
u	Road disturbances in the Q-parametrization	m
v_x	Longitudinal vehicle velocity	$\frac{\mathrm{m}}{\mathrm{s}}$
w	Adaptation vector in the Q-parametrization	m
y	Output vector in the Q-parametrization	m
z_{def}	Damper piston deflection	m
z_r	Road profile	m
z_s	Vertical position of the sprung mass	m
$\ddot{z}_s$	Vertical acceleration of the sprung mass	$\frac{\mathrm{m}}{\mathrm{s}^2}$
z_{us}	Vertical position of the unsprung mass	m
$\ddot{z}_{us}$	Vertical acceleration of the unsprung mass	$\frac{\mathrm{m}}{\mathrm{s}^2}$
$A \in \Re^{n_A}$	Denominator polynomial of the internal model	-
$B \in \Re^{n_B}$	Numerator polynomial of the internal model	-
$D \in \Re^{n_D}$	Denominator coprime polynomial in disturbance model	-
$N \in \Re^{n_N}$	Numerator coprime polynomial in disturbance model	-
$Q \in \Re^{n_Q}$	Adaptive parameter vector in the observer	-
$R_0 \in \Re^{n_R}$	Polynomial in the central regulation controller	-
$R \in \Re^{n_R}$	Polynomial of a stable controller	-
$S_0 \in \Re^{n_S}$	Polynomial in the central regulation controller	-
$S \in \Re^{n_S}$	Polynomial of a stable controller	-

4.2 Design of the $\mathcal{H}_\infty$ observer

The design of the road profile estimation algorithm is carried out on a QoV model. The system considers a sprung mass (m_s) and an unsprung mass (m_{us}). A spring with stiffness coefficient k_s and a semi-active shock absorber represent the suspension between both masses. The spring is considered

linear since it is around 95% of its operating zone in an automotive application. However, the semi-active damping force (F_{sa}) depends on a control input variable (electric current or voltage) and is highly nonlinear with respect to the suspension motion. The stiffness coefficient k_t models the wheel tire. The vertical position of the mass m_s (m_{us}) is defined by z_s (z_{us}), while z_r corresponds to the unknown road profile.
Then, the *QoV* system dynamics used to design the observer, given in a state-space representation, is written as:

$$\begin{aligned}
\underbrace{\begin{bmatrix} \dot{z}_s \\ \ddot{z}_s \\ \dot{z}_{us} \\ \ddot{z}_{us} \end{bmatrix}}_{\dot{x}} &= \underbrace{\begin{bmatrix} 0 & 1 & 0 & 0 \\ \frac{-k_s}{m_s} & 0 & \frac{k_s}{m_s} & 0 \\ 0 & 0 & 0 & 1 \\ \frac{k_s}{m_{us}} & 0 & \frac{-k_s-k_t}{m_{us}} & 0 \end{bmatrix}}_{A} \underbrace{\begin{bmatrix} z_s \\ \dot{z}_s \\ z_{us} \\ \dot{z}_{us} \end{bmatrix}}_{x} + \underbrace{\begin{bmatrix} 0 & 0 \\ \frac{-1}{m_s} & 0 \\ 0 & 0 \\ \frac{1}{m_{us}} & \frac{k_t}{m_{us}} \end{bmatrix}}_{B} \underbrace{\begin{bmatrix} F_{MR} \\ z_r \end{bmatrix}}_{u} \\
\underbrace{\begin{bmatrix} y_1 \\ y_2 \end{bmatrix}}_{y} &= \underbrace{\begin{bmatrix} \frac{-k_s}{m_s} & 0 & \frac{k_s}{m_s} & 0 \\ \frac{k_s}{m_{us}} & 0 & \frac{-k_s-k_t}{m_{us}} & 0 \end{bmatrix}}_{C} \begin{bmatrix} z_s \\ \dot{z}_s \\ z_{us} \\ \dot{z}_{us} \end{bmatrix} + \underbrace{\begin{bmatrix} \frac{-1}{m_s} & 0 \\ \frac{1}{m_{us}} & \frac{k_t}{m_{us}} \end{bmatrix}}_{D} \begin{bmatrix} F_{MR} \\ z_r \end{bmatrix} + \underbrace{\begin{bmatrix} v_1 \\ v_2 \end{bmatrix}}_{v}
\end{aligned} \tag{4.1}$$

where v is the noise in the accelerometers of the sprung ($\ddot{z}_s$) and unsprung mass ($\ddot{z}_{us}$). These measurements are related to the comfort and road holding performances, that depend on the semi-active damper properties and obviously on the road irregularities.

An $\mathcal{H}_\infty$ robust observer is designed to be unsensitive to measurements noise; also, it includes a weighting function to take into account the unknown road profiles. The performance is monitored by reducing the estimation error in the state variables; W_{e_i} represents the weighting function for each variable used to minimize the estimation error in the frequency range of interest for the suspension motion, while W_{zr} shapes the road irregularities in the observer design.

$$W_{zr} = \frac{K_{zr}\omega_{zr}s}{s+\omega_{zr}} \quad W_{e_i} = \frac{K_{e_{1_i}}\left(s^2+2\zeta_{e_{1_i}}\omega_{e_{1_i}}s+\omega_{e_{1_i}}^2\right)}{s^2+2\zeta_{e_{2_i}}\omega_{e_{2_i}}s+\omega_{e_{2_i}}^2} \tag{4.2}$$

By considering the filtering specifications (chosen to emphasize the interesting frequency range), the generalized model $\mathcal{P}$ used for the synthesis of the $\mathcal{H}_\infty$ observer is given by (4.3).

$$\mathcal{P} := \begin{cases} \dot{x} = & A \cdot x + B \cdot w \\ \tilde{y} = & C_2 \cdot x + D_2 \cdot w \\ z = & W_{e_i} \cdot (x - \hat{x}) \end{cases} \tag{4.3}$$

where $w = \begin{bmatrix} F_{MR} \\ W_{zr} \cdot \tilde{z}_r \end{bmatrix}$, $C_2 = \begin{bmatrix} C \\ 0_{1\times 4} \end{bmatrix}$, $D_2 = \begin{bmatrix} D \\ 1 \quad 0 \end{bmatrix}$ and, $W_{e_i} = [W_{e_1} W_{e_2} W_{e_3} W_{e_4}]^T$.
Figure 4.1 shows the structure of its design.
The observer is given as:

$$\dot{\hat{x}} = \quad A_{obs} \cdot \hat{x} + B_{obs} \cdot \begin{bmatrix} \ddot{z}_s & \ddot{z}_{us} & F_{MR} \end{bmatrix}^T \tag{4.4}$$

where A_{obs} and B_{obs} are the matrices of the $\mathcal{H}_\infty$ observer, which is quadratically stable by solving an optimization problem with *LMI* techniques, (Scherer *et al.*, 1997). Indeed, from the practical point of

view, variables related to the suspension motion (z_s, z_{us}) and their time derivatives ($\dot{z}_s$, $\dot{z}_{us}$) used to monitor the vertical vehicle performance, are not easy to measure. Therefore, an $\mathcal{H}_\infty$ observer can be used to estimate them because of its robustness to uncertainties. However, the observer reduces the effect of the measurement noise and avoid drifting in the estimated variables by decreasing asymptomatically the error dynamics, given by: $\dot{e} = \dot{x} - \dot{\hat{x}}$

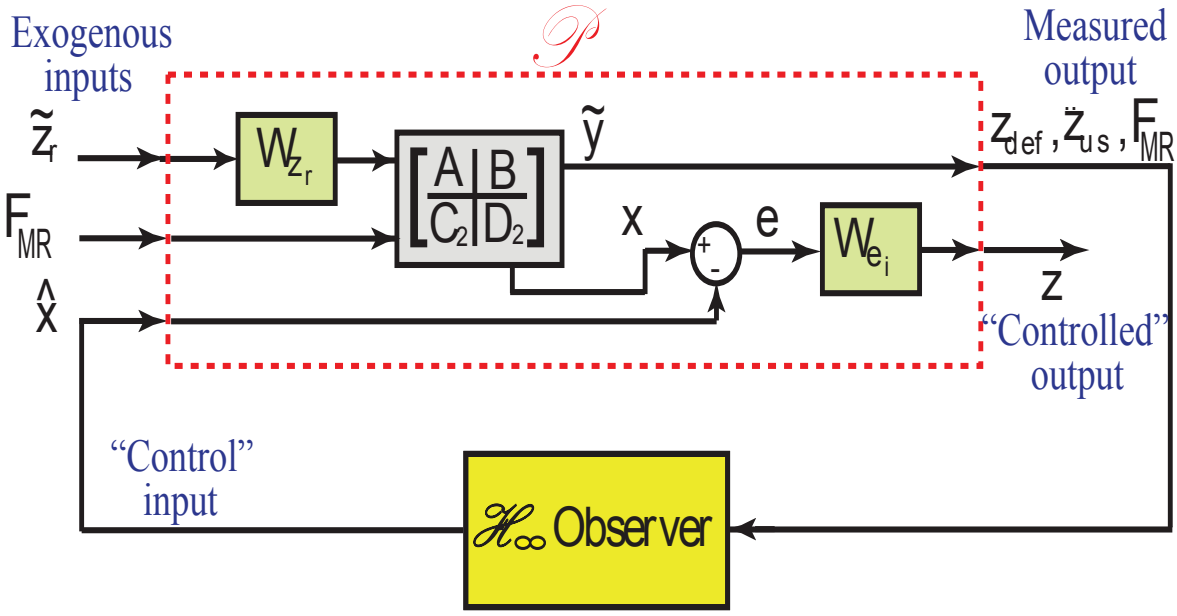

Figure 4.1: $\mathcal{H}_\infty$ observer design in a *QoV* system.

Remark: As it will be detailed later in this chapter, using the estimated states, the road profile can be estimated from the static equation of the unsprung mass acceleration, such that:

$$\hat{z}_r = [m_{us}\ddot{z}_{us} - k_s(\hat{z}_s - \hat{z}_{us}) + k_t\hat{z}_{us} - F_{MR}] \cdot k_t^{-1} \tag{4.5}$$

where F_{MR} is measured or modeled from experimental data.

4.2.1 Results of the $\mathcal{H}_\infty$ observer

To prove the efficiency of the proposed observer, an experimental implementation procedures were used and will be detailed in the following see subsection. 3.5.

Let us mention that experiments concern a predefined road profile (from ISO Norms) applied to the Gipsa-Lab test bench which is a $1/5$ of a real vehicle prototype designed to highlight on the vertical performances of the vehicle.
Table 4.2 shows the parameters of the weighting functions that minimize the estimation error of the designed $\mathcal{H}_\infty$ observer.

Table 4.2: Parameters of design in the $\mathcal{H}_\infty$ observer.

Filter W_{zr}		Filters W_{e_i}			
K_{zr}	3	K_{e1}	0.5	ω_{e1}	571 rad/s
ω_{zr}	1 rad/s	ζ_{e1}, ζ_{e2}	1	ω_{e2}	127 rad/s

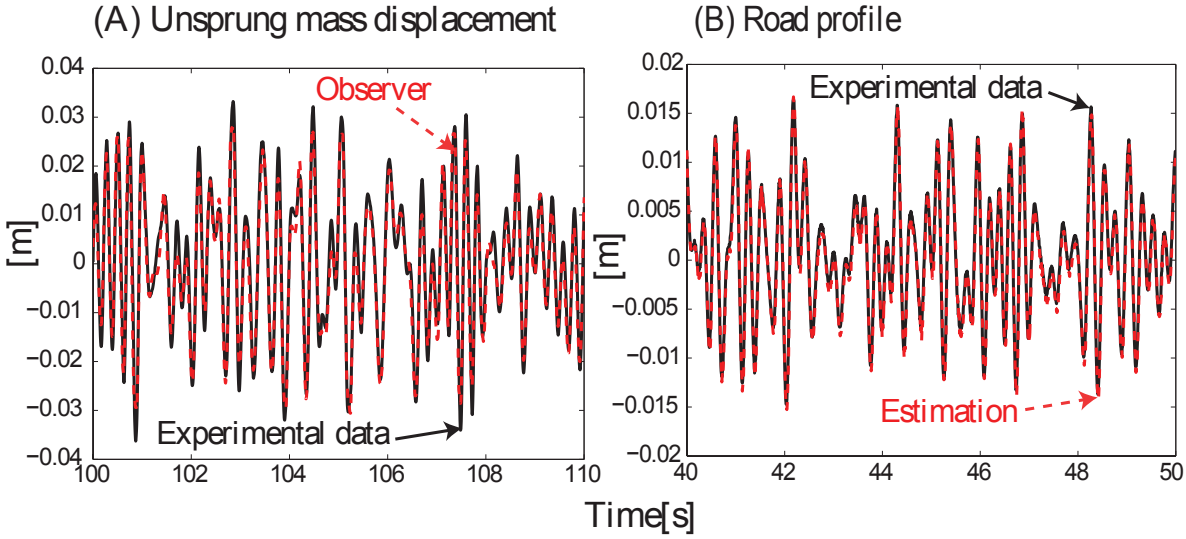

Figure 4.2: Performance of the $\mathcal{H}_\infty$ observer.

The efficiency of the $\mathcal{H}_\infty$ observer is shown in Fig. 4.2. The estimated state z_{us} follows the transient response of the measurement with an **ESR** (Error to State Ratio) error index of 0.11; a similar *ESR* index is obtained in other estimated state variables. Also, the estimated road profile $\hat{z}_r$ (see Fig. 4.2) is very close to the real one and proves the efficiency of the proposed $\mathcal{H}_\infty$ observer.

4.3 Method 2: Design of an Algebraic flat observer

This section is devoted to the estimation of a road profile method based on an algebraic observer with unknown inputs. This estimation method uses and is also applied on a quarter of vehicle model of the suspension.
For this road profile estimation, the classical quarter of vehicle (QoV) model of a suspension system as illustrated in figure 4.3 is used . This model describes the motions of the sprung and unsprung masses. The QoV system dynamics is governed by the following equations:

$$\begin{cases} m_s\ddot{z}_s = -k_s z_s + k_s z_{us} - \omega_1 \\ m_{us}\ddot{z}_{us} = -k_s z_s - (k_s + k_t) z_{us} + \omega_1 + k_t\omega_2 \end{cases} \tag{4.6}$$

For (4.6), the damping force ($F_{MR} = \omega_1$) and the road profile ($z_r = \omega_2$) are assumed to be the unknown inputs for the algebraic observer design procedure.

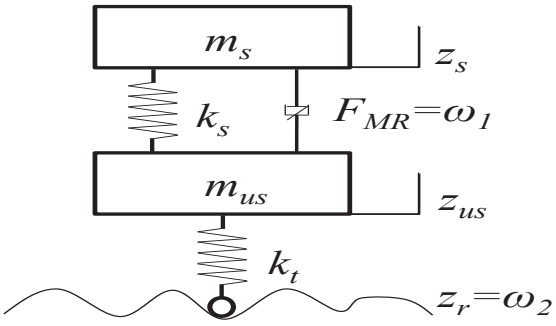

Figure 4.3: Quarter vehicle model for a semi-active suspension

Remark: Let us recall that the estimation method addressed in this section uses the algebraic framework devoted to the design of algebraic observers with unknown inputs (Barbot *et al.*, 2007), (Daafouz *et al.*, 2006), (Fliess and Join, 2008), (Ibrir, 2003), (Guerra *et al.*, 2007). The estimation approach uses also the algebraic identification methods for the numerical differentiation of noisy signals (Fliess and Join, 2008).

4.3.1 Road profile estimation method based on algebraic observer with unknown input

To establish the estimation method of road profile, we choose the displacements of sprung mass z_s and unsprung mass z_{us} as flat outputs.

$$y = \begin{bmatrix} y_1 \\ y_2 \end{bmatrix} = \begin{bmatrix} z_s \\ z_{us} \end{bmatrix} \tag{4.7}$$

The following algebraic observer estimation method of the road profile is established using the algebraic observability properties 8.4.1 and 8.4.2 and the definitions 8.4.2 and 8.4.3, the measured outputs (4.7) and the quarter vehicle model of suspension system (4.6):

$$\begin{cases} \hat{\dot{z}}_s = \dot{y}_1 \\ \hat{\dot{z}}_{us} = \dot{y}_2 \\ \hat{\omega}_1 = k_s y_2 - k_s y_1 - m_s \ddot{y}_1 \\ \hat{\omega}_2 = \frac{1}{k_t}\left(m_s \ddot{y}_1 + m_{us}\ddot{y}_2 + 2k_s y_1 + k_t y_2\right) \end{cases} \tag{4.8}$$

According to the properties 8.4.1 and 8.4.2, the system (4.6) is flat and the chosen outputs y_1 and y_2 are flat outputs. Let us recall that $\hat{\omega}_2 = \hat{z}_r$.

Remark: The algebraic observer with unknown inputs (4.8) is established thanks to the algebraic numerical differentiator (8.28) used to estimate the time derivatives of the measured flat outputs y_1 and y_2.

4.4 Algebraic identification

To have a robust filtering and a numerical differentiation of noisy signals, the algebraic estimation techniques are used. This estimation is performed using the recent advances in (Fliess and Join, 2008), which yield efficient real-time filters. For our study, these estimators are used to compute the derivatives of the flat outputs to design an input-free estimator of road profile.
The block diagram of figure 4.4 shows two parts of the road profile estimation method: the first one is concerned by the filtering and numerical differentiation of the measured outputs, while the second one illustrates the road profile estimation using an algebraic observer with unknown input.

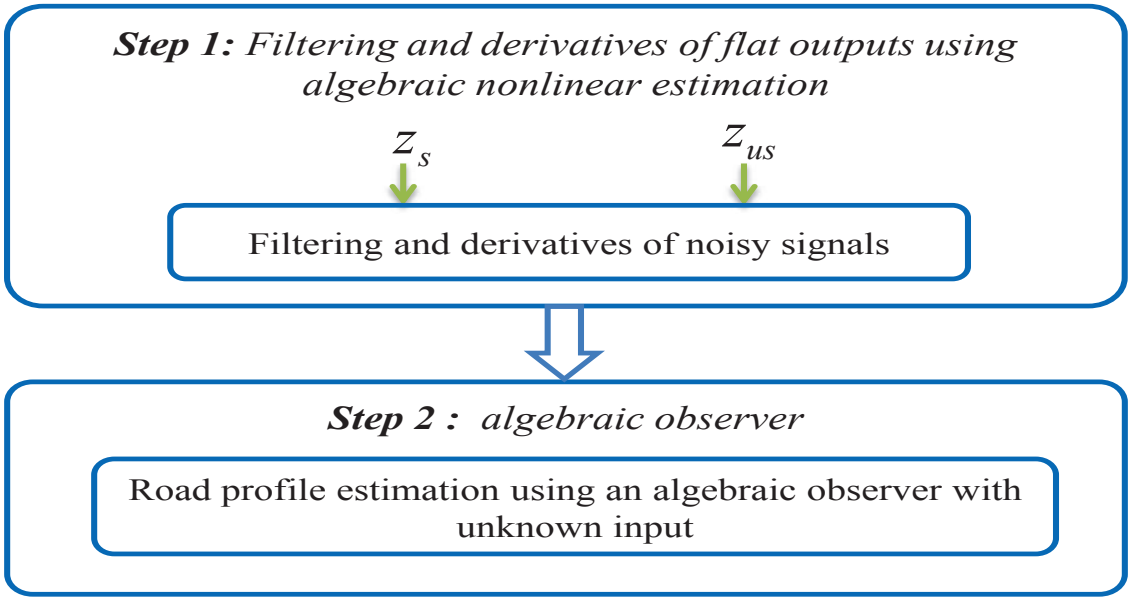

Figure 4.4: Block diagram of road profile estimation method

4.4.1 A short definition of algebraic denoising and numerical differentiation

The numerical estimators[1] (8.28) are deduced from operational calculation and algebraic manipulations. For this, consider the following real-valued polynomial time function $x_N(t) \in \mathbb{R}[t]$ of degree N

$$x_N(t) = \sum_{\nu=0}^{N} x^{(\nu)}(0)\frac{t^\nu}{\nu!}, \ t \geq 0. \tag{4.9}$$

In the operational domain[2] (see e.g. (Yosida, 1984)), (8.15) becomes

$$X_N(s) = \sum_{\nu=0}^{N} \frac{x^{(\nu)}(0)}{s^{\nu+1}}. \tag{4.10}$$

Multiplying the left-side and the right-side of equation (8.16) on the left by $\frac{d^\alpha}{ds^\alpha} s^{N+1}$, $\alpha = 0, 1, \cdots, N$. The quantities $x^{(\nu)}(0)$, $\nu = 0, 1, \ldots, N$, which are linearly identifiable satisfy the following triangular

[1] For the details related to the developments used in this work, we refer the reader to (Fliess and Join, 2008)
[2] $\frac{d}{ds}$ corresponds in time domain to the multiplication both sides by $-t$.

system of linear equations:

$$\frac{d^\alpha s^{N+1} X_N}{ds^\alpha} = \frac{d^\alpha}{ds^\alpha}\left(\sum_{\nu=0}^{N} x^{(\nu)}(0) s^{N-\nu}\right),\ 0 \leq \alpha \leq N-1. \tag{4.11}$$

The time derivatives in (8.17) ($s^\mu \frac{d^\iota X_N}{ds^\iota}$, $\mu = 1, \ldots, N$, $0 \leq \iota \leq N$), are removed by multiplying both sides of equation (8.17) by $s^{-\bar{N}}$, $\bar{N} > N$. Now, consider an analytic time function, defined by the power series $x(t) = \sum_{\nu=0}^{\infty} x^{(\nu)}(0)\frac{t^\nu}{\nu!}$, which is assumed to be convergent around $t = 0$. Approximate $x(t)$ by the truncated Taylor expansion $x_N(t) = \sum_{\nu=0}^{N} x^{(\nu)}(0)\frac{t^\nu}{\nu!}$ of order N. Good estimates of the derivatives are obtained by the same calculations as above.

Then, the following formulae may be obtained and used to estimate the 1st order derivative of y:

$$\hat{\dot{y}}(t) = -\frac{3!}{h^3}\int_{t-h}^{t} (2h(t-\tau) - h) y(\tau) d\tau \tag{4.12}$$

Note that the sliding time window $[t-h,\ t]$ may be quite short.

Remark: The estimation method (8.28) is not of asymptotic type and does not require any statistical knowledge of the corrupting noises (see (Fliess, 2006*b*) for details).

4.4.2 Application

To design the algebraic observer (4.8), the estimation of the outputs derivatives is required. These derivatives are achieved thanks to the algebraic estimation (8.28). Then, the numerical differentiation of y_1 and y_2 are computed as follows:

$$\begin{bmatrix} \hat{\dot{y}}_1(t) \\ \hat{\dot{y}}_2(t) \\ \hat{\ddot{y}}_1(t) \\ \hat{\ddot{y}}_2(t) \end{bmatrix} = -\frac{3!}{h^3}\int_{t-h}^{t} (2h(t-\tau) - h) \begin{bmatrix} y_1(\tau) \\ y_2(\tau) \\ \hat{\dot{y}}_1(\tau) \\ \hat{\dot{y}}_2(\tau) \end{bmatrix} d\tau \tag{4.13}$$

4.4.3 Simulation Results of the Algebraic Observer

To test the efficiency of proposed algebraic observer with unknown input, a quarter-car model is considered subject to a measured road profile excitation (see Fig. 4.6). The measured output signals considered as the flat output of the algebraic observer are z_s and z_{us} (the chassis displacement and wheel motion, resp), as shown in Fig. 4.5. Then, the road profile estimation is very well achieved as shown in Fig. 4.6.

Fig. 4.6 shows the efficiency of the proposed non linear algebraic estimation. The observer estimates perfectly the considered road profile. It will be used in the control strategy, designed below.

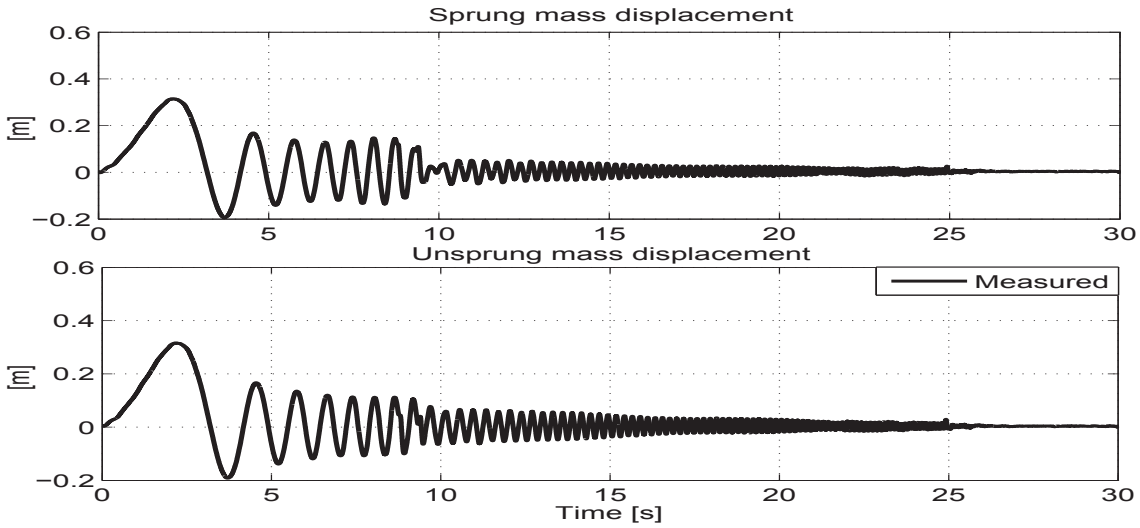

Figure 4.5: Used flat outputs: sprung and unsprung mass displacements

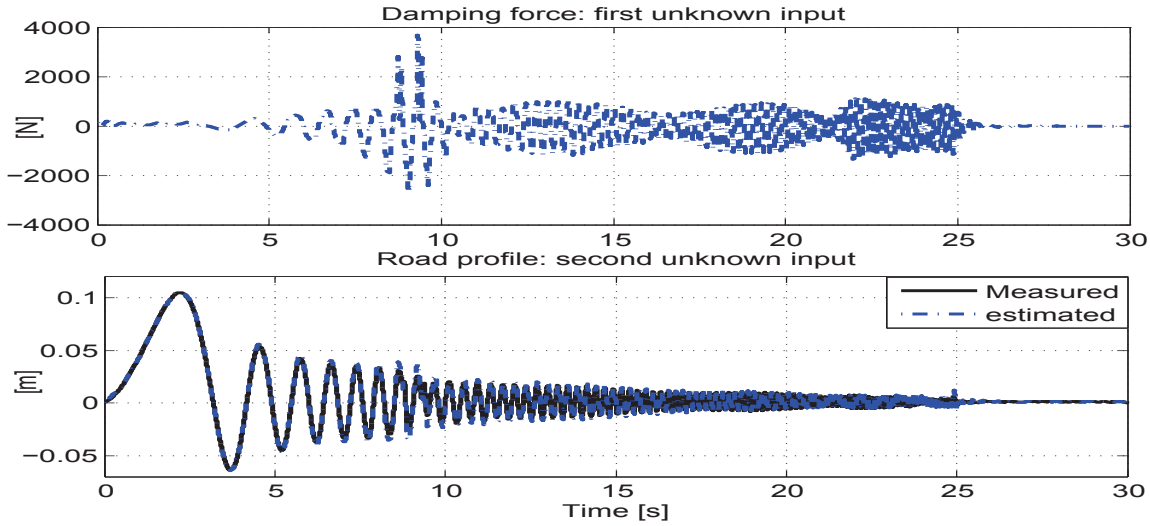

Figure 4.6: Unknown inputs estimation: damping force and road profile

4.5 Method 3: Desing of the Parametric Adaptive Observation of Road Disturbances

Inspired from a regulation control scheme, it is possible to estimate the road disturbances which must theoretically be compensated. Here, we make use of the internal model principle (Landau *et al.*, 2005) and the *YK* parametrization (known also as the *Q*-parametrization) to adjust a parametric vector $Q(z^{-1})$ that allows the online road estimation. In order to reduce the computing cost and minimize the implementation complexity, the Youla-Kučera (*YK*) parametrization approach is used to estimate the road profile by considering an internal model of the disturbance into the observer through adjusting a parameter vector. The parametric adaptive algorithm used to estimate the road profile is inspired of the tracking control proposed to the disturbance rejection (Landau *et al.*, 2005), (Martinez

and Alma, 2012).

Figure 4.7 illustrates a block diagram of the adaptive parametric observer using the Q-parametrization approach; the polynomials $R_0(z^{-1})$ and $S_0(z^{-1})$ represent a *central* controller which satisfies the reference-servo performances (Landau *et al.*, 2005).

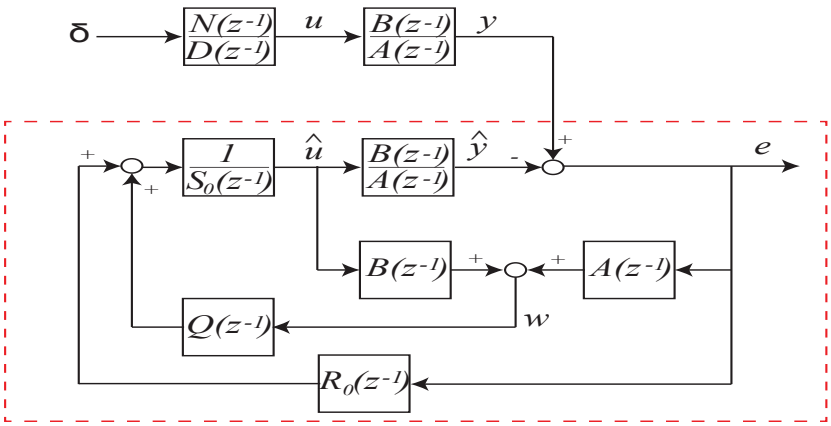

Figure 4.7: Parametric adaptive observation scheme for road profile disturbances

Because the road profile is deduced from the available car measurements, the observability condition must be guaranteed. In (Yu *et al.*, 2013), it is verified that the *QoV* model is fully observable when the sprung mass acceleration, suspension deflection or a combination of both is considered as measurement vector; even if the road disturbance model is a sum of sinusoidal waves, the *Gilbert observability criterion* assures full observability. In this section, the sprung mass position is considered as the output vector ($y = z_s$) because it has a softer transient response (more damped) than the sprung mass acceleration $\ddot{z}_s$ and because it offers sufficient information for a fully observable system representation. The discrete-time transfer function of z_s with respect to the unknown road input ($u = z_r$) with sampling time T_s is:

$$G_y(z^{-1}) = \frac{z^{-d}B(z^{-1})}{A(z^{-1})} \tag{4.14}$$

where d is an integer time delay in the process (in this case $d = 0$) and $A(z^{-1})$ and $B(z^{-1})$ are polynomials in the complex variable z^{-1} with orders n_A and n_B respectively, given by:

$$\begin{aligned} A(z^{-1}) &= 1 + a_1 z^{-1} + a_2 z^{-2} + \ldots + a_{n_A} z^{-n_A} \\ B(z^{-1}) &= b_1 z^{-1} + b_2 z^{-2} + \ldots + b_{n_B} z^{-n_B} \end{aligned} \tag{4.15}$$

By considering a reliable identified model, the central controller is used to specify the desired closed loop poles (Zito and Landau, 2005), whose characteristic polynomial is defined by:

$$P(z^{-1}) = A(z^{-1})S_0(z^{-1}) + z^{-d}B(z^{-1})R_0(z^{-1}) \tag{4.16}$$

The polynomials $S_0(z^{-1}) = 1+s_1 z^{-1}+\ldots+s_{n_S} z^{-n_S}$ and $R_0(z^{-1}) = r_0+r_1 z^{-1}+\ldots+r_{n_R} z^{-n_R}$ can be obtained by the *Bezout* equation as in (Martinez and Alma, 2012) to obtain a stable solution with the minimal pair (S_0, R_0).

Define the road disturbance as a deterministic process:

$$u(k) = \frac{N(z^{-1})}{D(z^{-1})}\delta(k) \tag{4.17}$$

where $\delta(k)$ is a *Dirac impulse function* and N and D are coprime polynomials of degrees n_N and n_D, respectively. Based on the internal model principle (Landau *et al.*, 2005), the transfer function between the road and the vehicle dynamics is given by the output sensitivity function S_y as:

$$y(k) = \underbrace{\frac{S(z^{-1})A(z^{-1})}{P(z^{-1})}}_{S_y} u(k) \tag{4.18}$$

In terms of the parametric vector Q, the reference output $y(k)$ can be defined by:

$$y(k) = \frac{S_0(z^{-1}) - z^{-d}B(z^{-1})Q(z^{-1})}{P(z^{-1})}A(z^{-1})u(k) \tag{4.19}$$

where $S(z^{-1}) = S_0(z^{-1}) - z^{-d}B(z^{-1})Q(z^{-1})$ belongs to the family of stable controllers, in the Q-parametrization, that assigns the closed loop poles defined by (4.16). By incorporating the internal model of the disturbance into the polynomial $Q(z^{-1})$, the diophantine equation (Landau *et al.*, 2005) is established , as:

$$S_0(z^{-1}) - z^{-d}B(z^{-1})Q(z^{-1}) = S'(z^{-1})D(z^{-1}) \tag{4.20}$$

such that,

$$y(k) = \frac{S'(z^{-1})A(z^{-1})N(z^{-1})}{P(z^{-1})}\delta(k) \tag{4.21}$$

whose unique solution for Q and S' allows to define a reference output model that leads a perfect disturbance rejection (Landau *et al.*, 2005), (Martinez and Alma, 2012).

For this application problem, the road disturbance is a time-varying signal (in frequency and amplitude) and an adaptation of the internal model is needed to match the actual disturbance. Thus, the adaptation error is given by:

$$e(k) = y(k) - \hat{y}(k) \tag{4.22}$$

Because $y(k)$ and $\hat{y}(k)$ can be represented by the parametric vector $Q(z^{-1})$ and $\hat{Q}(z^{-1})$ respectively using (4.19), the adaptation error (4.22), after some mathematical manipulations, can be rewritten as:

$$e(k) = \left[Q(z^{-1}) - \hat{Q}(z^{-1})\right] H(z^{-1})A(z^{-1})u(k) \tag{4.23}$$

where $H(z^{-1}) = \frac{z^{-d}B(z^{-1})}{P(z^{-1})}$. Since in practice there is no information about the unknown optimal parameter $Q(z^{-1}) = \theta_0 + \theta_1 z^{-1} + \ldots + \theta_{nQ} z^{-nQ}$ (Martinez and Alma, 2012), the adaptation error ϵ proposed in (Landau *et al.*, 2005) represents a solution to minimize the disturbance propagation, such that:

$$\epsilon(k) = \frac{S_0(z^{-1}) - z^{-d}B(z^{-1})\hat{Q}(z^{-1})}{P(z^{-1})}w(k) \tag{4.24}$$

where $w(k)$ represents the effect of the road disturbance on the system output $y(k)$ coming from an output sensor, and is given by:

$$w(k) = A(z^{-1})e(k) + z^{-d}B(z^{-1})u(k) \tag{4.25}$$

The adaptation error ϵ can be directly written in terms of the adaptation coefficients $\hat{\theta}$, (4.24) can be rewritten as:

$$\epsilon(k) = \frac{S_0(z^{-1})}{P(z^{-1})} w(k) - \hat{\theta}^T \psi(k) \tag{4.26}$$

where $\psi(k) = \begin{bmatrix} 1 & z^{-1} & \dots & z^{-nQ} \end{bmatrix}^T H(z^{-1}) w(k)$, θ and $\hat{\theta}$ are the parameter vector and their estimation. By using a *gradient algorithm* to minimize the error function cost $J = \frac{1}{2}\epsilon^2(\hat{\theta})$, the parametric adaptation law is:

$$\dot{\hat{\theta}} = \frac{\partial J}{\partial \hat{\theta}} = \epsilon \frac{\partial \epsilon}{\partial \hat{\theta}} = -\epsilon \cdot \psi \tag{4.27}$$

In order to make J small, the adaptation algorithm performs in the direction of the negative gradient with a gain of adaptation F (see (Martinez and Alma, 2012)), such that in discrete time the adaptation law becomes:

$$\hat{\theta}(k+1) = \hat{\theta}(k) + F\epsilon(k)\psi(k) \tag{4.28}$$

From (4.25) and applying the *YK* parameterizacion, the adaptive estimation of the unknown road disturbance $[\hat{z}_r(k) = \hat{u}(k)]$ is given by:

$$\hat{u}(k) = \frac{1}{S_0(z^{-1})} \left[\underbrace{\hat{Q}(z^{-1}) w(k)}_{\theta^T(k)\phi(k)} + R_0(z^{-1}) e(k) \right] \tag{4.29}$$

where $\phi(k) = \begin{bmatrix} 1 & z^{-1} & \dots & z^{-nQ} \end{bmatrix} w(k)$. The adaptation gain must be chosen to increase the convergence time of the parameters but with sensitivity to noise around the optimum (see (Zito and Landau, 2005)); generally at the beginning of the algorithm, the gain is enough big and then is decreased. Based on a robust stability analysis with proof in (Martinez and Alma, 2012), the adaptation gain is given by:

$$F(k+1) = \frac{F(k)}{\lambda + \psi^T(k) F(k) \psi(k)} \tag{4.30}$$

where λ is the forgetting factor to weight older gain values.

In the *narrow-band* disturbance rejection problem, the parameter vector $\hat{\theta}$ allows a straightforward determination of the disturbance frequency by $f_{z_r} = f_s \, arcos(-\hat{\theta}_1/2)$ where f_s is the sampling frequency (Martinez and Alma, 2012), (Airimitoaie and Landau, 2013), i.e. two coefficients in $\hat{Q}$ are enough to characterize the frequency of an unknown sinusoidal disturbance. However, because the road profiles are composed by an indeterminate series of sinusoidal waves, the online estimation of the road frequency through the parameter vector $\hat{\theta}$ is complex. Thus, a frequency estimation module based on the effective value of the road profile is considered.

4.5.1 Results of the Parametric Adaptive Observation of Road Disturbances

To test the efficiency of the Parametric Adaptive road profile observation the following scenario is used. A sinusoidal wave at constant frequency (7 Hz) is considered as road signal, and the automotive suspension system is at passive mode (without actuation). Figure 4.8a illustrates that the parametric adaptive algorithm allows a very accurate road estimation by using only two parameters in the Q vector, as it is established in (Martinez and Alma, 2012), (Airimitoaie and Landau, 2013). Indeed, in

around three seconds the estimation parameters converge, Fig. 4.8b, by using a higher adaptation gain at the beginning of the algorithm which decreases once the Q-parameters values are being adapted, Fig. 4.8c. Note in Fig. 4.8a that meanwhile the parameter vector Q is online adapted, the amplitude of the road signal is increases until it reaches the real value (10 cm).

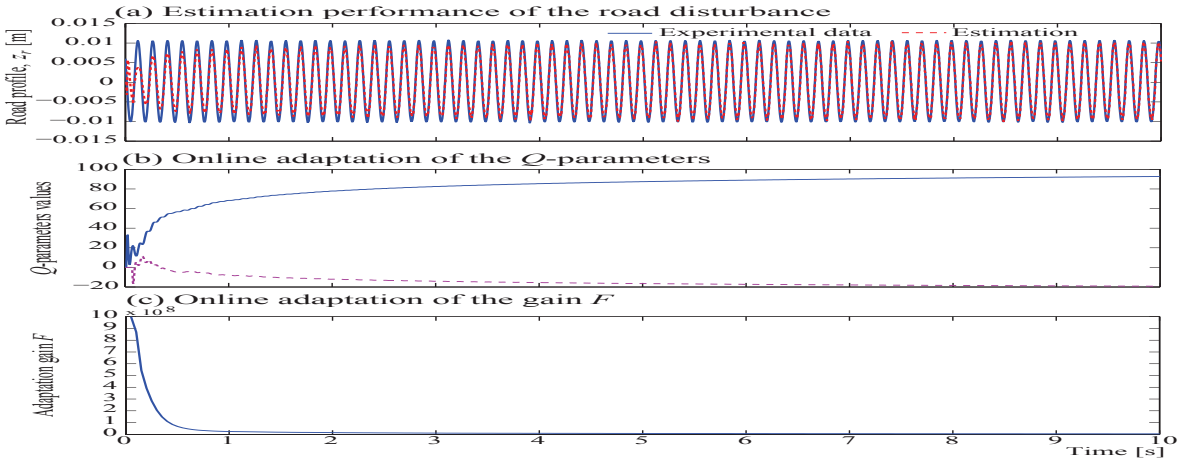

Figure 4.8: Road disturbance estimation with Q-parametrization, when z_r is a sinusoidal wave at 7 Hz and the car has passive damping suspension.

Remark: Results of the Q-parametrization algorithm to estimate the road disturbances are discussed, a forgetting factor $\lambda = 1$ was used.

4.6 Road Roughness Estimation and Classification

The road roughness estimation and classification approach is common to the 3 road profile reconstructions. Indeed, with the estimations of frequency and amplitude of the road disturbances, it is possible to define the type of road profile on which the vehicle is driven.

4.6.1 Frequency estimation of the road profile

According to the ISO 8608, a road profile satisfies a periodic motion whose fundamental frequency is not straightforward to compute. Thus, by assuming an harmonic motion in the road, this unknown input could be represented by one wave or a sum of sinusoidal waves of the form:

$$z_r(t) \approx A_{z_r} \cdot sin(2\pi \cdot f_{zr} \cdot t) \tag{4.31}$$

$$\dot{z}_r(t) \approx 2\pi \cdot f_{zr} \cdot A_{z_r} \cdot cos(2\pi \cdot f_{zr} \cdot t) \tag{4.32}$$

where there is no feasible prior information of the road frequency f_{zr}, which depends on: 1) the suspension capability, 2) road surface (number of waveforms), 3) tire dynamics and 4) vehicle velocity. By relating this harmonic motion to an uniform circular motion, it is possible to determine the frequency of excitation by:

$$f_{z_r} = v_{z_r} / (2\pi \cdot p_{z_r}) \tag{4.33}$$

where $2\pi f_{z_r}$ is the angular velocity, v_{z_r} is the tangential velocity and p_{z_r} is the radius of the circle. In this problem, p_{z_r} can be interpreted as the amplitude of the road disturbance and v_{z_r} the amplitude of its time derivative, such that the online estimation of z_r and $\dot{z}_r$ can be used to estimate f_{z_r}.

In (Cartwright, 2007), it is shown that one wave or a sum of two or more sinusoidal waveforms with different amplitudes and frequencies, such as an ISO 8608 road, can be obtained by the effective *RMS* value; thus, the road profile frequency can be estimated by the *RMS* values of the road disturbance computed by (4.29) and its numerical differentiation $f'(\hat{z}_r)$, inspired from (4.33), such that:

$$\hat{f}_{z_r}(k) = \sqrt{\frac{\left[f'(\hat{z}_r)^2(k)+f'(\hat{z}_r)^2(k-1)+\cdots+f'(\hat{z}_r)^2(k-n)\right]}{\left[\hat{z}_r^2(k)+\hat{z}_r^2(k-1)+\cdots+\hat{z}_r^2(k-n)\right]\cdot 4\pi^2}} \quad [\text{Hz}] \tag{4.34}$$

where n is the number of samples in a time window which guarantees at least 2 cycles of the estimated frequency (Lozoya-Santos *et al.*, 2011).

4.6.2 Amplitude estimation of the road profile

By using a discrete time Fourier analysis of the estimated road signal ($\hat{z}_r$) over a running window of one cycle of its fundamental frequency, it is possible to estimate the magnitude of the road by:

$$\hat{A}_{z_r}(k) = \sqrt{\alpha^2(k) + \beta^2(k)} \tag{4.35}$$

where the terms of the Fourier series, related to the fundamental component, are:

$$\begin{aligned} \alpha(k) &= \tfrac{1}{N}\textstyle\sum_{n=0}^{N-1} \hat{z}_r(n) cos\left(2\pi \hat{f}_{z_r} nk\right) \\ \beta(k) &= \tfrac{1}{N}\textstyle\sum_{n=0}^{N-1} \hat{z}_r(n) sin\left(2\pi \hat{f}_{z_r} nk\right) \end{aligned} \tag{4.36}$$

The online estimated frequency $\hat{f}_{z_r}$ is the fundamental frequency of the road over the running window, i.e. $N = 1/\hat{f}_{z_r}$. Thus, the estimations of the frequency and amplitude of the road disturbances are used to monitor its roughness. The roughness Power Spectral Density (*PSD*) function, $S_{z_r}(f_{z_r})$, is used to characterize a road in the frequency domain, (Wong, 2001):

$$S_{z_r}(f_{z_r}) = \frac{\hat{A}_{z_r}^2}{2\Delta f} \tag{4.37}$$

where Δf is defined by the frequency range of interest. By using the limits of roughness for each type of standard road, defined by the ISO 8608, one performs an online classification of the road on which the vehicle is driven. The thresholds are computed by using the vehicle velocity and the *PSD* of each road based, on the limit of the roughness coefficient (c_r) associated with the pavement quality. The lower/upper control limits for each road profile are given by:

$$S_{z_{r_{TH}}}(f_{z_r}) = \frac{c_r}{v_x} \cdot \left[\frac{f_{z_r}}{(f_0 \cdot v_x)}\right]^{-n_r} \qquad [\text{m}^2/\text{Hz}] \tag{4.38}$$

where f_{z_r} is the on-line estimated frequency by given (4.34), f_0 is the critical spatial frequency made equal $1/2\pi$ cycles/m, v_x is the longitudinal vehicle velocity and n_r is a dimensionless constant related to the road waves (Robson, 1979); for disturbances with high wave length (greater than 6 m) $n_r > 2$ (Genta and Morello, 2009). The Table 4.3 shows the c_r coefficient values used to define the thresholds of different ISO roads in the road identification algorithm.

Table 4.3: Classification of road profiles (ISO 8608).

Type of Road	Class	Lower c_r $\mathrm{m}^2/(\mathrm{cycles/m})$	Upper c_r $\mathrm{m}^2/(\mathrm{cycles/m})$	n_r
Smooth runway	A	1.6×10^{-14}	3.2×10^{-7}	3.8
Smooth highway	B	3.2×10^{-7}	1.2×10^{-6}	3.5
Highway with gravel	C	1.2×10^{-6}	5.1×10^{-6}	2.1
Rough runway	D	5.1×10^{-6}	2.0×10^{-5}	2.0
Pasture	E	2.0×10^{-5}	8.2×10^{-5}	2.0
Plowed field	F	8.2×10^{-5}	3.3×10^{-4}	1.6

4.7 Experimental Results: vehicle 1:5 scale test bed

The experimental platform is composed by a host computer used to design and develop the proposed road profile estimation algorithm in Matlab/Simulink™. The host computer is connected to a target computer by ethernet to run the Simulink™ development in real-time with a *xPC Target* software of Mathworks™. The target computer also contains a data acquisition card that establishes a bidirectional communication with the sensors and actuators of the experimental vehicle. The *xPC Target* enables control, monitoring, and on-the-spot parameter tuning of the real-time application directly from the Simulink™ model even if the program is running. Figure 4.9 shows a conceptual communication scheme of the experimental platform, the sampling frequency was 200 Hz. A test-bench

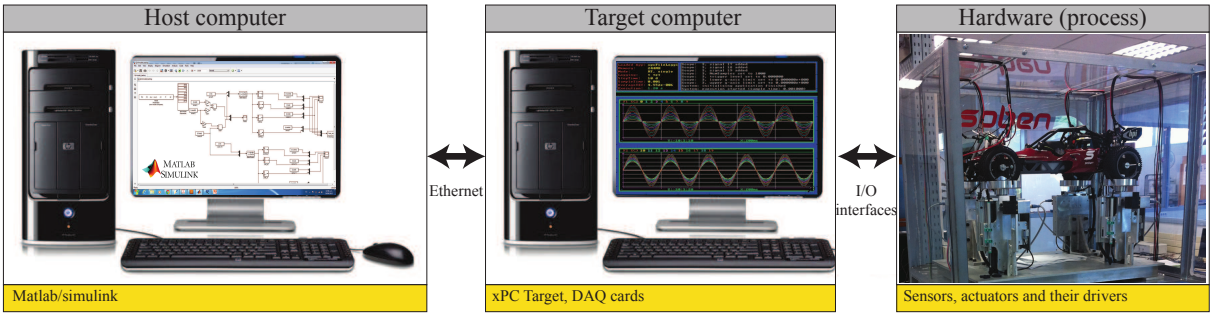

Figure 4.9: Experimental platform used to validate the proposed road profile estimation algorithm.

vehicle of 1:5 scale was developed by Soben™ in the context of the French national project INOVE ANR 2010 BLAN 0308. Fig. 4.10. The vehicle is equipped with *ER* dampers, one at each corner, and is fully instrumented to measure its vertical motion. Each corner has a DC motor to implement the road profile excitation, whose maximum height is 50 mm and the system can be verticaly excited by a mechanical system that simulates various road profiles excitations is controlled by a frequency variator.

Figure 4.10: Experimental vehicle of scale 1:5, developed in the context of the INOVE ANR 2010 BLAN 0308 project.

For simplicity, the road profile estimation algorithm is carried out on the rear-left QoV with the following available measurements: road profile z_r, unsprung mass position z_{us}, unsprung mass acceleration $\ddot{z}_{us}$, *ER* damping force F_{ER} and suspension deflection z_{def}.

4.7.1 Results of the road roughness estimation and classification

All the following results are performed on the INOVE platform.

4.7.1.1 Results using $\mathcal{H}_\infty$ observer

Based on the frequency and amplitude estimation of the road irregularities z_r, it is possible to define the type of ISO road profile on which the vehicle is driven. Indeed, Fig. 4.11 sums up the road roughness estimation and classification using strategy the $\mathcal{H}_\infty$ observer.
The following test is designed to evaluate the performance of the road estimation algorithm along a random road sequence among all ISO roads, by using the classification procedure.
A random sequence has a duration of 260 s at constant vehicle speed ($v_x = 30km/h$), i.e. around $2,167$ m of path is used.

Fig. 4.12A shows the estimation of the road signal obtained by the robust observer and compared to the measurement of the fully instrumented vehicle. The on-line roughness estimation, by considering the log operator is presented in Fig. 4.12B; the thresholds, which are online computed by using the limits of c_r for each road, are used to obtain the road classification result, Fig. 4.12C. In general, all roads are well classified with only some misclassifications among the neighbors roads. A 2 seconds time window is used to plot the PSD road roughness in order to have a softer estimation (blue solid line in Fig. 4.12B).

The efficiency of this classification can be also computed. Indeed, a ROC (Receiver Operating Characteristic) curve (see Fig. 4.13) is used to compute the probability of right classification of each road

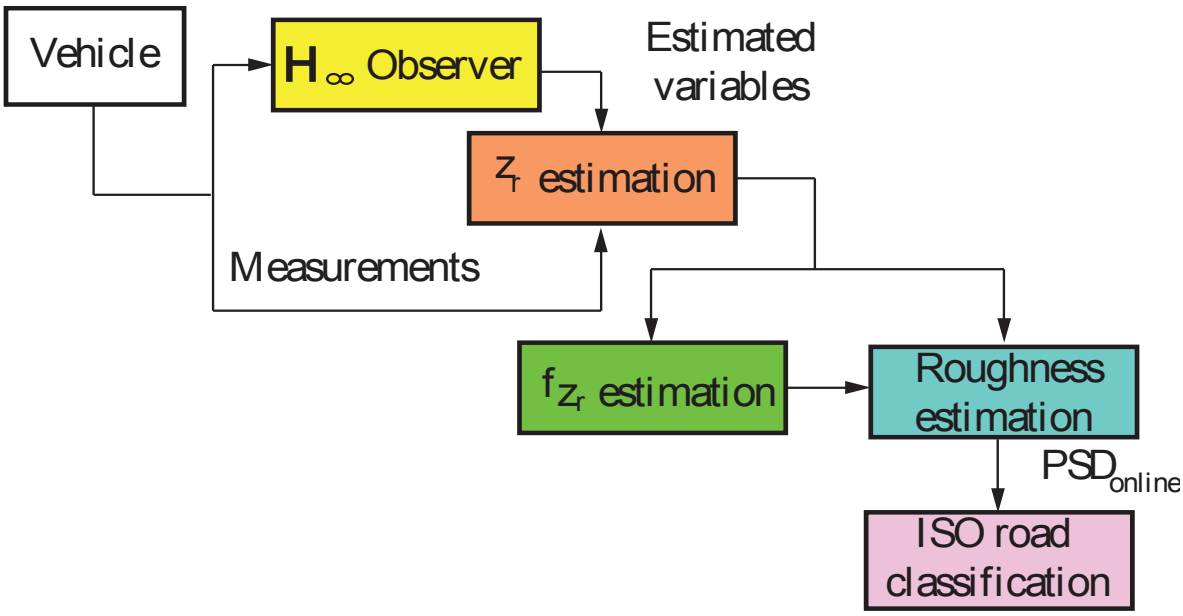

Figure 4.11: Road estimation and classification using the $\mathcal{H}_\infty$ observer.

profile, P_c, and its respective false alarm probability, P_f a.

Indeed, Fig. 4.13 shows that the identification results, for all ISO roads, are successful and the probability of correct identification is greater than 70% with minimal false alarm rate (lower than 5%).

Remark: A *ROC* curve is used to analyze the probability of right classification for each road profile, $P_c = TP/(TP + FN)$, and its respective false alarm probability, $P_{fa} = FP/(FP + TN)$. In this case, a True Positive (*TP*) is when the road class i occurs and is well classified and a False Negative (*FN*) is when this road is incorrectly identified as a road class j; inversely, a False Positive (*FP*) is when a road class j occurs but is classified as a road class i and a True Negative (*TN*) is when the road class i is correctly not classified because really occurs the road class j.

Then, the average error of classification can be computed as follows:

$$e = \sum_{i=1}^{r} P_i(\sum_{j \neq i} Q_{ij}). \tag{4.39}$$

where r is the number of classes of road, P_i is the probability of each road and Q_{ij} is the number of elements when the class of road i is incorrectly detected as a road j.

Table 4.4: ERROR OF CLASSIFICATION.

	Road profile					
	A	B	C	D	E	F
e (%)	0.48	4.57	4.55	4.39	1.23	2.24

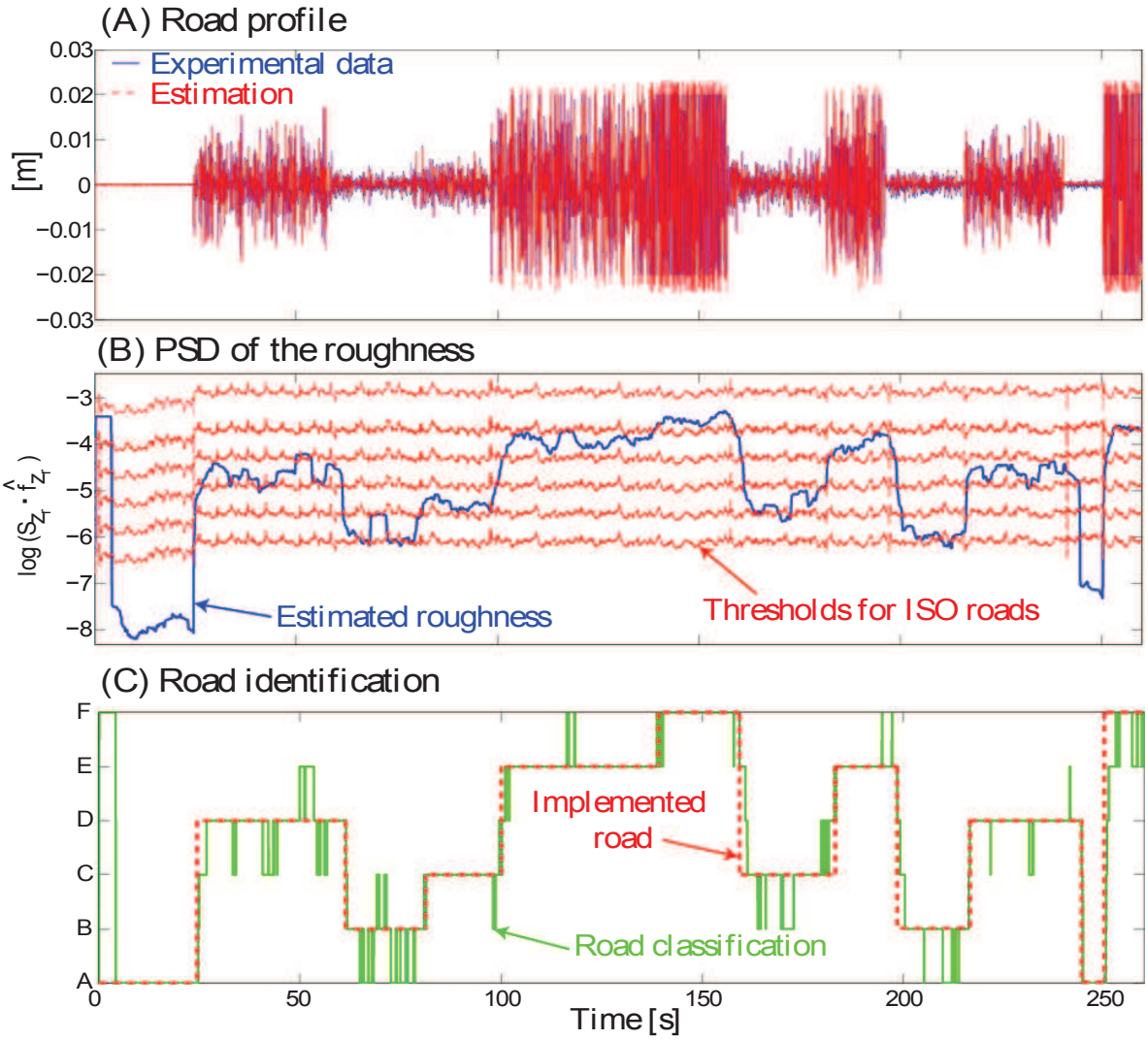

Figure 4.12: Results: implemented road sequence (A), on-line roughness estimation (B) and final result in the road identification algorithm (C).

Table. 4.4 shows that the roads B, C and D have the greatest error of identification, but this is less than 5%. Globally, all over the proposed test scenario, the error of classification did not exceed $e = 17.5\%$;

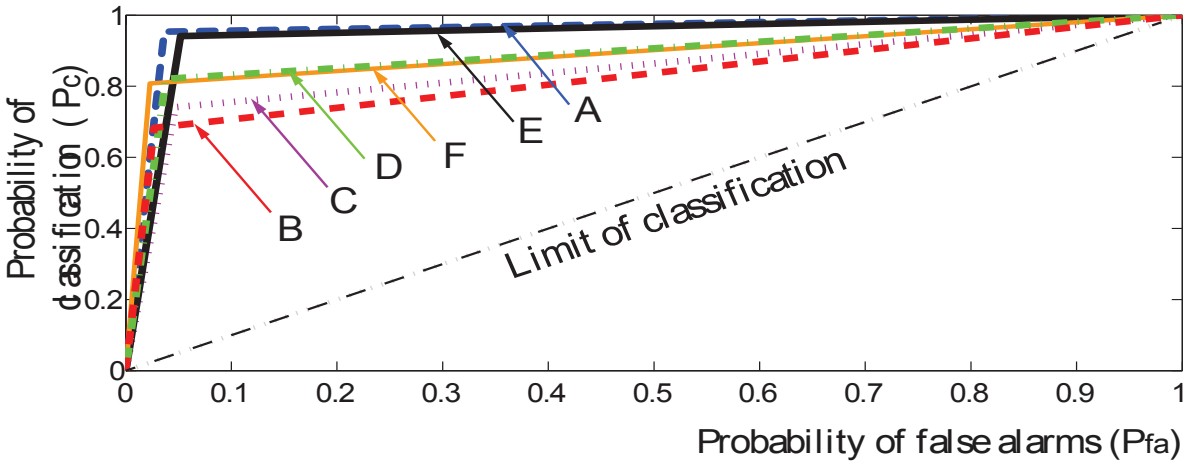

Figure 4.13: ROC curve for the classification of ISO road profiles.

4.7.1.2 Results using the algebraic observer

Fig.4.14 shows a summary of the the road roughness estimation and classification strategy using the algebraic observer.

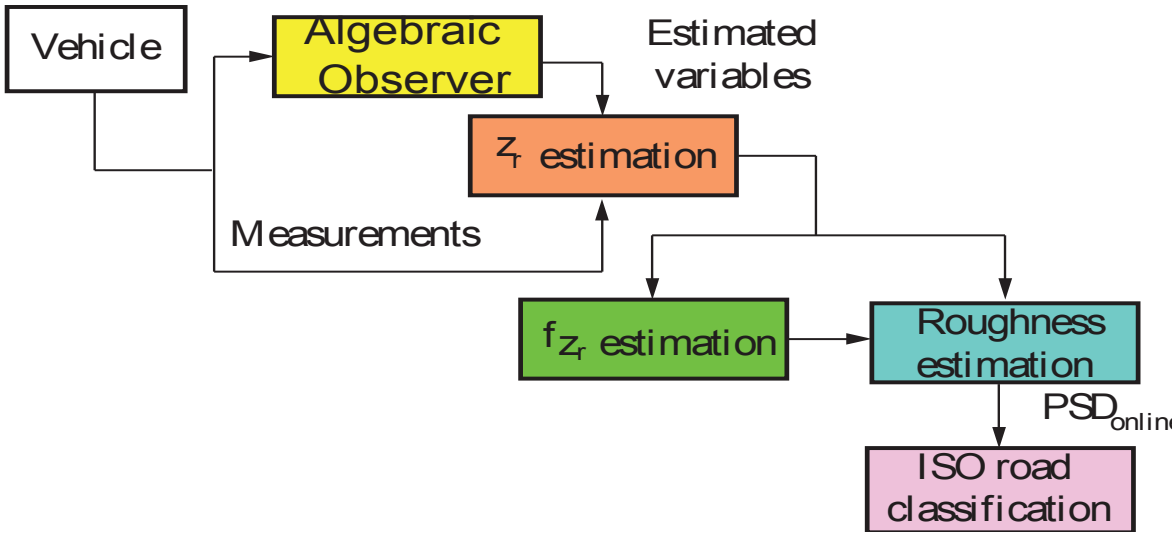

Figure 4.14: Road estimation and classification using the algebraic observer.

The efficiency of the algebraic observer can be seen trough Fig. 4.15. The road profile is well reconstructed and the frequency is well estimated.

Then, to evaluate the proposed road roughness estimation approach, a sequence of 120 s with various ISO roads was implemented at $v_x = 30\ Km/h$ (dashed line in Fig. 4.16.b).

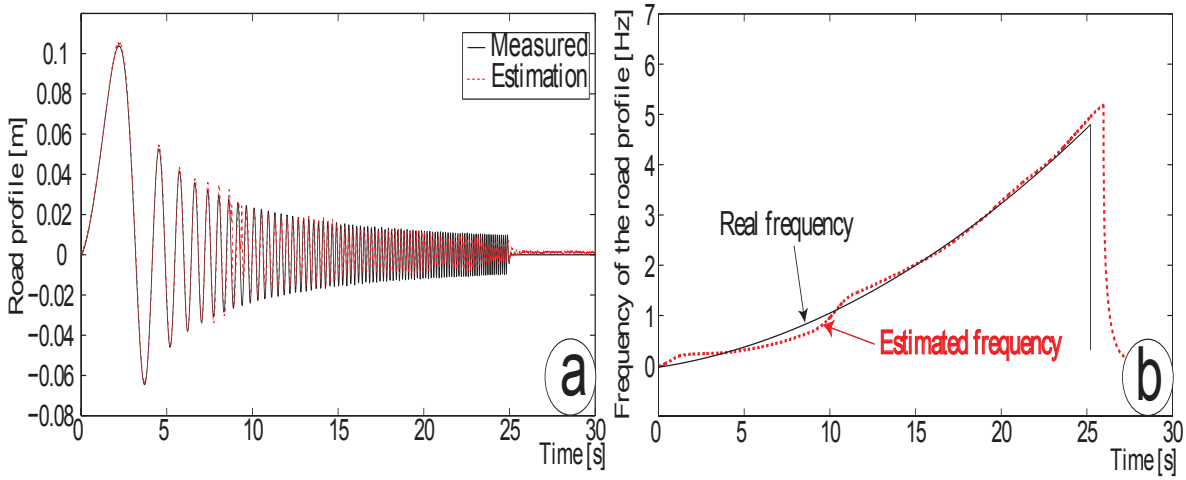

Figure 4.15: Algebraic Observer performances.

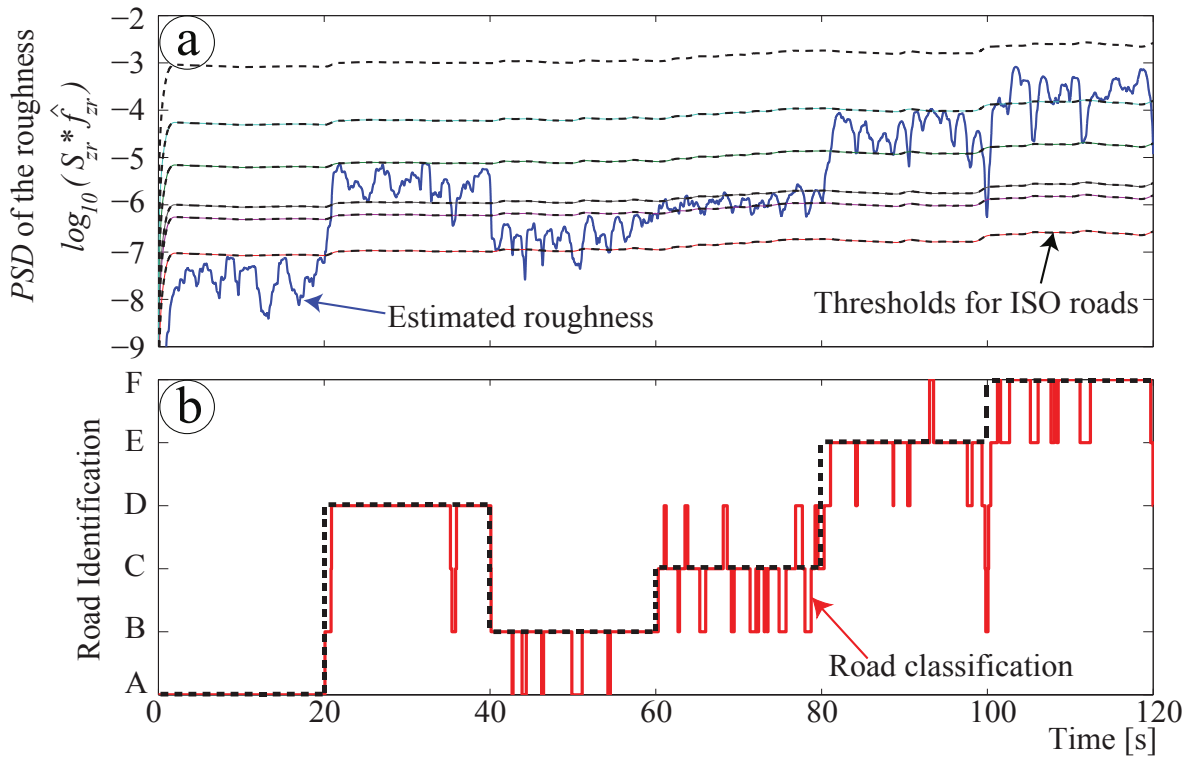

Figure 4.16: On-line roughness estimation and the road identification based on the algebraic observation.

Fig. 4.16.a shows the on-line roughness estimation, in a semi-log scale; additionally the thresholds, which are computed on-line by using the limits of c_r for each road, are used to obtain the road classification result, Fig. 4.16.b. The road type C is more complicated to detect because it has a lower operating zone between the thresholds.

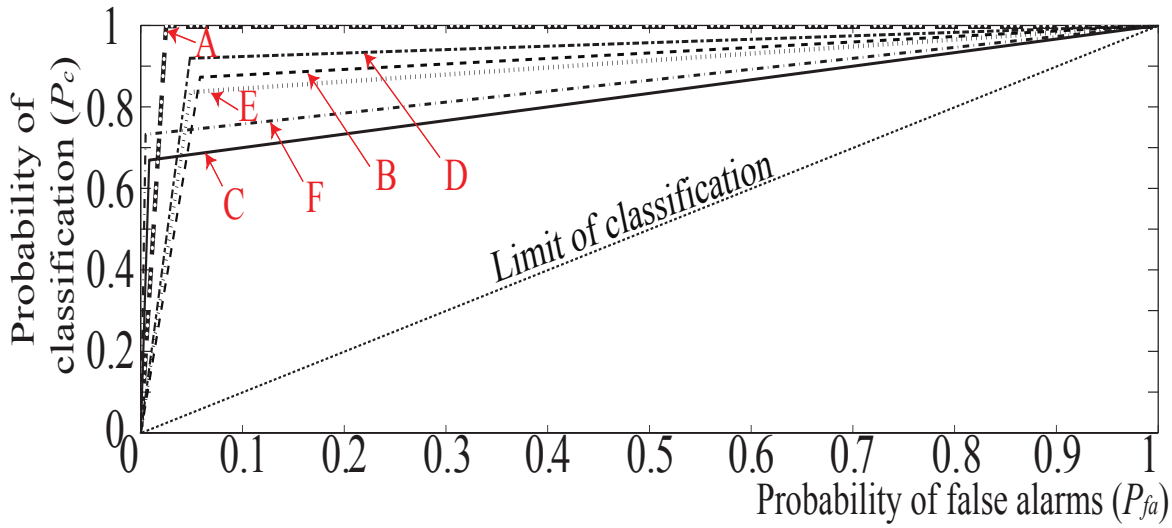

Figure 4.17: *ROC* curve for the classification of ISO road profiles.

Fig. 4.17 shows the *ROC* curve obtained by the proposed identification system of road profile. The detection result of the ISO roads A, B, D and E was successful, the probability of correct identification is greater than 80% with minimal false alarm rate (lower than 5%). Also, in the implemented test, $e = 14.1\%$, i.e. the road was well classified during 100 of 120 s.

4.7.1.3 Results using the Parametric Adaptive observation algorithm

To test the efficiency of the Parametric Adaptive observation algorithm, the following test was performed.
A random sequence of road profile disturbances at constant vehicle velocity is applied to the test bed. The random sequence has a duration of 260 s at constant vehicle velocity ($v_x = 30$ Km/h), i.e. representing around 2,167 m of path; the suspension system is semi-active with a constant damping (without controller). Figure 4.18a illustrates the road estimation result; the circles show a close up of the Q-parametrization performance at different ISO roads, in all cases the estimation follows the experimental road signal, used as a reference.

Remark: This test allows the evaluation of the Q-parametrization to adapt the disturbance estimation along a random road sequence among different ISO roads.

Figure 4.18b displays the online adaptation of the parameter vector Q. Note in this plot that, at the beginning of the adaptive algorithm (during the road type A), the parameters converge almost to the same value; then, all parameters are adapted again and dispersed when the vehicle passes on a rougher road (type D). Afterwards the parameter vector maintains almost constant values because the next roads are less rough than the road D. When the vehicle is driven on the road E at $t = 100$ s, the parameters are adapted again with more dispersion and much more even when the road F is present at $t = 138$ s. From $t = 160$ to 250 s, the path is less rough than the road F and consequently the current parameter vector Q can estimate correctly these disturbances without a readaptation. Finally, when

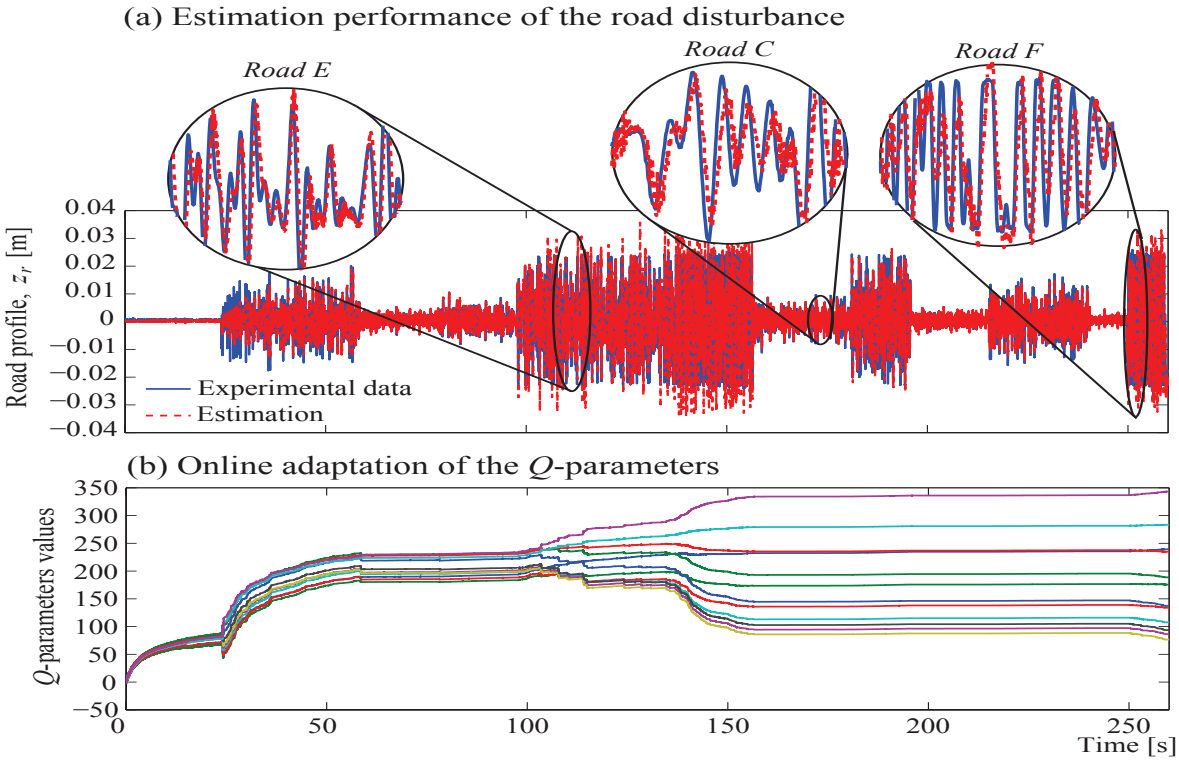

Figure 4.18: Road disturbance estimation with the Q-parametrization, when z_r is a random sequence with various ISO road profiles, and the car goes at constant velocity with medium damping in the *ER* damper.

occurs again the road F, at $t = 250$ s, the parameters are slightly modified.

Then, the road roughness estimation and classification corresponding to this scenario are the following. By using the estimated road signal, illustrated in Fig. 4.18a, and its frequency estimation, the on-line road roughness estimation outcome is presented in Fig. 4.19 in a semi-log scale on $S_{z_r} \times \hat{f}_{z_r}$; additionally the thresholds $S_{z_{r_{TH}}}$, which are computed online by using the limits of c_r for each road, eq. (4.38), are used to obtain the road classification result displayed in Fig. 4.19b. The computation of the *PSD* road roughness uses the *RMS* value of $\hat{A}_{z_r}(k)$ in a time window of 1 s in order to have a softer road identification outcome (blue solid line in Fig. 4.19a).

Figure 4.19b shows qualitatively that in general, all roads are well classified only with some misclassifications among the neighbors roads. In order to determine a quantitative performance, each road was studied individually by a binary classifier system (i.e. a two-class classification problem: positive or negative result). Figure 4.20 illustrates the basic concept of a *confusion matrix* used to determine the evaluation metrics of the road classifier.

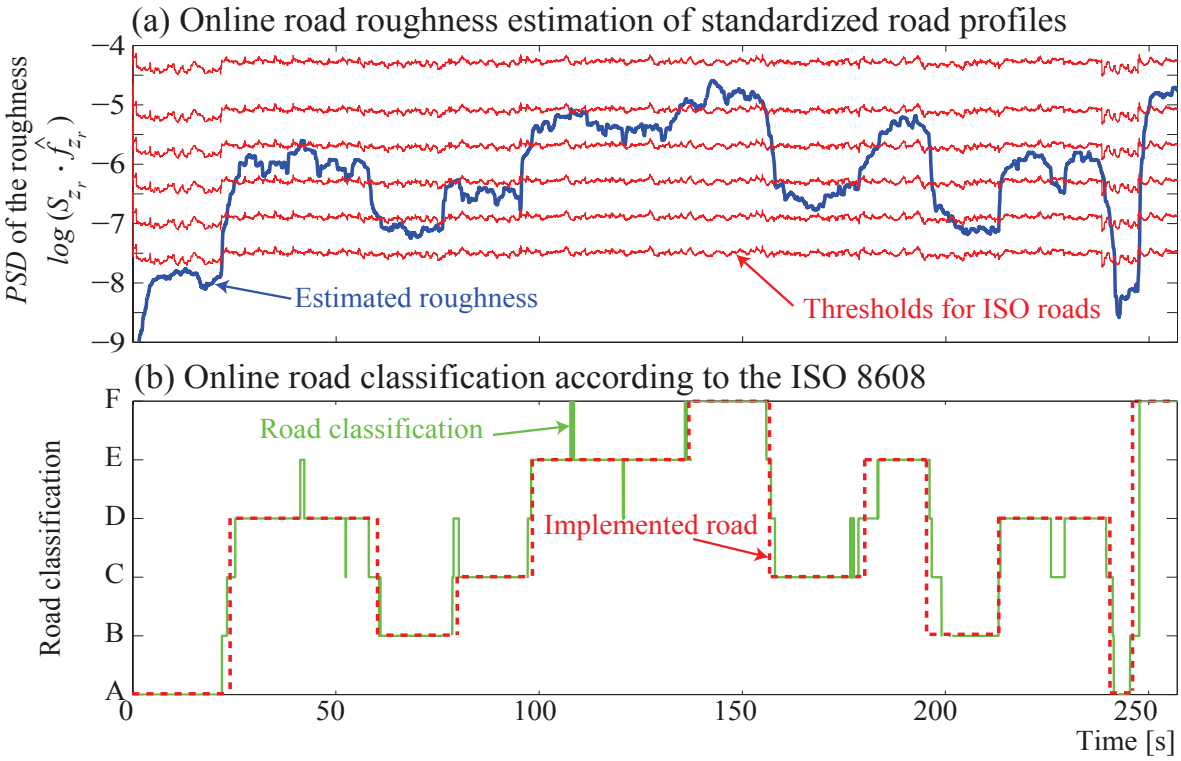

Figure 4.19: Online estimation of road roughness, and classification outcome.

		Real condition (Reference)		
		Condition positive	Condition negative	
Test Outcome	Positive	*TP*	*FP* (Type I error)	*Positive Precision* *TP/(TP + FP)*
	Negative	*FN* (Type II error)	*TN*	*Negative Precision* *TN/(FN + TN)*
		Sensitivity *Pc=TP/(TP + FN)*	*Specificity* *Pfa=FP/(FP + TN)*	*Accuracy* *(TP+TN)/(P+N)*

Figure 4.20: Confusion matrix of the test outcome of a classifier.

where, for each road class, there exist four classification outcome states as previously defined: (*TP*), (*FP*), (*FN*), (*TN*).

By using these outcome states, it is possible to determine the stronger metrics of a classifier: (1) the *sensitivity degree* of the classifier for each road, i.e. the probability of correct classification P_c, (2) the *specificity degree* associated to the probability of false alarm P_{fa}, and the *accuracy degree* that quantifies the general performance of the classifier. When plotting the sensitivity vs specificity degree, named the *Receiver Operating Characteristic* (*ROC*) curve, it is possible to quantify the performance of the classifier; the best possible result of classification generates a point in the upper left corner or coordinate (0,1) of the *ROC* space, representing 100% sensitivity (no False Negatives) and 100% specificity (no False Positives).

With the use of the confusion matrix was built the probability P_c and P_{fa} were determined for each ISO road profile, then it was built the *ROC* space in the classifier. Figure 4.21 shows that the classification outcome for all ISO roads was successful, all points are above the diagonal which represents a random outcome. Indeed, the classification outcome for all roads presents a probability of correct classification greater than 70% with minimal false alarm rate (P_{fa} lower than 8%). Table 4.5 shows that the accuracy degree of the classifier, in general, is greater than 90% for all road types. Notice that the types A and F roads are the easiest to classify.

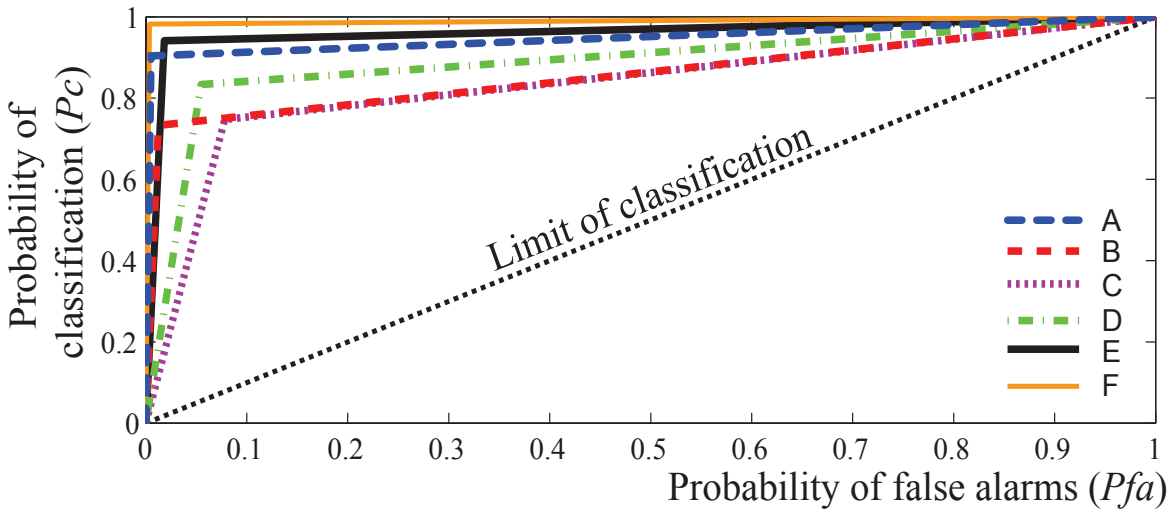

Figure 4.21: *ROC* curve for the classification of ISO 8608 road profiles.

Table 4.5: Accuracy degree of the classification outcome.

	Road profile					
	A	B	C	D	E	F
Accuracy degree (%)	98.7	94.7	90.5	90.8	96.6	99.5

4.8 Conclusion

In this chapter, 3 different road profile estimation and identification methods approaches are developed. These strategies were successfully implemented on the test bed developed in Gipsa-lab within ANR INOVE project (see chapter. 1.2). The experimental results show the efficiency and the accuracy of these approaches for the road roughness estimation and identification.
In the sequel, the road roughness estimation will be used to develop adaptive suspension controllers to achieve the desired performance objectives.

CHAPTER 5

LPV/$\mathcal{H}_\infty$ Road profile Adaptation control: application to the ground vehicle Renault Megane coupe

5.1 Introduction

Some researches have shown that the roughness estimation of the road surface can be used in an active or semi-active suspension control system to improve the comfort and handling stability of a car, [(Hong *et al.*, 2002), (Kim *et al.*, 2002), (Fialho and Balas, 2002)]. However, in these adaptive suspension systems, there is no integrated approach where the road roughness estimation and control strategies are developed in a single control objective.

In road adaptive suspension control, an extension to the *Sky-Hook* controller with adaptation to the road profile is proposed in (Hong *et al.*, 2002). The road estimator is based on the Fourier transform of the road profile signal where the fundamental frequency is constant, i.e. an online estimation of the frequency of motion, which depends on the vehicle velocity, is not used. Moreover, the road estimation is based on conventional filtering and the control strategy does not ensure the continuous and saturated actuation of the semi-active damper. In (Kim *et al.*, 2002) an active suspension controller with road adaptation is proposed: the road-sensing system uses two laser height-meters which are susceptible to be contaminated; additionally, if their location is not good, the controller performance could be deteriorated. An interesting Linear Parameter-Varying (*LPV*) controller with road adaptation is proposed in (Fialho and Balas, 2002) where the roughness is used as a scheduling parameter in order to design the controller; however, it is assumed to have an available signal of the road roughness (estimated or measured).
Very recently, car manufacturers have tried to develop a road adaptive suspension systems. FOr instance, Mercedes-Benz started the first world's first suspension system with eyes called *Magic body control* in 2014. It consists in using an embedded stereo camera that scans the road to detect different road unevenness in advance and then to adapt the suspension control to provide more passengers comfort. While this technic is very expensive since it uses cameras and image data processing, here, the proposed strategy uses data coming from sensors available in most of the commercial cars. Also, the LPV framework allows a better on line adaptation of the suspension control to the road profile.

In this chapter two LPV/$\mathcal{H}_\infty$ controllers, based on the previously detailed estimation strategies in chapter. 4, are developed:

- The first one is a new road LPV adaptive semi-active suspension controller for a quarter vehicle based on robust observer estimation of the road profile. This work was achieved in collaboration with colleagues from Tec Monterrey in Mexico (J.C. Tudon Matinez and Rubben Morales Mendez). This collaboration has led to the following publication in (Tudon-Martinez *et al.*, 2013*b*) and a future journal publication.

- The second one is a new LPV/$\mathcal{H}_\infty$ semi-active suspension control strategy with performance adaptation to roll behavior for the full vehicle, based on a non linear algebraic road profile estimation. This work was achieved in collaboration with colleagues from Mines-Paristech (Lghani Menhour and Brijitte D'Andréa Novel). It has led to the following publication in (Fergani *et al.*, 2014*a*) and a future journal article.

Here, one of the main contributions is that the road control adaptation is ensured using only the commonly available sensors on the commercial cars. This allows to reach better performances at a lower cost.

5.2 Road Adaptive Semi-Active Suspension for $1/4$ vehicle using an LPV/$\mathcal{H}_\infty$ Controller

In this section, a novel road adaptive Linear Parameter-Varying (*LPV*) based controller for the semi-active suspension system of an automotive vehicle is proposed. The analysis is carried on the front-left Quarter of Vehicle (*QoV*) model generated via CarSim^{TM} vehicle simulator. By using an on-line road roughness estimation, considered as a scheduling parameter, the proposed $LPV/\mathcal{H}_\infty$ controller is designed to improve comfort and road holding.

5.2.1 Problem statement

A customized vehicle model obtained by experimental data on a pick up truck in collaboration with Tech Monterrey is used as a test-bed for this work. The dynamics of this $1/4$ pick up is generated via CarSim^{TM} vehicle simulator. The analysis is carried on the front-left corner on the considered car. The system considers a sprung mass ($m_s = 470\ Kg$) and an unsprung mass ($m_{us} = 110\ Kg$). A spring with stiffness coefficient k_s ($86,378\ N/m$) and a Magneto-Rheological (*MR*) damper model represent the suspension between both masses. The stiffness coefficient k_t ($270,000\ N/m$) models the wheel tire. The vertical position of the mass m_s (m_{us}) is defined by z_s (z_{us}), while z_r corresponds to the unknown road profile.
This *QoV* is considered to be equipped with a Magneto-Rheological semi active damper. Indeed, as previously presented in subsection 3.3.1, the spring is considered as linear because around 95% of its operating zone in an automotive application is linear; however, the semi-active damping force (F_{MR}) depends on an electric current value and is highly nonlinear with respect to the suspension motion.

Experimental data obtained from a commercial *MR* damper are used to model the nonlinearities of this actuator by using (7.21) (for more details about the MR dampers see (Jorge De-J *et al.*, 2012)). This strategy is developed among the LPV *Qov* model (for more details see 3.3.1).

The used model is based on measurements related to the comfort and road holding performances,(the accelerometers of the sprung ($\ddot{z}_s$) and unsprung mass ($\ddot{z}_{us}$)) that depend on the semi-active damper properties and obviously on the road irregularities.
The main objective of this work is to design a road adaptive *LPV* controller Based on the road roughness and the profile estimation strategy (see chapter. 4) using an $\mathcal{H}_\infty$ observer for the semi-active suspension system of an automotive vehicle by including the non-linearities of the actuator into the *QoV* model (see 3.3.1), such that:

$$\begin{aligned} \dot{x} &= \mathcal{A}(\rho)\cdot x + \mathcal{B}\cdot u \\ y &= \mathcal{C}\cdot x + \mathcal{D}\cdot u \\ u &= \mathcal{K}(\rho)\cdot x \end{aligned} \tag{5.1}$$

which $\mathcal{K}(\rho) = \sum_{i=1}^{N} \xi_i(\rho)\mathcal{K}_i = \sum_{i=1}^{N} \xi_i(\rho) \begin{bmatrix} Ac_i & Bc_i \\ Cc_i & Dc_i \end{bmatrix}$ by appropriately choosing the gains $\mathcal{K}_i$, $i = 1, \ldots, N$ such that the closed-loop system (5.1) be asymptotically stable for all parameter variations.

Since three varying parameters are used in the *LPV* control design : ρ_1 and ρ_2 represent the actuator constraints and ρ_3 monitors on-line the road quality (roughness estimation as presented in the previous chapter. 4), then $N = 8$ vertices have to be considered.

5.2.2 Semi-Active Suspension Control Synthesis

By considering the vertical dynamics in a *QoV* model, eq. (7.22), the *MR* damping force is the key element to attenuate vibrations caused by road irregularities and to ensure good road holding. By using the parametric model of (Guo *et al.*, 2006*a*), it is possible to represent the non-linear dynamics of the semi-active damper as a scheduling parameter and to include it in the *LPV* control design, (see (Do *et al.*, 2012*b*) and (Anh lam, 2011)).

5.2.2.1 Recall on the LPV *QoV* model formulation

Let us recall the *QoV LPV* model considered in this section:

$$\begin{cases} \dot{x}_{_{lpv}} = A_{_{lpv}}(\rho_1, \rho_2)\, x_{_{lpv}} + B_1 u_c + B_2 w \\ y_{_{lpv}} = C_1 x_{_{lpv}} \end{cases} \tag{5.2}$$

where

$$x_{_{lpv}} = \begin{pmatrix} x_s \\ x_f \end{pmatrix}^T, A_{_{lpv}}(\rho_1, \rho_2) = \begin{pmatrix} A_s + \rho_2 B_{s1} C_{s1} & \rho_1 B_s C_f \\ 0 & A_f \end{pmatrix},$$

$$B_1 = \begin{pmatrix} 0 \\ B_f \end{pmatrix}, B_2 = \begin{pmatrix} B_{s1} \\ 0 \end{pmatrix}, C_1 = \begin{pmatrix} C_s \\ 0 \end{pmatrix}^T$$

$$C_s = \begin{bmatrix} 1 & 0 & -1 & 0 \\ 0 & 1 & 0 & -1 \end{bmatrix}$$

$$C_{s1} = (k_1\ C_1\ -k_1\ -C_1)$$

$$B_{s1} = (0\ \tfrac{-f_0}{m_s}\ 0\ \tfrac{-f_0}{m_s})$$

$$\rho_1 = \tanh(C_{s1}x_s)\tanh(\tfrac{C_f x_f}{F_1})\tfrac{F_1}{C_f x_f}, \rho_2 = \tfrac{\tanh(C_{s1}x_s)}{C_{s2}x_s}$$

$x_s = (z_s, \dot{z}_s, z_{us}, \dot{z}_{us})$, A_s, B_s, B_{s1}, B_{s2}, C_s and C_{s2} are the state and matrices of a state-space representation of the *QoV* model by including the *MR* damper model in (7.22), $w = z_r$ and considering z_{def} and $\dot{z}_{def}$ as the output; x_f, A_f, B_f, C_f are the state and matrices of a representation of the low-pass filter $W_{filter} = \omega_f/(s + \omega_f)$ which is added to the system to make the control input matrices parameter independent. Let us recal that all the parameters (f_0, m_s...) are defined in 7.22.

Remark: This model is obtained, based on the non linear equations (see subsection3.3.1 and Eq.3.7), after some mathematical transformations as in (Do *et al.*, 2012*b*). It is a control oriented *LPV* model considering an input saturation u_c provided with two scheduling parameters ρ_1 and ρ_2.

5.2.2.2 LPV/$\mathcal{H}_\infty$ control synthesis

The main contribution of this part is the use of a varying parameter (ρ_3) that schedules the suspension actuator work according to a new road estimation strategy. Indeed, depending on the value of the road roughness, the suspension control is adapted to meet the required performances. This scheduling parameter is included in the *LPV* control synthesis shown in Fig 5.1. The weighting functions are designed as:

- $W_{filter} = \omega_f/(s+\omega_f)$, with a large bandwidth to decouple the input and the varying parameters;
- $W_{\ddot{z}_s} = k_{\ddot{z}_s} \frac{s^2+2\zeta_{11}\omega_{11}s+{\omega_{11}}^2}{s^2+2\zeta_{12}\omega_{12}s+{\omega_{12}}^2}$, to account for passengers comfort at low frequencies;
- $W_{z_{us}} = k_{z_{us}} \frac{s^2+2\zeta_{21}\omega_{21}s+{\omega_{21}}^2}{s^2+2\zeta_{22}\omega_{22}s+{\omega_{22}}^2}$, to account for road holding at high frequencies;
- $W_{z_r} = 5 \times \rho_3 \times 10^{-2}$, is the road profile gain scheduled by the road roughness estimation to adapt the control synthesis.

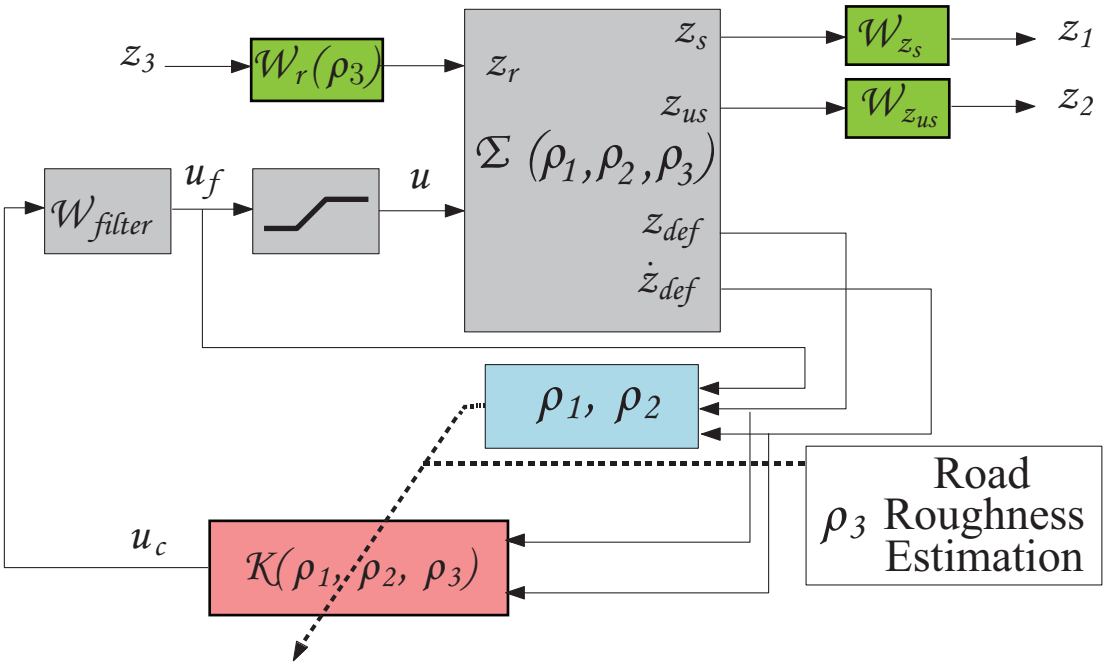

Figure 5.1: Suspension control implementation scheme.

The parameters of these weighting functions are obtained by genetic algorithms, as explained in (Do *et al.*, 2012*b*). Thus, the corresponding generalized plant is a 3 linear parameter depending system as follows:

$$\Sigma_{gv}(\rho_1,\rho_2,\rho_3) := \begin{cases} \dot{\xi} = A(\rho_1,\rho_2,\rho_3)\xi + B_1 u + B_2\tilde{w} \\ \tilde{z} = \tilde{C}_1\xi + D_{11}u + D_{12}\tilde{w} \\ y = \tilde{C}_2\xi + D_{21}u + D_{22}\tilde{w} \end{cases} \tag{5.3}$$

where $\xi = [\chi_{vert}\ \chi_w]^T$; $\tilde{z} = [z_1\ z_2\ z_3]^T$; $\tilde{w} = z_r$; $y = [z_{def}\ \dot{z}_{def}]^T$; $u = u_{ij}^{\mathcal{H}_\infty}$; χ_{vert} is the state vector in the vertical dynamics of the *QoV* model and χ_w is the vertical weighting functions state vector.

5.2.2.3 Scheduling parameters

In this part, both the considered *QoV* model for synthesis and the controller are parameters dependent; ρ_1 and ρ_2 allow to ensure that the suspension control respects the *MR* damper constraints and input saturation.

The varying parameter ρ_3 allows an on-line adaptation of the semi-active suspension system to road profiles (see chapter. 4) and is defined by:

$$\rho_3 = K_{\rho_3} \cdot S_{z_r}(f_{z_r}) \quad \in \quad [0,1] \tag{5.4}$$

where K_{ρ_3} is used to bound ρ_3, such that

$$I(\rho_3) := \begin{cases} I = I_{max} & if \quad \rho_3 \geq \overline{\rho_3} \\ I_{min} < I < I_{max} & if \quad \underline{\rho_3} < \rho_3 < \overline{\rho_3} \\ I = I_{min} & if \quad \rho_3 \leq \underline{\rho_3} \end{cases} \tag{5.5}$$

The main idea of this road adaptive control strategy is to provide a good on-line trade-off between road holding and passengers comfort, which are conflicting objectives, such that:

- When ρ_3 is high, the road roughness is high, and the semi-active damper is tuned to be *"harder"* ($u^{\mathcal{H}_\infty} \rightarrow I_{max}$) in order to improve the car road holding and to guarantee the vehicle safety at high velocities or comfort at low velocities.

- Conversely, when ρ_3 is low, the road roughness is low, and the *MR* damper is set to be *"softer"* to enhance comfort at low velocities or road holding at high velocities.

- Considering a varying parameter related to the road roughness in the LPV strategy allows to adapt the suspension damping characteristics to the road conditions.

Indeed, the proposed LPV/$\mathcal{H}_\infty$ control strategy allows to provide an innovative and a reliable solution to the road adaptive suspension control problem. Let us give some of this control design strategy specifications:

- The proposed *LPV/*$\mathcal{H}_\infty$ robust controller is synthesized by using *LMIs* solution for polytopic systems; all varying parameters are considered bounded: $\rho_1 \in [-1,1]$, $\rho_2 \in [0,1]$ and $\rho_3 \in [0,1]$.

- In this work, since 3 varying parameters are used, the considered polytope has 8 vertices (8 local controllers, more details on *LPV* robust control design in (Scherer *et al.*, 1997)).

5.2.3 Simulation Results

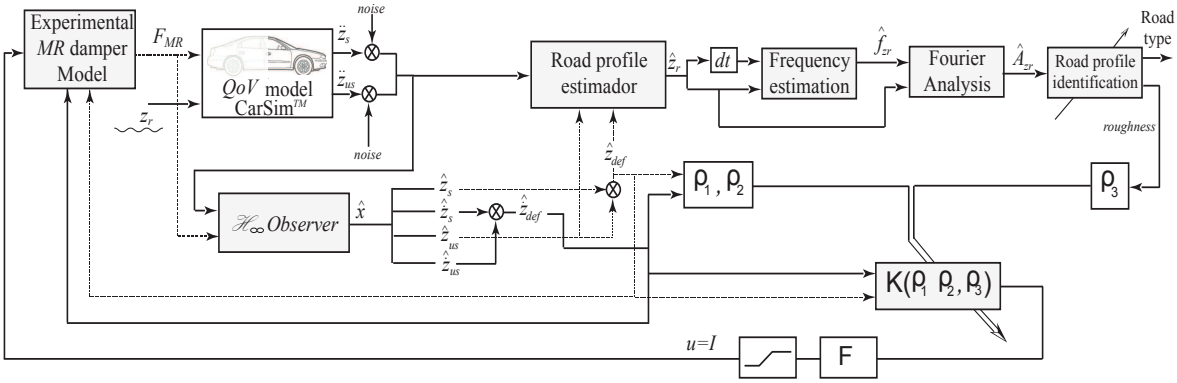

Figure 5.2: Block diagram of the proposed road adaptive semi-active suspension control system.

Figure 5.2 shows the block diagram of the proposed road adaptive semi-active suspension control system. The estimated states of the $\mathcal{H}_\infty$ observer are used in the proposed road estimation algorithm (see chapter. 4) and are also the controller inputs.
Table 5.1 shows the parameters used to guarantee the performance specifications of the designed *LPV*/$\mathcal{H}_\infty$ controller. Some simulation results in the time domain are presented to emphasize the interest of the proposed road adaptive *LPV* controller.

$k_{\ddot{z}_s}$	10	ζ_{12}	1	ω_{11}	6.3 rad/s	ω_{22}	56.5 rad/s
$k_{z_u s}$	1	ζ_{21}	0.3	ω_{12}	19 rad/s	ω_f	90 rad/s
ζ_{11}	0.3	ζ_{22}	1	ω_{21}	56.5 rad/s		

Table 5.1: $LPV/\mathcal{H}_\infty$ controller parameters.

To prove the efficiency of this strategy, two driving scenarios are considered:

5.2.3.1 Scenario 1: ISO road F at $v_x = 30\ Km/h$.

In this test, since the vehicle runs at low velocity on a plowed field (ISO road F), the suspension displacement increases considerably and the passengers comfort is deteriorated. Then, a comfort performance oriented suspension control is necessary to enhance the ride comfort of the passengers. Indeed, the controller performances for comfort (sprung mass acceleration) and road holding (unsprung mass displacement) are depicted in Fig. 5.3. The results show that:

1. The road adaptive controller reduces considerably the magnitude of oscillations of the sprung mass acceleration in the *QoV*, Fig. 5.3a, the improvement of comfort according to the *RMS* value of $\ddot{z}_s$ is 35.8% (reduction of 6.5 m/s^2);

2. The road holding index (z_{us}) is also reduced with the road adaptive semi-active suspension; the reduction of motion in the tire is 11.8% (8.1 mm), Fig. 5.3b.

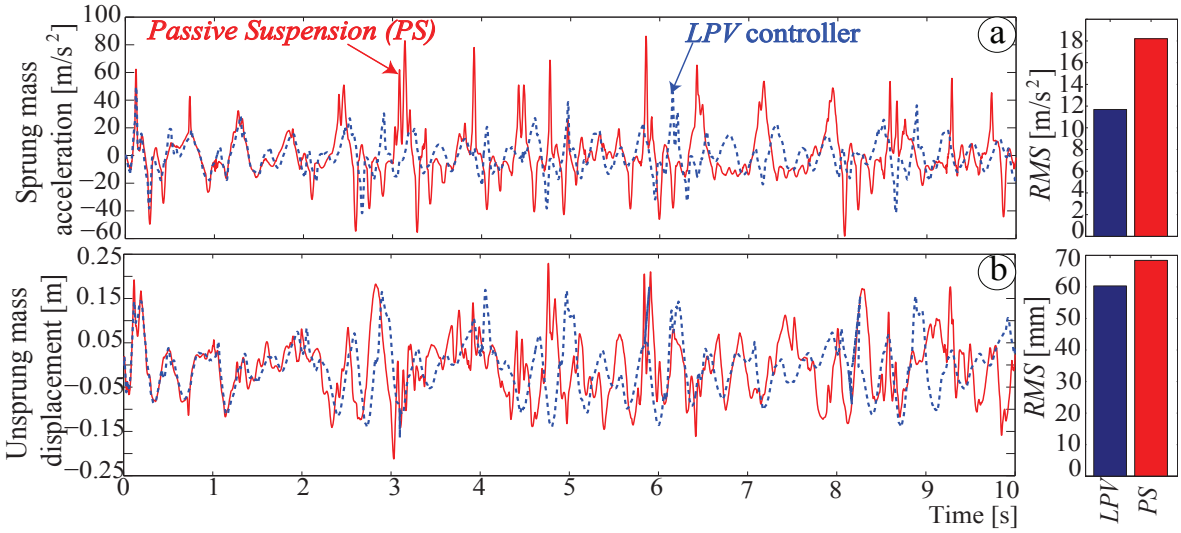

Figure 5.3: Performance of the road adaptive *LPV* controller compared to an uncontrolled damper (*passive*), by using test 1.

5.2.3.2 Scenario 2: ISO road A at $v_x = 100\ Km/h$.

For this scenario, the vehicle is driven at high velocities on highways, minimal road disturbances could affect the vehicle stability; thus, it is critical to increase the road holding index. Figure 5.4 shows the controller performance with respect to the *passive* suspension system. The results show that:

1. The unsprung mass displacement is reduced up to 6 mm by using the road adaptive controller, i.e. the vehicle stability is increased of 50% according to the *RMS* value of z_{us}, Fig. 5.4b;

2. The comfort performance is practically the same in both suspension systems, Fig. 5.4a .

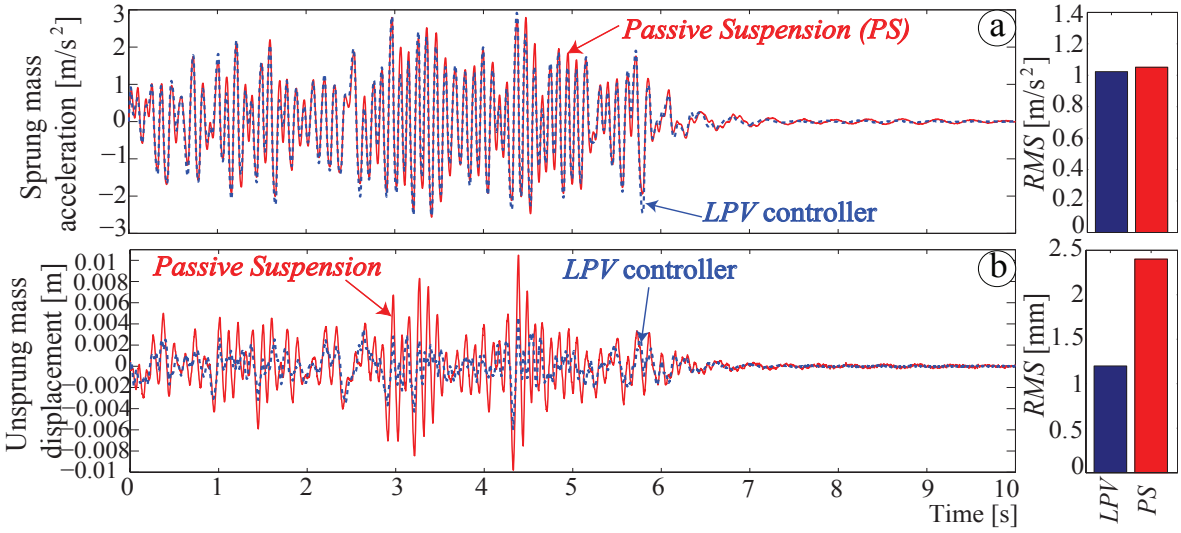

Figure 5.4: Performance of the road adaptive *LPV* controller compared to an uncontrolled damper passive), scenarios 2.

Thus, both tests confirm the efficiency of the proposed road adaptive *LPV* controller to manage the trade-off between comfort and road holding of an automotive suspension system equipped with an *MR* damper.

5.2.4 Concluding remarks

A novel road adaptive controller for the semi-active suspension system of an automotive vehicle is proposed. The front-left Quarter of Vehicle (*QoV*) model is used to evaluate the controller by using the CarSim^{TM} vehicle simulator. The control law is scheduled/adapted by using a Linear Parameter-Varying (*LPV*) based controller. Three scheduling parameters are used in the *LPV* control design, two linked to the nonlinearities and saturation of the actuator and one more for the road adaptation. A comparison between the road adaptive controller for the *MR* damper and an uncontrolled damper (*passive* suspension) shows the effectiveness of the proposed semi-active suspension control system to manage the trade-off between comfort and road holding.

Simulation results show that the road adaptive controller improves the comfort (35.8%) when the vehicle is driven on a road of bad quality at 30 Km/h while, when the vehicle is driven on a smooth runway at 100 Km/h, the road holding is improved, i.e. the unsprung mass displacement is reduced up to 6 mm (the vehicle stability is increased).

5.3 A new LPV/$\mathcal{H}_\infty$ semi-active suspension control strategy for the full car with performance adaptation to roll behavior based on a non linear algebraic road profile estimation

This section presents a new LPV/$\mathcal{H}_\infty$ semi-active suspension control strategy for a commercial vehicle equipped with 4 Magneto-Rheological dampers. The proposed approach concerns the road

adaptation using on-line road profile identification based on a non linear algebraic observer with unknown input. Then, a suspension forces distribution at each corner of vehicle is performed depending on the roll dynamics. In this LPV/$\mathcal{H}_\infty$ strategy, 2 varying parameters are used to model the semi-active behaviour of the MR dampers, and 2 other ones, namely, the road roughness identification and roll dynamics, are considered for the road adaptation and the full vehicle vertical dynamics control.

5.3.1 LPV/$\mathcal{H}_\infty$ Semi-Active Suspension Controller synthesis

The distribution of the suspension forces is performed using the evaluation of the load transfer, given by the roll dynamics, as a varying parameter in the road adaptation control strategy. This strategy is also based on the road profile estimation given by the non linear algebraic observer with unknown input.

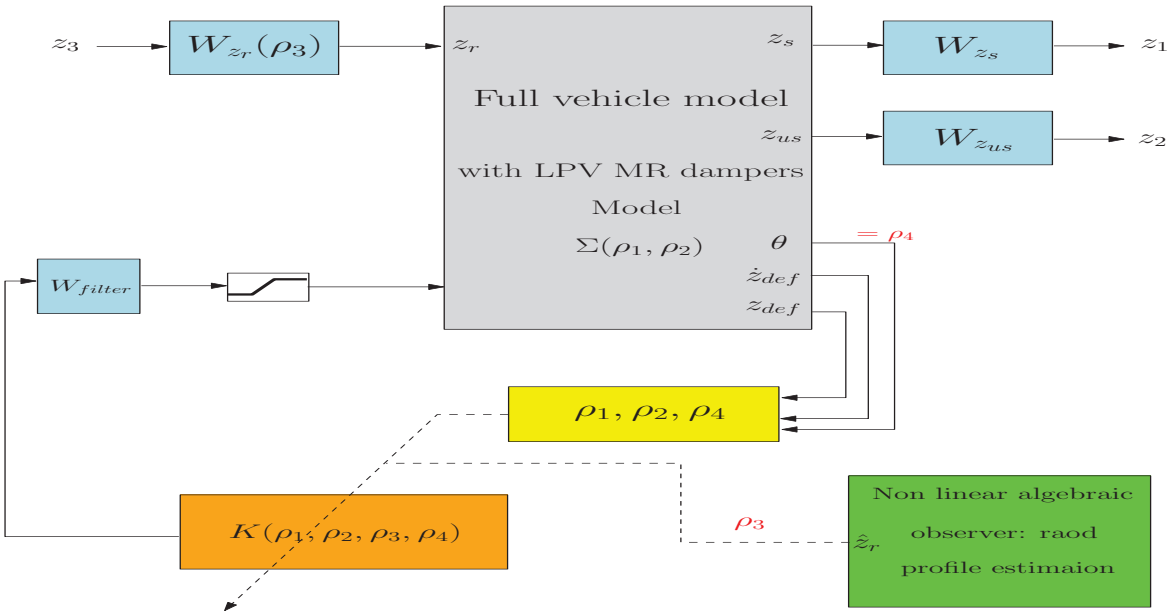

Figure 5.5: Suspension control design scheme.

As previously presented in 5.2.2.1, the considered model of the damper at each one of the four corner of the vehicle is an LPV Model.
The main contribution in this section compared to the previous one, beside the use of the full vehicle in the strategy, is the use of 2 new varying parameters in the control synthesis, in addition to the 2 parameters ρ_1, ρ_2 representing the damper non linearities.

The first one (ρ_3) (see Fig. 4.12) schedules the suspension actuator work according to a new algebraic road estimation strategy, as shown in Fig. 5.5. Indeed, depending on the value of the road roughness, the suspension control is adapted to meet the required performances as in the previous section (see section 5.2.2.3).

The second one is strictly dedicated to the roll dynamics $\rho_4 = \theta$ (see 5.13) to schedule the distribution of the left & right suspensions to the four corners of the vehicle. Moreover, the suspension

dampers smoothly, thanks to the LPV frame work, from "soft" to "hard" to improve the car performances according to the driving situation.

The varying parameter ρ_4 ensures the accurate distribution of the suspension forces, based on the load distribution of the vehicle. Here, left & right load transfer is considered. To ensure this distribution, the roll dynamics are used to schedule the semi-active suspensions effort ($\rho_4 = \theta$). This will alow to optimise the use of the different suspensions actuators to enhance vertical car's dynamics.

5.3.2 Suspension Control synthesis

Thus, the corresponding generalized plant (see Fig. 5.5) is a 3 linear parameter depending system as follows:

$$\Sigma_{gv}(\rho_1, \rho_2, \rho_3) := \begin{cases} \dot{\xi} = A(\rho_1, \rho_2, \rho_3)\xi + B_1 u + B_2 \tilde{w} \\ \tilde{z} = \tilde{C}_1 \xi + D_{11} u + D_{12} \tilde{w} \\ y = \tilde{C}_2 \xi + D_{21} u + D_{22} \tilde{w} \end{cases} \tag{5.6}$$

where $\xi = [\chi_{vert}\ \chi_w]^T$; $\tilde{z} = [z_1\ z_2\ z_3]^T$; $\tilde{w} = z_r$; $y = [z_{def}\ \dot{z}_{def}]^T$; $u = u_{ij}^{\mathcal{H}_\infty}$; χ_{vert} is the states vector in the vertical dynamics of the *QoV* model and χ_w is the vertical weighting functions states vector.
Then, we aim at using a specific structure of the suspension controller, the suspension forces distribution is handled as follows:

$$K_s(\rho_n) := \begin{cases} \dot{x}_c(t) = A_c(\rho_n)x_c(t) + B_c(\rho_n)y(t) \\ \begin{pmatrix} u_{fl}^{\mathcal{H}_\infty}(t) \\ u_{fr}^{\mathcal{H}_\infty}(t) \\ u_{rl}^{\mathcal{H}_\infty}(t) \\ u_{rr}^{\mathcal{H}_\infty}(t) \end{pmatrix} = \underbrace{U(\rho_4)C_c^0(\rho_4)}_{C_c(\rho_4)} x_c(t) \end{cases} \tag{5.7}$$

where

$$U(\rho_4) = \begin{pmatrix} 1-|\rho_4| & 0 & 0 & 0 \\ 0 & |\rho_4| & 0 & 0 \\ 0 & 0 & 1-|\rho_4| & 0 \\ 0 & 0 & 0 & |\rho_4| \end{pmatrix} \tag{5.8}$$

ρ_n, $n = 1, 2, 3$, $x_c(t)$ is the controller state, $A_c(\rho_n)$, $B_c(\rho_n)$ and $C_c(\rho_4)$ are the state matrices of the controller.
$u^{\mathcal{H}_\infty}(t) = [u_{fl}^{\mathcal{H}_\infty}(t) u_{fr}^{\mathcal{H}_\infty}(t) u_{rl}^{\mathcal{H}_\infty}(t) u_{rr}^{\mathcal{H}_\infty}(t)]$ the input control of the suspension actuators and $y(t) = z_{def}(t)$.

Remark: The proposed *LPV/*$\mathcal{H}_\infty$ robust controller is synthesized by using *LMIs* solution for polytopic systems; all varying parameters are considered bounded: $\rho_1 \in [-1, 1]$, $\rho_2 \in [0, 1]$, $\rho_3 \in [0, 1]$ and $\rho_4 \in [-1, 1]$.

5.3.3 Simulation Results

In this scenario, the road profile estimated in the previous chapter is applied at the left side of the vehicle, namely, under the front left wheel $z_{us_{fr}}$ and the rear left wheel $z_{us_{rr}}$.

Fig. 5.6 represents the implementation scheme for the proposed LPV/$\mathcal{H}_\infty$ strategy based on algebraic estimation:

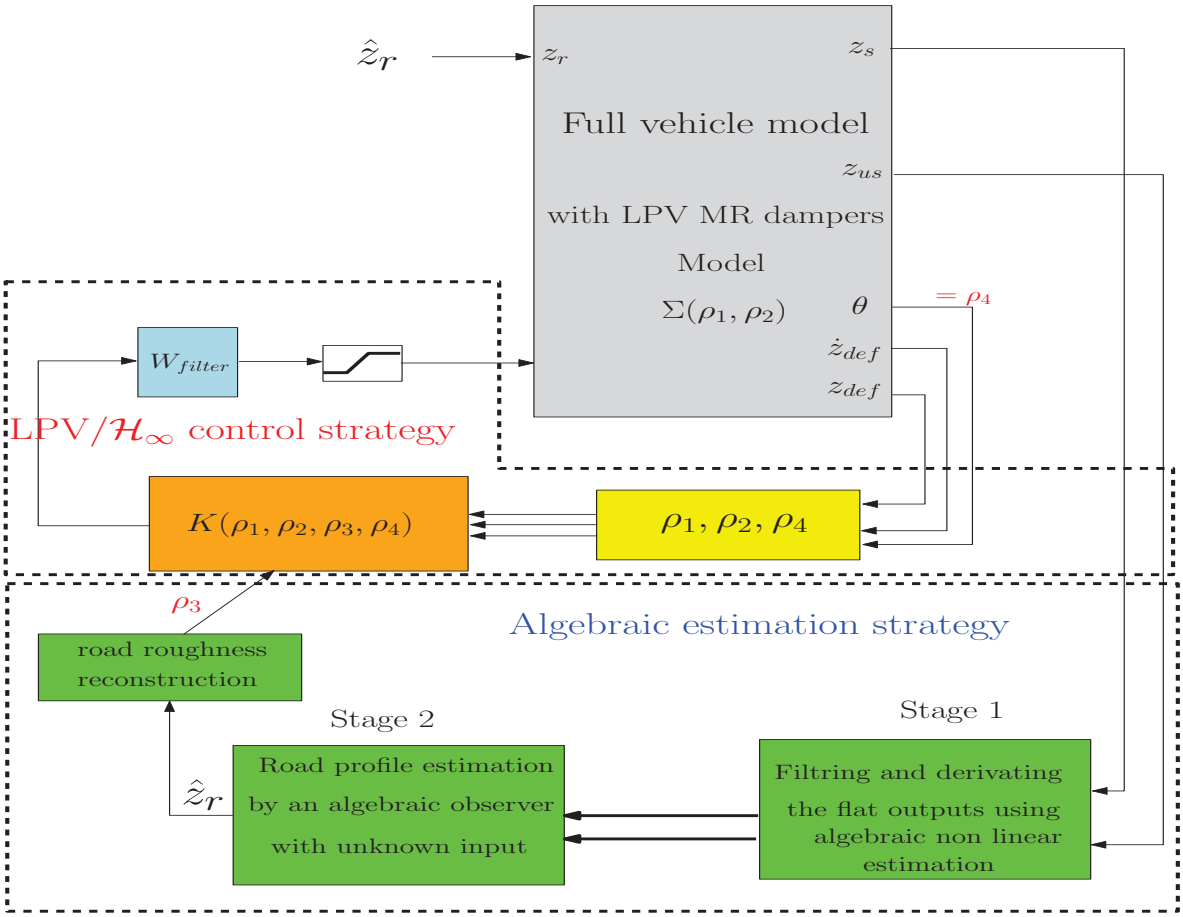

Figure 5.6: Implementation scheme of the proposed LPV/$\mathcal{H}_\infty$.

Let us recall that simulations are performed on a non linear full vehicle model. The model parameters are those of a Renault Mégane Coupé, obtained during a collaborative study with the MIPS laboratory in Mulhouse, through identification with real data.
The full vehicle model allows to emphasize the effect of the varying parameter $\rho_4 = \theta$ (roll dynamics) for the distribution of the suspensions forces to enhance the passengers comfort and the road holding of the vehicle.

To show the efficiency of the proposed LPV/$\mathcal{H}_\infty$ full vehicle semi-active suspension control strategy, two scenarios are proposed. The first one will be used to test the ability of the proposed control structure to enhance the passengers comfort while running safely on a bad road. The second one emphasizes the efficiency of the strategy to improve vehicle roadholding in dangerous situations.

Results

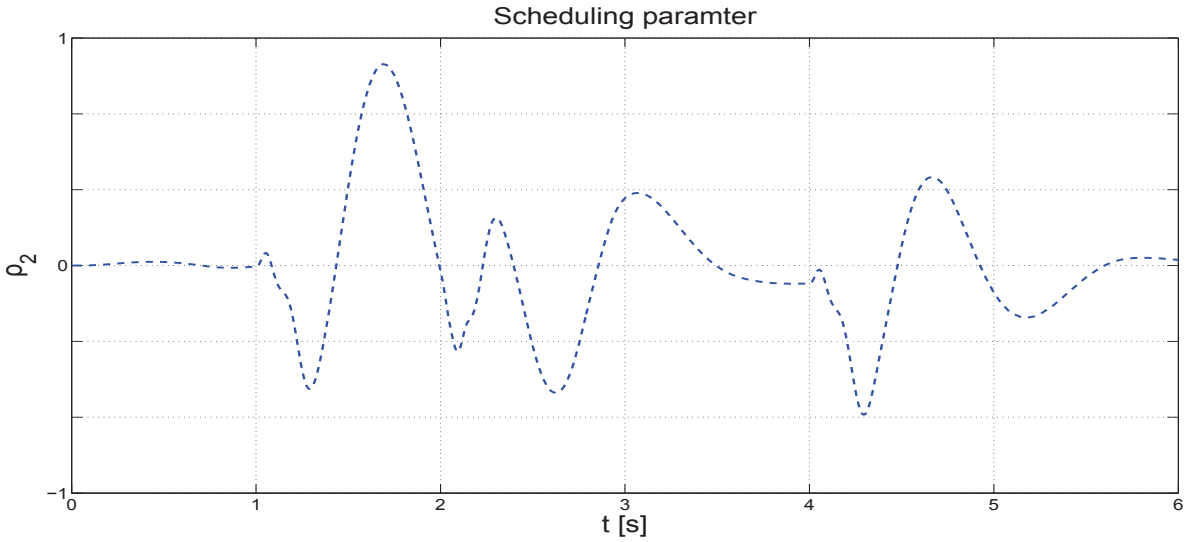

Figure 5.7: Scheduling parameter ρ_2.

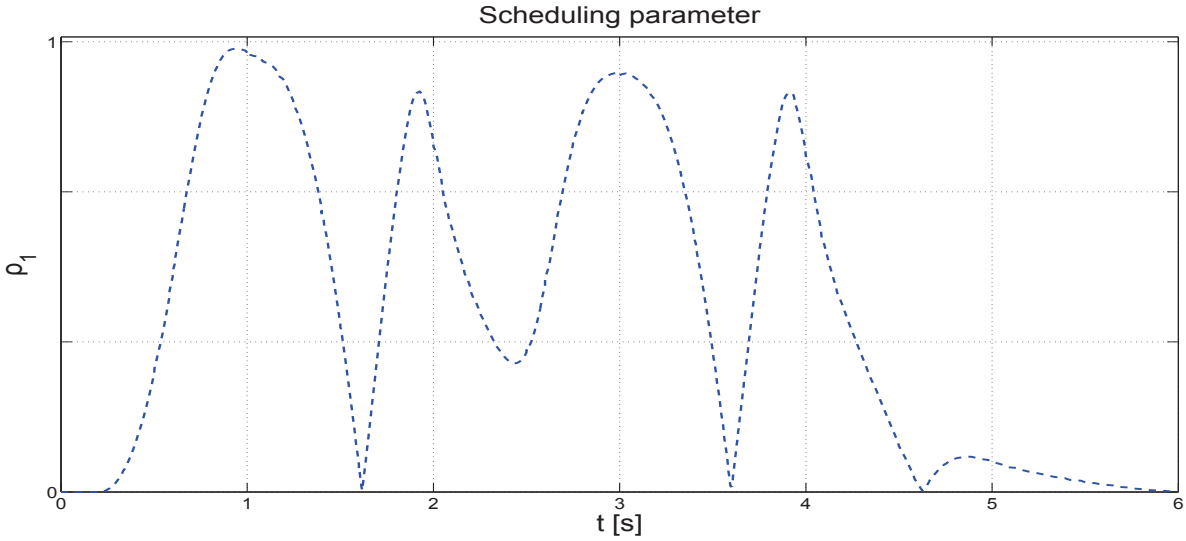

Figure 5.8: Scheduling parameter ρ_1.

Fig. 5.7 and Fig. 5.8 show the varying parameters ρ_1 and ρ_2 used to model the semi-active behaviour of the magneto-rheological dampers.

5.3.3.1 First simulation scenario

The first one concerns the vehicle running on a plowed field (see Table.4.3) at $v_x = 30$ kmh. In this case the predominating performance objective is the passengers comfort.
Indeed, this kind of road involves a lot of irregularities. This will cause a lot of vibration and will considerably degrade the displacement and the acceleration of the chassis. Then the passengers comfort

even at low velocities is deteriorated.

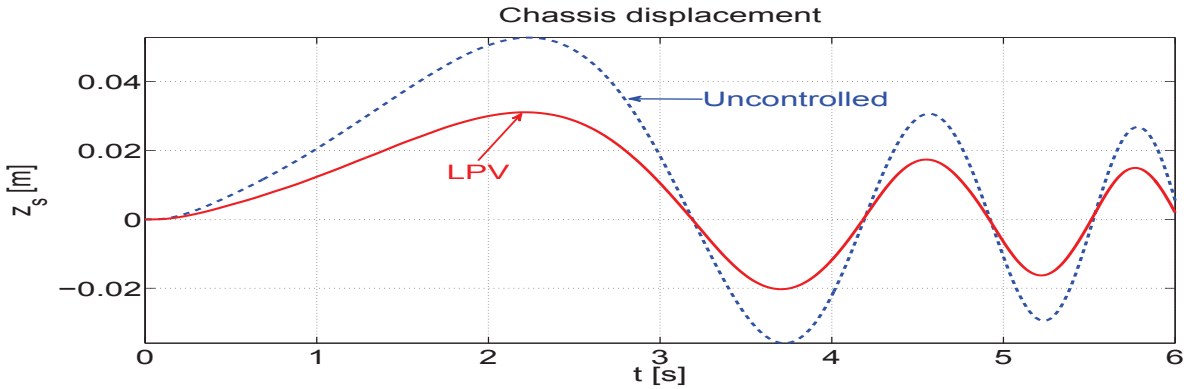

Figure 5.9: Chassis displacement of the gravity center z_s.

Fig. 5.9 and Fig. 5.10 show the chassis displacement at the center of gravity (chassis acceleration in the center of gravity respectively).
It can be noticed that the proposed LPV/$\mathcal{H}_\infty$ controller (in red) enhances better these dynamics representative of the passenger comfort, than in the case of the passive suspension system (in blue).

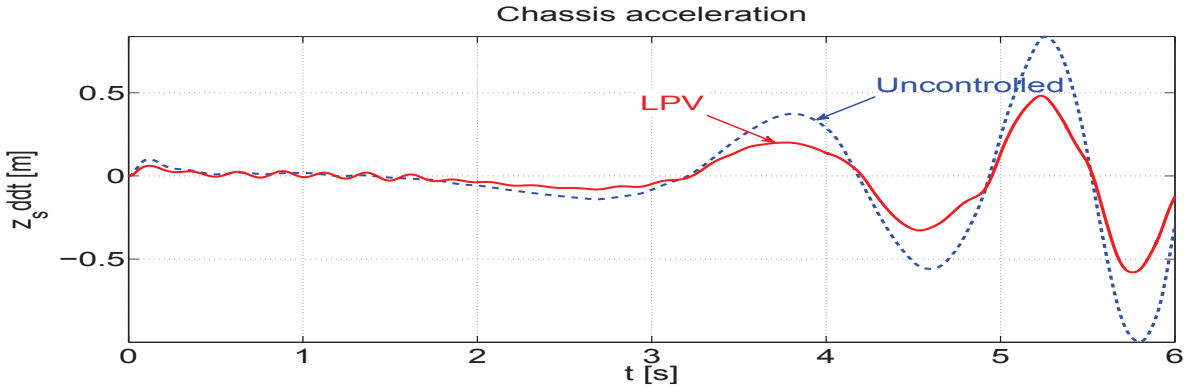

Figure 5.10: Chassis acceleration of the gravity center $\ddot{z}_s$.

In Fig. 5.11 and Fig. 5.12, the front right and left chassis displacements are shown. The effect of the suspensions forces distribution can be seen. Since the road profile is applied on the left side of the vehicle, it is clear that a larger load is applied at the right side, and then with the LPV scheduling strategy, larger suspensions forces can be applied on this side.

Here, one can see that the chassis displacement is better attenuated at the right corners of the vehicle than at the left ones, which copes with the proposed approach objectives.

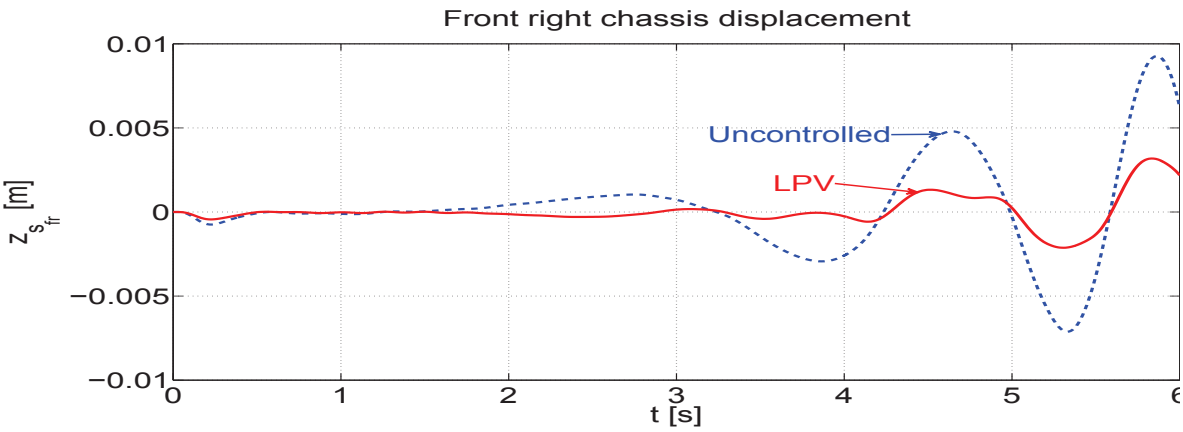

Figure 5.11: Front right chassis displacement $z_{s_{fr}}$.

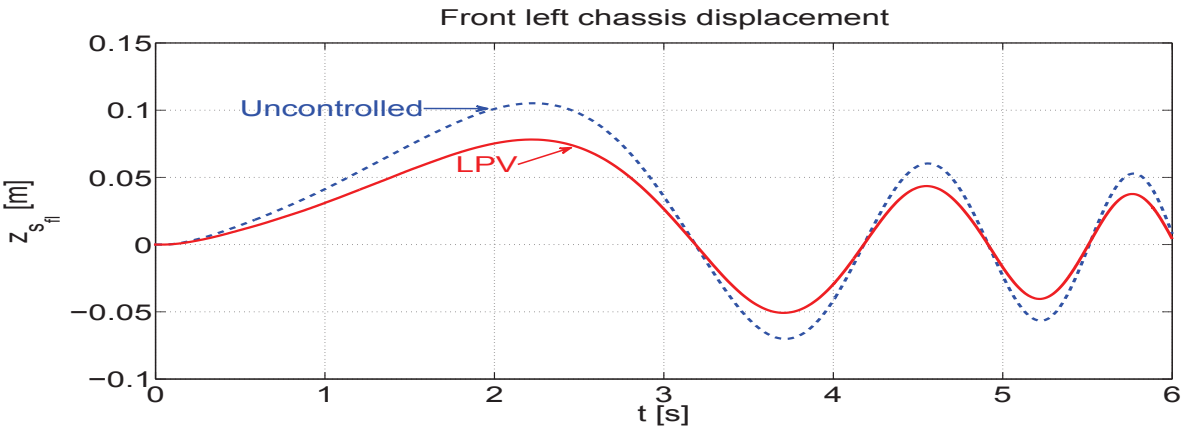

Figure 5.12: Front left chassis displacement $z_{s_{fl}}$.

Actually, by calculating the *RMS* (root mean square) of the chassis displacement (z_s) and the chassis acceleration ($\ddot{z}_s$), one can notice an improvement of 30% using the LPV/$\mathcal{H}_\infty$ control of the MR dampers.

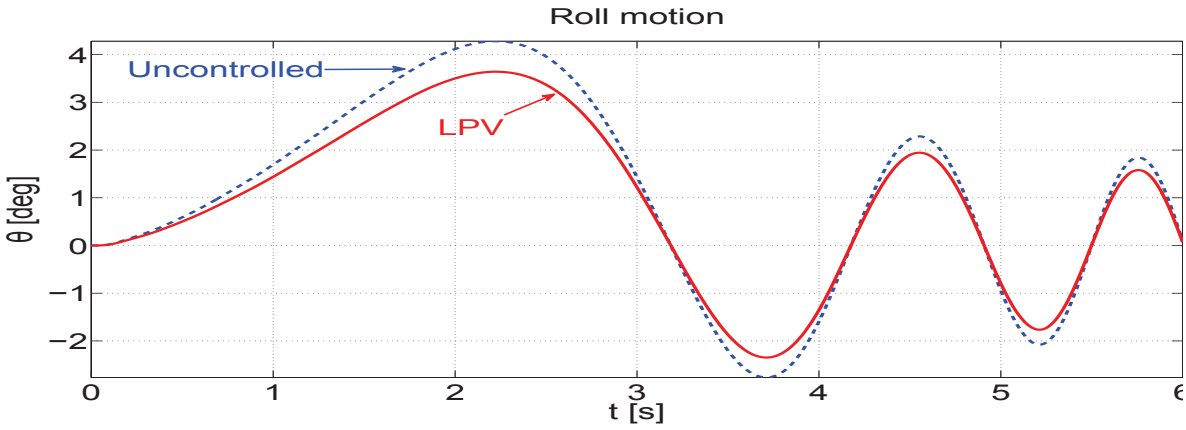

Figure 5.13: Roll motion θ.

Remark: The varying parameter $\rho_4 = \theta$ is normalized to evolve in the variation interval $\rho_4 \in [-1, 1]$.

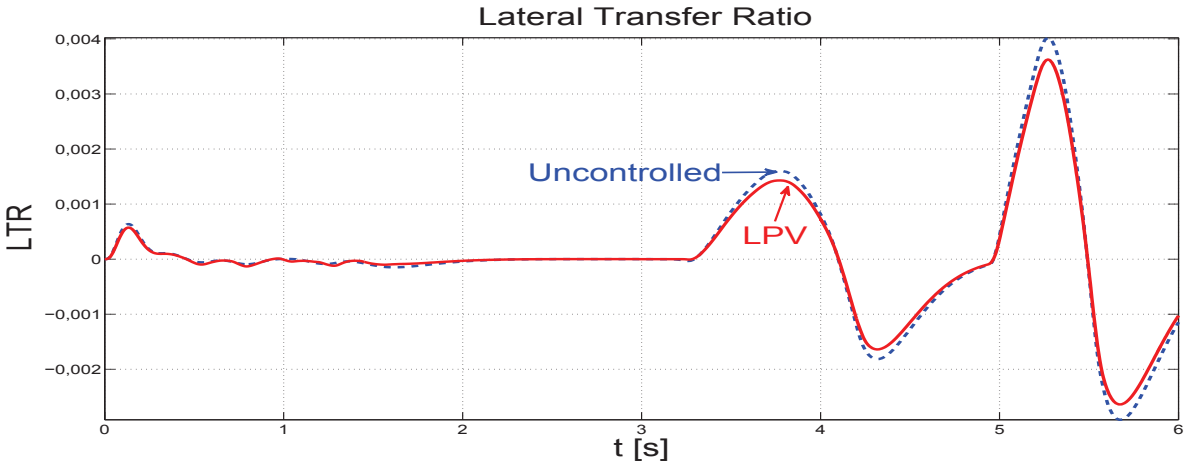

Figure 5.14: Load transfer ratio, LTR.

Fig. 5.13, Fig. 5.14, Fig. 5.15 and Fig. 5.16 show the roll motion, lateral transfer ratio, front left wheel and front right wheel displacement respectively, representative of the road holding of the vehicle. The improvement brought to these dynamics can be noticed, even if it is less than that for the passengers comfort car's dynamic.

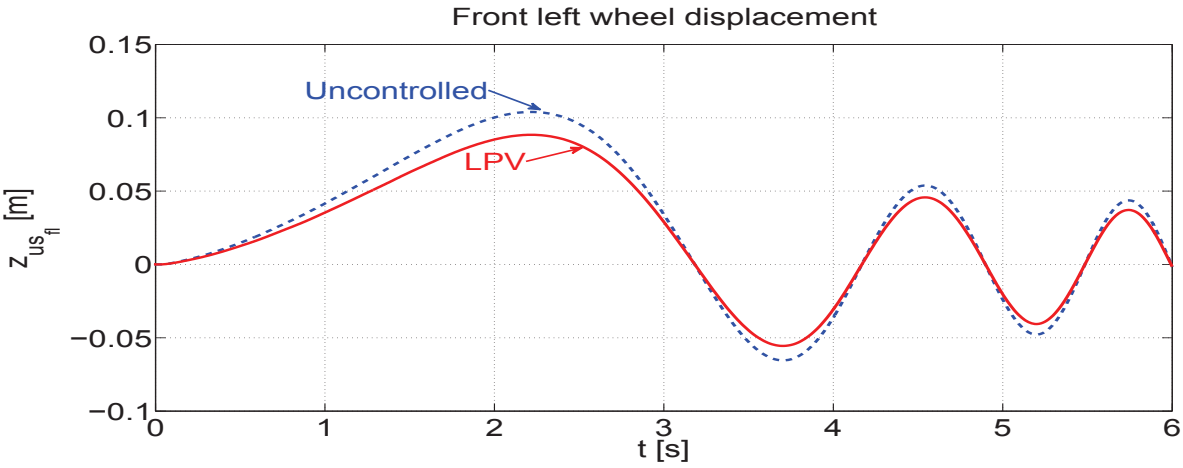

Figure 5.15: Front left wheel displacement $z_{us_{fl}}$.

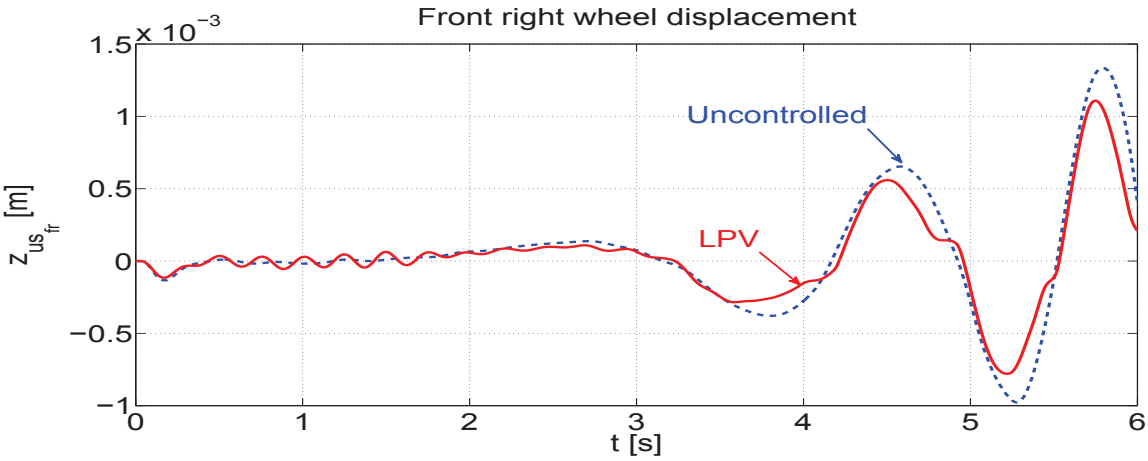

Figure 5.16: Front right wheel displacement $z_{us_{fr}}$

Now, calculating the *RMS* of the roll motion and the right wheel displacement proves that they have been improved up of 15% and the lateral transfer ratio and the left wheel displacement up to 5% compared to the passive case. This can be also explained by the distribution of the semi-active suspension forces on the vehicle sides. It is worth noting that the proposed strategy provides a good trade-off between the two conflicting performance objectives, passenger comfort and vehicle road holding.

5.3.3.2 Second simulation scenario

In the second scenario, the vehicle runs at a high speed, $v_x = 100$ kmh, on a smooth road (ISO road A, see Table. 4.3). Under these conditions, the predominating performance objective is the vehicle road holding represented by the roll motion θ and wheels displacement z_{us} .

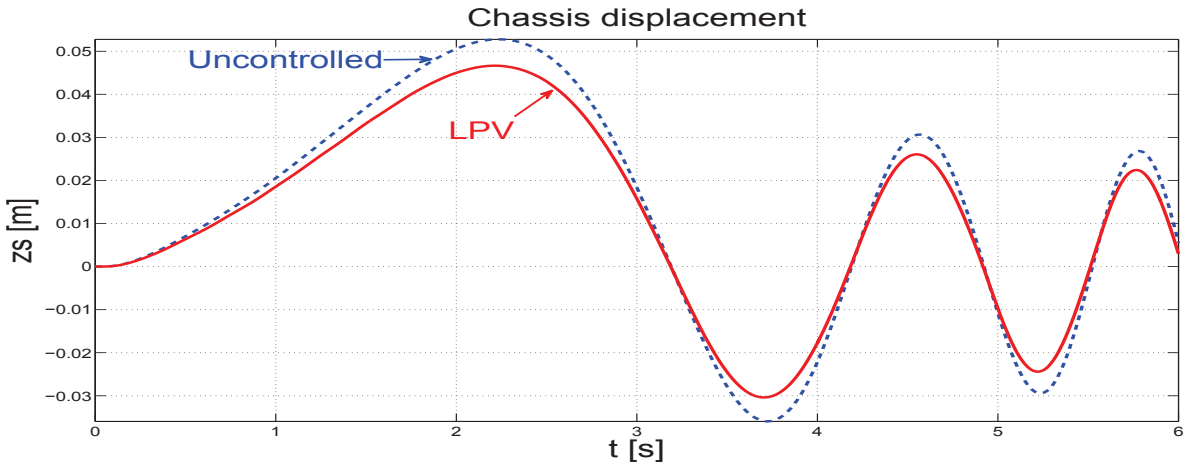

Figure 5.17: Chassis displacement of the gravity center z_s.

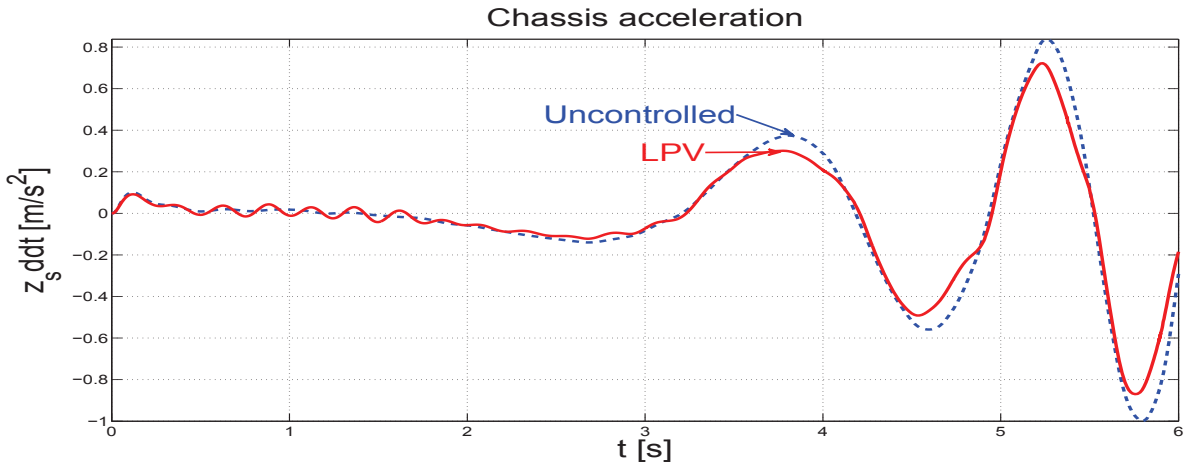

Figure 5.18: Chassis acceleration of the gravity center $\ddot{z}_s$.

Fig. 5.17 and Fig. 5.18 show the chassis displacement at the center of gravity (chassis acceleration at the center of gravity respectively). Calculating the *RMS* of these signals resulting from the LPV/$\mathcal{H}_\infty$ controller shows an improvement of 10% compared to the passive case. The improvement seems small since the controller, under these driving conditions, is oriented to enhance the road holding of the vehicle.

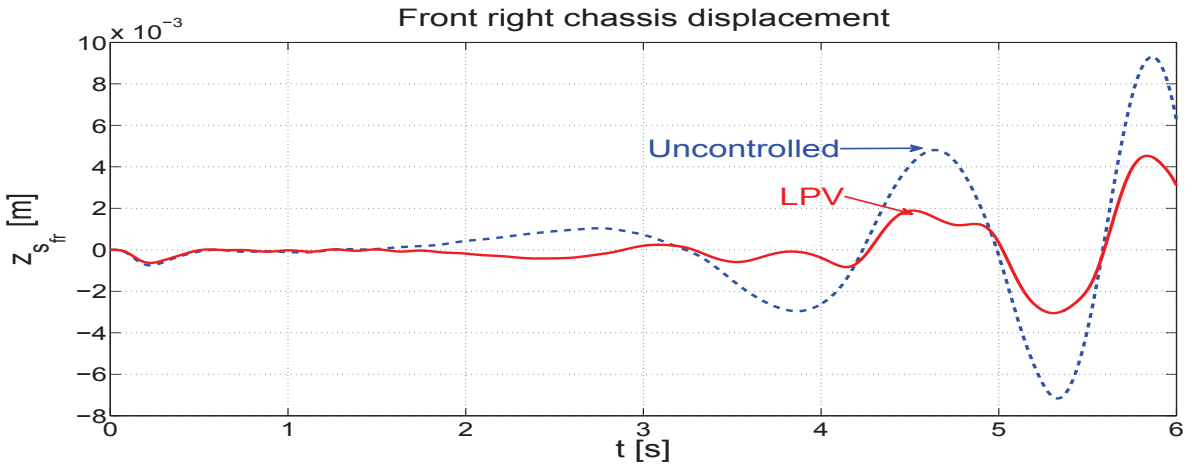

Figure 5.19: Front right chassis displacement $z_{s_{fr}}$.

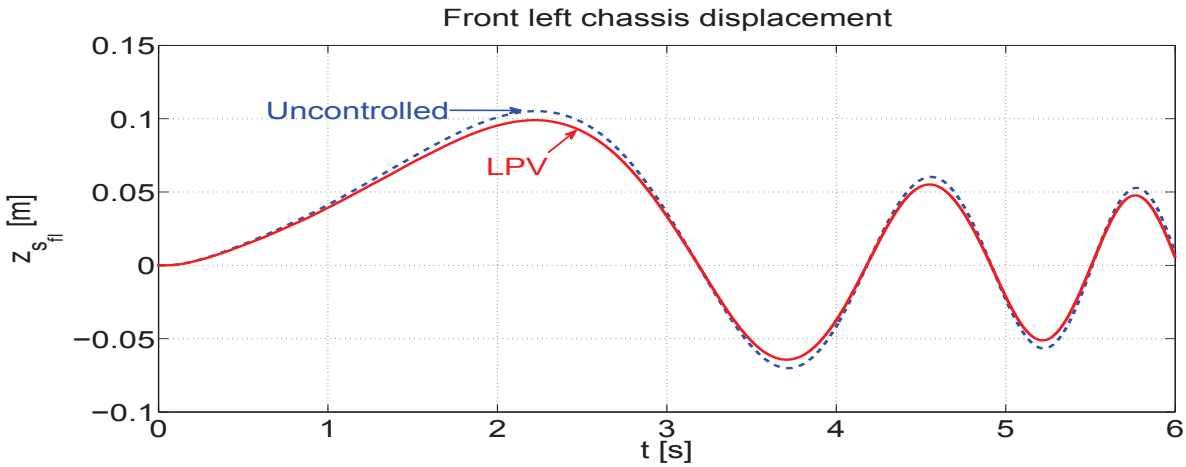

Figure 5.20: Front left chassis displacement $z_{s_{fl}}$.

Fig. 5.19 and Fig. 5.20 show the front right and left chassis displacements. It can be noticed that the right chassis displacement is better attenuated than the left one, even if the improvement remains small. This can be explained by the semi-active suspension forces distribution process, thanks to the varying parameter $\rho_4 = \theta$.

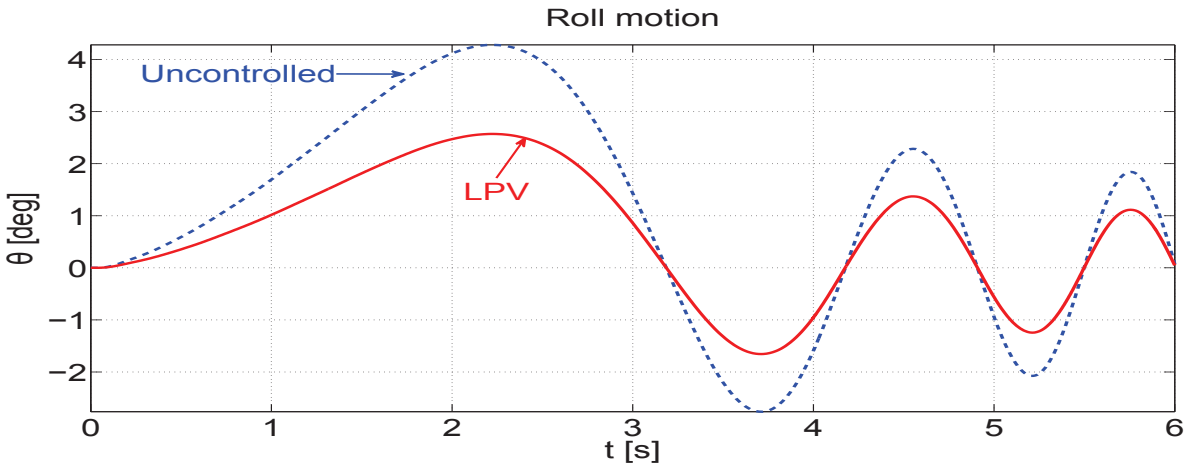

Figure 5.21: Roll motion θ.

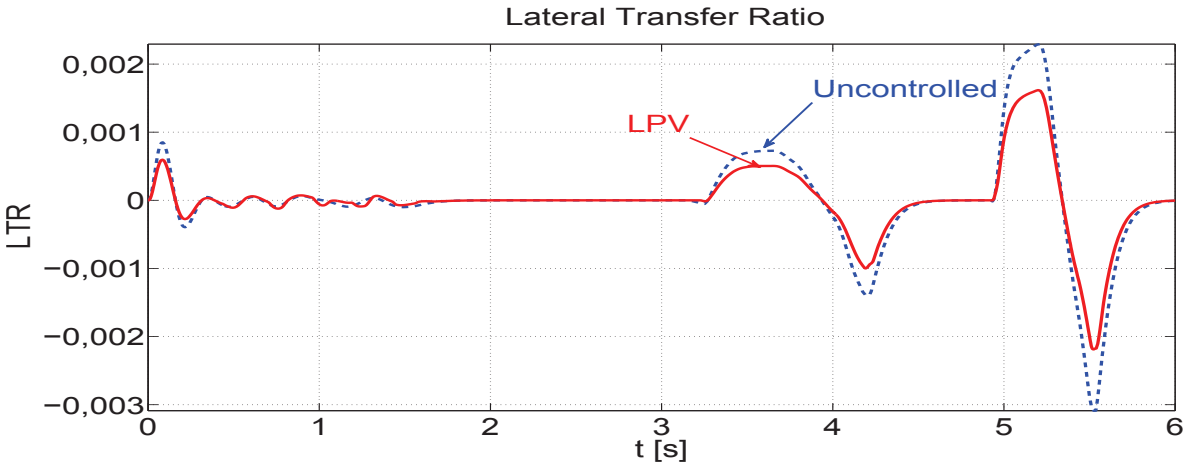

Figure 5.22: Load transfer ratio, LTR.

Fig. 5.21, Fig. 5.22, Fig. 5.23 and Fig. 5.24 are roll motion, lateral transfer ratio, front left wheel and front right wheel displacement respectively. Here, by calculating the *RMS* of each signal, it can be seen that the roll motion is enhanced up to "40%" compared to the passive case. Also the lateral transfer ratio is decreasing by "30%".

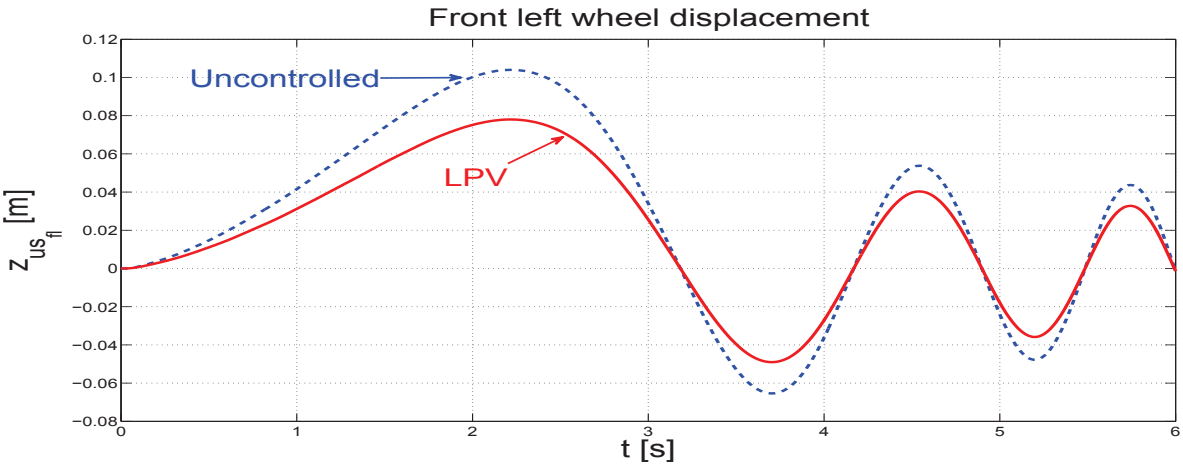

Figure 5.23: Front left wheel displacement $z_{us_{fl}}$.

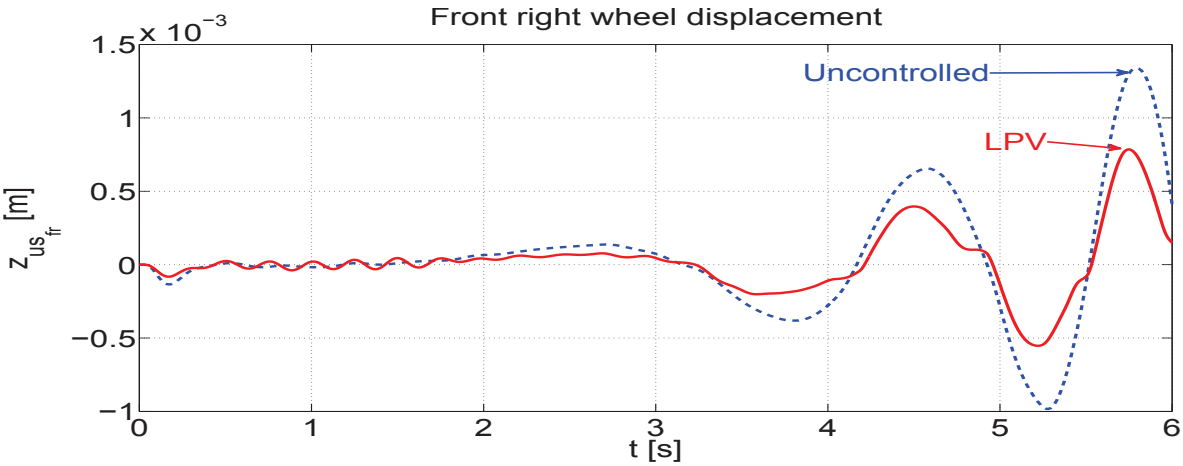

Figure 5.24: Front right wheel displacement $z_{us_{fr}}$

The front right and left wheel displacements are improved up to "40% (resp. up to "25%) compared to the uncontrolled vehicle.This improvement is important for vehicle safety.

It is worth noticing that one of the main interest of LPV/$\mathcal{H}_\infty$ control for automotive systems is that it ensures a smooth transition between the conflicting performance objectives, namely, the passengers comfort and the car's road holding and then ensure the online suspension control adaptation.

5.4 Conclusion

In this chapter, two road adaptive controllers were presented using some of the road estimation strategies developed in the previous chapter. The first controller was used to adapt the performance of only one quarter of the vehicle to the road, depending on the road roughness estimation obtained with an $\mathcal{H}_\infty$ robust observer. The second controller can be seen as an extension of the preliminary results obtained in the first part. The road control adaptation is used to handle the overall vertical dynamic of the car through non linear algebraic road roughness observation and estimation, and a suspension allocating control, depending on the roll behaviour of the car.
Simulation results were carried out on an experimentally validated model (either for the QoV or the full vehicle model). Very promising results prove the efficiency of the proposed strategies. The structure of the LPV performance adaptation to the road profile allows to implement these strategies easily without requiring other sensors or means that the commonly ones available on the commercial vehicles.

Part III

Global Chassis Control using several actuators

CHAPTER 6

An $LPV/\mathcal{H}_\infty$ integrated VDC

6.1 Introduction

This chapter presents an innovative LPV/H_∞ global chassis control strategy. It uses the suspension, steering and braking actuators to achieve the desired performance objectives and to ensures vehicle stability in the dangerous driving situations.

In this chapter, a new LPV/H_∞ control strategy (see Fig. 7.25) proposes a hierarchical collaborative coordination between the various actuators of semi-active suspension, steering and braking subsystems to enhance the vehicle dynamics to prevent conflicts in terms of performance objectives. This GCC (Global Chassis Control) strategy combines the monitoring of the driving situation and the corresponding coordination of the actuators. The LPV/H_∞ frame allows a smooth and flexible use of these actuators with adaptation to the driving situation while guaranteeing the robustness of the proposed control. The controllers design focuses on enhancing the overall vehicle dynamics, namely, vertical, lateral and longitudinal dynamics.

6.1.1 Motivations

Road safety has been an international stake in the last decades. A close examination of road traffic accident data (1.24 million death and more than 50 million of injuries in 2013, by World Health Organisation) reveals that the loss of vehicle control is largely responsible of road accidents. Therefore, enhancing driving characteristics by ensuring stability in critical situations (i.e safer vehicles) has been the main issue for both academical and industrial communities.

Also, the increasing request of the customers in term of driving performances has led several car manufacturers to seek new efficient strategies that improve the vehicles stability and prevent them from drifting, spinning or rolling over in order to enhance driving characteristics in critical situations. The automotive vehicles are highly complex systems including various components achieving different tasks. The main subsystems that act on vertical, lateral and longitudinal dynamics are influenced specifically by the (semi-active) suspensions, electro-mechanical braking and active steering actuators.

Conventionally, the controls of these subsystems are designed separately by the vehicle manufacturers. This aims at locally solving each problem related to the car's dynamics. In the last years, it has been proven that this strategy has a major weakness: the interactions between the dynamics of the automotive subsystems are not taken into account. The lack of or inappropriate communication between the different actuators of braking, steering and suspension subsystems may induce poor performances and generate conflicts between the objectives of the controllers.

So, a new trend is to develop multivariable global chassis control strategies involving several actuators and enhancing the car's dynamics. The purpose of the integrated multivariable vehicle control is to use, in a collaborative way, the available actuators acting on the vehicle dynamics. The synthesis of

such a multivariable controller allows to adapt the vehicle behaviour to the driving situations. It also focuses here on improving both comfort and safety objectives by coordinating the use of the actuators controllers of braking, steering and semi-active suspensions subsystems.

6.1.2 Related works

6.1.2.1 Vehicle stability via multivariable Steering/Braking control

In the last decade, a lot of literature and studies dealing with the control dynamics have been proposed, starting from SISO control solutions as in (Denny, 2005) ,(Tanelli *et al.*, 2007), (Botero *et al.*, 2007) where only the braking control was used separately to improve the lateral and yaw behaviours of the vehicle and to tackle critical driving situations and also as in (S.Mammar and D.Koenig, 2002) where a strategy using active steering for vehicle handling improvement was presented.
Recently, many studies have been carried out on the multivariable control design for the global chassis stabilization and vehicle dynamics improvement. First, research on vehicle stability and handling has focused on improving the lateral dynamics behaviour using braking and steering actuators. Multivariable controllers using braking/steering actuators have been widely investigated by the control communities. Indeed, in (Canale *et al.*, 2007) a robust non-parametric approach to improve vehicle yaw rate dynamics by means of a rear active differential is introduced. Also, (Acarman, 2009) proposed an optimal non linear vehicle control based on individual braking torque and steering angle with online control allocation to improve vehicle performances. Another recent result given by (Németh and Gáspár, 2011) shows a new design of actuator intervention for trajectory tracking. In (Gáspár *et al.*, 2005), a heavy vehicle LPV model is introduced with a scheduled robust control, involving suspensions and braking actions. An adaptive braking control coupled with active steering is used in (Tjonnas and Johansen, 2010) for vehicle stabilization. (Di Cairano *et al.*, 2013) gives an approach for yaw stability control by coordinating active steering and differential braking in the tire sideslip angles domain. Another interesting coupled non linear lateral dynamics control is introduced in (Menhour *et al.*, 2014).
In (Poussot-Vassal *et al.*, 2011*a*), (Doumiati *et al.*, 2010*b*) and (Doumiati *et al.*, 2013*b*), some smart scheduling policies of braking /steering actuators have been presented, a step towards a full coordinated control. New strategies using steering and braking actuators are detailed in (Poussot *et al.*, 2013).

As part of the automotive system dynamical behaviour study, an interesting comparative study between a non linear flatness control and LPV/$\mathcal{H}_\infty$ control has explained the advantage of using the steering/braking actuators for the vehicle stability in (Fergani *et al.*, 2013*a*). The scheme given in Fig. 6.1 shows the comparative study of these two control strategies applied to the considered vehicle:

The first one concerns a controller based on the differential algebraic flatness of non linear systems and an algebraic non linear estimation applied to commercial vehicles. The second one is a LPV/$\mathcal{H}_\infty$ (Linear Varying Parameter with the $\mathcal{H}_\infty$ norm) control using a stability monitoring system to achieve the vehicle dynamics control objective. These two strategies use Active Steering and Electro-Mechanical Braking actuators and aim at improving the vehicle stability and steerability by designing a multivariable controller that acts simultaneously on the lateral and longitudinal dynamics

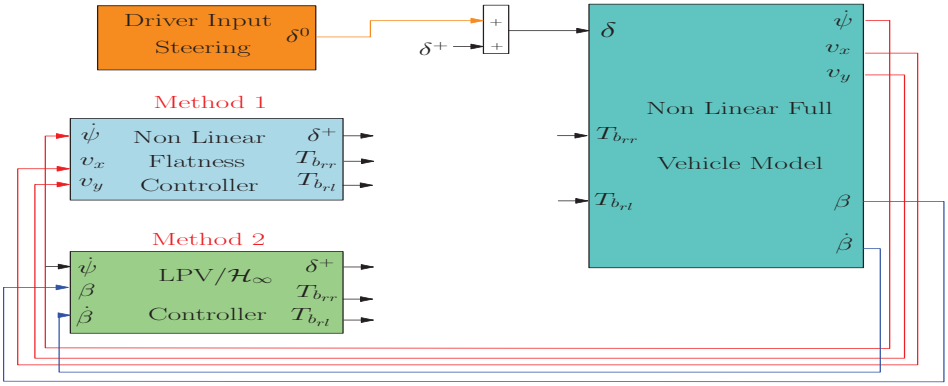

Figure 6.1: Design of The Vehicle dynamics Control Strategies (steer, brake)

of the car. Also, it is worth noting that the results have proven the efficiency of the two strategies for the vehicle stability improvement even if one is linear and the other non linear. Indeed, the LPV/$\mathcal{H}_\infty$ control strategy allows a smooth transition between performance objectives and to handle non linearities in a simple way, while remaining robust through the $\mathcal{H}_\infty$ framework.

However, it has been proven that steering and braking actuators are not sufficient to improve all the vehicle dynamical behaviours. Indeed, road holding characteristics and passengers comfort, which are crucial commercial arguments for the automotive manufacturers, can not be handled when using only steering and braking actuators. Both industry and academic communities have therefore been interested by studying vertical dynamics through suspensions systems to improve the overall vehicle dynamics.

6.1.2.2 Road holding and passengers comfort through suspension systems control

The importance of suspension systems in the vehicle dynamical behaviour has raised much interest in the last years. Since the suspension system ensures the link between the chassis and the wheels, it plays a key role in the automotive vertical dynamical attitude. The control strategies developed for such systems allow to achieve the performance objectives concerning the passengers comfort and the car roadholding.

Many studies have been dedicated to the suspensions control. A summary of some recent suspensions control strategies has been presented in (Poussot-Vassal *et al.*, 2012). Also, (Savaresi *et al.*, 2010*b*) presents a detailed description of different suspension systems and summarizes several control approaches applied to semi-active suspensions such as groundhook, skyhook, ADD and LPV control strategies. Many of recent works (see e.g. (Jonasson and Roos, 2008), (Giua *et al.*, 2004), (Lu, 2004), (Savaresi and Spelta, 2007) and references therein) tried to present new and reliable suspensions control strategies to enhance both safety and comfort of passengers. In (Zin *et al.*, 2008) only the suspensions control is designed to improve either comfort or roadholding using $\mathcal{H}_\infty$ control theory. Also, several non linear control strategies have been developed to cope with the different dynamics induced by several types of suspensions. In (Li *et al.*, 2012) a reliable fuzzy control for active suspension systems with actuator delay and fault is presented. (Sun *et al.*, 2011) presents a finite frequency H_∞ control for vehicle active suspension systems. Many works have also developed various control strategies for suspensions system to enhance both passengers comfort and road handling as in

(Do *et al.*, 2010*b*) where an LPV control approach for comfort and suspension travel improvements of semi-active suspension systems is presented. In (Do *et al.*, 2011), another interesting strategy is proposed, dealing with semi-active LPV suspensions control under actuators constraint, using an anti-wind up approach.

6.1.2.3 Global chassis control (GCC) strategy

The study of each of the suspension, steering and braking systems has shown that an independent design for each of them may lead to performance conflicts due to the different interactions between the vehicle dynamics. The solution to this problem is to handle all the vehicle dynamics in the same control strategy.

Recently, several works have been concerned with the integrated control strategies since they allow to manage multiple-objective performances from the available actuators and sensors used in these control tasks. The interest for this type of vehicle control increased in several academic and industrial research centers. As a result of the interactions between the vertical and lateral dynamics, as previously mentioned, new vehicle control methodologies including suspension and braking or steering actuators have been presented: in (Lin, 2007) a nonlinear backstepping control design of anti-lock braking systems with assistance of active suspension, in (Chou and d'Andréa Novel, 2005*a*), an interesting nonlinear control law using suspension and braking actuators for commercial cars and a hierarchical fuzzy-neural control of anti-lock braking system and active suspension in (Wang *et al.*, 2012).

A detailed survey of all these studies shows about the importance of providing new global chassis control strategies. The previously cited approaches yield good results. So we have tried to combine the strength of the mutlivariable control for the multiple performance objectives and the adaptation of the use of the actuators to the driving situations that influence considerably the dynamical behaviour of the vehicle. For this purpose, we have proposed several $LPV/\mathcal{H}_\infty$ robust control design strategies.

Furthermore, in this thesis, a new structure of robust controllers have been developed to enhance the overall vehicle dynamics using a coordination approach for the steering, braking and magneto-rheological semi-active dampers. A robust $LPV/\mathcal{H}_\infty$ based on LMI's resolution in the LPV framework for those subsystems is developed in (Fergani *et al.*, 2012*a*). Also, some first results concerning multivariable robust control including the three actuators were established and validated in (Fergani *et al.*, 2012*b*).
Moreover, here, semi-active suspensions are considered (while in (Poussot-Vassal *et al.*, 2011*b*) active systems were used), which suits better to the industrial requirements (energy saving). This strategy is adapted to driver-aid, depending on the dangerousness of the situation, selects the best actuator coordination to avoid accidents, and limits the unnecessary use of the actuators for energy saving sake.
This strategy is summarized in the following implementation scheme (see Fig. 7.25) which includes the vehicle's model, the monitoring approach and the subsystems controllers. This proposed control strategy has led to several contribution in (Fergani *et al.*, 2012*a*) and (Fergani *et al.*, 2012*b*).
This chapiter is organized as follows: Section 2 presents the overview of the main contribution of the study which is the coordination between semi-active suspension, steering and braking actuators and the synthesis of different controllers to enhance vehicle performances and attitude. Controllers synthesis and performance analysis are detailed in Section 3 and 4 through frequency domain sim-

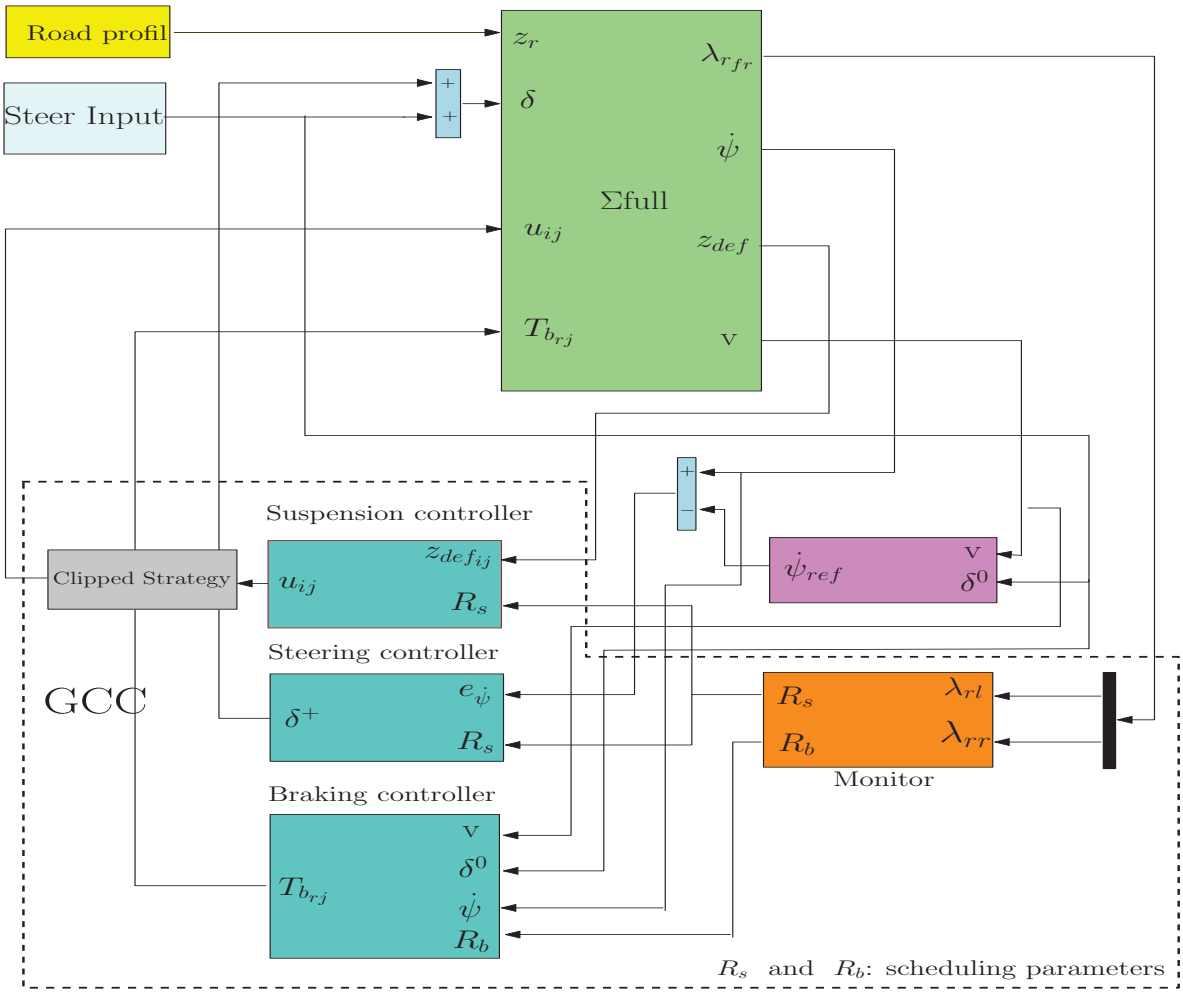

Figure 6.2: Global chassis control implementation scheme.

ulations. In Section 5, time domain simulations are performed on a complex nonlinear full vehicle model equipped with semi-active suspension dampers (Magneto Rheological Dampers). It also emphasizes the contribution of the proposed LPV strategy by comparing it to the LTI one. Conclusions and discussions are given in the last Section.

6.2 A New Global Chassis Control Strategy: Supervision and Synthesis

This section presents the main result of the chapter, namely, the multivariable Global Chassis Control (GCC) involving front active steering, rear braking and semi-active suspension (see Fig.6.3). Such a strategy, preliminary introduced in previous works (see (Poussot-Vassal *et al.*, 2011*b*)) involves 2 monitoring parameters R_b and R_s, used to evaluate the dangerousness of the driving situation and to schedule the control actions.

The main idea is to synthesize two controllers, one dedicated to the lateral dynamics and the other to the vertical dynamics, that will be coordinated thanks to the scheduling parameters R_b (braking)

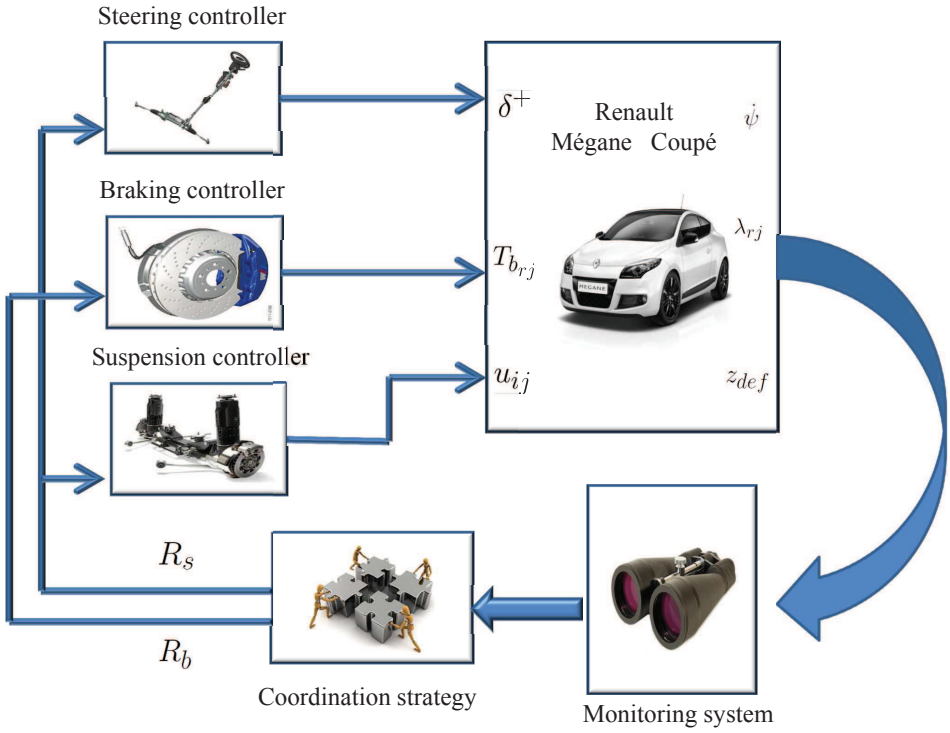

Figure 6.3: General structure scheme

and R_s (suspension and steering). The controllers synthesis is presented in the following subsections.

6.2.1 Driving situation monitoring

The monitoring of the driving situation has been selected following (Poussot-Vassal *et al.*, 2011*b*) from the longitudinal slip ratio of the rear wheels (s_{ij}), since it considerably affects the yaw stability and the car handling attitude.

- **Braking monitor:**

$$R_b = \min_{j=l,r}(r_{b_j}) \tag{6.1}$$

, is a function of the absolute value of the slip ratio ($|s_{rj}|$). r_{b_j} is defined as a relay (hysteresis like) function: $\rightarrow 0$ when 'on', $\rightarrow 1$ when 'off'. The switch 'on' (resp. 'off') threshold is s^+ (resp s^-).

When the slipping is low, the vehicle is in a normal situation, hence $R_b \rightarrow 1$. When the slip ratio raises and becomes greater than s^+, a critical situation is detected, then $R_b \rightarrow 0$. As R_b is function of the slip ratio, the choice of s^+ (resp. s^-) is done according to the tire friction curve. Here (and in a general case), $s^+ = 9\%$ and $s^- = 8\%$, in order to delimitate the linear and peak

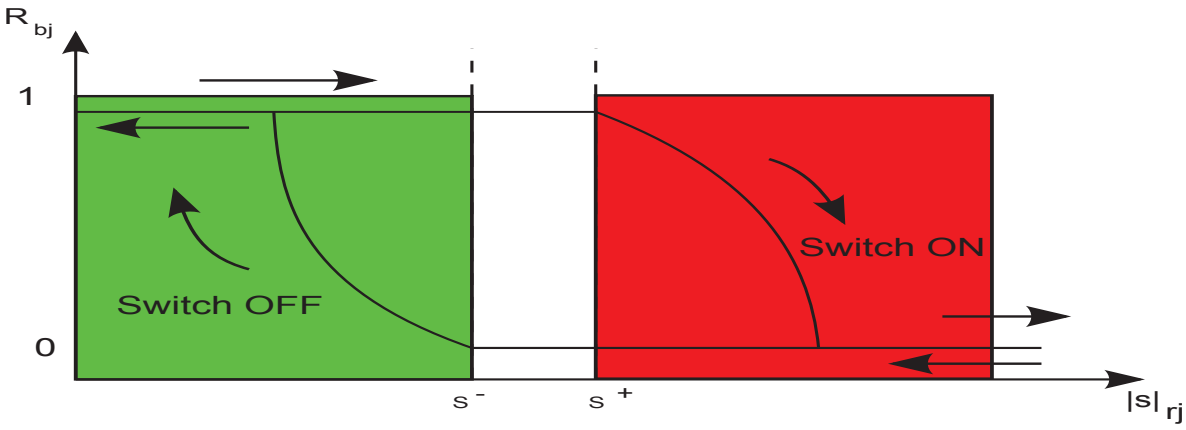

Figure 6.4: R_{bj} as a function of the rear slip $|s_{rj}|$.

tire friction force with the unstable part of the tire.

6.2.2 Classification of the driving situations

Based on the previously defined driving situation monitor R_b, the other varying parameter R_s allows to classify these driving situations depending on the dangerousness and on the degree of emergency under which the vehicle is running. This parameter R_s is introduced as follows:

$$R_s \begin{cases} =0 & \text{when } 1 > R_b > R^2_{crit} \\ = \frac{R_b - R^1_{crit}}{R^2_{crit} - R^1_{crit}} & \text{when } R^1_{crit} < R_b < R^2_{crit} \\ =1 & \text{when } 0 < R_b < R^1_{crit} \end{cases} \tag{6.2}$$

When $R_b > R^2_{crit}(= 0.9)$, i.e. when a low slip ($< s^-$) is detected, the vehicle is not in an emergency situation and R_s is set to 1. When $R_b < R^1_{crit}(= 0.7)$, i.e. when a high slip occurs ($> s^+$), a critical situation is reached and R_s is set to 0. Intermediate values of R_b correspond to intermediate driving situations.

The R_b and R_s varying parameters are used (as detailed later in the design step) to schedule the use of the Active steering, Semi-Active suspension and Electro-Mechanical Braking actuators according to the driving situation and optimize their operating range as described below, and summarized in Fig. 6.5 :

Normal situation: ($R_s = 1$, $R_b \rightarrow 0$) the driving cruise goes smoothly, with no emergency situations. Since there is no risk of wheel locking, as $R_b \rightarrow 0$, the rear braking torques will not be limited. The semi-active suspension will be tuned in order to preserve the passengers comfort, without deteriorating the road holding (i.e soft suspension damping), thanks to the scheduling parameter $R_s = 1$. Also, since the driving situation is safe, no corrective steering action is needed to stabilise the vehicle which will correspond to the scheduling parameter value $R_s = 1$.

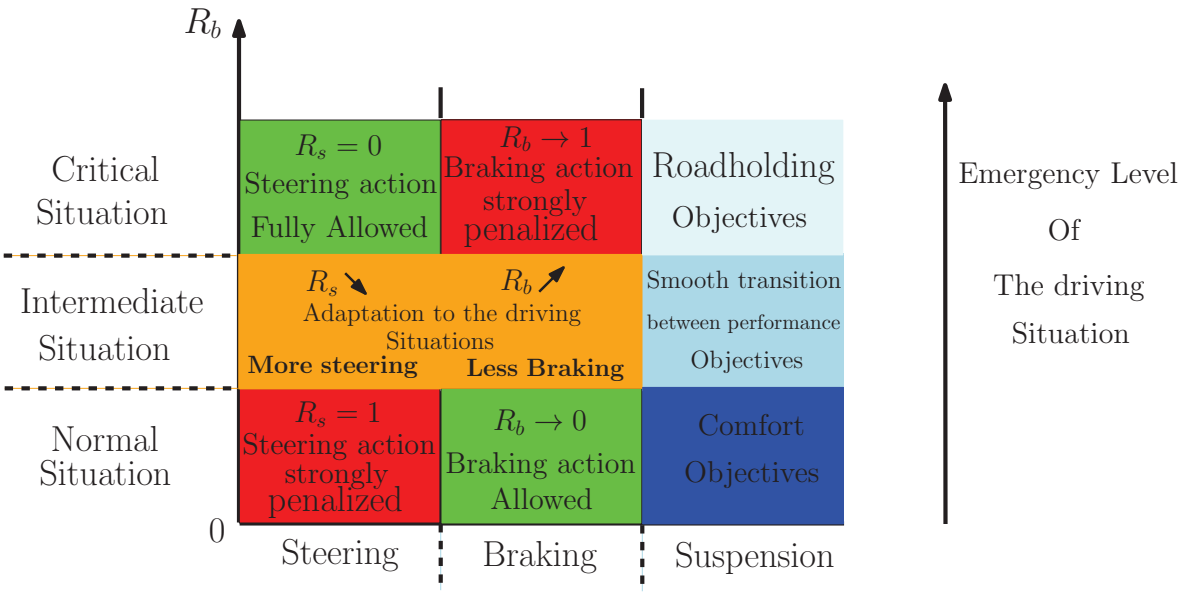

Figure 6.5: Actuators monitoring and scheduling strategy

Intermediate situation: ($R_s \searrow$, $R_b \nearrow$) As the driving situation becomes dangerous, the values of the scheduling parameters R_s and R_b change. The tire forces approach the non linear zone of the tire characteristic. As a result, the value of the monitor R_b starts to rise and the braking torques will be penalized to prevent the wheel locking. At the same time, the varying parameter R_s decreases and an a corrective steering action is allowed to help the driver to overcome this situation. Also, the semi-active suspension characteristics will be set to change smoothly, from soft to hard, depending on the value of R_s to further improve the car road holding without deteriorating the passengers comfort.

Critical situation: ($R_s = 0$, $R_b \to 1$) When a dangerous situation is detected through the braking monitor $R_b = 1$ (in terms of longitudinal tire slip), the braking torques are limited accordingly in order to bring back the forces into the linear stable zone of the tire characteristic. As R_s reaches zero, the maximum additive steering angle will be generated and the semi-active Magneto-Rheological dampers will be tuned to be "hard" in order to ensure a good roadholding (a small wheel rebound). This will help the driver to overcome the critical driving situation and prevent the vehicle from imminent accidents.

Remark:

- While in (Poussot-Vassal *et al.*, 2011*b*) the scheduling parameters are considered to coordinate the use of braking/active suspension actuators, here, they aim at coordinating steering, braking and semi-active suspensions (which is more complex).
- The controllers will be derived thanks to the LPV/$\mathcal{H}_\infty$ methodology. This framework allows to smoothly tune the control performances thanks to the scheduling parameters R_b et R_s, guar-

anteeing internal stability (by avoiding switching) and ensuring $\mathcal{H}_\infty$ performances, for any parameters variations.

6.2.3 Global chassis controllers design synthesis

The scheme in Fig. 7.25 shows the proposed 2 steps GCC LPV/$\mathcal{H}_\infty$ strategy. The first one based on the extended bicycle vehicle model is dedicated to the front steering/ rear braking controller, that aims at improving the yaw stability and the lateral dynamics. The other one corresponds to the 4 MRD semi-active suspension system, to enhance the vertical behaviour (comfort/roadholding performances of the car). The coupling effects are handled through the scheduling parameter R_s and thanks to an "anti-roll" action of the semi-active suspension.
The main strategy is to adapt the control action to the driving situation as previously presented in Fig.6.5, using a self-scheduled controller, function of R_b and R_s. This will be achieved thanks to a good coordination and communication between the actuators of Active front Steering, Electro-Mechanical rear Braking, and the Semi-Active MRD Suspension systems.

Remark: While in (Poussot-Vassal *et al.*, 2011*b*) only the braking action (scheduled by R_b) is used , the lateral dynamics are controlled here using both the braking and steering actions, scheduled by R_b and R_s respectively. Also, here, suspension systems are considered equipped with Magneto-Rheological semi-active damper (of high interest for both industries and research communities). In the sequel, LPV/$\mathcal{H}_\infty$ controllers (scheduled by R_b and R_s) are developed within the polytopic approach.

6.3 First step: the braking/steering control problem formulation

The LPV/$\mathcal{H}_\infty$ controller synthesis for the braking/steering subsystems is achieved with the use of the following extended bicycle model (see Fig. 6.6).

6.3.1 Control oriented extended lateral bicycle vehicle model:

The model describes the lateral dynamics of the vehicle. It has been used in many studies in order to synthesize braking and steering control to enhance several behaviours such as the yaw rate, the lateral acceleration and the lateral sideslip dynamics.

$$\begin{bmatrix} \dot{v}_y \\ \dot{\psi} \\ \beta \end{bmatrix} = \begin{bmatrix} \frac{-C_f-C_r}{mv} & v-\frac{-C_f l_f+C_r l_r}{mv} & 0 \\ \frac{-C_f l_f+C_r l_r}{I_z v} & \frac{-C_f l_f^2-C_r l_r^2}{I_z v} & 0 \\ 0 & 1+\frac{l_r C_r-l_f C_f}{mv^2} & -\frac{C_f+C_r}{mv} \end{bmatrix} \begin{bmatrix} v_y \\ \psi \\ \beta \end{bmatrix} + \begin{bmatrix} \frac{C_f}{m} & -\frac{1}{m} & 0 \\ \frac{C_f l_f}{I_z} & 0 & \frac{t_r}{RI_z} \\ \frac{C_f}{mv} & 0 & \frac{1}{mv} \end{bmatrix} \begin{bmatrix} \delta \\ F_{dy} \\ T_{b_{rj}} \end{bmatrix} \tag{6.3}$$

where, δ= δ^0 + δ^+ (the driver and **controller additive steering angle** input respectively). $\dot{v}_y$: the lateral acceleration. v_y: vehicle lateral velocity. $\dot{\psi}$: the yaw rate of the vehicle. β: the sideslip of the car. v: the vehicle speed. $C_{f,r}$: the front and rear linear stiffness of the lateral tire. R: the nominal wheel radius. m: the vehicle mass. Iz: yaw inertia. F_{dy}: the disturbance lateral force. $T_{b_{rj}}$: the rear braking torques. $t_{r,f}$ and l_{rf}: (front, rear) axle and COG- front, rear) distance, respectively.

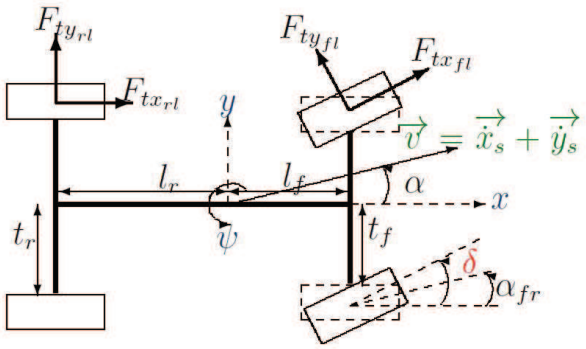

Figure 6.6: Bicycle vehicle model

6.3.2 The LPV/$\mathcal{H}_\infty$ braking/steering controller synthesis method:

The following general control configuration (including gain scheduled weighting functions) is considered:

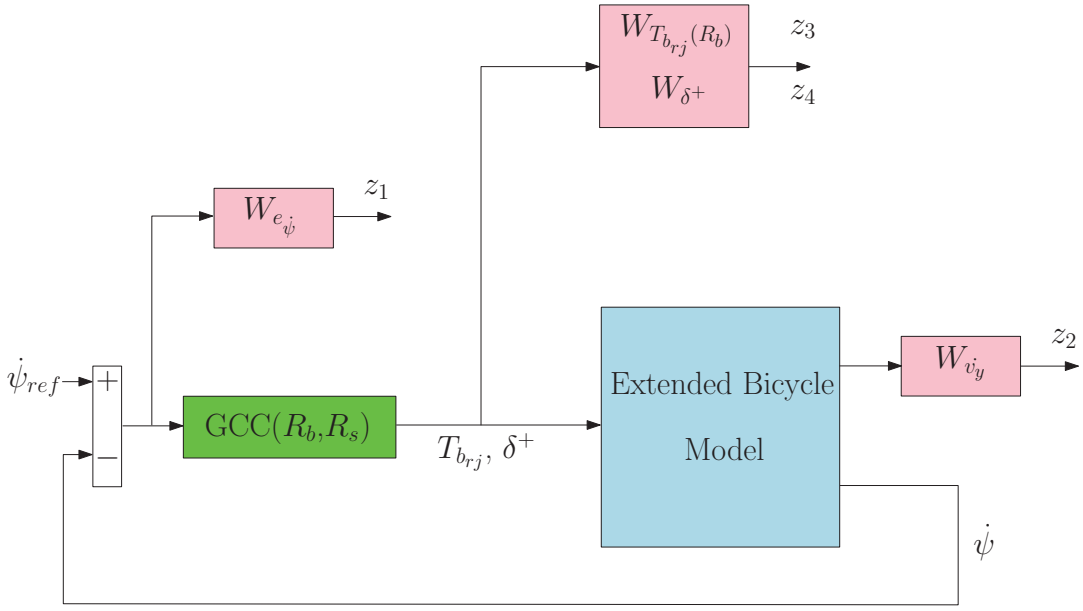

Figure 6.7: Generalized plant for braking/steering control synthesis.

where:

- $W_{e_{\dot\psi}} = 10\frac{s/500+1}{s/50+1}$, is used to shape the yaw rate error ($e_{\dot\psi} = \dot\psi_{ref} - \dot\psi$)
- $W_{\dot v_y} = 10^{-3}$, attenuates the lateral acceleration.
- $W_{T_{b_{rj}}}(R_b) = R_b\frac{s/10\varpi+1}{s/100\varpi+1}$, attenuates the yaw moment control input according to the value of R_b.

- $W_{\delta^+}(R_s) = R_s \frac{s/\kappa+1}{s/10\kappa+1}$, attenuates the steering control input according to the value of R_s.

Remark: The reference yaw rate $\dot{\psi}$ is calculated using the bicycle model, the steering input and the vehicle speed. It corresponds to the accurate yaw rate that the vehicle has to track to achieve the desired scenario and the performance objectives

where ϖ (resp.κ) is the braking (resp.steering) actuator cut-off frequency.

The controller is chosen to be scheduled by the varying parameters R_b and R_s (according to the diagram in Fig.6.5) in order to achieve the following objectives:

- **Normal situation:** The tire force is in the linear zone, i.e. there is no risk of wheel locking; so $R_b \to 0$ and the weighting function gain of $W_{T_{b_{rj}}}$ is chosen to be low. Therefore, the braking control is allowed to stabilize the vehicle. At the same time $R_s = 1$, the gain of the weighting function on the steering control is high and no additive steering angle is necessary and allowed.
- **Intermediate situation:** Since the proposed strategy in within the LPV framework, as the driving situation becomes more dangerous, the gains of the weighting functions on the braking and steering actions change to cope with the needs for the vehicle stabilization. Indeed, the braking action is more and more reduced to avoid the wheels skidding, while a more corrective steering angle is supplied to help keeping the vehicle stable.
- **Critical situation:** When a high slip ratio is detected (critical situation), so $R_b \to 1$, the gain of the weighting function is set to be high to deactivate the braking torques and prevent the wheels from locking. Then, the value of the varying parameter R_s is set to 0, the steering weighting function is not penalized any more and a maximum corrective action by the steering actuators is allowed to compensate for the lack of braking and to preserve the handling and stability of the vehicle. This may help the driver to overcome the critical driving situations.

The corresponding LPV generalized plant is modeled as:

$$\Sigma(R(.)) : \left[\begin{array}{c} \dot{x} \\ \hline z \\ y \end{array}\right] = \left[\begin{array}{c|cc} A(R_s,R_b) & B_1(R_s,R_b) & B_2 \\ \hline C_1(R_s,R_b) & D_{11}(R_s,R_b) & D_{12} \\ C_2 & 0 & 0 \end{array}\right] \left[\begin{array}{c} x \\ \hline w \\ u \end{array}\right] \tag{6.4}$$

where x includes the state variables of the system and of the weighing functions, $w = F_{dy}$ and $u = [\delta^+, T_{b_{rj}}]$ are the exogenous and control inputs respectively;
$z = [z_1, z_2, z_3, z_4] = [W_{e_{\dot{\psi}}} e_{\dot{\psi}}, W_{\dot{v}_y} \dot{v}_y, W_{T_{b_{rj}}}(R_b) T_{b_{rj}}, W_{\delta^+}(R_s)\delta^+]$ holds for the controlled output, and $y = \dot{\psi}_{ref}(v) - \dot{\psi}$ is the controller input, where $\dot{\psi}_{ref}(v)$ is provided by a reference bicycle model as the one described in (6.3).

According to this general plant formulation, the LPV controller $GCC_s(R_s, R_b)$ obtained is defined as,

$$\left[\begin{array}{c} \dot{x_c} \\ u \end{array}\right] = \left[\begin{array}{cc} A_c(R_s,R_b) & B_c(R_s,R_b) \\ C_c(R_s,R_b) & D_c(R_s,R_b) \end{array}\right] \left[\begin{array}{c} x_c \\ y \end{array}\right] \tag{6.5}$$

where $x_c \in \mathbb{R}^n$ includes the controller state variables, $u \in \mathbb{R}^{n_u}$, $y \in \mathbb{R}^{n_y}$. Then, $R_s \in \mathcal{P}_{R_s}$, s.t.

$$\mathcal{P}_{R_s} = \{R_s \in \left[\begin{array}{cc} \underline{R}_s & \overline{R}_s \end{array}\right]\}, \text{where, } \underline{R}_s = R_{min} \text{ and } \overline{R}_s = R_{max} \tag{6.6}$$

and $R_b \in \mathcal{P}_{R_b}$, s.t.

$$R_b \in \left[\begin{array}{cc} \underline{R}_b & \overline{R}_b \end{array} \right] \text{, where, } \underline{R}_b = R_{min} \text{ and } \overline{R}_b = R_{max} \tag{6.7}$$

Notice that the LPV model (7.33) is here affine w.r.t the parameters R_s and R_b and can be described as a polytopic system, i.e. a convex combination of the systems defined at each vertex formed by $\mathcal{P}_R(.)$, namely $\Sigma(\underline{R}(.))$ and $\Sigma(\overline{R}(.))$. The controller is then a convex combination of 4 vertiex controllers obtained at the min/max of R_b/R_s. From the affine generalized plant of Fig. 6.7, an LPV polytopic controller is designed in the framework of the quadratic stabilisation, (as presented in appendix).

The following frequency domain plots are provided here for performance analysis of the lateral dynamics control.

6.3.3 Performances Analysis:

Analysis of the steering control input:
The following figures represent the LPV/$\mathcal{H}_\infty$ steering input control and the yaw rate tracking error with the value of the varying parameter $R_s = 0$ and $R_s = 1$ (upper and lower bounds of the variation interval of the varying parameter).

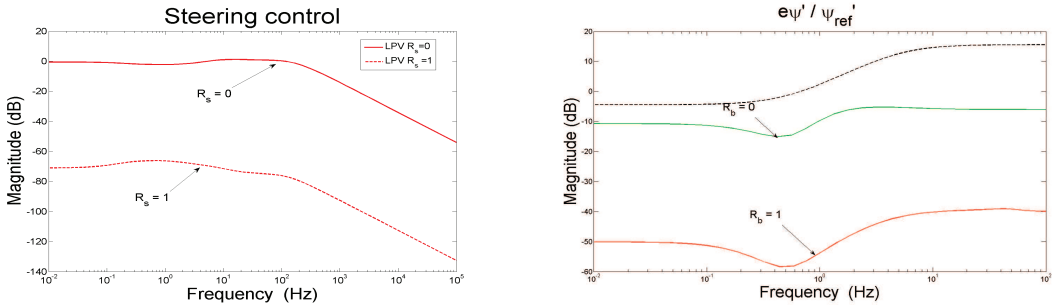

Figure 6.8: LPV Steering control (left), yaw rate tracking error (right)

In Normal situation: $R_s = 1$, the steering control action is penalized and no additional steering angle is delivered.

In Critical situation: $R_s = 0$, the steering control action is enabled since the driver can not manage a critical driving situation by using only the braking action.
Fig. 6.8 (right) illustrates the performance of the tracking control problem of the yaw reference, which is, in any case, satisfactory according to the required performance specifications.

Analysis of the braking control input:

The following figures represent the LPV/$\mathcal{H}_\infty$ braking input controls (the braking torques) of the rear right/left wheels, function of the value of the varying parameter $R_b = 0$ and $R_b = 1$ (upper and lower bounds of the variation interval of the varying parameter). In Fig.6.9, the use of the braking actuators

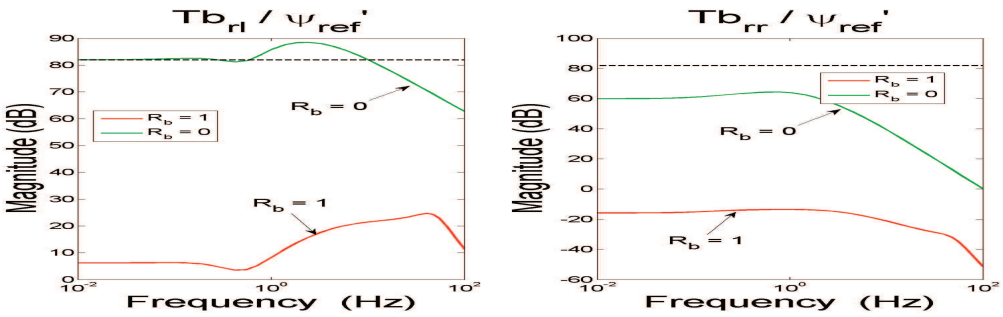

Figure 6.9: Braking torques $T_{b_{rl}}(left)$, $T_{b_{rr}}(right)$

is emphasized, as a function of the braking monitor R_b:

In Normal situation: $R_b = 0$, the braking weighting function is low and the braking action is allowed to stabilize the vehicle.
In Critical situation: $R_b = 1$, the braking action is penalized, the weighing function gain limits the braking torques on the rear wheels to avoid tire locking and vehicle roll-over.

6.4 Second step: the suspension control problem formulation

The control of the semi-active MR dampers is synthesized using the classical 7-DOF vertical model (see Fig. 6.10) in order to handle the trade-off between the chassis motion (comfort) and the roll motion (handling).

6.4.1 Control oriented full vertical vehicle model

This model includes the vertical dynamics of the chassis, the vertical motions of the wheels, the pitch and roll, respectively, z_s, $z_{us_{ij}}$, θ,and ϕ. The dynamical equations are:

$$\left\{\begin{array}{rcl} \ddot{z}_s & = & -\big(F_{sz_f} + F_{sz_r} + F_{dz}\big)/m_s \\ \ddot{z}_{us_{ij}} & = & \big(F_{sz_{ij}} - F_{tz_{ij}}\big)/m_{us_{ij}} \\ \ddot{\theta} & = & \big((F_{sz_{rl}} - F_{sz_{rr}})t_r + (F_{sz_{fl}} - F_{sz_{fr}})t_f\big)/I_x \\ \ddot{\phi} & = & \big(F_{sz_f} l_f - F_{sz_r} l_r\big)/I_y \end{array}\right. \tag{6.8}$$

where, F_{sz_i} are the vertical suspension forces, $F_{tz_{ij}}$ the vertical tire forces, I_x, I_y, I_z : the roll, pitch and yaw moments and F_{dz} the disturbance yaw moment and

$$\left\{\begin{array}{rcll} F_{tz_{ij}} & = & k_t(z_{us_{ij}} - z_{r_{ij}}) + c_t(\dot{z}_{us_{ij}} - \dot{z}_{r_{ij}}) & \\ F_{sz_{ij}} & = & F_k(z_{s_{ij}} - z_{us_{ij}}) + F_c(\dot{z}_{s_{ij}} - \dot{z}_{us_{ij}}) & \text{(passive suspension case)} \\ F_{sz_{ij}} & = & F_k(z_{s_{ij}} - z_{us_{ij}}) + u_{ij}^{\mathcal{H}_\infty} & \text{(controlled suspension case)} \end{array}\right. \tag{6.9}$$

k_t and c_t denoting the linear tire stiffness and damping factors.

Here, one considers a vehicle equipped with "Magneto-Rheological" semi-active dampers. The Magneto-Rheological (MR) damper is a non-linear component with dissipative capability used in automotive suspension control systems, where the damping property varies according to the applied

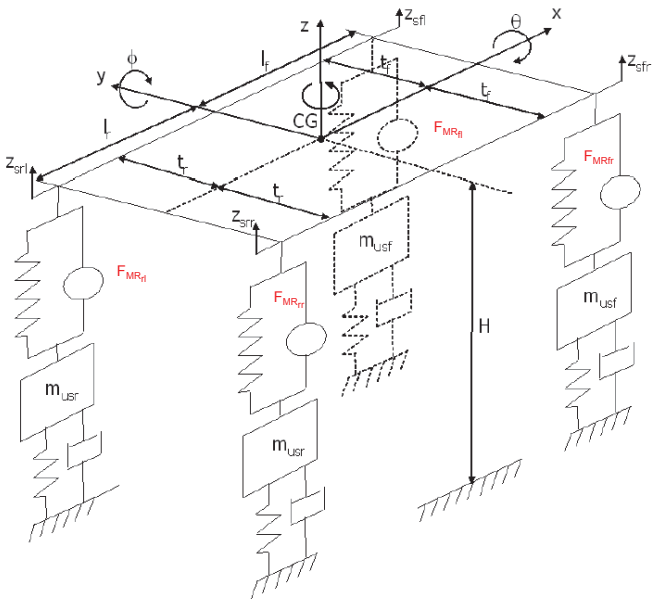

Figure 6.10: Full vertical vehicle model

magnetic field. Such a damper is able to provide adaptive performances in terms of comfort and road holding.
For control purpose, the semi-phenomenological model given in (Guo *et al.*, 2006*b*; Do *et al.*, 2010*a*) is considered since it allows to account for the hysteresis and bi-viscous damper characteristics.

Remark: The bicycle model (see Fig. 6.6) and the vertical model (see Fig. 6.10) are linear models, extracted from the non linear full vehicle model. They are used for the controllers synthesis purpose.

6.4.2 LPV/$\mathcal{H}_\infty$ suspension controller synthesis:

The control of suspension systems aims at enhancing the vertical dynamics of the vehicle in order to achieve frequency specification performances, see (Savaresi *et al.*, 2010*b*) and (Poussot-Vassal *et al.*, 2006). Here the control objectives are oriented towards bounce and roll motions characterized by the frequency-domain weighting functions in the $\mathcal{H}_\infty$ control framework of Fig. 6.11.

where $W_{z_s}(R_s) = R_s \frac{s^2+2\xi_{11}\Omega_{11}s+{\Omega_{11}}^2}{s^2+2\xi_{12}\Omega_{12}s+{\Omega_{12}}^2}$ is shaped in order to reduce the bounce amplification of the suspended mass (z_s) between $[0, 12]$Hz, when R_s is high.
$W_\theta(R_s) = (1-R_s)\frac{s^2+2\xi_{21}\Omega_{21}s+{\Omega_{21}}^2}{s^2+2\xi_{22}\Omega_{22}s+{\Omega_{22}}^2}$ attenuates the roll amplification in low frequencies, when R_s is low.
$W_u = 3.10^{-2}$ is set to shape the control signal.

This control design schedules the use of the semi-active suspensions and the vehicle performance as follows:

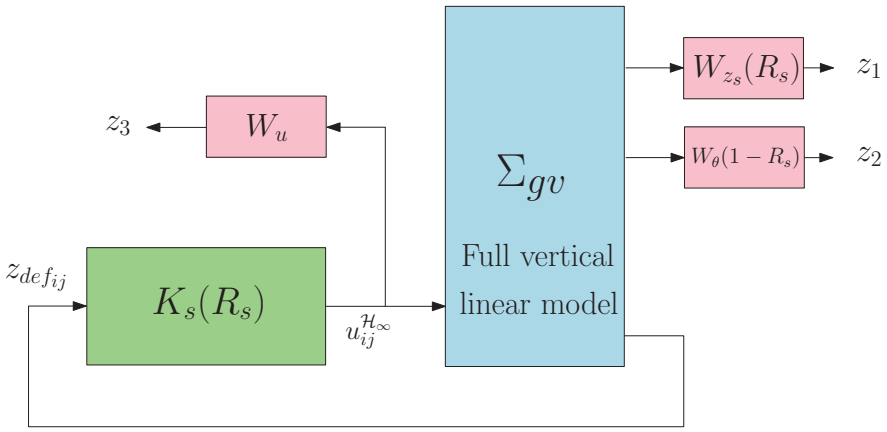

Figure 6.11: Suspension system generalized plant.

In Normal situation: $R_s = 1$, the semi-active suspension control enhances the passengers comfort objectives by using a high gain of the weighting function on the chassis displacement z_s. The undesirable vibrations of the chassis are then absorbed by the Magneto-Rheological semi-active dampers which are tuned to have a soft damping characteristic (see later the illustration Fig. 6.15).

Intermediate situation: As the driving situation changes, the value of the varying parameter R_s decreases, such that the suspension control changes the performance objectives from the passenger comfort (by reducing the weighting function on the chassis displacement) to the roadholding by increasing the weighting on the roll dynamics of the car caused by the lateral load transfers. The LPV framework used in the proposed strategy ensures a smooth and efficient transition between these performance objectives while ensuring the stability conditions.

In Critical situation: $R_s = 0$, the semi-active suspension control acts to improve the roadholding. The weighting on the chassis motion is relaxed since the passengers comfort is no longer a priority and a high penalization on the roll motion is set to reduce the load transfer that may lead to vehicle instability (close to accident).
The configuration of the proposed LPV/$\mathcal{H}_\infty$ ensures the appropriate help to the driver by monitoring the driving situation and the related vehicle dynamics. The main purpose is to preserve the passengers safety and to help to overcome different emergencies while facing such situations.

Remark:

- The selection of the parameters of the weighting functions is a key step in $\mathcal{H}_\infty$ control. Usually, the choice of these parameters is achieved using empirical rules, thanks to the automotive engineers experience but it doesn't guarantee any optimal value for these parameters. Here, the choice of these parameters is done, following the methodology described in (Do *et al.*, 2010*a*) where a genetic algorithm optimization was used to obtain the parameter values that minimize

a criterion representative enough of the vehicle vertical performances in terms of comfort and roadholding.

- Let us also recall that when $R_b > R^2_{crit}$, the braking is in the linear zone (tire stable zone), hence, suspensions are tuned to improve comfort (i.e. $R_s \to 1$). Conversely, when $R_b < R^1_{crit}$, the braking becomes critical, hence, suspensions are harder (i.e. $R_s \to 0$).

According to Fig. 6.11, the following parameter dependent generalized plant ($\Sigma_{gv}(R_s)$) is obtained:

$$\left[\begin{array}{c} \dot{\xi} \\ \hline z \\ y \end{array}\right] = \left[\begin{array}{c|cc} A(R_s) & B_1(R_s) & B_2 \\ \hline C_1(R_s) & D_{11}(R_s) & D_{12} \\ C_2 & 0 & 0 \end{array}\right] \left[\begin{array}{c} \xi \\ \hline w \\ u \end{array}\right] \tag{6.10}$$

where $\xi = [\chi_{vert}\ \chi_w]^T$ is the state vector of the system plus the state vector of the weighting functions; $\tilde{z} = [z_1\ z_2\ z_3]^T$; $\tilde{w} = [z_{rij}\ F_{dx,y,z}\ M_{dx,y}]^T$; $y = z_{def_{ij}}$; $u = u_{ij}^{\mathcal{H}_\infty}$; and F_{dz} is the vertical disturbance and M_{dz} is the disturbance moment along z-axis.

The LPV system (8.39) includes a single scheduling parameter (R_s) and can be described as a polytopic system after some relaxations, i.e, a convex combination of the systems defined at each vertex of a polytope defined by the bounds of the varying parameter.

Remark: Since semi-active suspensions are considered, the LPV controllers are clipped in order to cope with the damper constraints The LPV/$\mathcal{H}_\infty$ suspension controller synthesis is obtained thanks

to LMI's resolution of the control problem presented as follows:

According to the general plant formulation, the LPV controller $K_s(R_s)$ obtained is defined as,

$$\left[\begin{array}{c} \dot{x_c} \\ u \end{array}\right] = \left[\begin{array}{cc} A_c(R_s) & B_c(R_s) \\ C_c(R_s) & D_c(R_s) \end{array}\right] \left[\begin{array}{c} x_c \\ y \end{array}\right] \tag{6.11}$$

where $x_c \in \mathbb{R}^n$ are the controller states, $u \in \mathbb{R}^{n_u}$, $y \in \mathbb{R}^{n_y}$. Then, $R_s \in \mathcal{P}_{R_s}$, s.t.

$$R_s \in \left[\begin{array}{cc} \underline{R}_s & \overline{R}_s \end{array}\right], where, \underline{R}_s = R_{min}\ and\ \overline{R}_s = R_{max} \tag{6.12}$$

Then the LPV/$\mathcal{H}_\infty$ control synthesis solution is obtained, using the mathematical development given in (Scherer, 2004).

6.4.3 Performances Analysis

Analysis of the vertical dynamical performance:

The following frequency domain plots allow to analyse the vertical performances of the suspension controller.

First in Fig. 6.12, the vertical dynamics of the vehicle (position of the sprung mass and roll angle) are given. Indeed, a comparison between passive vehicle with performances set to enhance only

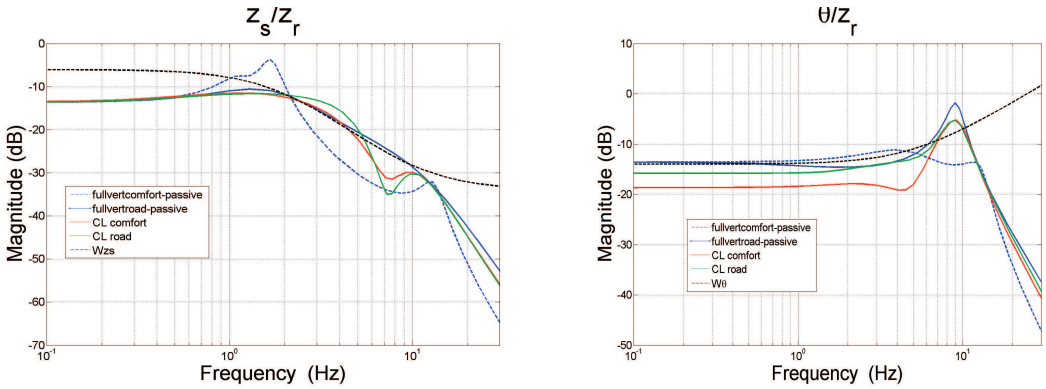

Figure 6.12: Vertical dynamics: chassis displacement (left) and roll motion (right)

the comfort or the road holding (fullvertcomfort-passsive and fullvertroad-passsive) and closed loop system with the designed LPV/$\mathcal{H}_\infty$ controller. When $R_s = 1$ (obtained from the LPV controller by solving the previous $\mathcal{H}_\infty$ frozen with $R_s = 1$), the suspension control improves the comfort by reducing the chassis displacement z_s thanks to the weighting function that penalizes this degree of freedom , while when $R_s = 0$ (obtained from the LPV controller by solving the previous $\mathcal{H}_\infty$ frozen with $R_s = 0$), the suspension dampers are set to "hard", the charge transfers are reduced and the roll motion θ is reduced to enhance passengers safety.

Analysis of the suspension control input:

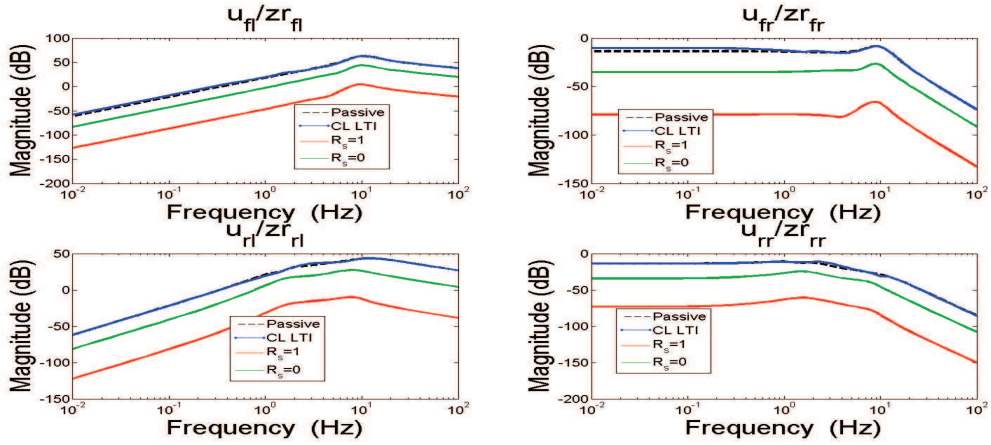

Figure 6.13: Suspension Forces

In Fig. 6.13 the suspension systems forces gain are plotted. It shows that the required additional forces $u_{ij}^{\mathcal{H}_\infty}$ are quite low, compared to the passive nominal forces: $F_{s_{ij}} = k_{ij}(z_{s_{ij}} - z_{us_{ij}}) + c_{ij}(\dot{z}_{s_{ij}} - \dot{z}_{us_{ij}})$.
The control inputs given by the LPV controllers obtained by solving the previous $\mathcal{H}_\infty$ frozen with $R_s = 0$, and $R_s = 1$ are also shown. It shows that the LPV controllers better handle the limit of the control inputs, ensuring then energy saving.

6.4.4 The semi-active suspension control implementation

The semi-active control of the considered suspension is achieved here by the clipped strategy, see Fig. 6.14, using the data characteristics of the Magneto-Rheological dampers obtained with the experimental procedure in collaboration with colleagues from Technological institute of Monterry, Mexico (see (Jorge De-J *et al.*, 2012)).
Here, the simple "Clipped approach" is used to focus the contribution on the actuator coordination (and then to avoid a too large number of scheduling parameters). This approach is depicted in Fig.6.14: for a given deflection speed ($\dot{z}_{def}$), if the controller computes a force F^* out of the achievable damper range, the force provided to the system will be the projection $F^\perp$ of F^* on the admissible force area.

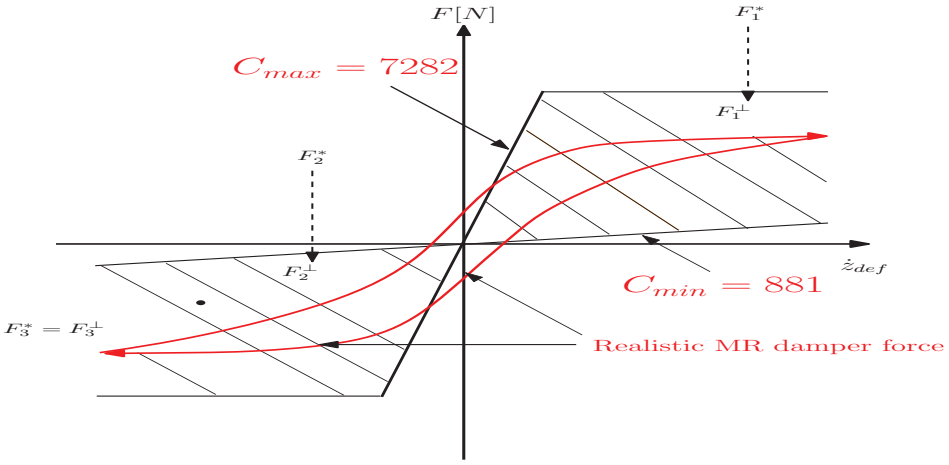

Figure 6.14: Illustration of projection principle of the semi-active controlled damper model (F_1^* and F_2^* are out of the allowed area and F_3^* is inside) + the MR damper force with bi-viscosity "$C_{min} = 881$, $C_{max} = 7282$"

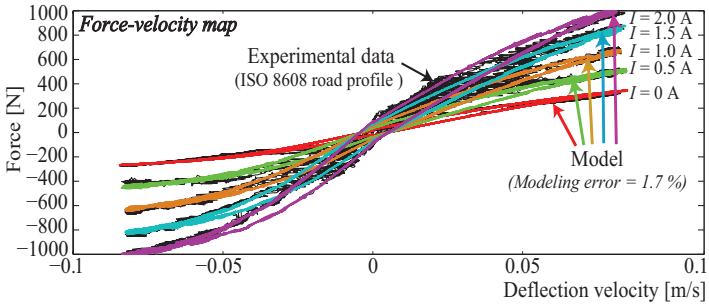

Figure 6.15: Model of the *MR* damper for different I values.

This damper allows to achieve good comfort, to enhance the road holding and to keep a safety suspension deflection.
In the parametric model given in (Guo *et al.*, 2006*b*), the hysteresis force-velocity loop is well modeled by an hyperbolic tangent function and the *MR* damping force is modeled by:

$$F_{MR} = I f_c \tanh\left(a_1 \dot{z}_{def} + a_2 z_{def}\right) + b_1 \dot{z}_{def} + b_2 z_{def} \tag{6.13}$$

where the electric current is bounded between $0 \leq I_{min} \leq I \leq I_{max} \leq 2.5$. I_{min} and I_{max} depend on the *MR* damper specifications. Figure 6.15 shows the characteristics of the *MR* damper model used in this analysis; the parameters $fc = 600.9$, $a_1 = 37.8$, $a_2 = 22.1$, $b_1 = 2830.8$ and $b_2 = -7897.2$ were obtained by an experimental study of the Magneto-Rheological dampers.

The strategy proposed in this chapter is valid for other types of semi-active dampers since it requires only upper and lower bounds of the considered actuator. For the used M-R dampers, these boundaries are $C_{min} = 881$ and $C_{max} = 7282$.
It is worth noting that the dissipativity constraint of semi-active dampers can be taken into account in the LPV framework as presented in (Do *et al.*, 2010*a*) but at the price of an increased complexity. This could be handled in future works.

The LPV solution allows to use optimally each actuator depending on the driving situation and to smoothly switch between them to overcome critical cases. The robustness of the solutions is ensured through the $\mathcal{H}_\infty$ framework. The whole controllers synthesis is achieved thanks to the LMI's resolution.

6.5 Simulation study

In this section, the complete and validated non linear model of the vehicle is considered for simulation purpose (see section model). Then, 2 different simulation scenarios are given and the corresponding results are analysed.

All along this section, the proposed LPV/$\mathcal{H}_\infty$ VDC , denoted as 'LPV', will be analyzed and compared to the Renault Mégane Coupé car (without control denoted "open Loop") and, for sake of completeness, with the standard LTI/$\mathcal{H}_\infty$ design of both Active Steering/ Braking controller and semi-active suspension controller (without scheduled gains), denoted as 'LTI', which was achieved by solving the previous $\mathcal{H}_\infty$ problems with constant values for the varying parameter ($R_s = 0.1$ and $R_b = 0.9$).

6.5.1 Simulation. First scenario:

The following scenario is considered (see Fig.6.16).
When the vehicle runs at 100km/h in straight line,

1. from $t = 0.5$s to $t = 1$s: 5cm bump on the left wheels ,
2. from $t = 2$s to $t = 6$s: a double line change manoeuvre is performed by the driver,
3. from $t = 2.5$s to $t = 3$s: a lateral wind occurs at vehicle's front, generating an undesirable yaw moment,
4. from $t = 3$s to $t = 3.5$s: 5cm bump on the left wheels, during the manoeuvre,

In this scenario, the road is considered as wet ($\mu = 0.5$, the road adherence parameter), which reduces the road/tire adhesion and the lateral tire contact forces.
The resulting monitored signals R_b (see Eq.(6.1)) and R_s (see Eq.(6.2)) are shown in Fig. 6.17 and they entail the LPV framework of the strategy.

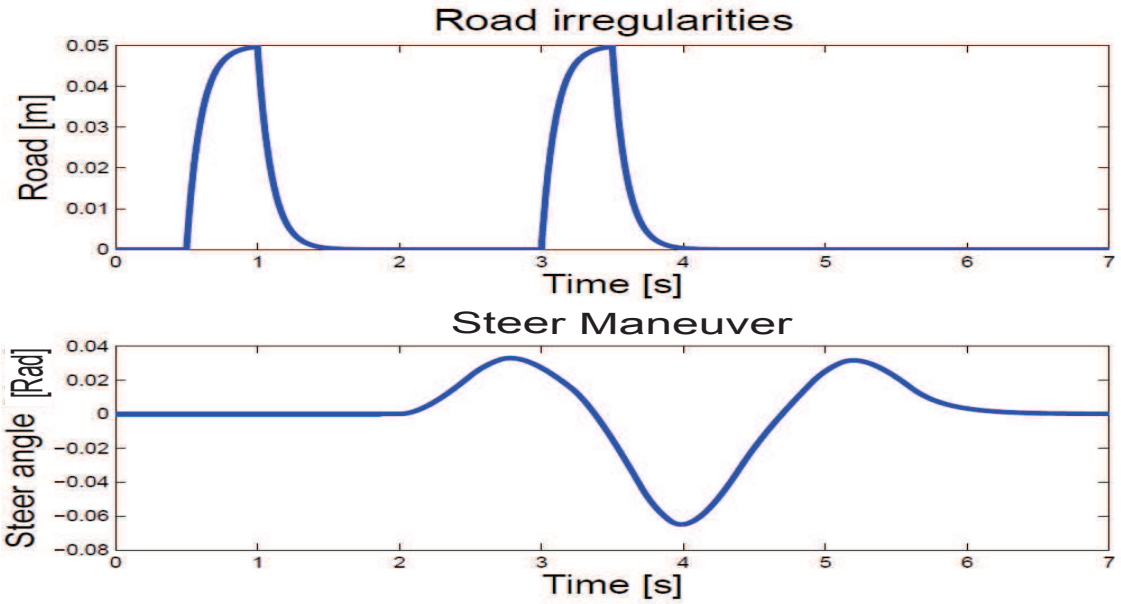

Figure 6.16: Input signals

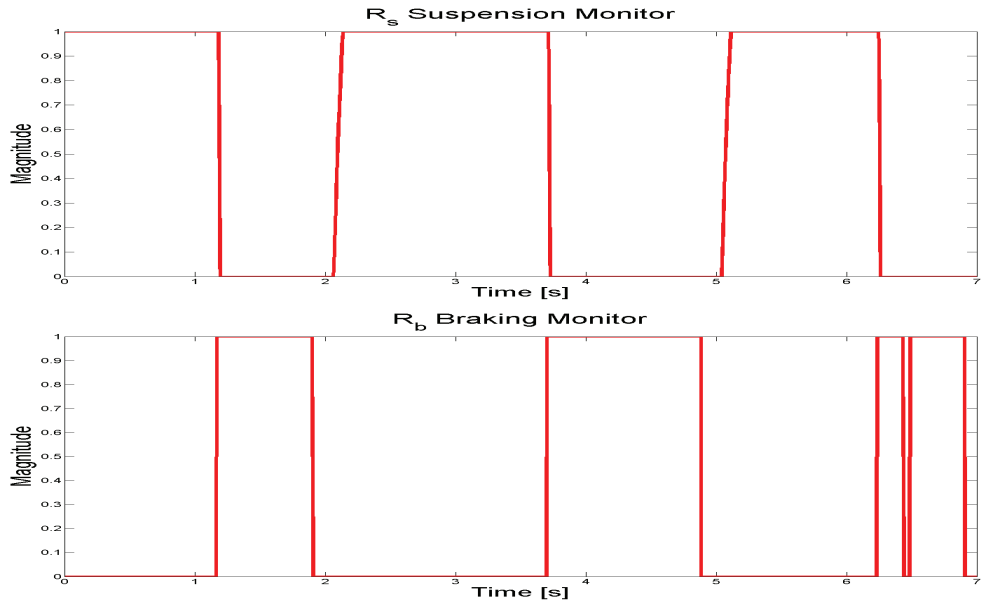

Figure 6.17: Monitoring signals

The varying parameters R_b and R_s allow to activate, limit or deactivate the control action when required (for braking and steering actuators). Let recall that the R_s scheduling parameter depends on the value of R_b, which itself monitors the slip ratio dynamics. Those parameters are very important since they define the behavior of the vehicle subject to critical driving situations. They will allow to provide the necessary assistance to the driver using the steering, braking and suspension subsystems.

6.5.1.1 Lateral dynamics behaviour analysis

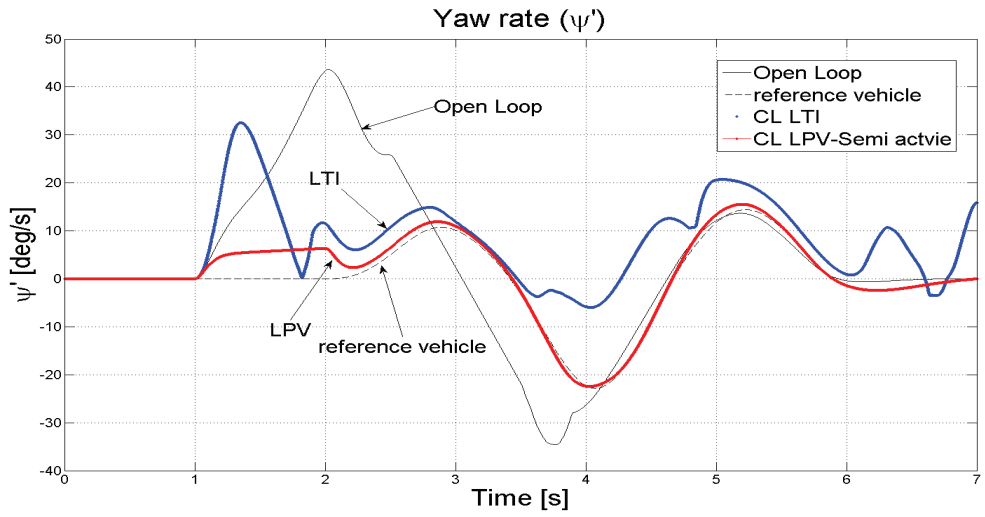

Figure 6.18: Yaw rate

It can been seen from Fig. 7.12 that the proposed LPV/$\mathcal{H}_\infty$ strategy enhances better the lateral dynamics, namely here, the vehicle yaw tracking. Compared to the LTI/$\mathcal{H}_\infty$ controller, it gives good results in terms of vehicle lateral stability.

Remark: Simulations using the extended bicycle model with the driver input give the "ideal" reference to be tracked by the vehicle (black dashed line). It helps to compare and to emphasize the improvements brought by the proposed LPV/$\mathcal{H}_\infty$ strategy

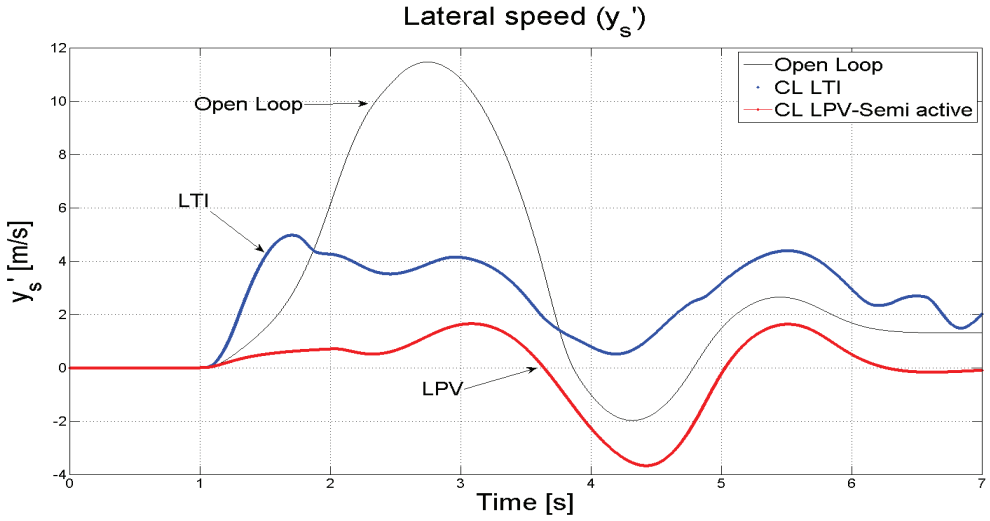

Figure 6.19: Lateral speed

Fig. 6.19 shows clearly that the LPV strategy first improves the lateral dynamics by reducing

the lateral speed (and implicitly the lateral acceleration) and then allows a better yaw rate tracking see Fig. 7.12) which enhances therefore the stability of the vehicle subject to this critical driving situation.

6.5.1.2 Vertical dynamics behaviour analysis

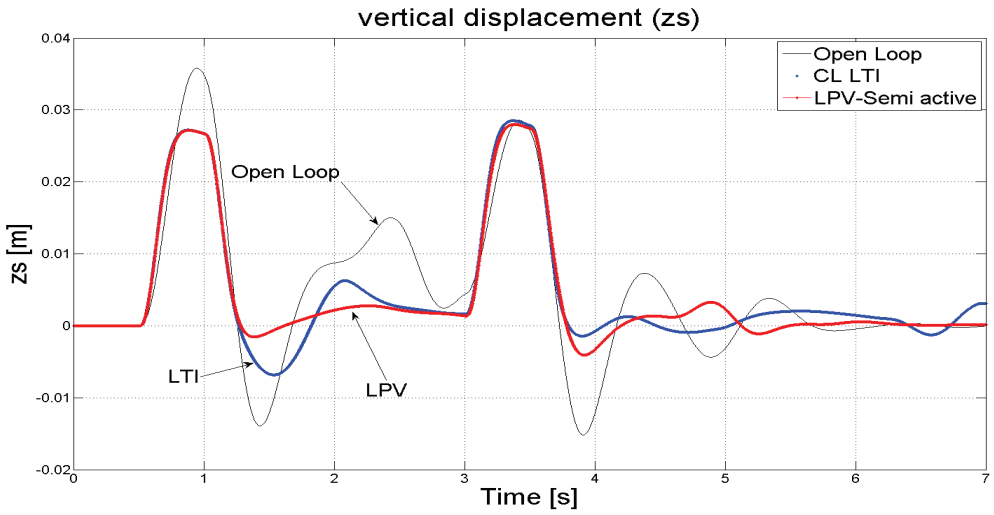

Figure 6.20: Vertical chassis displacement z_s

The vertical motion of the chassis is shown in Fig. 7.29. The LPV/$\mathcal{H}_\infty$ controller improves better the vertical dynamics than the LTI/$\mathcal{H}_\infty$ one does. The chassis displacement is considerably reduced by the proposed LPV/$\mathcal{H}_\infty$ strategy. This enhances the passengers comfort while driving on uneven roads.

Fig. 6.21 represents the improvement brought in term of the load transfer mitigation. The roll motion

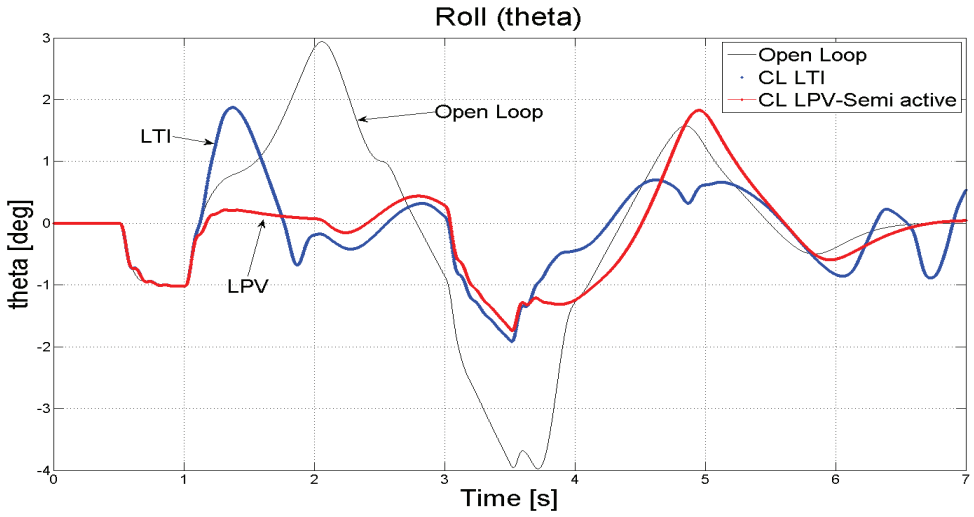

Figure 6.21: Roll motion of the chassis θ

is well attenuated which, in addition to enhance the vehicle stability, ensures a good road handling of the vehicle running in dangerous driving situations. It can be seen that the use of the semi-active suspension control in the coordinated "LPV/$\mathcal{H}_\infty$" strategy (with hierarchical activation of the different actuators depending on the driving situations needs) gives better results than in the "LTI" case.

6.5.1.3 Actuators dynamics behaviour analysis

In addition of enhancing the vehicle various dynamics, the proposed LPV/$\mathcal{H}_\infty$ improves the use of the actuators of electromechanical braking, active steering and semi-active suspensions considered for the car under study. The following figures show interesting results for the actuators activation:

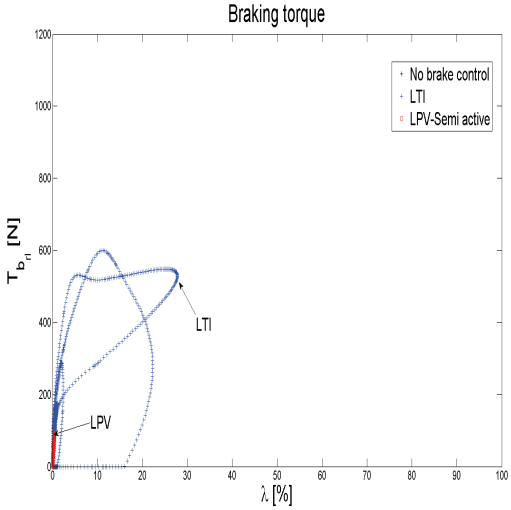

Figure 6.22: Rear right Breaking torque.

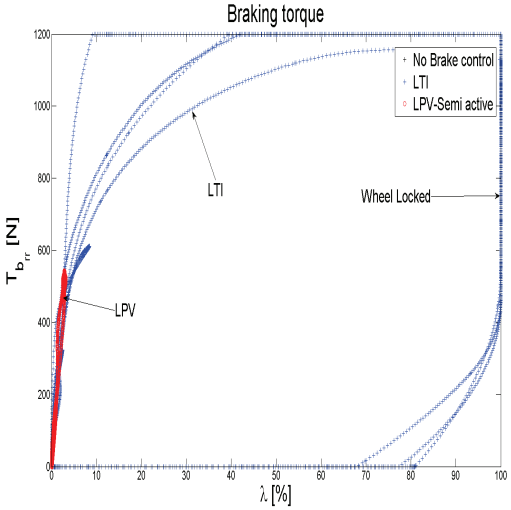

Figure 6.23: Rear left Breaking torque.

Fig. 6.22 and Fig. 6.23 show the braking torques provided by the vehicle to perform the previously defined scenario. The braking torques provided by the LPV/$\mathcal{H}_\infty$ controller are depicted in red. It is clear that the torques are much lower than those provided in the LTI controller case, which saturate. Also, the use of the LPV/$\mathcal{H}_\infty$ strategy avoids wheel locking, while, Fig. 6.23 shows that for the LTI case, the longitudinal slip ration λ_{rl} reaches the value of 100% which indicates that the left rear wheel is locked.

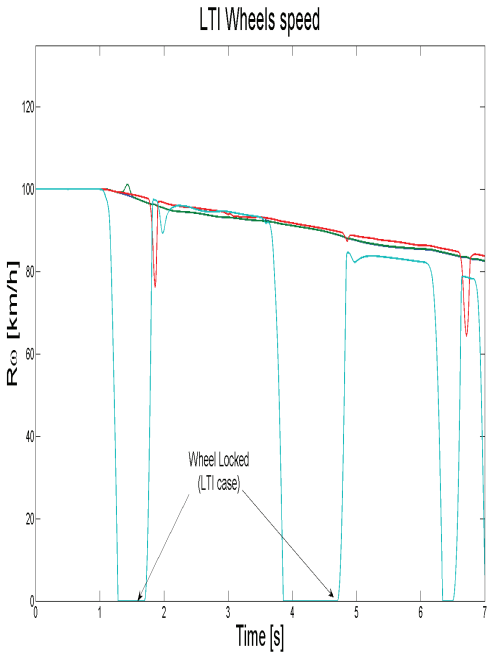

Figure 6.24: Wheels speed LTI

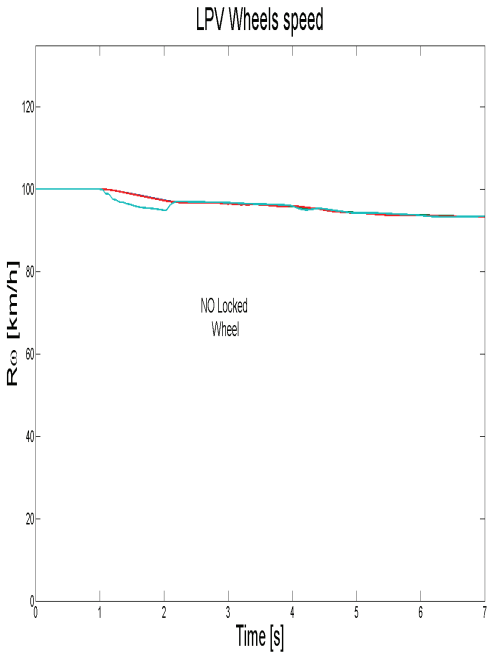

Figure 6.25: Wheels speed LPV

In Fig. 6.24, the rotational speed of the rear left wheel subject to $T_{b_{rl}}$ decreases to reach 0 for the LTI controlled car, causing the wheel locking and the loss of manoeuvrability.

This is not the case for the LPV controlled car which only undergoes a small speed decrease, see Fig. 6.25.
Fig. 6.26 shows that the active steering actuators are saturated using the LTI/$\mathcal{H}_\infty$ during this scenario. The proposed LPV/$\mathcal{H}_\infty$ strategy limits the use of the steering actuator, gives a smoother action and never saturates the actuator (see blue curve).

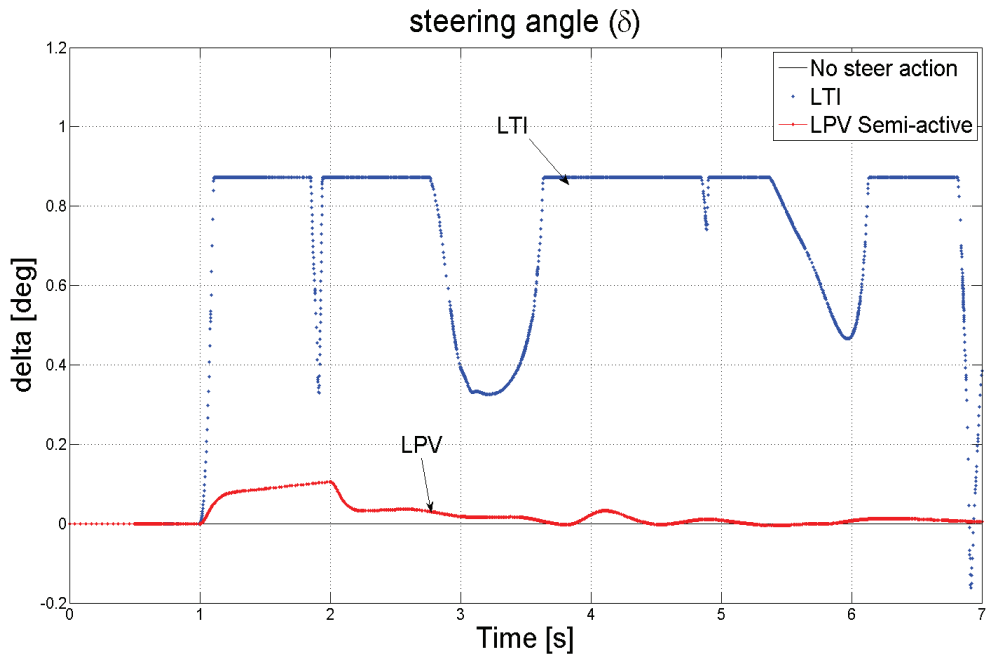

Figure 6.26: Steer control input

Fig. 6.26 shows also that the ”LPV coordination strategy” can help the driver to keep the vehicle stable with a minimum effort. The steer control considerably decreases in the ”LPV” case compared to the ”LTI” case, and is activated only when the driving situation is dangerous enough.

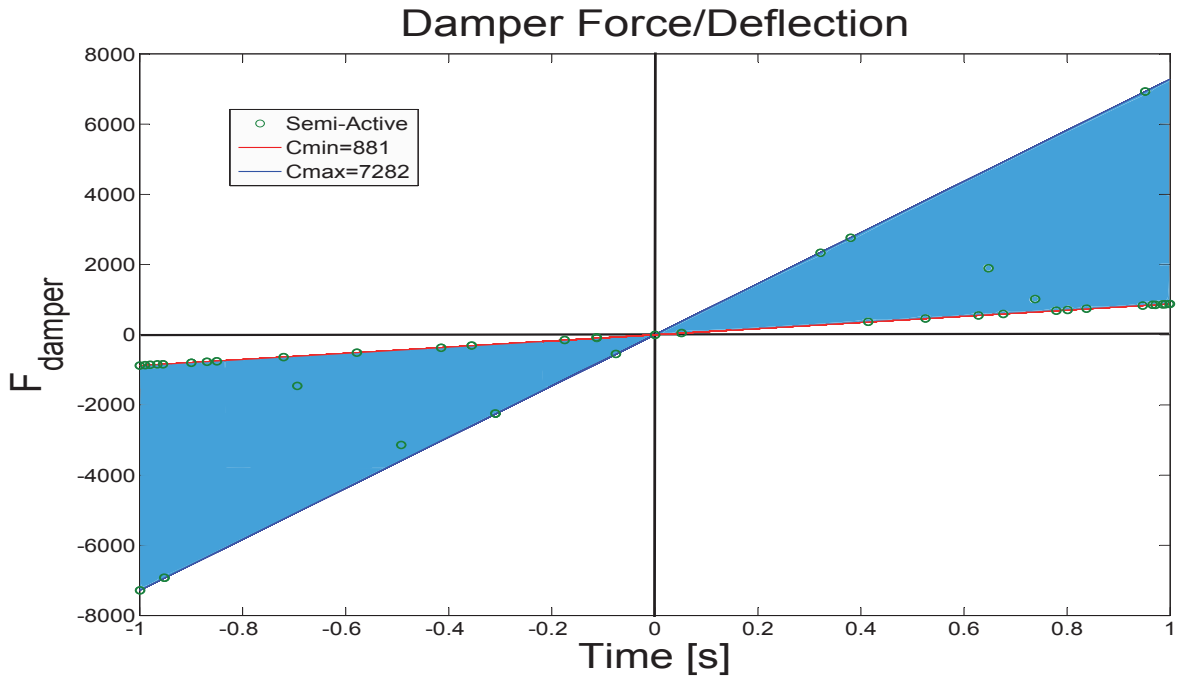

Figure 6.27: Damper force/deflection

Finally, Fig. 6.27 shows the force/deflection characteristic of the semi-active suspension control. The semi-activeness is obtained by the "Clipped Strategy" that takes into account the min and max damping limits of the Magneto Rheological dampers, namely $C_{min} = 881$ and $C_{max} = 7282$. These types of dampers have been studied and their characteristics analysed in previous works (more details in (Jorge De-J *et al.*, 2012)).

Remark: In the previous simulations, the LTI control strategy gives fairly good results. However, since the rear wheels lock during the manoeuvre as shown in Fig. 6.23 leading to a very high risk of loss of manoeuvrability and safety degradation, the LPV control appears to be a very efficient way to deal with the braking issues. Moreover, it enhances performances and stability, using the previously presented integrated control strategy. Furthermore, the LPV controller uses the actuators of braking, steering and suspensions in a coordinated way to enhance first the overall vehicle dynamics, and second to cope better with the actuators characteristics and limitations.

6.5.2 Simulation. Second scenario:

This scenario has been performed, for the uncontrolled car, on a professional real race track by a professional driver. The data used in the simulation were collected during these tests. It is also worth noting that the non linear full vehicle model used for the simulations was also validated during this test procedure.
There, the moose test is made at a velocity of $90km.h^{-1}$ to assess the efficiency for obstacles avoidance of the designed controllers (see Fig.6.28). This circuit includes a left bend and then an obstacle

avoidance in emergency situation to determine how well a vehicle evades a suddenly appearing obstacle. Here, the same scenario for identification is used to compare with a passive vehicle.

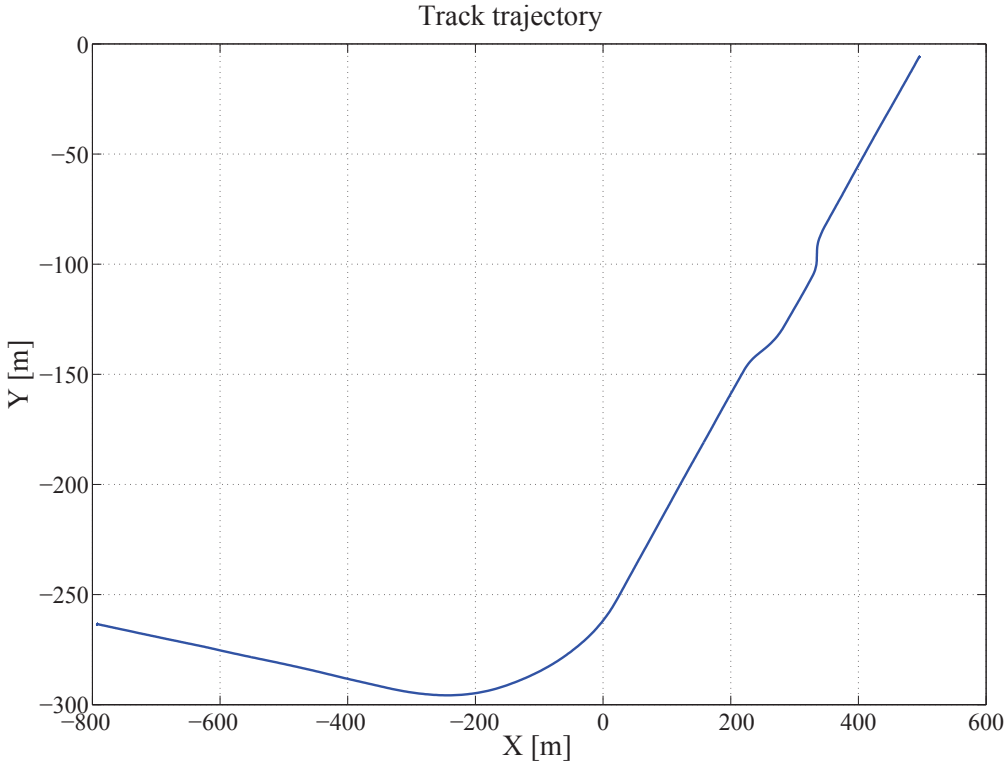

Figure 6.28: Second scenario trajectory

The resulting varying parameters that schedule the coordination of the 3 actuator's controllers (Semi-Active Suspension, Active Steering and Electro-Mechanical Braking) R_b and R_s are shown on Fig. 6.29.

These parameters are complementary, which is coherent with the previously presented monitoring strategy.

Remark: All the passive vehicle dynamical behaviours presented in this section were measured on the real vehicle (Renault Mégane Coupé) while performing this simulation scenario on a real circuit path.

Fig. 6.30 shows the yaw rate behaviour of the vehicle using the presented $LPV/\mathcal{H}_\infty$ compared to the passive vehicle behaviour. One can notice that the yaw rate dynamics of the vehicle are well improved even if the vehicle is running with a quite high velocity $90km.h^{-1}$ on the left bend when avoiding the obstacle.

The Fig. 6.31 clearly shows that the lateral acceleration of the vehicle is considerably reduced with the controller scheduled by the varying parameters. The stability of the vehicle is then improved

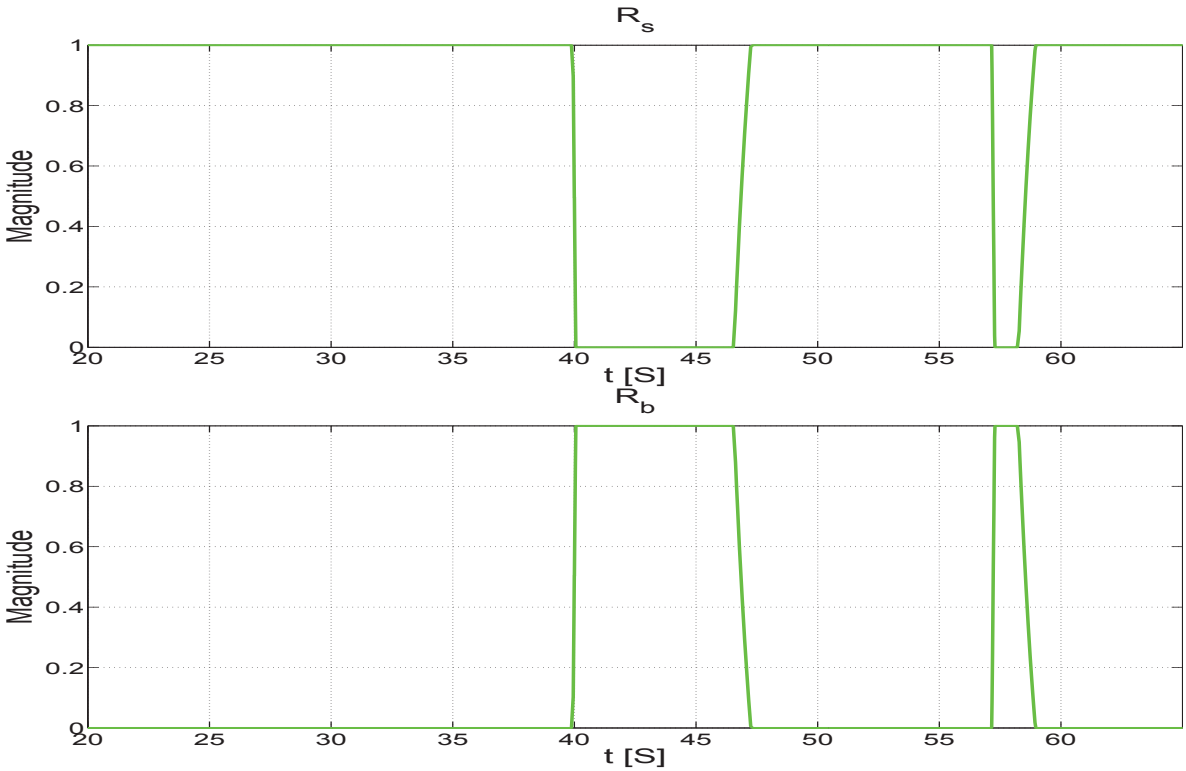

Figure 6.29: Monitoring R_s and R_b signals

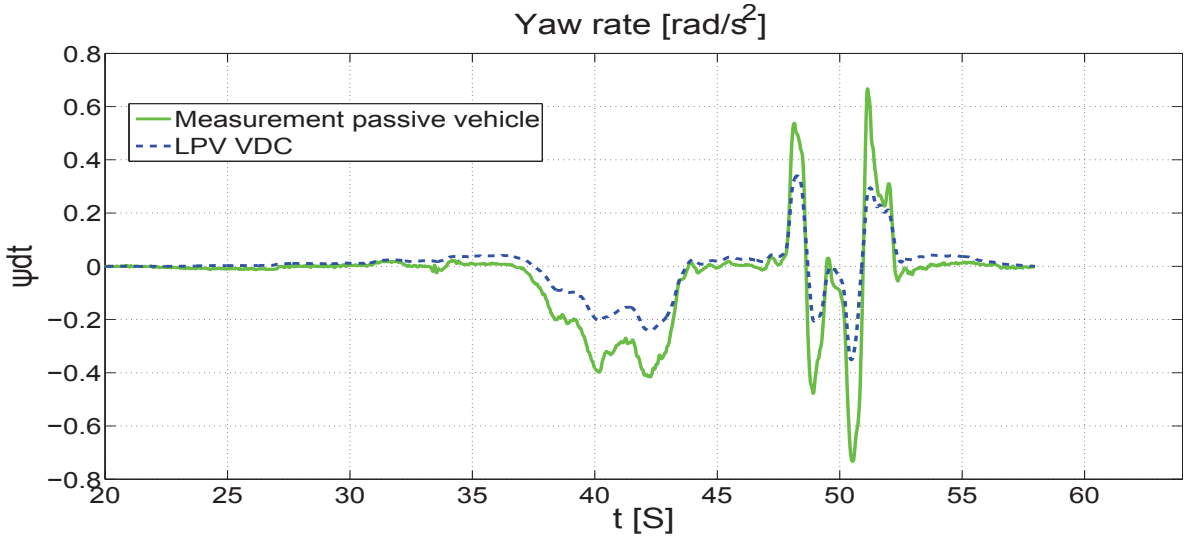

Figure 6.30: Yaw rate $\dot{\psi}$

and the lateral dynamics of the car are well improved.

Fig. 6.32 shows the improvement of the roll velocity. Indeed, using the designed $LPV/\mathcal{H}_\infty$ controllers that coordinate the use of the semi-active suspension, steering and braking, the roll motion is considerably reduced (47% less than that of the passive car). It is obvious that the vertical dynamics

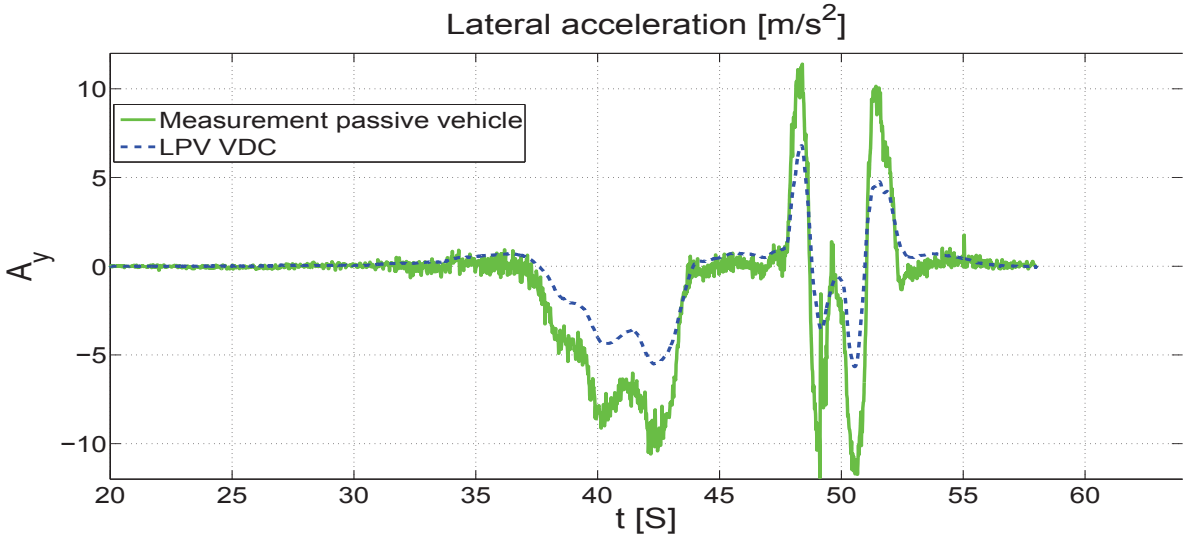

Figure 6.31: Lateral acceleration a_y

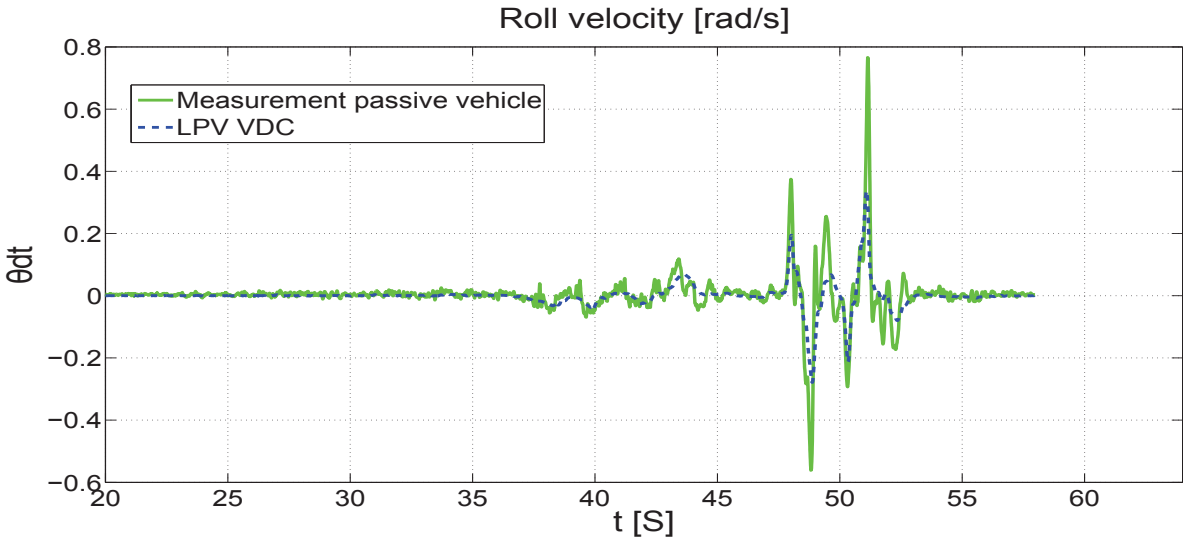

Figure 6.32: Roll velocity of the chassis $\dot{\theta}$

are better enhanced using an $LPV/\mathcal{H}_\infty$ robust controller in emergency situations.

In Fig. 6.33, the longitudinal speed of the vehicle during the driving scenario decreases using the $LPV/\mathcal{H}_\infty$. This allows to better handle the vehicle in critical driving situation and to improve the vehicle stability in emergency situations.

The Fig. 6.34 shows the measured rotation angle of the steering wheel that the driver carries out to perform the considered driving scenario. Then, the Fig. 6.35 shows the corrective steering angle that the controller supplies to help the driver to ensure the vehicle stability and manoeuvrability in critical driving situation. This corrective steering angle is considered to be directly applied on the wheels not on the steering wheel.

It is important to notice that the **steering ratio** of the car, which is the rotation angle of a steering

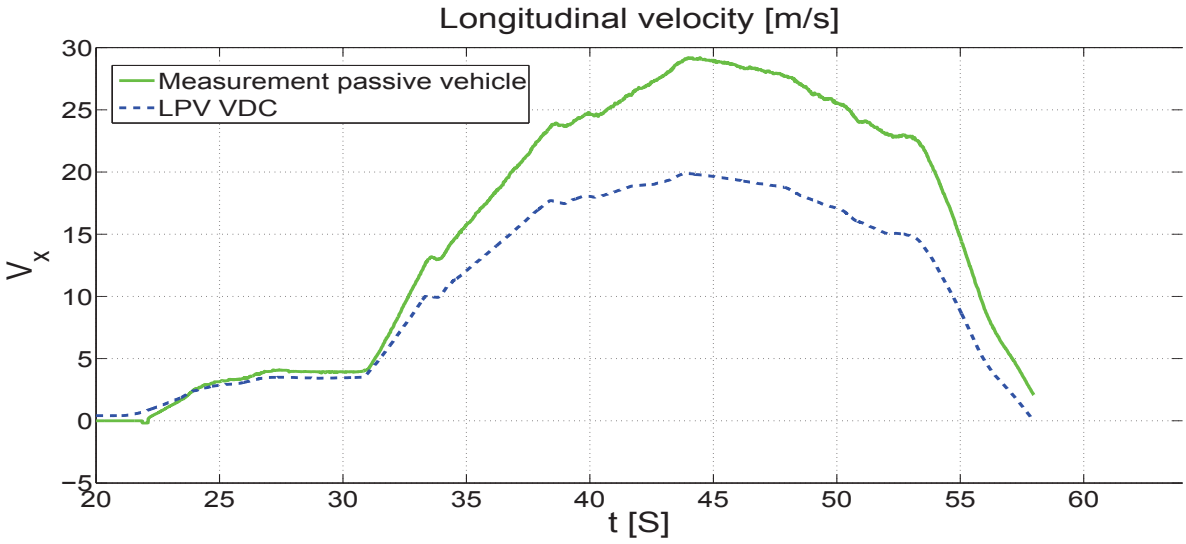

Figure 6.33: Longitudinal speed v_x

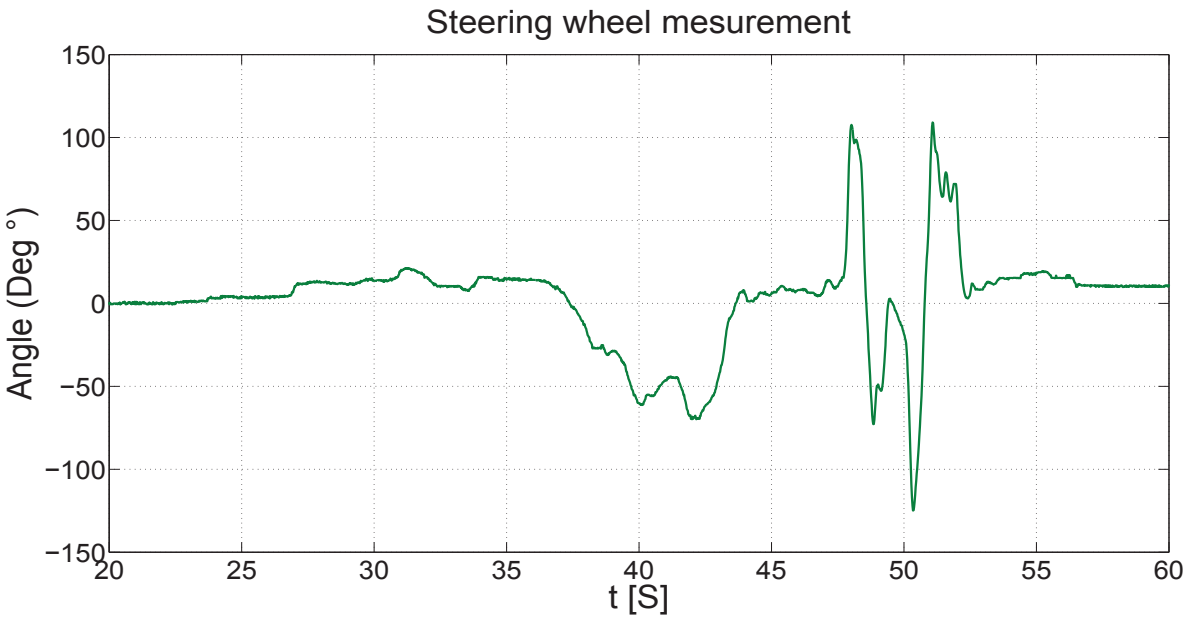

Figure 6.34: Steering wheel angle δ^0

wheel divided by the steer angle of the wheels, is around $10:1$ to $20:1$ depending on the car's type (commercial, race, sport...).

6.6 Conclusion

In this chapter, a global chassis control strategy has been proposed, involving active steering, electromechanical braking and semi-active suspension. It is shown to enhance the vehicle dynamical behaviour subject to critical driving situations. The originality of the proposed strategy is the coordinated use of these 3 actuators and the hierarchical activation of each one of them, depending on

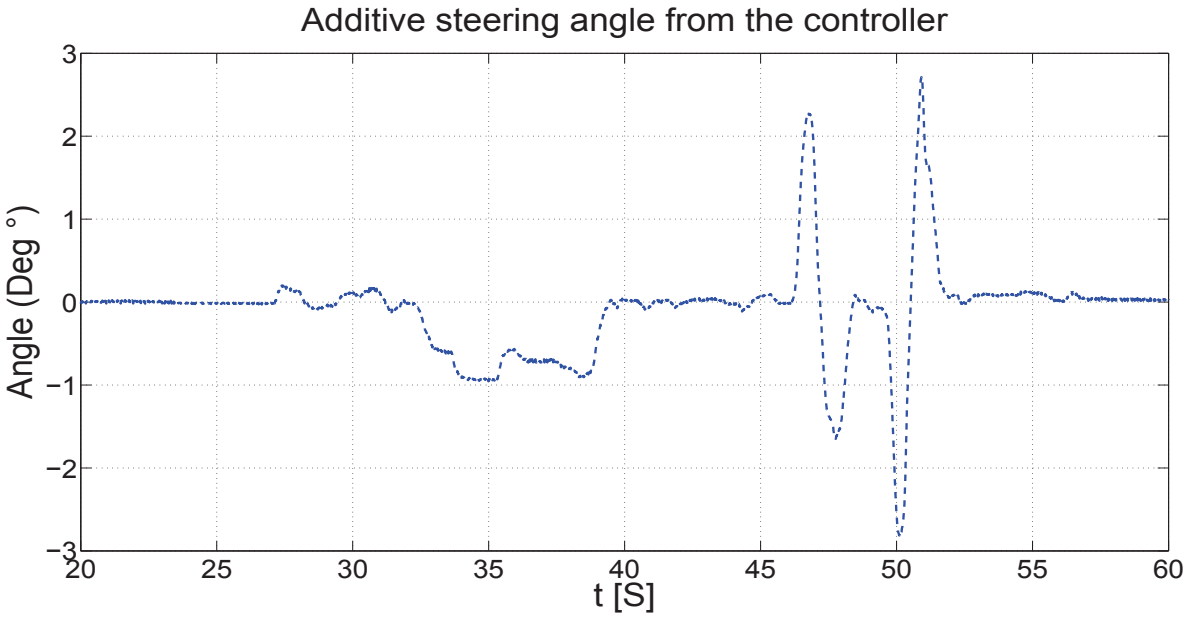

Figure 6.35: Corrective steering angle from the controller δ^+ (on the wheels)

the driving situations to reach the performance objectives in a unified way. This is achieved thanks to the LPV approach that provides an efficient coordination of these actuators. Another advantage is the reduction of the braking actuation in critical situations to avoid wheel locking and skidding, and compensating this action by combining and coordinating the intervention of the active steering and semi-active suspension controller to improve road handling and preserving the stability and manoeuvrability of the vehicle. Also, the actuator efficiency is well improved using the LPV framework compared to the classical LTI one. Simulation results upon dangerous driving situations, performed on a complex nonlinear model (validated on real experimental data (see appendix)), have shown the efficiency of the proposed approach.

Finally, it is worth noting that the efficiency of the previously detailed strategy has inspired to develop more strategies, as in (Sename *et al.*, 2013) where an innovative fault tolerant control strategy uses the smart coordination of the healthy actuators to compensate some other actuators loss or malfunction.

CHAPTER 7

Global Chassis and suspension LPV/$\mathcal{H}_\infty$ control allocation

ï»¿¿

7.1 Introduction

This chapter proposes a new multivariable LPV/H_∞ Global Chassis allocation control strategy. It allows to achieve several performance objectives using a smart control structure that adapts the control to the considered vehicle dynamical behaviour. In the following, two automotive based control objectives are achieved using the proposed LPV/H_∞ Global Chassis allocation strategy (see Fig. 7.1):

- A LPV suspension control with performance adaptation to roll behavior, embedded in a global vehicle dynamic control strategy: it uses the control allocation approach to manage the load transfer distribution and suspensions efforts generation (see (Fergani *et al.*, 2013*c*) and (Fergani *et al.*, 2013*b*)).
- A LPV methods for fault tolerant dynamics control: it uses the control allocation approach to handle an actuator failure: *e.g.* damper failure or braking actuators failure (see (Sename *et al.*, 2013) and (Fergani *et al.*, 2014*b*)).

The allocation control approach is very useful since it allows to provide the accurate inputs control to the system in order to achieve the desired purposes. This can be very interesting in terms of computation time and energy saving.

The main interesting contribution in this chapter is the use of the parameter ρ to schedule the distribution of the left & right suspensions on the four corners of the vehicle and tune the suspension dampers control. This distribution is handled using a specific partly fixed structure of the suspension controller, given as follows :

$$K_s(\rho) := \left\{ \begin{array}{l} \dot{x}_c(t) = A_c(\rho)x_c(t) + B_c(\rho)y(t) \\ \\ \begin{pmatrix} u_{fl}^{\mathcal{H}_\infty}(t) \\ u_{fr}^{\mathcal{H}_\infty}(t) \\ u_{rl}^{\mathcal{H}_\infty}(t) \\ u_{rr}^{\mathcal{H}_\infty}(t) \end{pmatrix} = \underbrace{U(\rho)C_c^0(\rho)}_{C_c(\rho)} x_c(t) \end{array} \right. \tag{7.1}$$

where $x_c(t)$ is the controller state, $A_c(\rho)$, $B_c(\rho)$ and $C_c(\rho)$ controller scheduled by ρ. $u^{\mathcal{H}_\infty}(t) = [u_{fl}^{\mathcal{H}_\infty}(t) u_{fr}^{\mathcal{H}_\infty}(t) u_{rl}^{\mathcal{H}_\infty}(t) u_{rr}^{\mathcal{H}_\infty}(t)]$ the input control of the suspension actuators and $y(t) = z_{def}(t)$.

Let us recall that ρ is the varying parameter used to perform the allocation control strategy. The choice of this parameter can vary depending on the monitoring approach and the control application for which the strategy is dedicated.

Remark: This partly fixed structured of the controller is used all over this chapter to perform the suspension control allocation either for GCC objectives or FTC (Fault Tolerant Control) objectives. The presentation of the control structure may appear several time trough this work to emphasize on the application objective. In this synthesis, the authors wish to stress that an interesting innovation is the

use of a partly fixed structure controller, combined with a parameter dependency on the control output matrix introduced to allow a smooth load transfer distribution, depending on the situation. Then, the LPV framework is obtained, thanks to the matrix $U(\rho_1)$,

$$U(\rho_1) = \begin{pmatrix} 1-\rho_1 & 0 & 0 & 0 \\ 0 & \rho_1 & 0 & 0 \\ 0 & 0 & 1-\rho_1 & 0 \\ 0 & 0 & 0 & \rho_1 \end{pmatrix} \tag{7.2}$$

Then this section is organised in two sections (see Fig. 7.1): section 7.2 introduces the developed LPV/H_∞ suspension control with performance adaptation to roll behavior, embedded in a global vehicle dynamic control strategy. Then, section 7.3 presents the use of the LPV methods for fault-tolerant vehicle dynamic control. Finally, in section 7.4 some conclusions to summarize the works presented in this chapter.

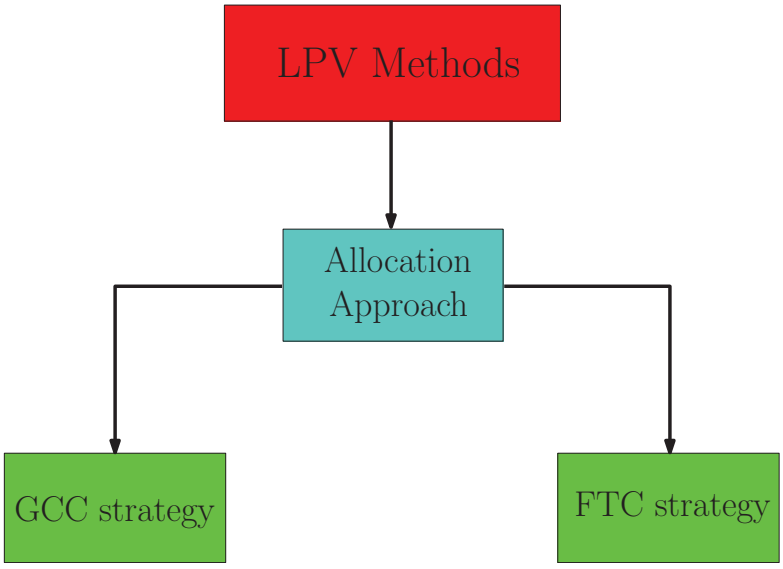

Figure 7.1: Control allocation strategies.

7.2 A LPV/H_∞ suspension control with performance adaptation to roll behavior, embedded in a global vehicle dynamic control strategy

This section presents a new LPV/H_∞ coordination strategy that improves the vehicle stability using suspension, active steering and electro-mechanical braking actuators. The vehicle stability is evaluated through a stability index and a defined stability region based on slip dynamics. The new coordination technic aims, by monitoring the load transfer distribution of the vehicle while facing road irregularities, at tuning the suspension forces in the four corners of the vehicle and improving the vertical performances. At the same time, the lateral and the longitudinal car dynamics are improved using braking and steering actuators scheduled through the stability index, based on slip dynamics. The proposed GCC (Global Chassis Control) provides a load transfer allocation on the four corners of the vehicle, ensures a good coordination between different actuators, and improves the vehicle stability and the car dynamics.
The main objectives of LPV/H_∞ suspension allocation control strategy are:

- The suspension performance is here adapted depending on the left/right load transfer. This allows to coordinate the suspension systems behavior and tune their control based on the vehicle dynamical one. This study is detailed in (Fergani *et al.*, 2013*c*).
- The strategy developed in this section allows to tune the suspension system to work either in a coordination mode with braking and steering systems to adapt to the driving situation, or alone when no other actions (steering and/or braking) are required to satisfy the specified performances (see (Fergani *et al.*, 2013*b*)).

The strategy proposed for the vehicle stabilization and the performance improvement is presented (see Fig. 7.2), involving front active steering, rear braking and active suspension actuators, scheduled by two monitoring parameters provided by some supervision systems.

Monitor 1 (see 7.2.1) allows to supervise the right/left load transfer dynamics that may induce the vehicle into instability. It provides a parameter (ρ_1) that is used in the suspension systems control design in the LPV framework to enhance passengers comfort to keep the road holding and to help maintaining the stability of the car.
Also, Monitor 2 (see 7.2.1) supervises the vehicle stability based on the lateral sideslip dynamics of the car see (Doumiati *et al.*, 2013*c*)). It provides a parameter (ρ_2) that is used in the steering and braking systems control design in the LPV framework to achieve the global chassis control strategy performance objectives.

This whole supervision strategy induces a hierarchical activation of the different actuators. The LPV framework provides, in addition to stability, a smooth use of the coordination between steering, braking and suspension actuators, as well as a considerable help to the driver to overcome critical situations.

7.2.1 Monitoring systems

The varying parameters involved in the proposed strategy are given by two monitoring systems. The first one is the suspension monitor that emphasizes the vehicle load transfer distribution and the other one is the braking/steering monitor that allows to supervise the lateral behaviour of the car.

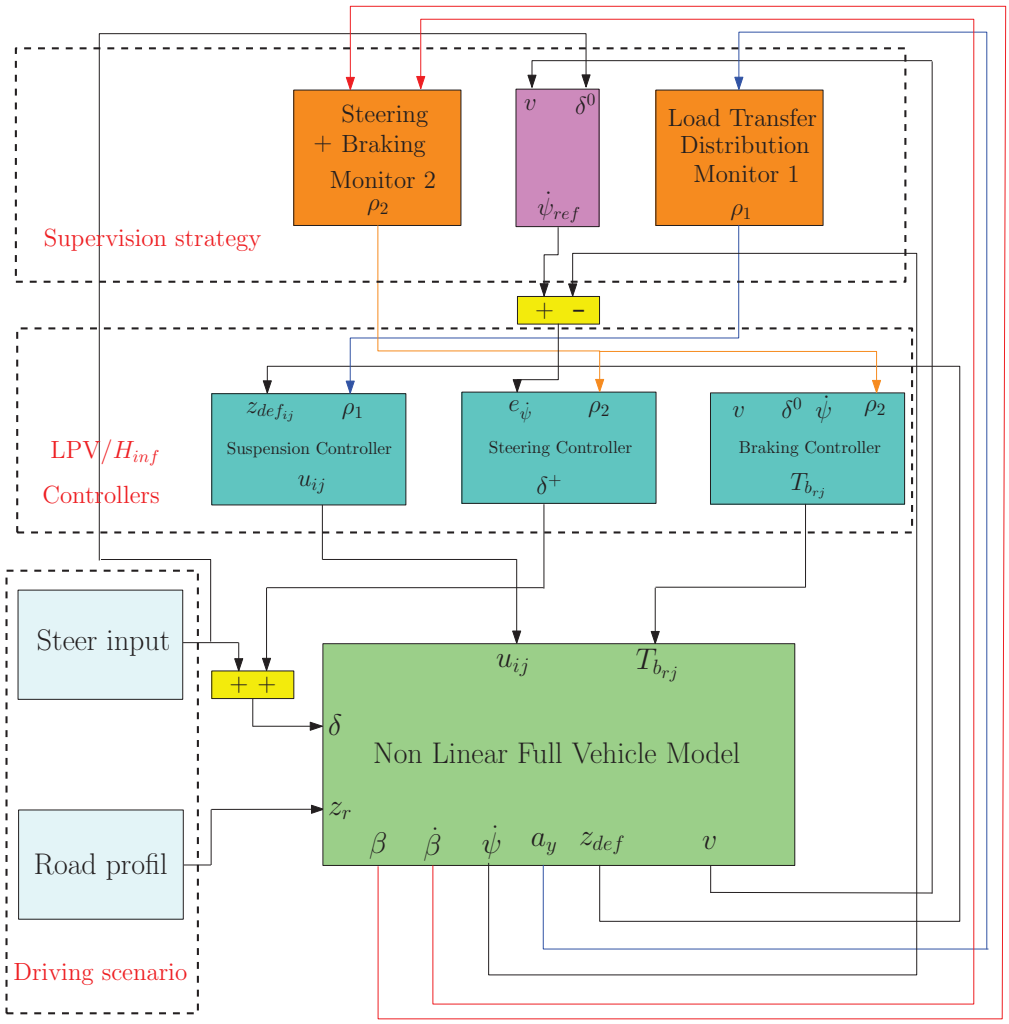

Figure 7.2: Global chassis control Implementation scheme.

- **Load transfer distribution monitoring system (ρ_1):**
  It is based on the evaluation of the roll load transfer when the vehicle is running in several situations. The main idea is to compute the difference between the right and left vertical forces at the four corners of the vehicle.

  This suspension monitor is characterized by the following equations:

$$\begin{cases} F_{z_l} &= m_s \times g/2 + m_s \times h \times a_y/l_f \\ F_{z_r} &= m_s \times g/2 - m_s \times h \times a_y/l_r \\ \rho_1 &= (F_{z_l} - F_{z_r})/(F_{z_l} + F_{z_r}); \end{cases} \tag{7.3}$$

  where, F_{z_l} and F_{z_r} are the vertical forces, a_y the lateral acceleration, ρ_1 the scheduling parameter (for other parameters see chapter. 3). Note that $\rho_1 \in [-1 \;\; 1]$.

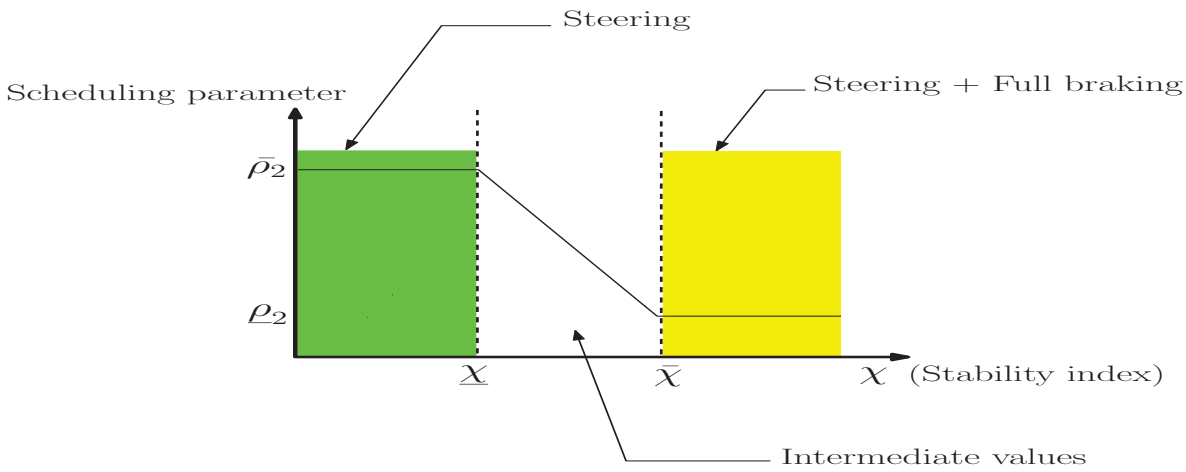

Figure 7.3: Control task selection according to the stability index variation.

- **Braking and Steering monitoring system (Doumiati *et al.*, 2013*c*) (ρ_2):**

  This supervision strategy was introduced in (Moustapha *et al.*, 2011). Since the vehicle stability is directly related to the sideslip motion of the vehicle, judging the vehicle stability region is derived from the phase-plane ($\beta - \dot{\beta}$) method. A stability bound defined in (He *et al.*, 2006) is used here, and is formulated as:

  $$\chi < 1, \tag{7.4}$$

  where $\chi = \left|2.49\dot{\beta} + 9.55\beta\right|$ is the "Stability Index".

  Hence, the scheduling parameter $\rho_2(\chi)$ can be defined as:

  $$\rho_2(\chi) := \begin{cases} \overline{\rho_2} & (steering\ control \\ & steering\ control\ task) \\ \dfrac{\overline{\chi} - \chi}{\overline{\chi} - \underline{\chi}}\overline{\rho_2} + \dfrac{\chi - \underline{\chi}}{\overline{\chi} - \underline{\chi}}\underline{\rho_2} & (steering + braking) \\ \underline{\rho_2} & (steering + braking \\ & stability\ control\ task) \end{cases} \tag{7.5}$$

  where $\underline{\chi} = 0.8$ (user defined) and $\overline{\chi} = 1$. The control task selection is illustrated in Figure 7.3.

  To calculate the actual stability index χ defined previously, a side-slip dynamics observer is used to evaluate $\dot{\beta}$ and β (the sideslip) in real-time:

  – $\dot{\beta}$ can be reconstructed using available sensors, according to the following relationship:

  $$\dot{\beta} = \frac{a_y}{v_x} - \dot{\psi}, \tag{7.6}$$

where a_y is the lateral acceleration and v_x is the forward vehicle speed that can be approximated by the mean of the rear wheel velocities.

– β is not available using standard sensors, and thus, it must be estimated. The "β-estimation" is widely discussed in the literature, and many papers are concerned with that topic (see (Lin-Hui *et al.*, 2010) and references therein). Here, the observer developed in (Doumiati *et al.*, 2010*a*), (Doumiati *et al.*, 2011) has been used, which is suitable for real-time implementation.

7.2.2 Design of the LPV/H_∞ Global Chassis allocation Control Strategy

The design procedure of the proposed strategy consists on a two step procedure is proposed for a hierarchical controllers synthesis. The first one is the braking and steering control synthesis, introduced previously by the authors in (Doumiati *et al.*, 2013*c*), that improves the stability of the vehicle through the supervision of the stability index evolution.
The second step is concerned with the suspension control at the four corners of the vehicle, based on the proposed new load transfer distribution.

First step: Yaw control design of the braking/steering actuators:

The generalized plant described in Fig 7.4 is used for the synthesis of the gain scheduled controller $K(\rho_2)$. This synthesis method uses a bicycle model (a lateral linear model of the vehicle (Poussot-Vassal *et al.*, 2011*a*)).

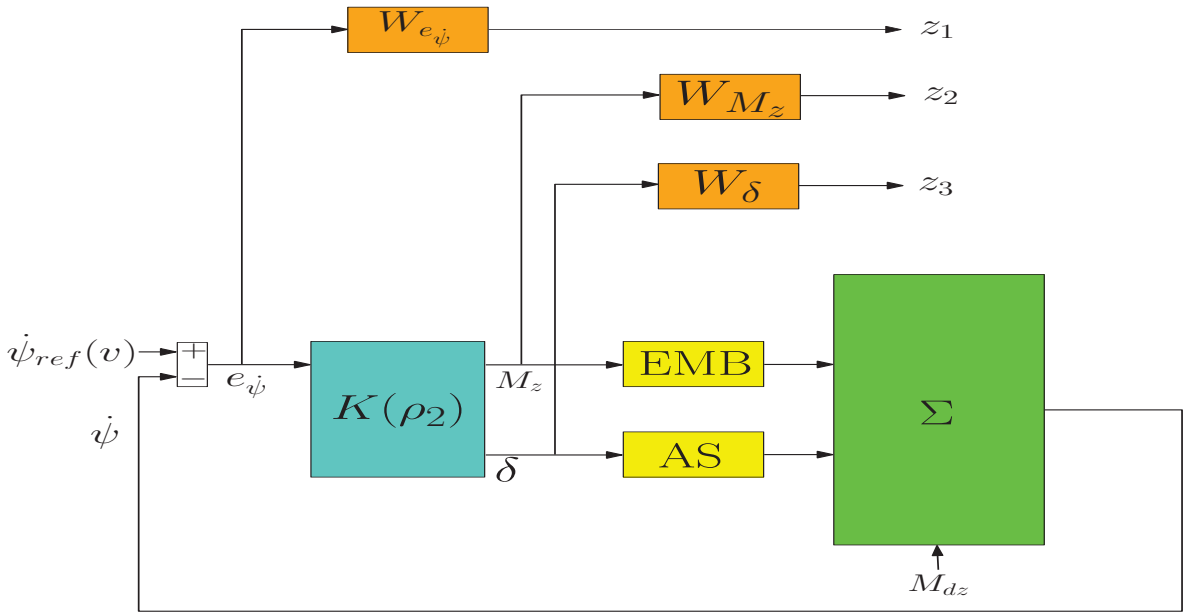

Figure 7.4: Generalized plant model.

Scheduling strategy w.r.t ρ_2:

- Σ, EMB and AS stand for the extended bicycle, electro-mechanical braking and active steering actuators models, respectively.
- z_1, the yaw rate error output signal, is the output of the tracking error performance, weighted by:

$$W_{e_{\dot{\psi}}} = \frac{1}{2G_e}\frac{sG_e/2\pi f_1 + 1}{s/2\pi f_1 + 1} \tag{7.7}$$

where $f_1 = 1$Hz is the cut-off frequency of the high pass filter. $G_e = 0.1$ is the attenuation level for low frequencies ($f < f_1$); in this case 0.1 means that the static tracking error should be less than 5%.

- z_2, the yaw moment control signal attenuation, is the output of the braking control, weighted by:

$$W_{M_z}(\rho_2) = \rho_2\frac{s/(2\pi f_2) + 1}{s/(\alpha 2\pi f_2) + 1} \tag{7.8}$$

where $f_2 = 10$Hz and $\alpha = 100$ are the braking actuator bandwidth and the roll-off parameters, respectively. These parameters are chosen to handle the dynamical braking actuator limitations. $W_{M_z}(\rho_2)$ is linearly parameterized by the considered varying parameter $\rho_2(.)$, where $\rho \in \left\{\underline{\rho_2} \leq \rho_2 \leq \overline{\rho_2}\right\}$ (with $\underline{\rho_2} = 0$ and $\overline{\rho_2} = 1$). Then, when $\rho_2 = \overline{\rho_2}$, the braking input is penalized, on the contrary, when $\rho_2 = \underline{\rho_2}$, the braking control signal is relaxed.

- z_3, the steering control signal attenuation, is the output of the steering control performance, weighted by:

$$\begin{aligned} W_\delta &= G_\delta^0\frac{(s/2\pi f_3 + 1)(s/2\pi f_4 + 1)}{(s/\alpha 2\pi f_4 + 1)^2} \\ G_\delta^0 &= G_\delta\frac{(\Delta_f/\alpha 2\pi f_4 + 1)^2}{(\Delta_f/2\pi f_3 + 1)(\Delta_f/2\pi f_4 + 1)} \\ \Delta_f &= 2\pi(f_4 + f_3)/2 \end{aligned} \tag{7.9}$$

where $G_\delta = 5.10^{-3}$, $f_4 = 10$Hz is the steering actuator bandwidth and $f_3 = 1$Hz is lower limit of the actuator intervention. For more details, see (Moustapha *et al.*, 2011).

The generalized plant is given by:

$$\Sigma : \left\{\begin{array}{lcl} \dot{\xi}(t) &=& A\xi(t) + B_1 w(t) + B_2(\rho)u(t) \\ z(t) &=& C_1(\rho_2)\xi(t) + D_{11}w(t) + D_{12}(\rho_2)u(t) \\ y(t) &=& C_2\xi(t) + D_{21}w(t) \end{array}\right. \tag{7.10}$$

where

$$\begin{array}{lcll} w(t) &=& [\dot{\psi}_{ref}(v)(t), M_{dz}(t)]^T & \text{are the exogenous inputs} \\ u(t) &=& [\delta^*(t), M_z^*(t)]^T & \text{are the control inputs} \\ y(t) &=& e_{\dot{\psi}}(t) & \text{are the measurements} \\ z(t) &=& [z_1(t), z_2(t), z_3(t)]^T & \text{are the controlled outputs} \end{array} \tag{7.11}$$

$\xi(t)$ collects the state variables of the linearized vehicle model, actuators and parameter dependent weighting functions.
The LPV controller is given by :

$$K(\rho_2)\left\{\begin{array}{l} \dot{x}_c(t) = A_c(\rho_1)x_c(t) + B_c(\rho_1)y(t) \\ \begin{pmatrix}\delta^*(t) \\ M_z^*\end{pmatrix} = C_c^0(\rho_2)\, x_c(t) \end{array}\right. \tag{7.12}$$

where $x_c(t)$ is the controller state, $y(t) = e_{\dot{\psi}}$, $u(t) = [\delta^*(t)\ M_z^*]^T$.

Then, this LPV controller working can be seen as the following: when the vehicle states move beyond the control boundaries and enter the unstable region, braking actuators will be involved to generate an additive corrective yaw moment, pulling the vehicle back into the stable region. As mentioned in (He *et al.*, 2006), one of the significant benefits of this stability index is that the reference region defined in (7.4) is largely independent of the road surface conditions and hence, the accurate estimation of the road surface coefficient of friction is not required.
Remember that the control task is also supposed to provide a seamless application of the direct yaw moment control when it is required.

Second step: A new LPV suspension control method for performance adaptation to the roll index:
Here, the main idea of the suspension control allocation with performance adaptation (see (Savaresi *et al.*, 2010*b*)), to be integrated in the global VDC strategy (Vehicle Dynamic Control), is presented. The following H_∞ control scheme is considered, including parameter varying weighting functions.

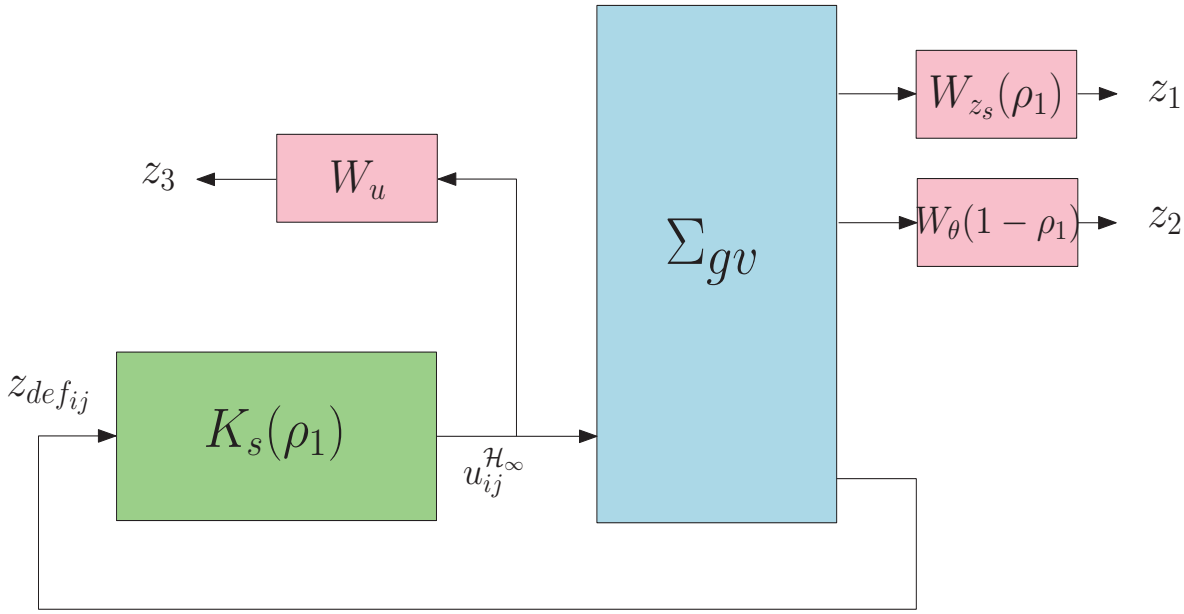

Figure 7.5: Suspension system generalized plant.

where $W_{z_s} = \rho_1 \frac{s^2+2\xi_{11}\Omega_{11}s+{\Omega_{11}}^2}{s^2+2\xi_{12}\Omega_{12}s+{\Omega_{12}}^2}$ is shaped in order to reduce the bounce amplification of the suspended mass (z_s) between $[0, 12]$Hz.
$W_\theta = (1-\rho_1)\frac{s^2+2\xi_{21}\Omega_{21}s+{\Omega_{21}}^2}{s^2+2\xi_{22}\Omega_{22}s+{\Omega_{22}}^2}$ attenuates the roll bounce amplification in low frequencies.
$W_u = 3.10^{-2}$ shapes the control signal.

Remark: The parameters of these weighting functions are obtained using genetic algorithm optimization as in (Do *et al.*, 2010*a*). Also, for this design procedure a 7 DOF vehicle model is considered.

According to Fig. 7.5, the following parameter dependent suspension generalized plant ($\Sigma_{gv}(\rho_1)$)

is obtained:

$$\Sigma_{gv}(\rho_1) := \begin{cases} \dot{\xi} = A(\rho_1)\xi + B_1\tilde{w} + B_2 u \\ \tilde{z} = C_1(\rho_1)\xi + D_{11}\tilde{w} + D_{12}u \\ y = C_2\xi + D_{21}\tilde{w} + D_{22}u \end{cases} \tag{7.13}$$

where $\xi = [\chi_{vert}\ \chi_w]^T$; $\tilde{z} = [z_1\ z_2\ z_3]^T$; $\tilde{w} = [z_{rij}\ F_{dx,y,z}\ M_{dx,y}]^T$; $y = z_{def_{ij}}$; $u = u_{ij}^{\mathcal{H}_\infty}$; and χ_w are the vertical weighting functions states.

Scheduling strategy w.r.t ρ_1:

One of the main interesting contributions is the use of the parameter ρ_1 to schedule the distribution of the left & right suspensions on the four corners of the vehicle and tune the suspension dampers smoothly, thanks to the LPV frame work, from "soft" to "hard" to improve the car performances according to the driving situation. This distribution is handled using a specific structure of the suspension controller, given as follows :

$$K_s(\rho_1) := \begin{cases} \dot{x}_c(t) = A_c(\rho_1)x_c(t) + B_c(\rho_1)y(t) \\ \begin{pmatrix} u_{fl}^{\mathcal{H}_\infty}(t) \\ u_{fr}^{\mathcal{H}_\infty}(t) \\ u_{rl}^{\mathcal{H}_\infty}(t) \\ u_{rr}^{\mathcal{H}_\infty}(t) \end{pmatrix} = \underbrace{U(\rho_1)C_c^0(\rho_1)}_{C_c(\rho_1)} x_c(t) \end{cases} \tag{7.14}$$

where $x_c(t)$ is the controller state, $A_c(\rho_1)$, $B_c(\rho_1)$ and $C_c(\rho_1)$ controller scheduled by ρ_1. $u^{\mathcal{H}_\infty}(t) = [u_{fl}^{\mathcal{H}_\infty}(t) u_{fr}^{\mathcal{H}_\infty}(t) u_{rl}^{\mathcal{H}_\infty}(t) u_{rr}^{\mathcal{H}_\infty}(t)]$ the input control of the suspension actuators and $y(t) = z_{def}(t)$.
In this synthesis, the authors wish to stress that an interesting innovation is the use of a partly fixed structure controller, combined with a parameter dependency on the control output matrix introduced to allow a smooth load transfer distribution, depending on the situation. Then, the LPV framework is obtained, thanks to the matrix $U(\rho_1)$,

$$U(\rho_1) = \begin{pmatrix} 1-\rho_1 & 0 & 0 & 0 \\ 0 & \rho_1 & 0 & 0 \\ 0 & 0 & 1-\rho_1 & 0 \\ 0 & 0 & 0 & \rho_1 \end{pmatrix} \tag{7.15}$$

The parameter $\rho_1 \in [0; 1]$ is used to distribute the load at the four corners of the vehicle, ensuring a good tuning of the suspensions. When a load transfer is performed from the right to the left side, $\rho_1 \to 1$, and the suspensions actuators are set to be "hard" and tuned to provide more force to handle the big load transfer (left $\leftrightarrows$ right). The suspensions control at each corner aims at handling the overweight, by providing the accurate suspension force to ensure better stability and handling for the vehicle. Conversely, when the load transfer is carried out on the right side, $\rho_1 \to 0$, this control allows to considerably reduce the roll motion of the vehicle when running, the suspensions actuators are then tuned to "soft", and aim at enhancing the passengers comfort.

The following figure summarize the main idea of the proposed LPV/H_∞ stratgey for the global chassis control:

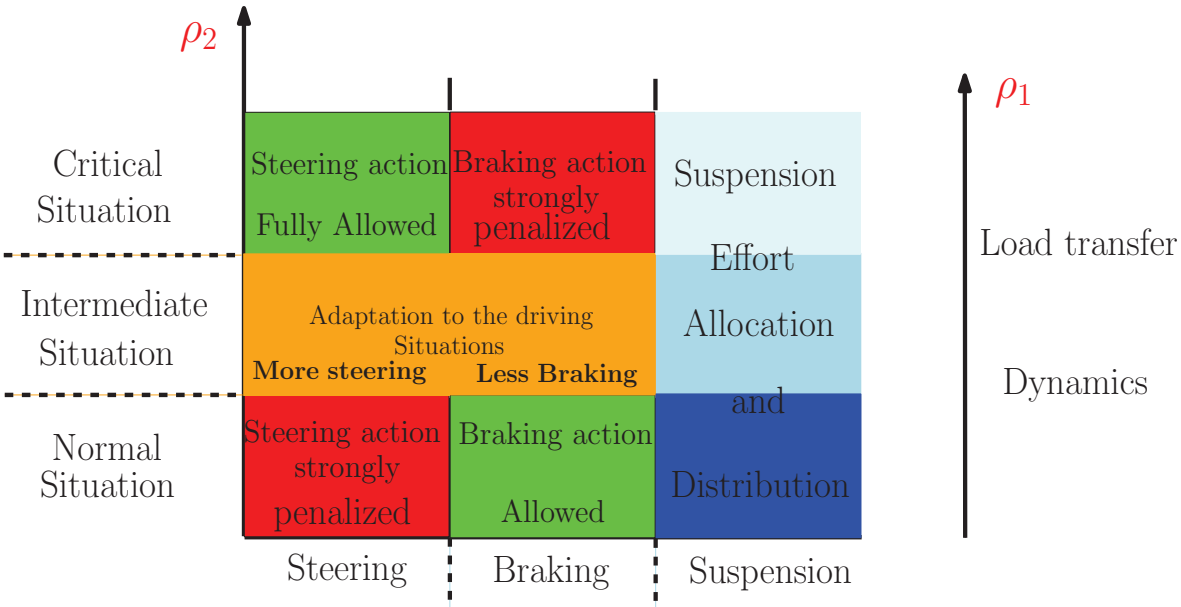

Figure 7.6: Control scheduling strategy .

Remark: The LPV system (8.39) includes a single scheduling parameter and can be described as a polytopic system, i.e, a convex combination of the systems defined at each vertex of a polytope defined by the bounds of the varying parameter. The synthesis of the controller is made under the framework of the $\mathcal{H}_\infty$ control of polytopic suspensions, (for more details, see (Scherer, 1996)).

All controllers presented along this study are synthesized in the LPV/H_∞ framework. This design is achieved, thanks to the LMI-based H_∞ resolution.

7.2.3 Simulation Results

To test the efficiency of the proposed LPV/H_∞ GCC, the following scenario in Fig. 7.7 is used:

1. the vehicle runs at 100km/h in straight line on wet road ($\mu = 0.5$, where μ is a coefficient representing the adherence to the road).

2. a 5cm bump on the left wheels (from $t = 0.5$s to $t = 1$s),

3. a line change manoeuvre is performed by the driver,

4. lateral wind occurs at vehicle's front, generating an undesirable yaw moment (from $t = 2$s to $t = 2.5$s),

5. a 5cm bump on the left wheels ($t = 2$s), another on the left wheels,($t = 2.5$s),

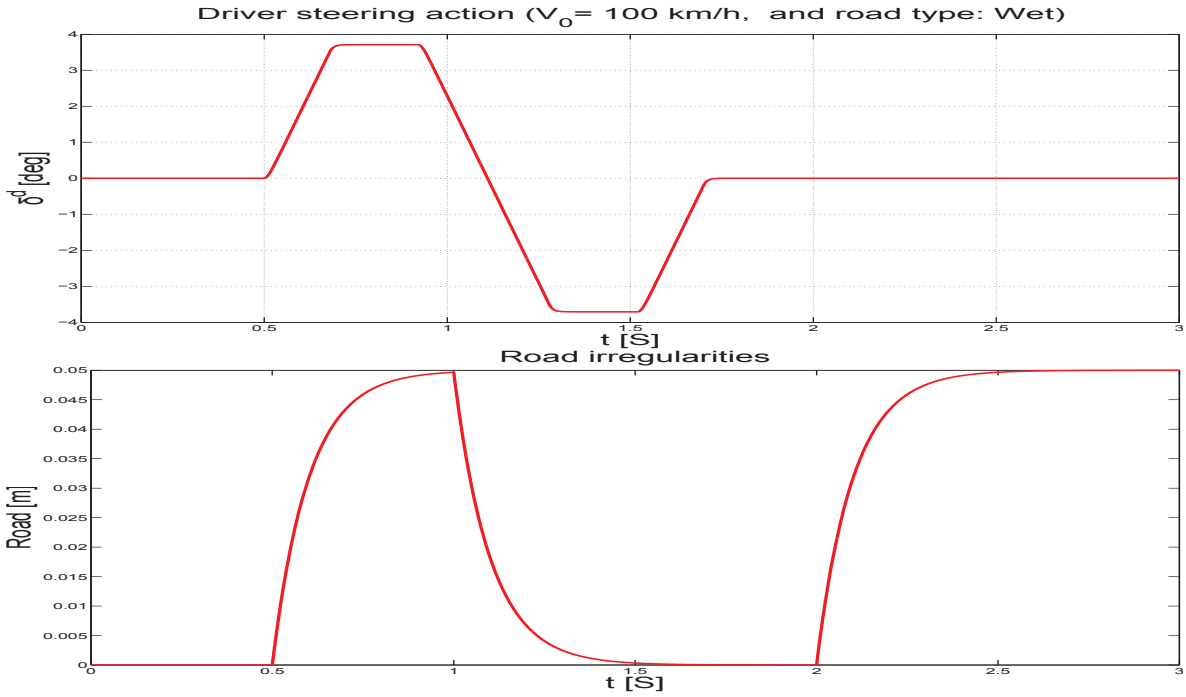

Figure 7.7: Driving scenario.

For sake of completeness, the new LPV/H_∞ GCC strategy is compared to the uncontrolled vehicle, to show the vehicle stability enhancement and the improvements of the different dynamics.

7.2.3.1 The monitors

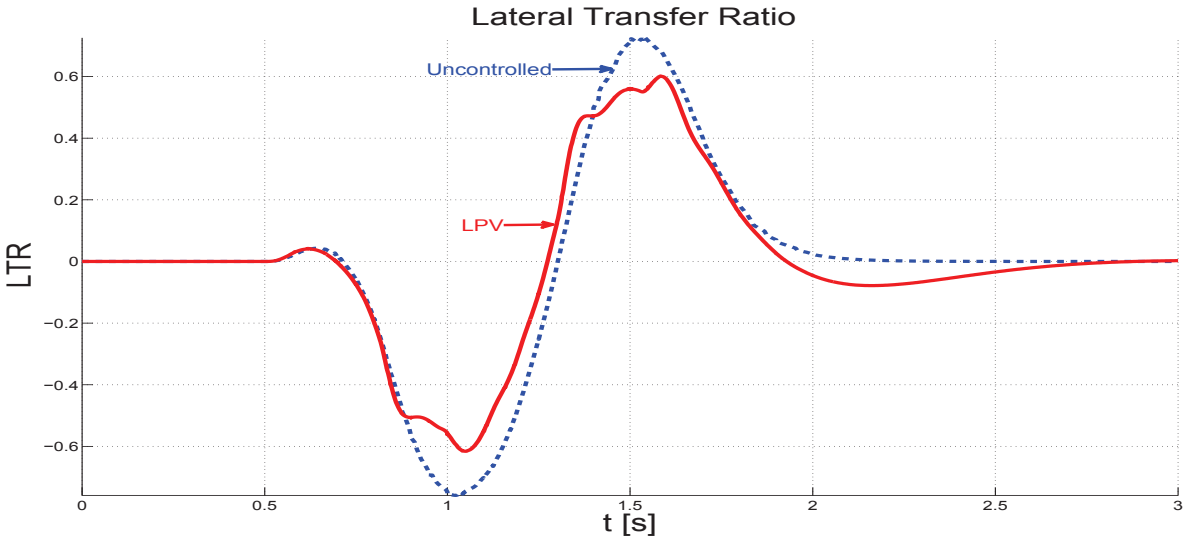

Figure 7.8: ρ_1: load transfer index.

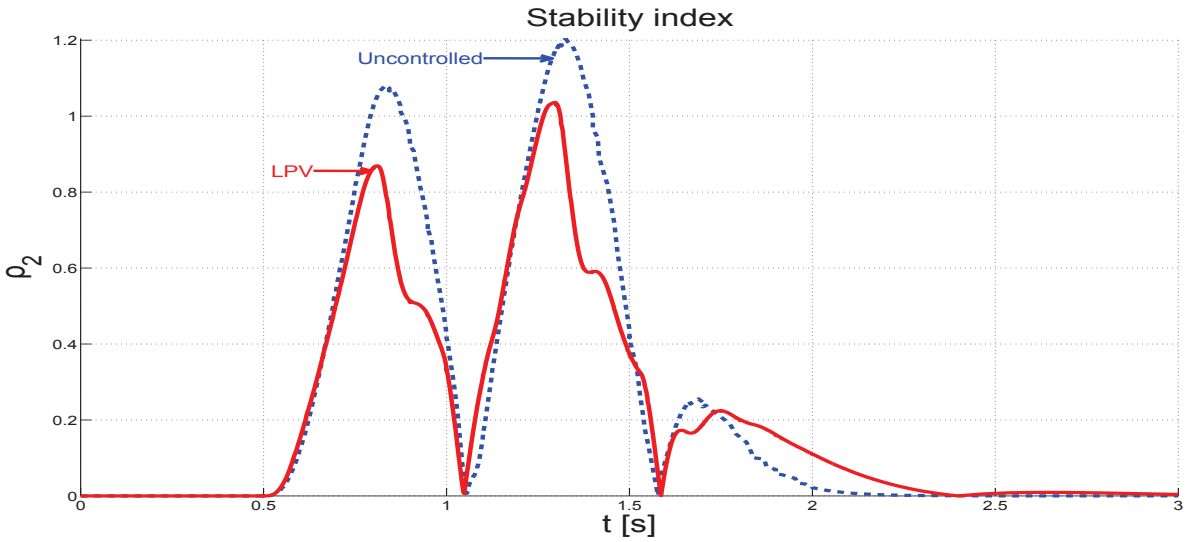

Figure 7.9: ρ_2: stability index.

Fig 7.8 and 7.9 show the monitors. The proposed LPV strategy enhances very well the car stability since the load transfer bounce is reduced and stability index is attenuated.

7.2.3.2 Vertical dynamics behaviour analysis

Fig 7.11 and 7.10 show the chassis displacement and the roll motion respectively. These two figures, representative of the vertical dynamics of the vehicle, show that the proposed strategy enhances very well the vertical behavior of the car.

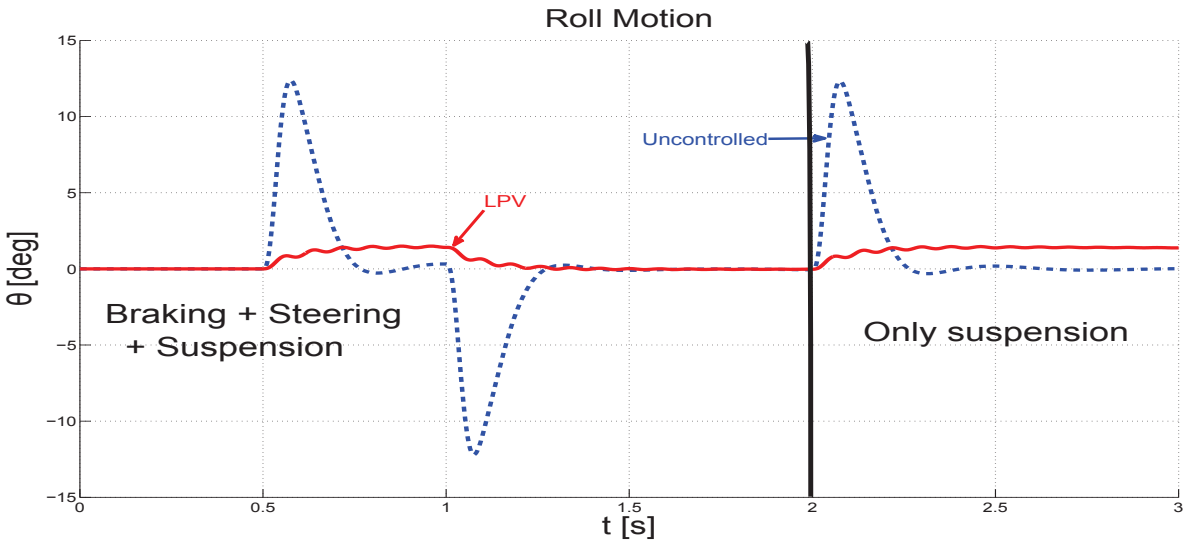

Figure 7.10: Roll motion.

Fig 7.10 represents one of the main results of this work since it shows the improvement brought

by the new load transfer distribution control strategy. It is clear that the use of the new scheduling parameter ρ_1 reduces the roll motion of this vehicle. This leads to a better vehicle stability and enhances driving safety when performing critical scenarios.

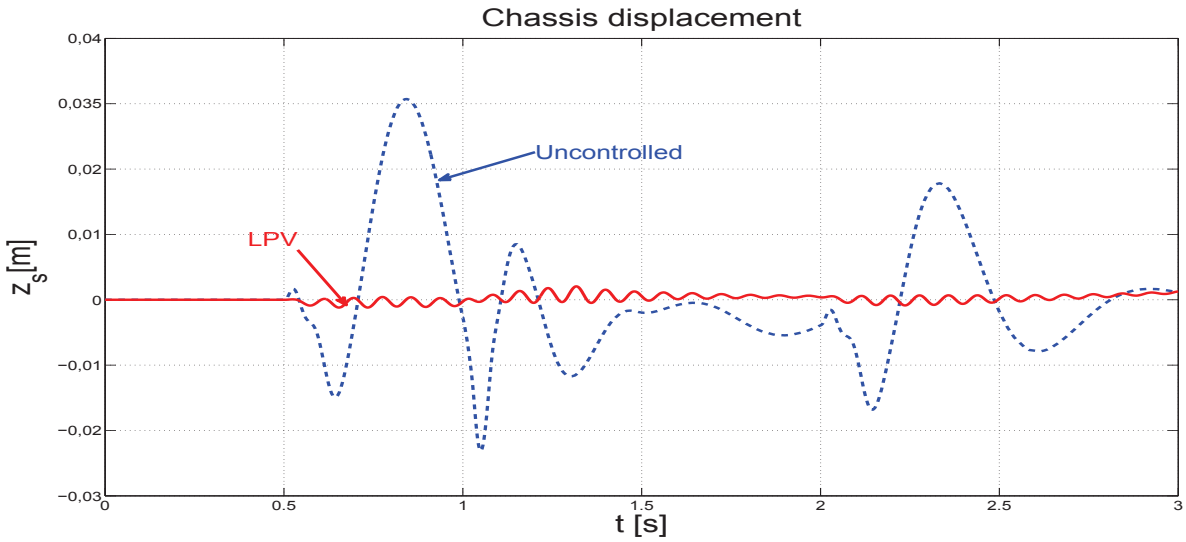

Figure 7.11: Chassis displacement.

Also, it can be clearly seen trough Fig. 7.11 that the chassis displacement of the vehicle is considerably attenuated and then the passengers comfort is improved.

7.2.3.3 Lateral and longitudinal dynamics behaviour analysis

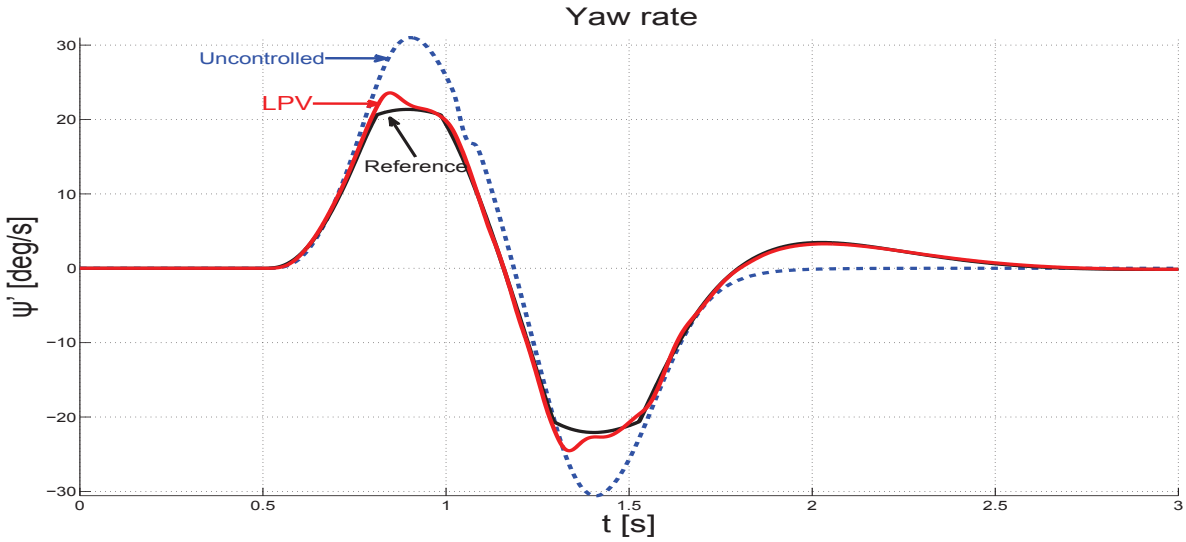

Figure 7.12: Yaw rate.

Figure 7.13: Yaw rate error.

Fig. 7.12 and Fig. 7.13 show the yaw rate tracking and yaw rate error, one of the main lateral car dynamics. It is clear that the designed LPV/H_∞ control strategy (in red) significantly enhances the vehicle stability since the results given by this approach fit well with the reference car performances (in black). Also, It minimizes the yaw rate error to ensure a good trajectory tracking. This comparison allows to emphasize the good results in terms of vehicle lateral stability and dynamics improvement brought by the proposed approach.

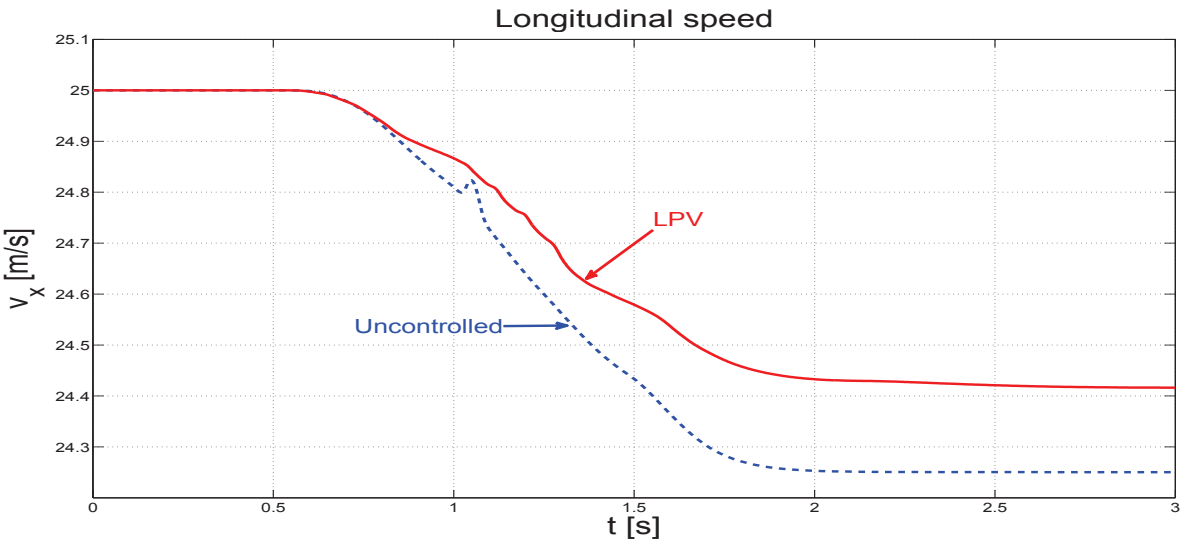

Figure 7.14: Evolution of the vehicle longitudinal speed v_x.

In Fig. 7.14, the longitudinal speed is lower with the proposed LPV control when performing the driving scenario. This property gives more stability for the vehicle in various driving situations, compared to the uncontrolled case (in blue).

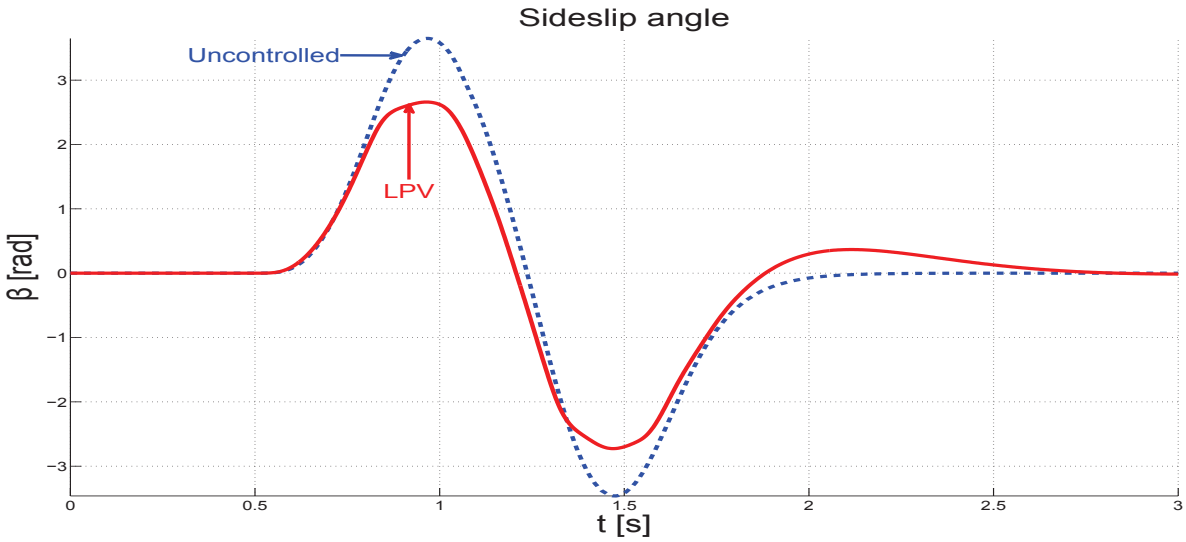

Figure 7.15: Sideslip angle.

In Fig 7.15, the sideslip angle is attenuated in the LPV case, which allows to maintain the handling of the vehicle.

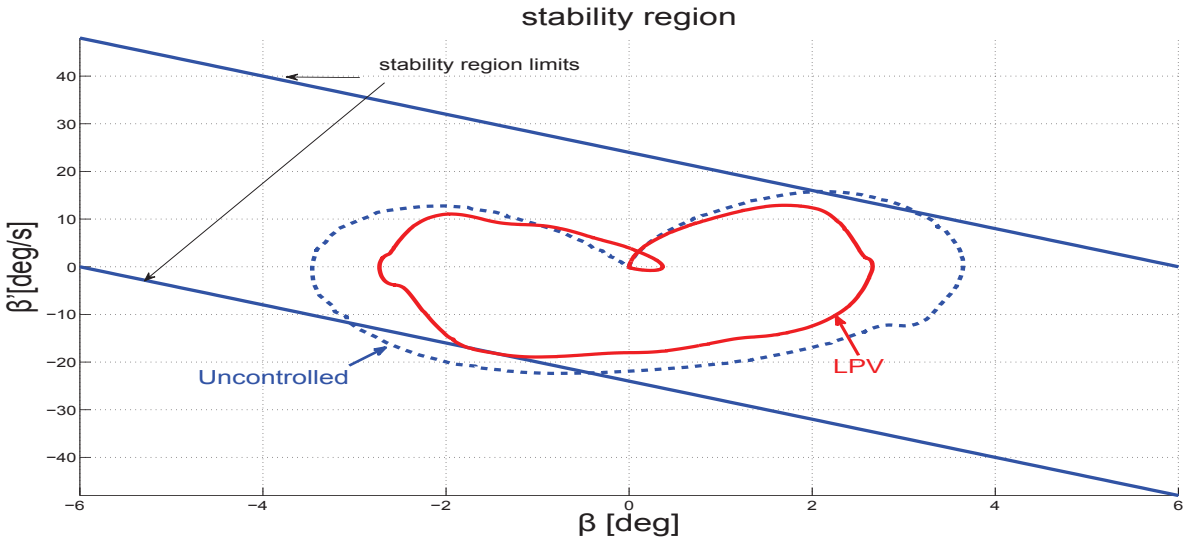

Figure 7.16: Evolution of the vehicle in the β-$\dot{\psi}$ plane.

Fig. 7.16 shows one important result, namely, the vehicle stability enhancement. The evolution of the vehicle in the β-$\dot{\beta}$ plane, clearly demonstrates that the LPV strategy prevents the car from going beyond the stability region limits. This proves the efficiency of the control designed to reach the performance objectives. Also, Fig. 7.15 shows the good attenuation of the sideslip dynamics of the car which enhance the vehicle stability in critical situations.

7.2.3.4 Actuators

The improvements of the vehicle stability and lateral/longtudinal behaviour are achieved thanks to the coordinated collaboration between the steering and braking actuators trough the LPV control framework.

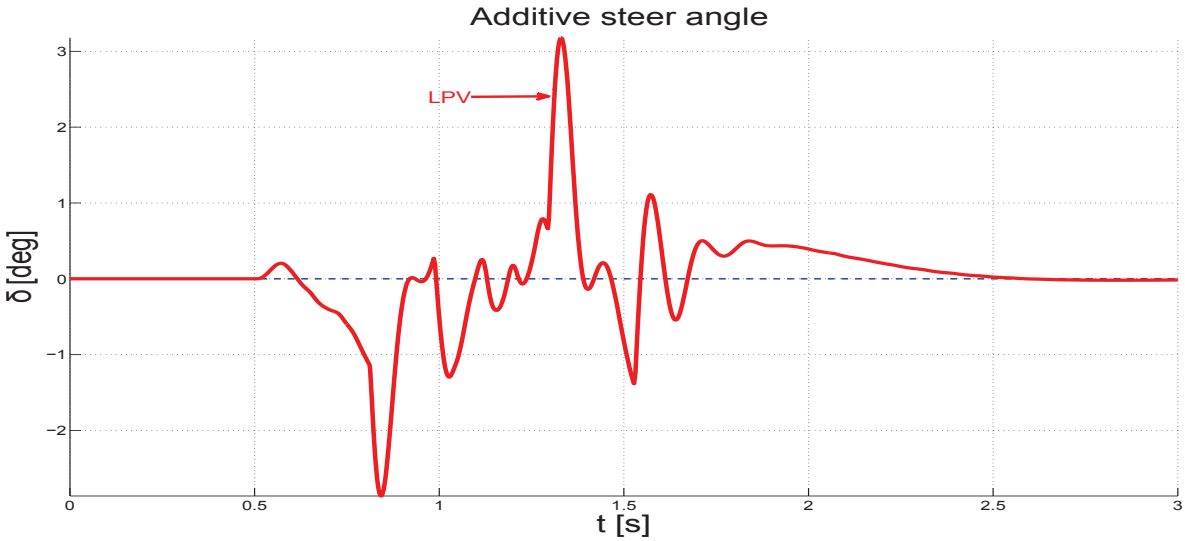

Figure 7.17: Additive steer angle δ^{+}.

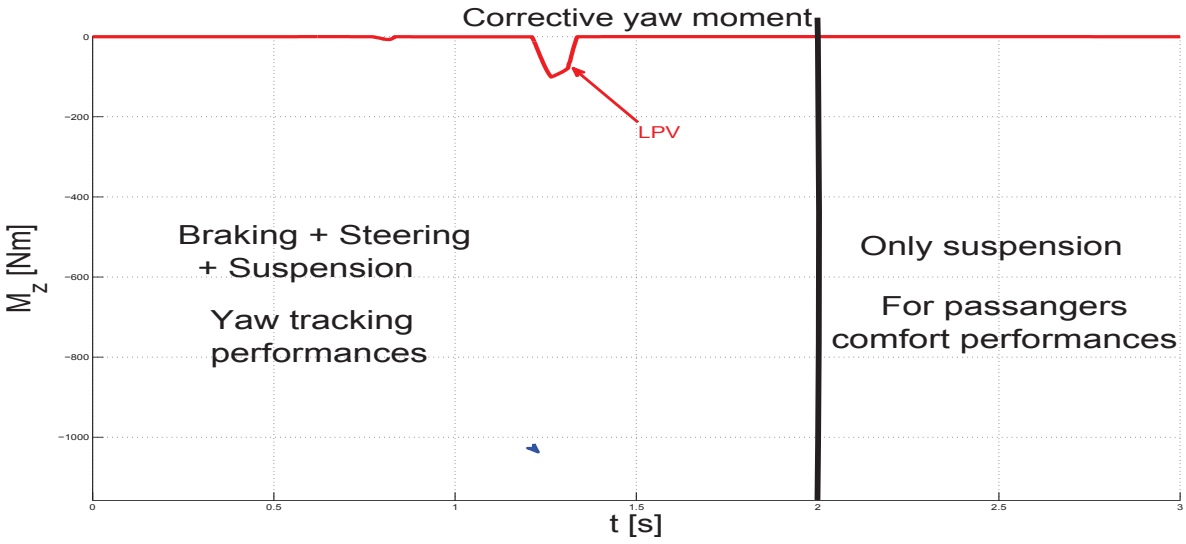

Figure 7.18: Corrective yaw moment.

The actuators contribution for improving the stability and the performances of the vehicle is illustrated via Fig 7.18 and 7.17. The braking control is activated for $\rho = \underline{\rho}$ and limited for $\rho = \overline{\rho}$ (see (Moustapha *et al.*, 2011)). The braking controller provides a corrective yaw moment:

$$M_z^* = \frac{t_r \Delta F_x}{2} \tag{7.16}$$

where t_r is the vehicle's rear axle length, ΔF_x is the longitudinal force between the left and right driving wheels of the same axle.

The braking torques can be deduced thanks to the following equation:

$$T_{b,ij} = R_w F x_{ij}, \tag{7.17}$$

where R_w is the effective tire radius and $Fx_{i,j}$, the longitudinal tire force (see (Park and Ahn, 1999)).

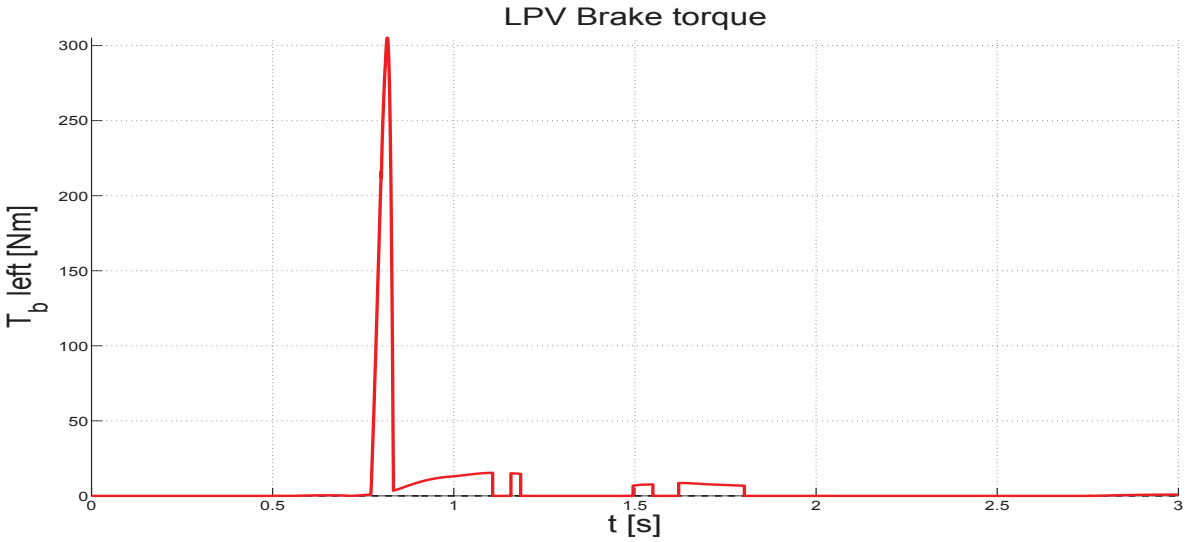

Figure 7.19: Rear left braking torque.

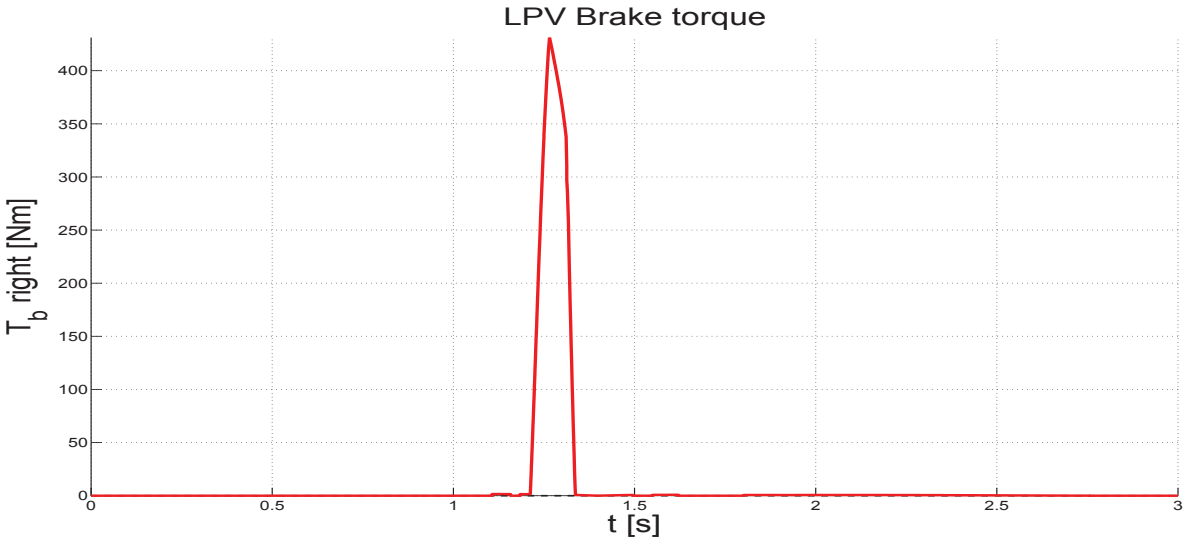

Figure 7.20: Rear right braking torque.

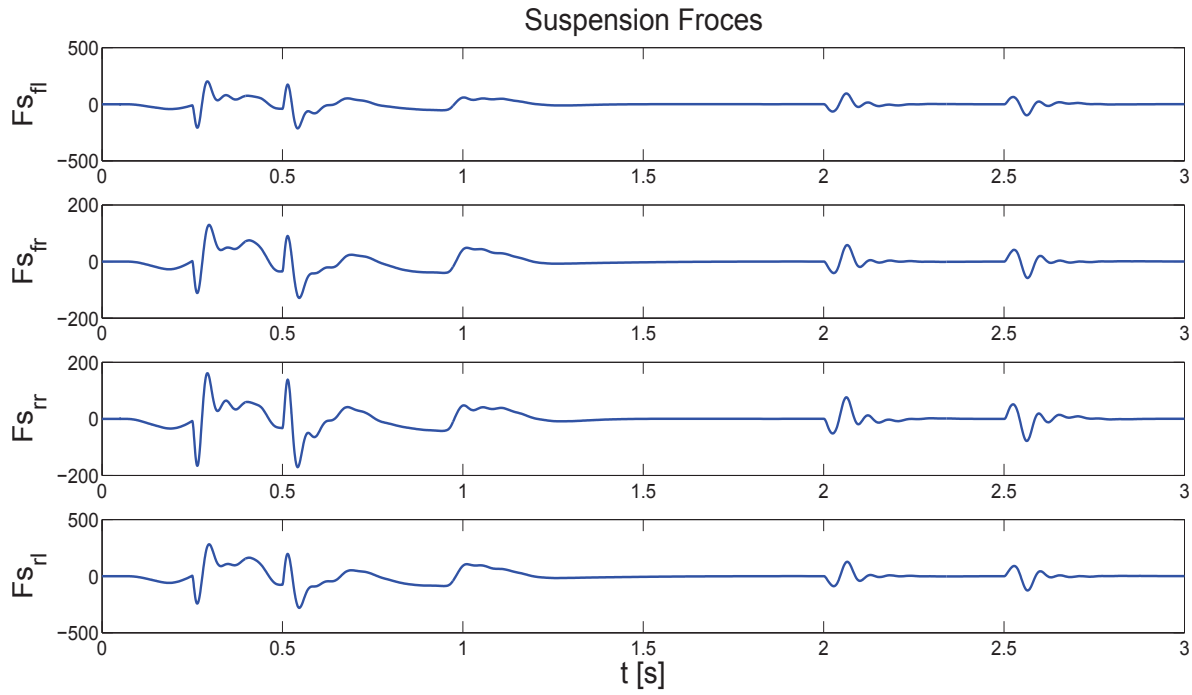

Figure 7.21: Suspension forces allocation.

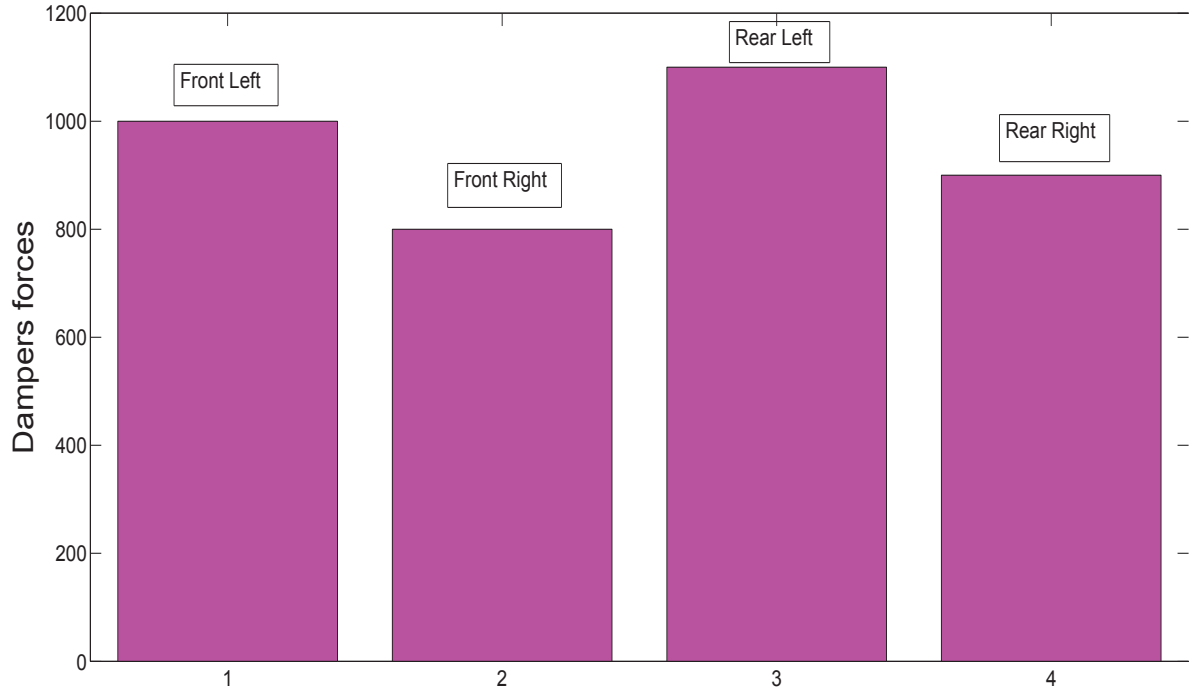

Figure 7.22: Damping forces comparison.

Fig. 7.21 and Fig. 7.22 show the distribution of the suspension forces in each corner of the vehicle. Indeed, it can be clearly seen that the forces provided by each suspension system is tuned separately and gives different value depending on the over load that it supports.

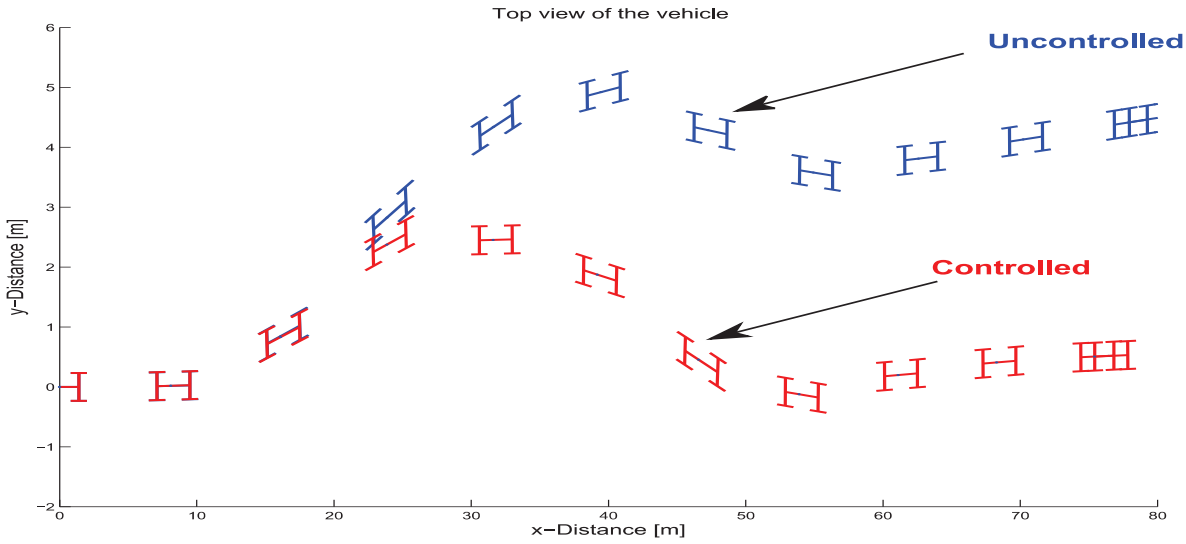

Figure 7.23: Top view of the controlled and uncontrolled vehicle.

Fig. 7.23 summarizes the vehicle stability and performance improvement. It is clear, through the trajectory tracking, that the vehicle controlled by the proposed LPV/H_∞ (in red) behaves better, in terms of car dynamics and stability, than the uncontrolled one does.

7.2.4 Conclusion

This section has presented a new LPV/H_∞ global chassis control strategy involving several actuators, namely, suspensions, electro-mechanical rear braking and active steering ones. It introduced an innovative solution to the problem of vehicle dynamical stability and performances improvement, based on roll vehicle motion attenuation and load transfer distribution control and monitoring.
Simulations of a consistent representative driving situation, performed on a complex nonlinear model, have shown the efficiency of the proposed approach. The results based on those simulations show also the improvements given by this LPV GCC design method. Then, the stability of the vehicle has been considerably enhanced using this new control strategy while improving the different car dynamics.
Also, one of the important results shown in the previous figures is that the proposed suspension system control can take part in the coordination strategy between braking, steering and suspension actuators when necessary (depending on the driving situations) to preserve vehicle stability, or work as an independent control system using load transfer distribution (thanks to the parameter ρ_1) when only the vertical dynamics are concerned without any braking and steering actions.

7.3 LPV methods for vehicle actuators (braking, suspension) fault-tolerant control

This section aims at presenting the efficiency of the Linear Parameter Varying methods for vehicle dynamics control, in particular when some actuators may be in failure. The cases of the semi-active suspension actuator failure, braking actuators failure and a scenarios combining the failure of the two of them consecutively are presented.
The LPV (Linear Parameter Varying) approach whose interest is now proven by many successful applications has been used to manage the actuators failures within a fault tolerant control strategies. Here, the study is interested on proven the efficiency of the LPV/$\mathcal{H}_\infty$ fault tolerant control applied to the automotive systems. This aims at enhancing the vehicle dynamics when actuators failures occurs through the suspension control (for comfort and road holding improvements) and the braking/steering control (for road handling and safety).
The first part of this section shows a LPV/$\mathcal{H}_\infty$ fault tolerant control strategy for roll dynamics handling under semi-active damper's malfunction. Indeed, in case of damper's malfunction, a lateral load transfer is generated, that amplifies the risks of vehicle instability and can lead to the car roll over.

A preliminary work was presented in (Tudon-Martinez *et al.*, 2013*a*) where only a pre-defined distribution of the suspension forces (computed from the steady state behaviour) is used to compensate a damper oil leakage while in this study, the suspension systems efficiency is monitored through the lateral (or longitudinal) load transfer induced by a damper's malfunction. The information given by the monitoring system is used in a partly fixed LPV/$\mathcal{H}_\infty$ controller structure that allows to manage the distribution of the four dampers forces in order to handle the over load caused by one damper's malfunction. The proposed LPV/$\mathcal{H}_\infty$ controller then uses the 3 remaining healthy semi-active dampers in a real time reconfiguration. Moreover, the performances of the car vertical dynamics (roll, bounce, pitch) are adapted to the varying parameter given by the monitoring of the suspension system efficiency, which allows to modify online the damping properties (soft/hard) to limit the induced load transfer.

The second part of this section presents an LPV/H_∞ fault tolerant MIMO gain-scheduled Vehicle Dynamic Control (VDSC) that involves the steering actuators, rear brakes and four active suspension, and aims at enhancing the yaw stability and lateral car performances (Poussot-Vassal *et al.*, 2011*c*),(Doumiati *et al.*, 2010*c*), (Doumiati *et al.*, 2013*b*).

This new LPV/H_∞ MIMO Global Chassis Controller (GCC) aims at handling the lateral dynamic control, i.e. the yaw control, and improving vehicle stability subject to critical driving situation.This strategy is scheduled by 3 parameters (ρ_b, ρ_s and ρ_l). Indeed, a special monitoring system is defined to evaluate how a driving situation is dangerous and to account for braking/suspension actuator failures. The control structure is such that the system become fault tolerant by construction. This means that it can handle one actuator failure by changing the configuration of control online.

Simulation results performed on a nonlinear model experimentally validated on the vehicle Renault Mégane Coupé MIPS (Mulhouse) subject to critical driving situations show that the proposed methodology is effective and robust.

7.3.1 A LPV/$\mathcal{H}_\infty$ fault tolerant control of vehicle roll dynamics under semi-active damper malfunction

This study focuses on the fault tolerant control reconfiguration of MR semi-active dampers. Indeed, few works have been concerned with the control reconfiguration in the presence of suspension

system malfunctions or failures.
While detecting a damper malfunction, the proposed strategy aims at keeping the vehicle stability and performance through an adequate distribution of the 3 remaining healthy suspension actuators.
The characteristics of magneto rheological dampers allow to compensate the lack of the vertical force in the faulty suspension corner by reconfiguring the global suspensions control.

To solve that problem a new LPV/$\mathcal{H}_\infty$ fault tolerant control is introduced to manage the deterioration of the vertical dynamics by using a varying parameter that coordinate the use of the healthy dampers. The main idea involves 2 steps. First, a monitoring system is introduced to evaluate the state of health of the suspension system. Here, the load transfer induced by a damper malfunction is considered, but different methods could be integrated in the proposed control strategy (observers, parity space, ...). Then the global suspension control is scheduled according to the monitor parameter to adapt on-line the damper control distribution, and the performances of the suspension systems as well (in term of comfort and road holding).

To achieve these objectives, the authors have chosen to fix the structure of the LPV/$\mathcal{H}_\infty$ controller by making the LMI's orthogonal with parameters dependency, as follow:

$$\begin{pmatrix} u_{fl}^{\mathcal{H}_\infty}(t) \\ u_{fr}^{\mathcal{H}_\infty}(t) \\ u_{rl}^{\mathcal{H}_\infty}(t) \\ u_{rr}^{\mathcal{H}_\infty}(t) \end{pmatrix} = \underbrace{U(\rho)C_c^0(\rho)}_{C_c(\rho)} x_c(t) \tag{7.18}$$

The suspension forces distribution is obtained through the matrix $U(\rho)$:

$$U(\rho) = \begin{pmatrix} \rho_1 & 0 & 0 & 0 \\ 0 & \rho_2 & 0 & 0 \\ 0 & 0 & \rho_3 & 0 \\ 0 & 0 & 0 & \rho_4 \end{pmatrix} \tag{7.19}$$

where ρ_i are the varying parameters given by the considered suspensions monitoring strategies.

Remark: This kind of structure has been used,as previously presented, for vehicle dynamics control with braking, steering and suspension actuators (Poussot-Vassal *et al.*, 2011*b*), (Fergani *et al.*, 2013*c*).

Here, this approach is extended to account for suspension actuator's malfunction. Since roll dynamics affect very much the vehicle behaviour, the authors have chosen to schedule the suspension control using the lateral load transfer as a varying parameter (ρ_l). The controller output matrix shows the dependency on this varying parameter and ensures the suspension efforts reconfiguration, as follows:

$$U(\rho_l) = \begin{pmatrix} 1-\rho_l & 0 & 0 & 0 \\ 0 & \rho_l & 0 & 0 \\ 0 & 0 & 1-\rho_l & 0 \\ 0 & 0 & 0 & \rho_l \end{pmatrix} \tag{7.20}$$

Remark: Before going further in this strategy presentation and analysis, it is worth to recall that:

- The model used for the controller synthesis is the linear vertical 7-DOF model. It includes several vertical dynamics as the chassis acceleration $\ddot{z}_s$, the four wheels accelerations $\ddot{z}_{us_{ij}}$, the roll bounce acceleration $\ddot{\theta}$ and the pitch acceleration $\ddot{\phi}$, see chapter. 3.

- The simulations presented in that work are provided using a nonlinear full vehicle model experimentally validated on the vehicle Renault Mégane Coupé MIPS (Mulhouse) (see. 3.1).

Here, the proposed strategy is applied to a vehicle equipped by four semi-active MR dampers. There are various approaches to model semi-active dampers. In the parametric model of (Guo *et al.*, 2006*a*), the hysteresis loop force-velocity is well modeled by an hyperbolic tangent function.

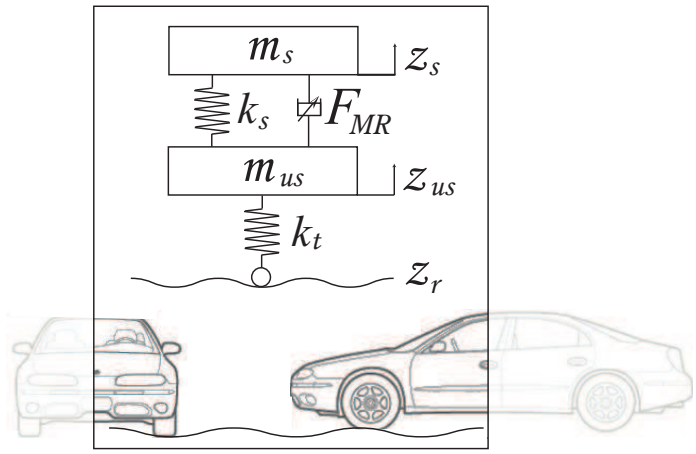

Figure 7.24: *QoV* model for a semi-active suspension in a vehicle.

The *MR* damping force is given by:

$$F_{MR} = I f_c \tanh\left(a_1 \dot{z}_{def} + a_2 z_{def}\right) + b_1 \dot{z}_{def} + b_2 z_{def} \tag{7.21}$$

where the electric current is bounded between $0 \leq I_{min} \leq I \leq I_{max} \leq 2.5$. I_{min} and I_{max} depend on the *MR* damper specifications. Experimental data obtained from a commercial *MR* damper are used to model the nonlinearities of this actuator by using (7.21). The parameters of the *MR* damper model used in this analysis are: $fc = 600.9$, $a_1 = 37.8$, $a_2 = 22.1$, $b_1 = 2830.8$ and $b_2 = -7897.2$.

The *QoV* system dynamics, given in a state-space representation, is written as:

$$\begin{aligned}
\underbrace{\begin{bmatrix} \dot{z}_s \\ \ddot{z}_s \\ \dot{z}_{us} \\ \ddot{z}_{us} \end{bmatrix}}_{\dot{x}} &= \underbrace{\begin{bmatrix} 0 & 1 & 0 & 0 \\ -\frac{k_s+b_2}{m_s} & -\frac{b_1}{m_s} & \frac{k_s+b_2}{m_s} & \frac{b_1}{m_s} \\ 0 & 0 & 0 & 1 \\ \frac{k_s+b_2}{m_{us}} & \frac{b_1}{m_{us}} & -\frac{k_s+k_t+b_2}{m_{us}} & -\frac{b_1}{m_{us}} \end{bmatrix}}_{A} \underbrace{\begin{bmatrix} z_s \\ \dot{z}_s \\ z_{us} \\ \dot{z}_{us} \end{bmatrix}}_{x} \\
&+ \underbrace{\begin{bmatrix} 0 & 0 \\ \frac{-\cdot\rho f_c}{m_s} & 0 \\ 0 & 0 \\ \frac{\cdot\rho f_c}{m_{us}} & \frac{k_t}{m_{us}} \end{bmatrix}}_{B} \underbrace{\begin{bmatrix} I \\ z_r \end{bmatrix}}_{u} \\
\underbrace{\begin{bmatrix} y_1 \\ y_2 \end{bmatrix}}_{y} &= \underbrace{\begin{bmatrix} 1 & 0 & -1 & 0 \\ 0 & 1 & 0 & -1 \end{bmatrix}}_{C} \begin{bmatrix} z_s \\ \dot{z}_s \\ z_{us} \\ \dot{z}_{us} \end{bmatrix}
\end{aligned} \tag{7.22}$$

where, $\rho = \tanh\left[a_1 \dot{z}_{def} + a_2 z_{def}\right] \in [0, 1]$ is a varying parameter, the accelerometers of the sprung ($\ddot{z}_s$) and unsprung mass ($\ddot{z}_{us}$). These measurements are related to the comfort and road holding performances, that depend on the semi-active damper properties and obviously on the road irregularities.

7.3.1.1 Design of the LPV/$\mathcal{H}_\infty$ fault tolerant control of vehicle roll dynamics under semi-active damper malfunction

Here, a new LPV/$\mathcal{H}_\infty$ fault tolerant control strategy is based on the monitoring of the semi-active dampers. When a fault is detected on one of the four semi-active dampers (i.e a lack in the vertical forces), the roll dynamics are amplified, causing vehicle instability and increasing car roll-over risks. To manage this instability, the proposed LPV/$\mathcal{H}_\infty$ suspension control is scheduled thanks to ρ_l the load transfer generated by the roll bounce of the vehicle ρ_l (by comparing the righ/letf forces) and tunes the 3 remaining healthy dampers to achieve fault compensation without reaching saturation. In addition, the performance objectives are set thanks to this varying parameter ρ_l which is included in the considered weighting functions on chassis displacement W_{z_s} and the roll dynamics of the car W_θ.

Remark: This strategy given in Fig. 7.25 includes 3 varying parameters. one is used for the control reconfiguration and adaptation to critical driving situations with damper malfunction, the two others parameters are needed to account for the dissipativity and saturation of the semi-active MR , as in (Mohammadpour and Scherer, 2012).

For sake of clarity, let us recall the LPV Quarter of Vehicle model used in this control synthesis for this strategy. Indeed, the semi-active force is modeled following (Jorge De-J *et al.*, 2012), as:

$$F_{sa} = \underbrace{b_1\left(\dot{z}_{s_i} - \dot{z}_{us_i}\right) + b_2\left(z_{s_i} - z_{us_i}\right)}_{passive} + \underbrace{I \cdot f_c \cdot \rho}_{semi-active} \tag{7.23}$$

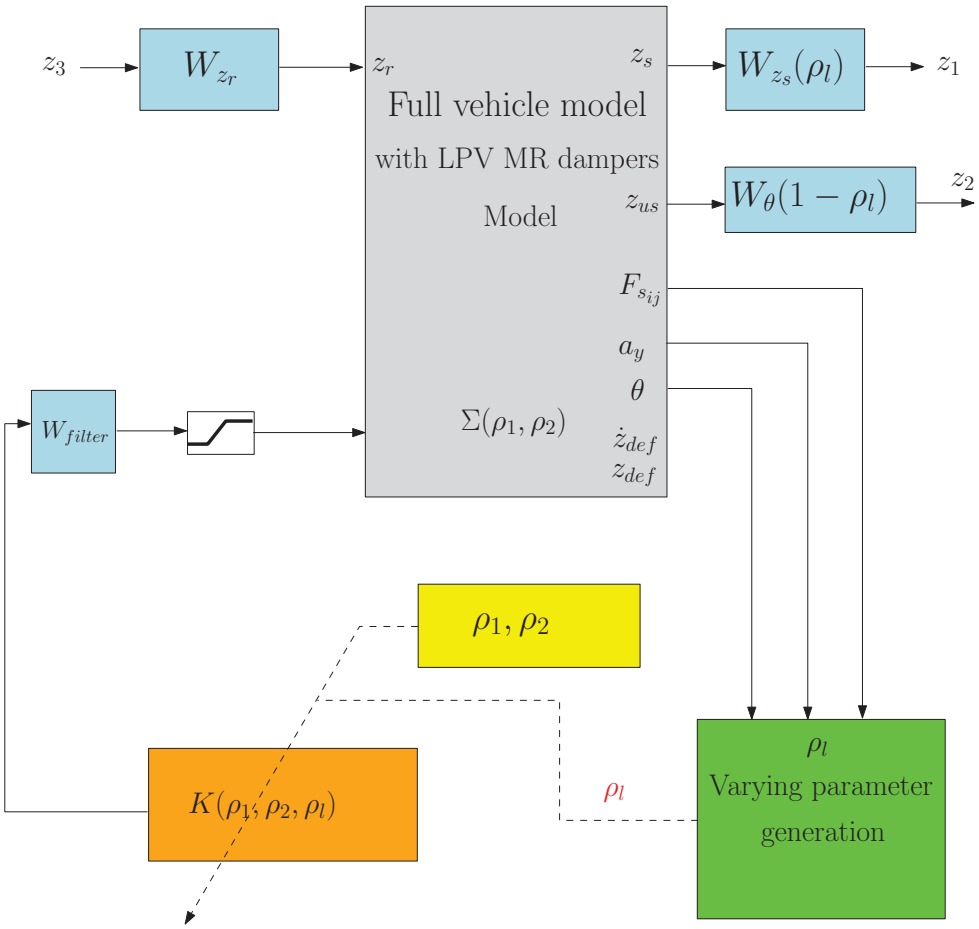

Figure 7.25: Global chassis control implementation scheme.

where I is the electric current to control the semi-active force based on the desired performances and $\rho = \tanh\left[a_1 \dot{z}_{def} + a_2 z_{def}\right] \in [0, 1]$ represents the nonlinearities of the shock absorber. In the control synthesis for FTC, the varying parameters ρ_1 and ρ_2 allow to ensure that the suspension control meets the semi-activeness and the saturation damper's constraints, respectively. Then, in this study the suspension in each corner is modeled as:

$$\begin{cases} \dot{x}_{_{lpv}} = A_{_{lpv}}\left(\rho_1, \rho_2\right) x_{_{lpv}} + B_1 u_c + B_2 w \\ y_{_{lpv}} = C_1 x_{_{lpv}} \end{cases} \tag{7.24}$$

where

$$x_{_{lpv}} = \begin{pmatrix} x_s \\ x_f \end{pmatrix}^T, A_{_{lpv}}\left(\rho_1, \rho_2\right) = \begin{pmatrix} A_s + \rho_2 B_{s2} C_{s2} & \rho_1 B_s C_f \\ 0 & A_f \end{pmatrix},$$
$$B_1 = \begin{pmatrix} 0 \\ B_f \end{pmatrix}, B_2 = \begin{pmatrix} B_{s1} \\ 0 \end{pmatrix}, C_1 = \begin{pmatrix} C_s \\ 0 \end{pmatrix}^T$$

$$\rho_1 = \tanh(C_{s2} x_s) \tanh(\tfrac{C_f x_f}{F_1}) \tfrac{F_1}{C_f x_f},$$
$$\rho_2 = \tfrac{\tanh(C_{s2} x_s)}{C_{s2} x_s}$$

x_s, A_s, B_s, B_{s1}, B_{s2}, C_s and C_{s2} are the state and matrices of a state-space representation of the *QoV* model by including the *MR* damper model in (7.22) and considering z_{def} and $\dot{z}_{def}$ as output; x_f, A_f,

B_f, C_f are the state and matrices of a representation of the low-pass filter $W_{filter} = \omega_f/(s+\omega_f)$ which is added to the system to make the control input matrices parameter independent.

7.3.1.2 LPV/$\mathcal{H}_\infty$ FTC structure for the suspension systems :

A smart LPV controller structure scheduled by ρ_l is used to achieve the fault tolerant control that manage suspension systems failures. The third scheduling parameter, ρ_l, acts in the presence of damper malfunction, which can be seen directly on the lateral load transfer of the vehicle. For this sake, the suspension control allocation is used to manage this malfunction. This parameter, as previously defined for the GCC actuators coordination, gives a good idea on the vertical behaviour of the car considering the suspensions vertical efforts and the lateral load transfer. Here, it will be used to reconfigurable the suspension effort in order to manage the damper loss. Let us recall how it is generated:

$$\begin{cases} F_{z_l} &= m_s \times g/2 + m_s \times h \times a_y/l_f \\ F_{z_r} &= m_s \times g/2 - m_s \times h \times a_y/l_r \\ \rho_l &= |(\delta_{fl}F_{z_{fl}} + \delta_{rl}F_{z_{rl}}) - (\delta_{fr}F_{z_{fr}} + \delta_{rr}F_{z_{rr}})| \\ & \quad /|(F_{z_{fl}} + F_{z_{rl}} + F_{z_{fr}} + F_{z_{rr}})|; \end{cases} \tag{7.25}$$

with δ_{ij}: the suspension systems efficiency given by the considered monitoring system, $F_{z_{ij}}$: the vertical forces, a_y lateral acceleration, $\rho_l \in [0\ \ 1]$: the monitoring parameter. The innovative solution which aims at stabilizing the vehicle in the presence of damper failure is the following: the controller has a partly fixed structure obtained by by making the LMIs structure orthogonal with a parameter dependency on the control output matrix, as follow:

$$\begin{pmatrix} u_{fl}^{\mathcal{H}_\infty}(t) \\ u_{fr}^{\mathcal{H}_\infty}(t) \\ u_{rl}^{\mathcal{H}_\infty}(t) \\ u_{rr}^{\mathcal{H}_\infty}(t) \end{pmatrix} = \underbrace{U(\rho_l)C_c^0(\rho_l)}_{C_c(\rho_l)} x_c(t) \tag{7.26}$$

The suspension forces distribution is obtained with the matrix $U(\rho_l)$:

$$U(\rho_l) = \begin{pmatrix} 1-\rho_l & 0 & 0 & 0 \\ 0 & \rho_l & 0 & 0 \\ 0 & 0 & 1-\rho_l & 0 \\ 0 & 0 & 0 & \rho_l \end{pmatrix} \tag{7.27}$$

The parameter ρ_l defined in (7.25) generates the adequate suspension forces distribution, depending on the load transfer (left $\leftrightarrows$ right) caused by the critical situation.
This suspension tuning is achieved as follows: When one of the suspension dampers is faulty, a load transfer is then generated and influences the vehicle stability and handling. When a malfunction is detected on one of the left front suspension systems, $\rho_l \to 1$, penalizing the provided output suspension force on the faulty corner, changing the level of saturation depending on the detected fault. Also, an overload appears on the right side. To managed that, the lacking suspension effort is compensated by the 3 healthy dampers to stabilise the vehicle. Indeed, left suspensions are set to ”hard” to handle the

overload caused by the loss of one of the right side dampers. On the other side, suspensions are relaxed and tuned to "soft" for the remaining healthy actuators (since the overload is on the other side) and a level of saturation is applied to the faulty one depending of the degree of deterioration detected. This distribution is handled thanks to the specific structure of the suspension controller, given as follows :

$$K_s(\rho) := \begin{cases} \dot{x}_c(t) = A_c(\rho_1,\rho_2,\rho_l)x_c(t) + B_c(\rho_1,\rho_2,\rho_l)y(t) \\ \begin{pmatrix} u_{fl}^{\mathcal{H}_\infty}(t) \\ u_{fr}^{\mathcal{H}_\infty}(t) \\ u_{rl}^{\mathcal{H}_\infty}(t) \\ u_{rr}^{\mathcal{H}_\infty}(t) \end{pmatrix} = \underbrace{U(\rho_l)C_c^0(\rho_1,\rho_2)}_{C_c(\rho_1,\rho_2,\rho_l)} x_c(t) \end{cases} \tag{7.28}$$

where $x_c(t)$ is the controller state, $A_c(\rho_1,\rho_2,\rho_l)$, $B_c(\rho_1,\rho_2,\rho_l)$ and $C_c(\rho_1,\rho_2,\rho_l)$ controller scheduled by ρ_l while ρ_1 and ρ_2 ensure the semi-activeness of the dampers.
$u^{\mathcal{H}_\infty}(t) = [u_{fl}^{\mathcal{H}_\infty}(t) u_{fr}^{\mathcal{H}_\infty}(t) u_{rl}^{\mathcal{H}_\infty}(t) u_{rr}^{\mathcal{H}_\infty}(t)]$ the input control of the suspension actuators and $y(t) = z_{def}(t)$ the suspension deflection.

Then, the LPV/$\mathcal{H}_\infty$ suspension control problem formulation regarding the previously described FTC structure is given as follows:
According to Fig. 7.25, the FTC is coupled with the the suspension control adaptation (see (Savaresi *et al.*, 2010*b*)). Indeed,a robust H_∞ control scheme is considered, including the following parameter varying weighting functions: where $W_{z_s} = \rho_l \frac{s^2+2\xi_{11}\Omega_{11}s+{\Omega_{11}}^2}{s^2+2\xi_{12}\Omega_{12}s+{\Omega_{12}}^2}$ is shaped in order to reduce the bounce amplification of the suspended mass (z_s) between $[0, 12]$Hz.
$W_\theta = (1-\rho_l)\frac{s^2+2\xi_{21}\Omega_{21}s+{\Omega_{21}}^2}{s^2+2\xi_{22}\Omega_{22}s+{\Omega_{22}}^2}$ attenuates the roll bounce amplification in low frequencies.
$W_u = 3.10^{-2}$ shapes the control signal.

According to Fig. 7.25, the following parameter dependent suspension generalized plant ($\Sigma_{gv}(\rho_1,\rho_2,\rho_l)$) is obtained:

$$\Sigma_{gv}(\rho_1,\rho_2,\rho_l) := \begin{cases} \dot{\xi} = A(\rho_1,\rho_2,\rho_l)\xi + B_1\tilde{w} + B_2 u \\ \tilde{z} = C_1(\rho_1,\rho_2,\rho_l)\xi + D_{11}\tilde{w} + D_{12}u \\ y = C_2\xi + D_{21}\tilde{w} + D_{22}u \end{cases} \tag{7.29}$$

where $\xi = [\chi_{vert}\ \chi_w]^T$; $\tilde{z} = [z_1\ z_2\ z_3]^T$; $\tilde{w} = [z_{rij}\ F_{dx,y,z}\ M_{dx,y}]^T$; $y = z_{def_{ij}}$; $u = u_{ij}^{\mathcal{H}_\infty}$; and χ_w are the vertical weighting functions states.

One of the main interesting contributions is the use of the parameter ρ_l that schedules the distribution of the left & right suspensions on the four corners of the vehicle and tune the suspension dampers smoothly. This is done thanks to the LPV frame work, from "soft" to "hard" to improve the car performances according to the driving situation.

In this synthesis, a very interesting innovation is the use of a partly fixed structure controller with a parameter dependency (ρ_l) on the control output matrix, combined with the scheduling of the weighting functions by the use of the varying parameter ρ_l, on the chassis displacement (z_s, considered as a comfort indicator) and the roll motion (θ, a road holding indicator). This allows , at the same time, to manage the dampers failures in FTC strategy and to tune various actuators controllers, depending on the driving situation, by a hierarchical activation to optimize their use (coordinate framework with smooth transition between different performance objectives even if they are contradictory).

The LPV system (8.39) includes 3 scheduling parameters and can be described as a polytopic system, i.e, a convex combination of the systems defined at each vertex of a polytope defined by the bounds of the varying parameter. The synthesis of the controller is made within the framework of the $\mathcal{H}_\infty$ control of polytopic suspensions, (for more details, see (Scherer, 1996)).

Remark:

- In this study, a 7 DOF vehicle model is considered, (see 3.3.2 and augmented with LPV damper model (7.23) for each corner of the vehicle.

- The parameters of these weighting functions are obtained using genetic algorithm optimization as in (Mohammadpour and Scherer, 2012).

- All controllers presented along the paper are synthesized in the LPV/H_∞ framework. This design is achieved, thanks to the LMI-based H_∞ resolution.

7.3.1.3 Simulation Results

Time domain simulations are performed on the full nonlinear vehicle model given in subsection 3.5. For sake of completeness, the results of the proposed LPV/$\mathcal{H}_\infty$ fault tolerant control are denoted "LPV strategy" in red and compared to the "vehicle with the damper failure" in blue.

To test the efficiency of the proposed LPV/$\mathcal{H}_\infty$ FTC of vehicle roll dynamics under semi-active damper malfunction, the following scenario is used:

1. The vehicle runs at 80km/h in straight line on wet road ($\mu = 0.5$, where μ is a coefficient representing the adherence to the road).

2. The front right damper of the vehicle is considered faulty (a failure of 70% on the nominal behaviour of the healthy dampers).

3. A 5cm bump on the left wheels (from $t = 0.5$s to $t = 1$s),

4. A Another bump on the right wheels (from $t = 3$s to $t = 4$s),

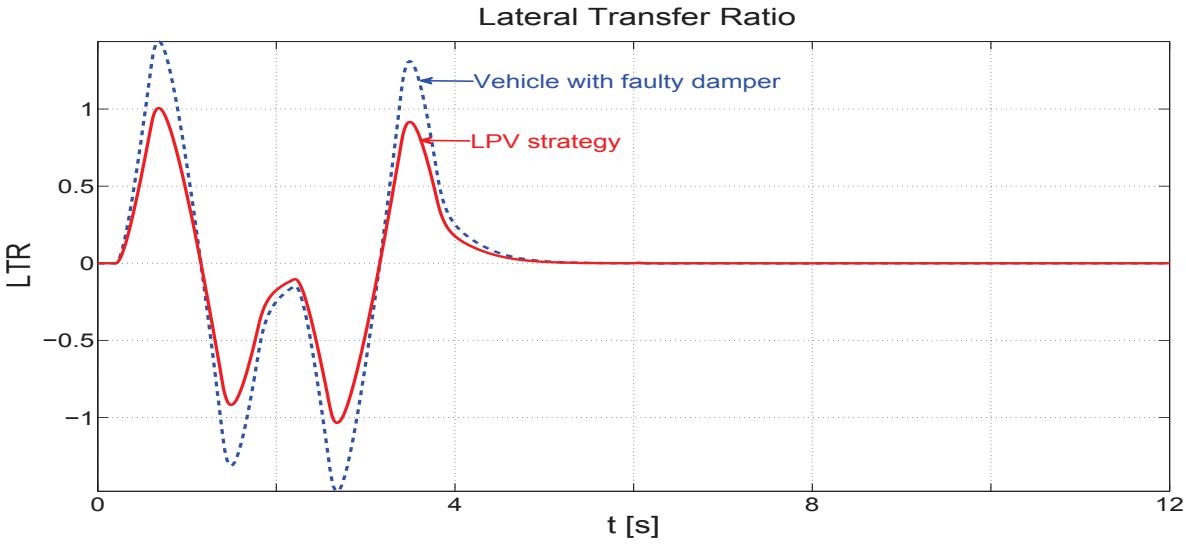

Figure 7.26: Lateral load transfer

Fig. 7.26 shows the lateral load transfer generated by the driving scenario; based on it, the scheduling parameter ρ_l is calculated by simply calculating the absolute value of the LTR parameter.

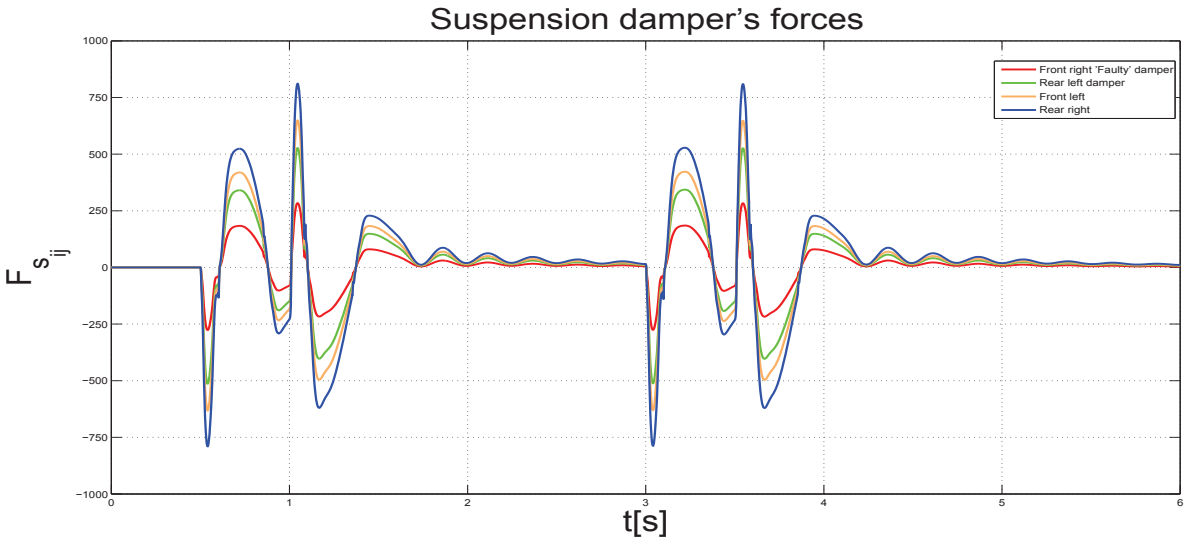

Figure 7.27: Suspension damper's forces: the faulty and healthy dampers efforts

In Fig. 7.27, the 4 semi-active dampers efforts provided by the designed fault tolerant LPV/$\mathcal{H}_\infty$ controller are given. It is clear that the failure occurs on the front rear damper which can not provide more then 30% of the nominal force of the healthy MR dampers. Also, it can be seen that the dampers forces distribution is scheduled, following the varying parameter ρ_l (generated by monitoring the lateral transfer ratio). The suspensions forces provided on the right side of the vehicle are larger than those on the right side, due to the big load supported by their dampers. Moreover, the force provided

by the front right damper is greater than the one provided by the rear right one, because it compensates the load due to the front left damper.

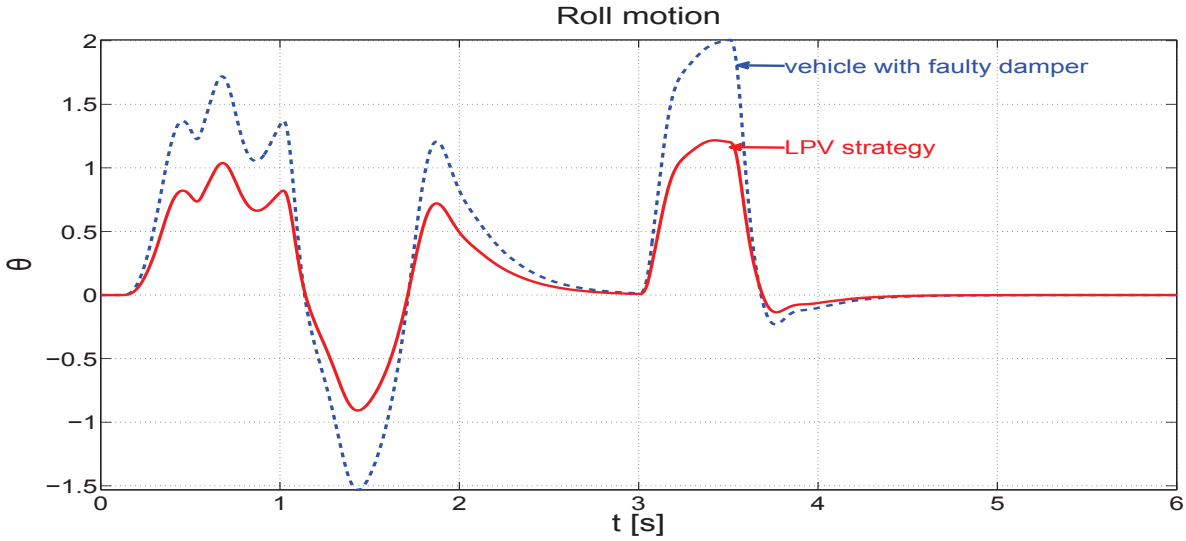

Figure 7.28: Roll motion of the vehicle θ

Fig. 7.28 represents one of the interesting results achieved by the proposed control structure. The roll dynamics are clearly attenuated by the proposed LPV/$\mathcal{H}_\infty$ FTC strategy. This allows to maintain a good road holding and stability of the vehicle.

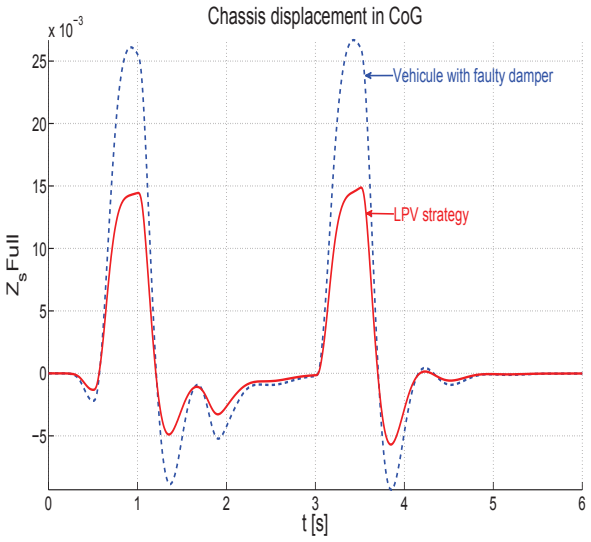

Figure 7.29: Chassis displacement in CoG z_s.

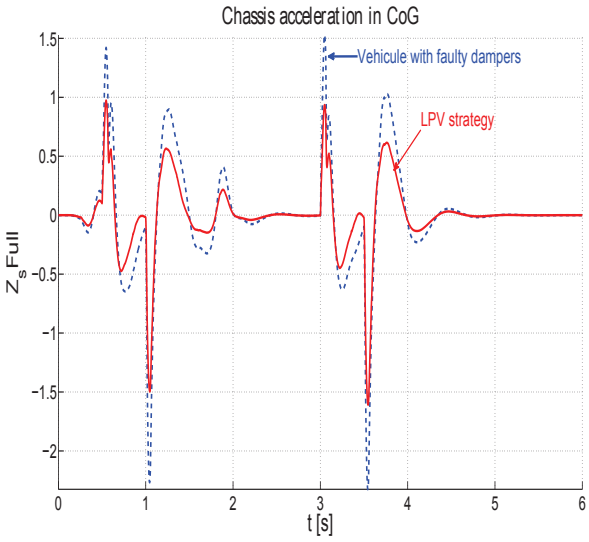

Figure 7.30: Chassis acceleration in CoG $\ddot{z}_s$.

From Fig. 7.29 and Fig. 7.30, it can be noticed that the developed strategy in addition on enhancing vehicle roadholding, it improves passengers comfort by reducing chassis acceleration $\ddot{z}_s$ and

displacement z_s in the four corners in the car (differently depending on the suspensions efforts allocation) while driving.

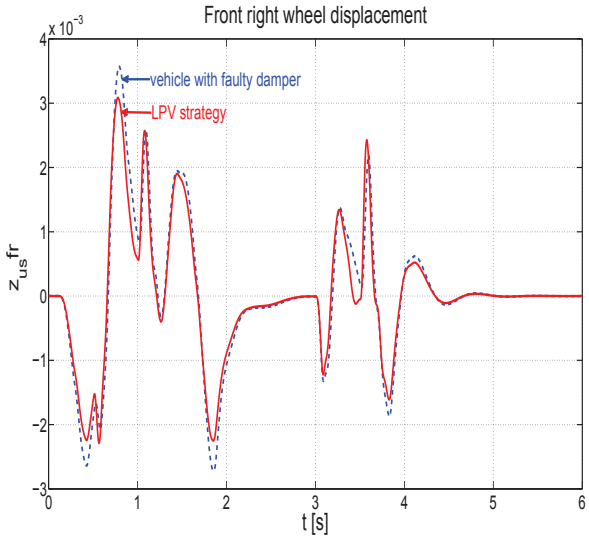

Figure 7.31: Wheel displacement in front right $z_{us_{fr}}$.

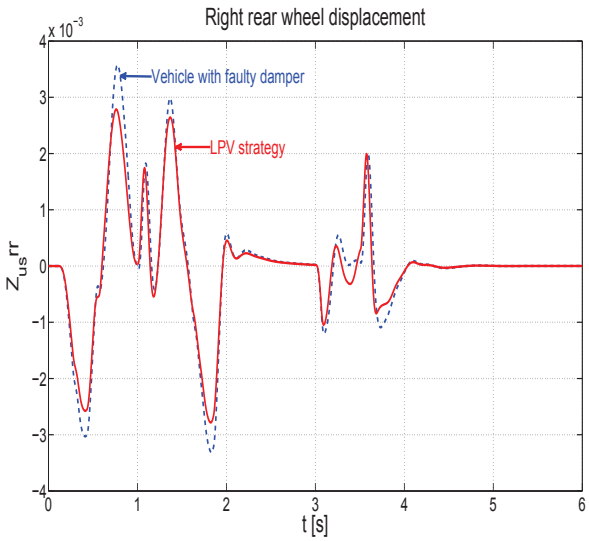

Figure 7.32: Wheel displacement in rear right $z_{us_{rr}}$.

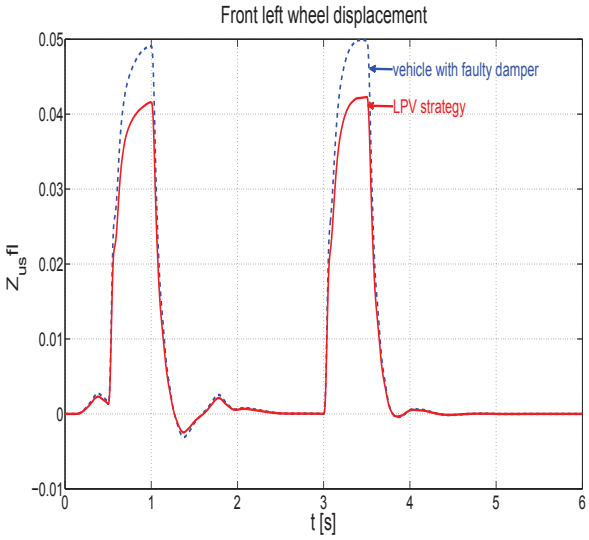

Figure 7.33: Wheel displacement in front left $z_{us_{fl}}$.

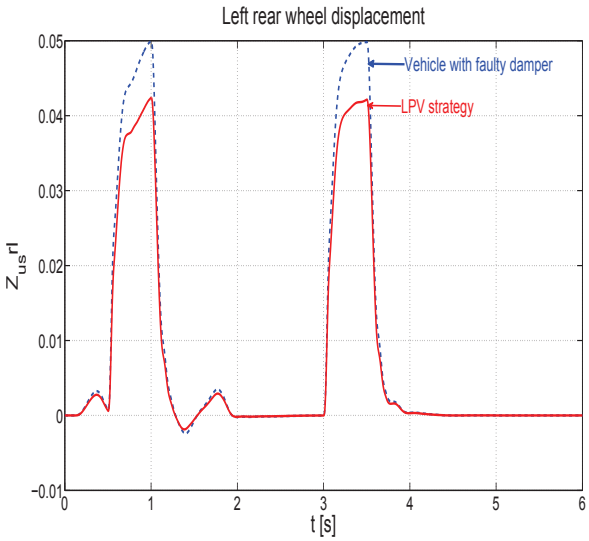

Figure 7.34: Wheel displacement in rear left $z_{us_{rl}}$.

In Fig. 7.31, 7.32, 7.33, 7.34, the four wheels bounce of the vehicle are shown. It can be seen also that the improvements brought by the designed controller on the left side are better than on the right side, due to the larger damping forces supplied on this side to handle the load transfer.

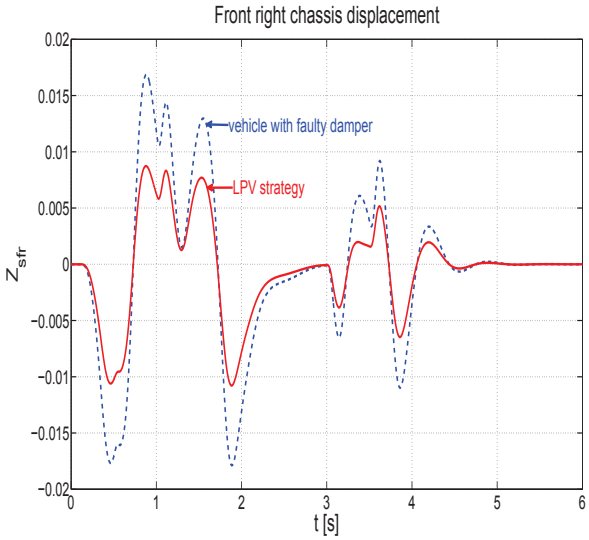

Figure 7.35: Chassis displacement in front right $z_{s_{fr}}$.

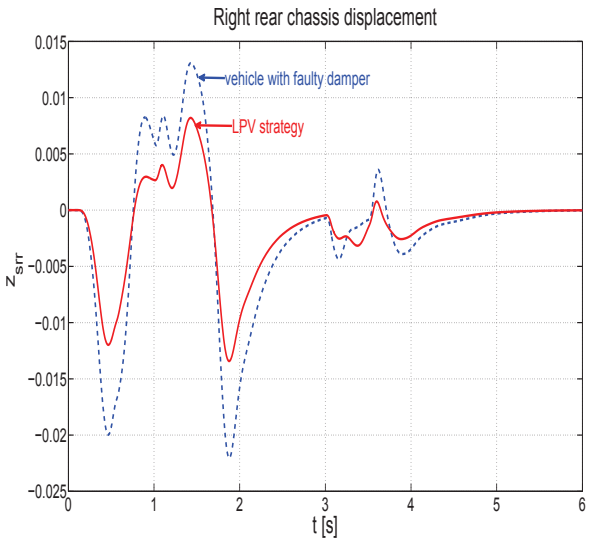

Figure 7.36: Chassis displacement in rear right $z_{s_{rr}}$.

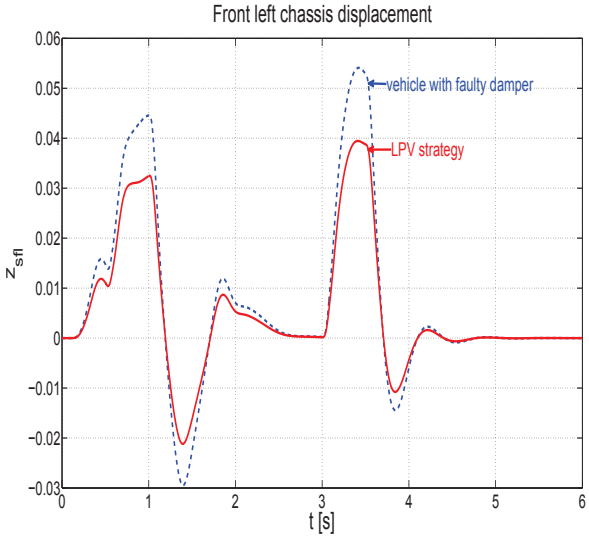

Figure 7.37: Chassis displacement in front left $z_{s_{fl}}$.

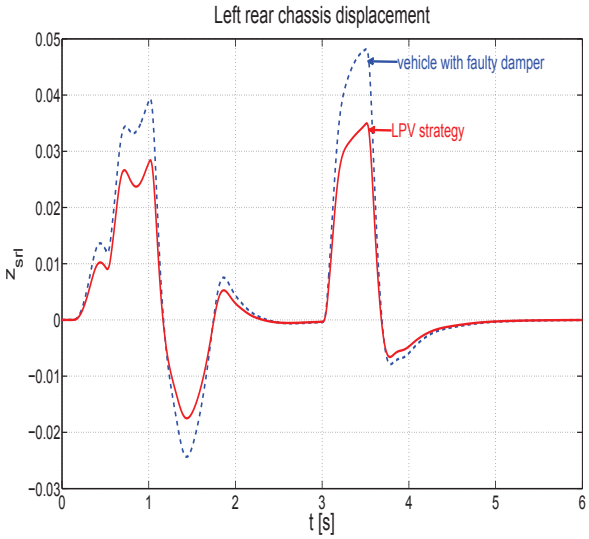

Figure 7.38: Chassis displacement in rear left $z_{s_{rl}}$.

Fig. 7.35, 7.36, 7.37, 7.38 shows the chassis displacement in the four corners of the vehicle. It can be clearly seen that the chassis displacement is differently attenuated in each corner. Indeed, the control allocation structure allows to tune each damper force depending on the evolution of the varying parameters thanks to the LPV framework. The dynamics improvements, then, is achieved according to this fault tolerant allocation control of the vehicle.

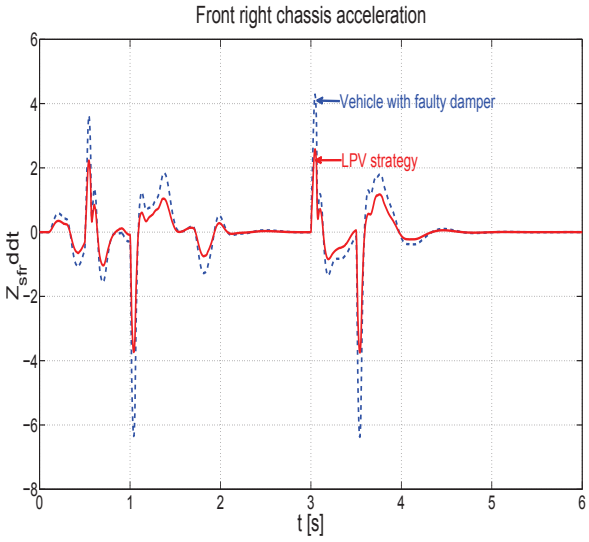

Figure 7.39: Chassis acceleration in front right $\ddot{z}_{s_{fr}}$.

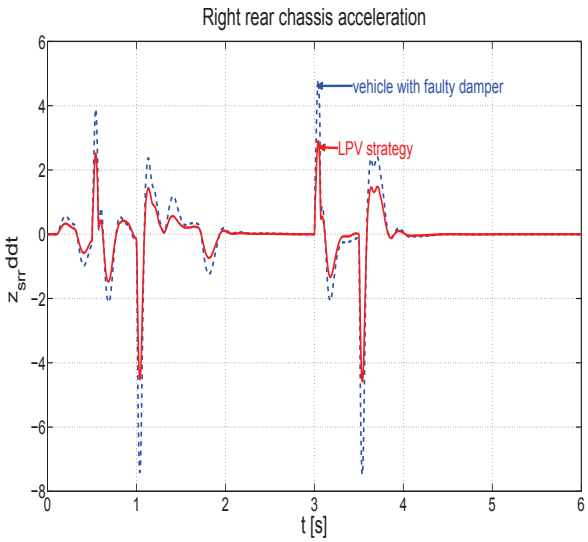

Figure 7.40: Chassis acceleration in rear right $\ddot{z}_{s_{rr}}$.

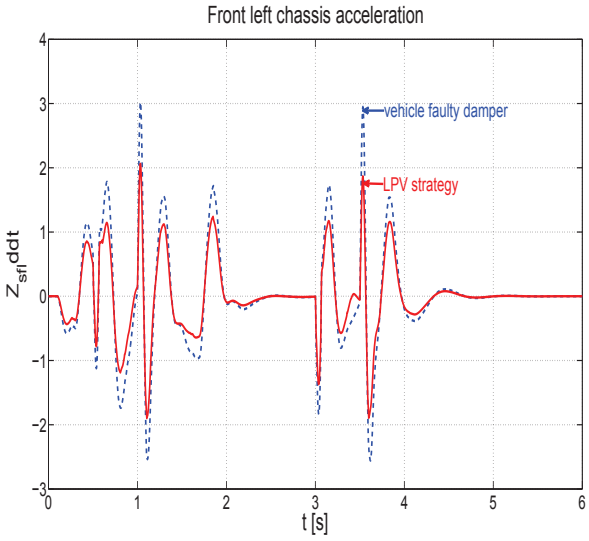

Figure 7.41: Chassis acceleration in front left $\ddot{z}_{s_{fl}}$.

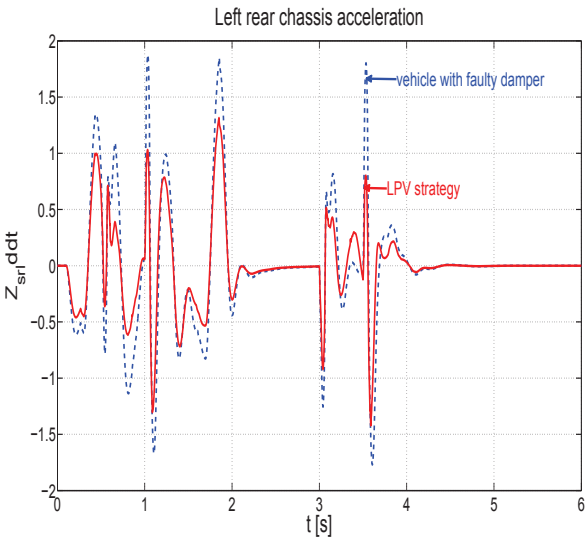

Figure 7.42: Chassis displacement in rear left $\ddot{z}_{s_{rl}}$.

Also, figures from Fig. 7.39 to Fig. 7.42 show various comfort performances, namely, the chassis acceleration on each corner of the vehicle. It is clearly noticed that the performance objectives are differently reached, depending on the suspension forces distribution and reconfiguration given by the proposed LPV/$\mathcal{H}_\infty$ fault tolerant control. This allows to handle the damper's failure effect on the vehicle dynamics in several driving situations.

7.3.1.4 Conclusion

A new LPV/H_∞ fault tolerant control strategy which handles vehicle roll dynamics under damper malfunction has been presented in this study. It proposes a new structure of the controller, by making the corresponding LMIs orthogonal with a parameter dependency on the controller matrix output. The varying parameter used in the developed strategy is obtained by monitoring the lateral transfer ratio caused by the roll bounce of the vehicle. This allows to online reconfigure the provided suspensions forces in the four corners of the vehicle to reach the desired performance objective. Simulations performed on a complex nonlinear model have shown the efficiency of the proposed approach. Let us recall that the LPV framework allows to simplify the implementation procedure.

7.3.2 LPV fault tolerant global chassis control for vehicle dynamics

In this study, a new fault tolerant global chassis control strategy is presented. It aims at managing simultaneously critical driving situations due to road/vehicle conditions as well as actuator malfunctions. Indeed, it allows to achieve several performance objectives such as enhancing the vehicle handling and the lateral dynamic control, i.e. the yaw control, and improving vehicle stability subject to critical driving situation.

This strategy is summarized in (see Fig.7.43). The FTC LPV controllers are scheduled by 3 parameters (ρ_b, ρ_s and ρ_l). Indeed, a special monitoring system is defined to evaluate how a driving situation is dangerous and to account for braking/suspension actuator failures. The control structure is such that the system become fault tolerant by construction. This means that it can handle one actuator failure by changing the configuration of control online.
Indeed, here the proposed strategy in addition of achieving the damper failure management allows to handle the braking malfunction to avoid critical driving within global chassis control strategy as shown in the following scheme:

Then, the LPV/$\mathcal{H}_\infty$ FT GCC strategy focuses on achieving in the same control structure the following objectives:

- **The suspension control reconfiguration under damper malfunction**: as previously presented in 7.3.1. It is worth noting that for this part of the study active suspensions are considered in the control and simulation procedures.

- **The control adaptation to critical driving situations and braking actuator malfunction**: Two scheduling parameters ρ_b and ρ_s will be used to coordinate the actuators and provide hierarchical use of the 3 VDSC actions (steering, braking and active suspension). When dangerous situation is detected, the GCC gives a torque reference to the braking system (that avoids slipping thanks to the ABS local controller), and if the braking system is not efficient enough and is not able to stabilize the vehicle (e.g. in case of low adherence or braking failure), the steering system is activated, and the suspension performances are changed from soft to hard, in order to handle the dynamical problem. First, in a normal situation, only the active suspension acts in order to keep the driving comfort, while not deteriorating the road handling (i.e soft suspension damping). When a dangerous situation is detected through the braking monitor ρ_b (in terms of tire slip), the braking torque is limited accordingly in order to bring back the tire forces into the linear stable zone of the tire characteristic and avoid slipping.

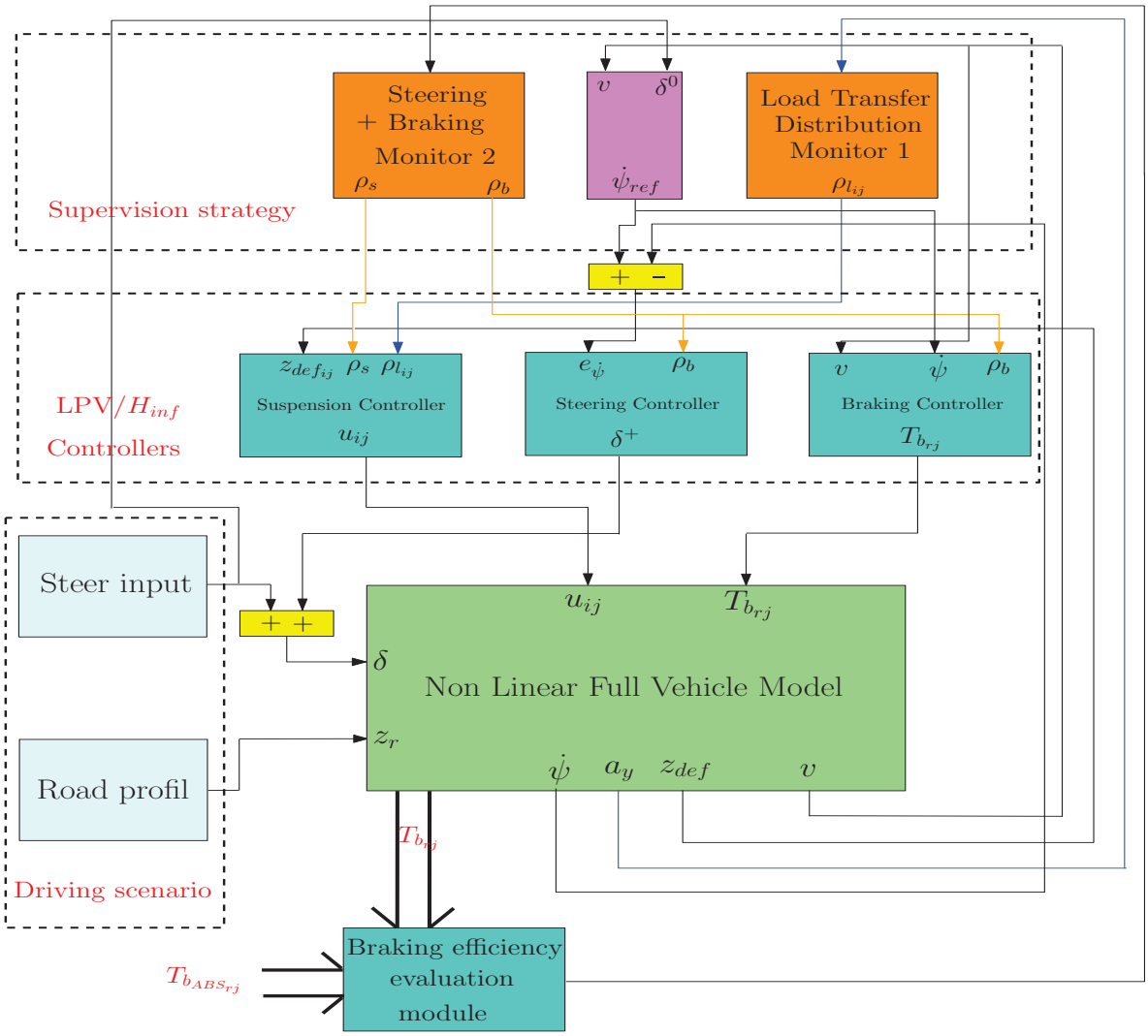

Figure 7.43: Global chassis control implementation scheme.

Defining some thresholds on the braking monitor ρ_b allows to handle more critical situations, thanks to the activation of the front steering actuator, as well as the performance adaptation of the active dampers that will improve the road handling through the attenuation of the roll movement.

In this strategy, the LPV framework is achieved thanks to some varying parameters that allow to adapt the control structure regarding the performance objective to be achieved.

7.3.2.1 Driving situation supervision and Scheduling parameters generation

The monitoring strategy presented below has been introduced by the authors in (Poussot-Vassal *et al.*, 2011*b*). Since attitude and yaw stability are concerned in this study, the strategy based on the

measurement of the longitudinal slip ratio of the rear wheels (s_{rj}) is efficient while being simple. Both scheduling parameters are defined as follows:

1. **Monitor on the braking efficiency:** The aim of the monitor is to schedule the GCC control to activate the steering system when braking is no longer efficient enough to guarantee safety. Then, one proposes the following scheduling strategy:

$$\rho_b = \max(|e_{T_{b_{rj}}}|)\,, j = \{l, r\} \tag{7.30}$$

where $e_{T_{b_{rj}}} = T_{b_{ABS_{rj}}} - T^*_{b_{rj}}$, and one defines the scheduling parameter $\xi(e)$ as:

$$\rho_b := \begin{cases} \overline{\xi} & \text{if } \rho_b \leq \underline{\chi} \\ \dfrac{\overline{\chi} - e}{\overline{\chi} - \underline{\chi}}\overline{\xi} + \dfrac{e - \underline{\chi}}{\overline{\chi} - \underline{\chi}}\underline{\xi} & \text{if } \underline{\chi} < \rho_b < \overline{\chi} \\ \underline{\xi} & \text{if } \rho_b \geq \overline{\chi} \end{cases} \tag{7.31}$$

where $\underline{\chi} = \frac{30}{100}T_{b_{max}}$ and $\overline{\chi} = \frac{70}{100}T_{b_{max}}$ are user defined brake efficiency measures. Note that other monitor strategies may be employed.

2. **Suspension and Steering monitor according to the braking efficiency:** ρ_s is defined as :

$$\rho_s \begin{cases} \to 1 & \text{when } 1 > \rho_b > R^2_{crit} \\ = \frac{\rho_b - R^1_{crit}}{R^2_{crit} - R^1_{crit}} & \text{when } R^1_{crit} < \rho_b < R^2_{crit} \\ \to 0 & \text{when } 0 < \rho_b < R^1_{crit} \end{cases} \tag{7.32}$$

when $\rho_b > R^2_{crit}(= 0.9)$, i.e. when a low slip ($< s^-$) is detected, the vehicle is not in an emergency situation and ρ_s is set to 0. When $\rho_b < R^1_{crit}(= 0.7)$, i.e. when a high slip occurs ($> s^+$), a critical situation is reached and ρ_s is set to 0. Intermediate values of ρ_b will give intermediate driving situations.

3. **The suspension control distribution for the dampers malfunction management**: the ρ_l as defined in 7.25 is used to generate the adequate suspension forces in the four corners of the vehicle depending on the load transfer (left $\leftrightarrows$ right) caused by the performed driving scenario.

Remark:

- It is worth noting that, while in (Poussot-Vassal *et al.*, 2011*b*) the scheduling parameters are considered to coordinate the use of braking/active suspension actuators, here, they aim at coordinating steering, braking and suspensions subsystems (which is more complex).

- The controllers are derived thanks to LPV/$\mathcal{H}_\infty$ methodology. This framework allows to smoothly tune the control performances thanks to the scheduling parameters ρ_b et ρ_s, guaranteeing internal stability (avoiding switching) and ensuring $\mathcal{H}_\infty$ performances.

7.3.2.2 Global chassis control design strategy

The synthesis of the different controllers is completed in 2 steps, to decouple lateral and vertical dynamics. The coupling effects are handled through the scheduling parameter ρ_s and thanks to an "anti-roll" action of the semi-active suspension.

- First the steering/braking controllers are designed using the linear bicycle model, to improve the lateral dynamics and to stabilize the vehicle.
- Then the suspension controllers are synthesized, using the linear vertical full car model, to improve the comfort/road handling performance objectives and the vertical dynamics behavior.

Below, LPV/$\mathcal{H}_\infty$ controllers (with ρ_b and ρ_s the scheduling parameters) are developed thanks to a dedicated polytopic approach.

step1: the braking/steering control Problem formulation For the the braking/steering controller design, the extended bicycle model introduced in subsection. 3.4 is used. The considered LPV/$\mathcal{H}_\infty$ control problem is described in Fig. (7.44) with the following scheduled weighting functions:

- $W_{e_{\dot\psi}} = 10\frac{s/500+1}{s/50+1}$, is used to shape the yaw rate error
- $W_{\dot v_y} = 10^{-3}$, attenuates the lateral acceleration
- $W_{T_{b_{rj}}}(R_b) = (1-\rho_b)\frac{s/10\varpi+1}{s/100\varpi+1}$, attenuates the yaw moment control input
- $W_{\delta^+}(\rho_s) = \rho_s\frac{s/\kappa+1}{s/10\kappa+1}$, attenuates the steering control input according to the value of ρ_s

where ϖ (resp.κ) is the braking (resp.steering) actuator cut-off frequency.

- When the tire force is in the linear zone, i.e. there is no risk of locking; so $\rho_b \to 1$ and the weighting function gain of $W_{T_{b_{rj}}}$ is chosen to be low. Therefore, the braking control is activated.
- When a high slip ratio is detected (critical situation) , the tire may lock, so $\rho_b \to 0$ and the gain of the weighting function is set to be high. This allows to deactivate the braking signal leading to a natural stabilisation of the slip dynamic.

On the other hand, when the driving situation is dangerous and presents a high risk for passengers, the steering control is activated through $W_{\delta^+}(\rho_s)$. The steering action depends on the varying parameter ρ_s, with $\rho_s(.) \in \mathcal{P}_{\rho_s}$ and $\mathcal{P}_{\rho_s} := \{\rho_s \in \mathbb{R} : \underline{\rho_s} \le \rho_s \le \overline{\rho_s}\}$ (where $\underline{\rho_s} = 0.1$ and $\overline{\rho_s} = 1$).

The generalized plant corresponding to Fig. 7.44 is LPV and can be modeled as,

$$\Sigma(R(.)) : \left[\begin{array}{c}\dot x\\ \hline z\\ y\end{array}\right] = \left[\begin{array}{c|cc} A(\rho(.)) & B_1(\rho(.)) & B_2\\ \hline C_1(\rho(.)) & D_{11}(\rho(.)) & D_{12}\\ C_2 & 0 & 0\end{array}\right]\left[\begin{array}{c} x\\ \hline w\\ u\end{array}\right] \tag{7.33}$$

where x includes the state variables of the system and of the weighing functions, $w = F_{dy}$ and $u = [\delta^+, T_{b_{rj}}]$ are the exogenous and control inputs respectively.

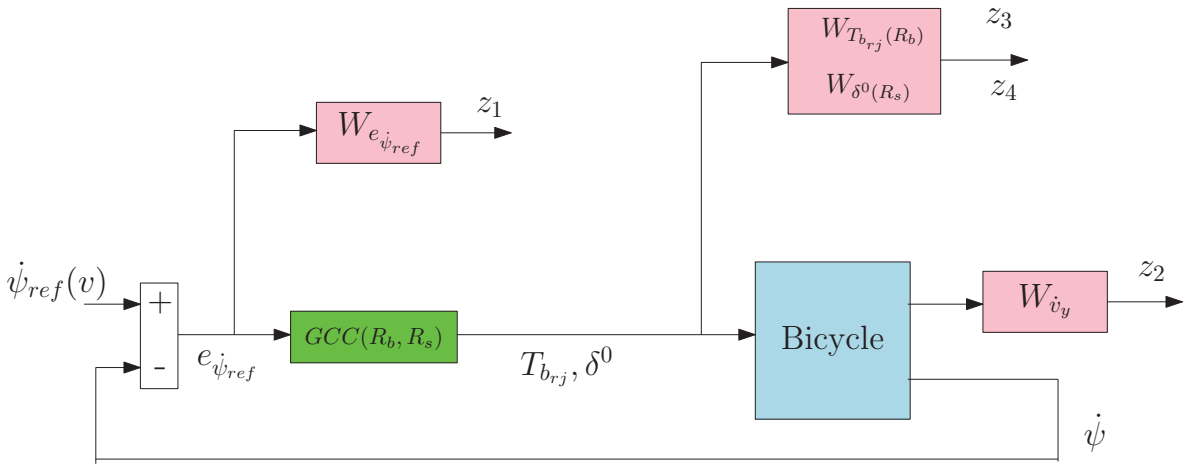

Figure 7.44: Generalized plant for braking/steering control synthesis.

$z = [z_1, z_2, z_3, z_4] = [W_{e_{\dot\psi}} e_{\dot\psi}, W_{\dot v_y} \dot v_y, W_{T_{b_{rj}}}(\rho_b) T_{b_{rj}}, W_{\delta^+}(\rho_s)\delta^+]$ holds for the controlled output, and $y = \dot\psi_{ref}(v) - \dot\psi$ is the controller input ($\dot\psi_{ref}(v)$ is provided by a reference bicycle model as the one described in subsection. 3.4).

Notice that the LPV model (7.33) is affine w.r.t parameters ρ_s and ρ_b and can be described as a polytopic system, i.e. a convex combination of the systems defined at each vertex formed by $\mathcal{P}_\rho(.)$, namely $\Sigma(\underline{\rho}(.))$ and $\Sigma(\overline{\rho}(.))$.

step 2: the suspension control problem formulation For this controller design, a 7 DOF vehicle model is considered, see sectin. 3.3.2. For the control design purposes, linear models are assumed for the stiffness k_{ij} and damping c_{ij} in the suspension force computation.
In this step, the suspension control with performance adaptation (see (Savaresi *et al.*, 2010*b*)), to be integrated in the global VDSC strategy (Vehicle Dynamic Control), is presented. The following H_∞ control scheme is considered, including parameter varying weighting functions.
The LPV/$\mathcal{H}_\infty$ FT control design for the suspensions is similar to the one presented in the previous section (see 7.3.1.2). Indeed, The following H_∞ control scheme is considered, including parameter varying weighting functions. where $W_{z_s} = \rho_1 \frac{s^2+2\xi_{11}\Omega_{11}s+{\Omega_{11}}^2}{s^2+2\xi_{12}\Omega_{12}s+{\Omega_{12}}^2}$ is shaped in order to reduce the bounce amplification of the suspended mass (z_s) between $[0, 12]$Hz.
$W_\theta = (1-\rho_1)\frac{s^2+2\xi_{21}\Omega_{21}s+{\Omega_{21}}^2}{s^2+2\xi_{22}\Omega_{22}s+{\Omega_{22}}^2}$ attenuates the roll bounce amplification in low frequencies.
$W_u = 3.10^{-2}$ shapes the control signal.

Remark: The parameters of these weighting functions are obtained using genetic algorithm optimization as in (Do *et al.*, 2010*a*).

According to Fig. 7.45, the following parameter dependent suspension generalized plant ($\Sigma_{gv}(\rho_s)$) is obtained:

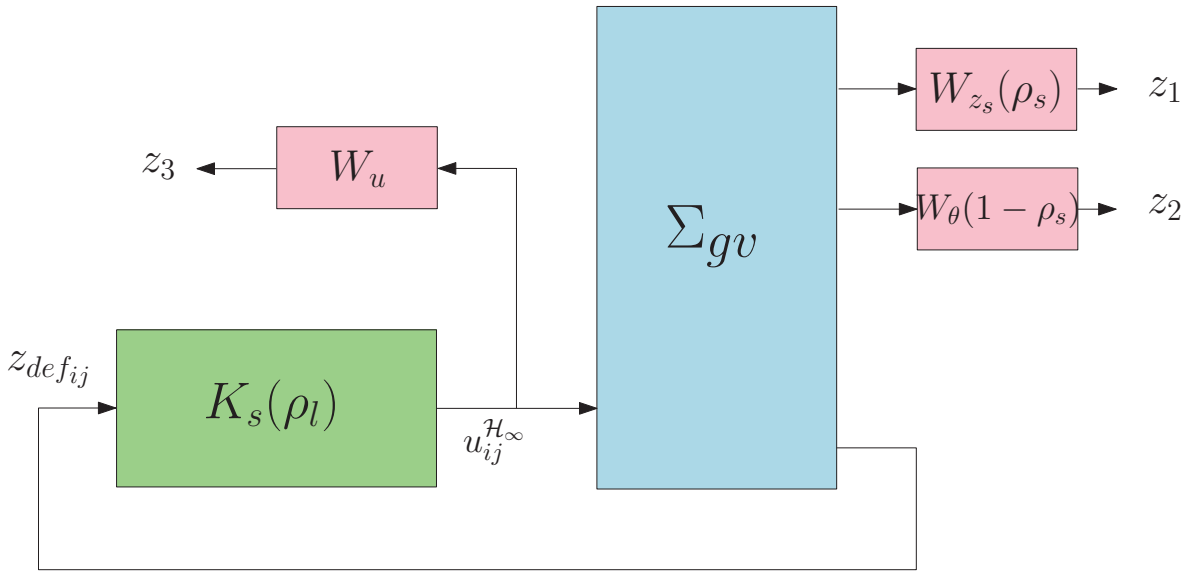

Figure 7.45: Suspension system generalized plant.

$$\Sigma_{gv}(\rho_s,\rho_l) := \begin{cases} \dot{\xi} = A(\rho_s,\rho_l)\xi + B_1\tilde{w} + B_2 u \\ \tilde{z} = C_1(\rho_s,\rho_l)\xi + D_{11}\tilde{w} + D_{12}u \\ y = C_2\xi + D_{21}\tilde{w} + D_{22}u \end{cases} \tag{7.34}$$

where $\xi = [\chi_{vert}\ \chi_w]^T$; $\tilde{z} = [z_1\ z_2\ z_3]^T$; $\tilde{w} = [z_{rij}\ F_{dx,y,z}\ M_{dx,y}]^T$; $y = z_{def_{ij}}$; $u = u_{ij}^{\mathcal{H}_\infty}$; and χ_w are the vertical weighting functions states.

As in previously defined,the parameter ρ_l to schedule the distribution of the left & right suspensions on the four corners of the vehicle and tune the suspension dampers smoothly, thanks to the LPV frame work, from "soft" to "hard" to improve the car performances according to the driving situation. This distribution is handled using a specific structure of the suspension controller, given as follows :

$$K_s(\rho_l) := \begin{cases} \dot{x}_c(t) = A_c(\rho_{l_{ij}})x_c(t) + B_c(\rho_{l_{ij}})y(t) \\ \begin{pmatrix} u_{fl}^{\mathcal{H}_\infty}(t) \\ u_{fr}^{\mathcal{H}_\infty}(t) \\ u_{rl}^{\mathcal{H}_\infty}(t) \\ u_{rr}^{\mathcal{H}_\infty}(t) \end{pmatrix} = \underbrace{U(\rho_l)C_c^0(\rho_s)}_{C_c(\rho_s,\rho_l)} x_c(t) \end{cases} \tag{7.35}$$

where $x_c(t)$ is the controller state, $A_c(\rho_s)$, $B_c(\rho_s)$ and $C_c(\rho_s)$ controller scheduled by ρ_s. $u^{\mathcal{H}_\infty}(t) = [u_{fl}^{\mathcal{H}_\infty}(t) u_{fr}^{\mathcal{H}_\infty}(t) u_{rl}^{\mathcal{H}_\infty}(t) u_{rr}^{\mathcal{H}_\infty}(t)]$ the input control of the suspension actuators and $y(t) = z_{def}(t)$.

It is worth noting that this control design structure allows to tune various actuators controllers depending on the driving situation, by a hierarchical activation to optimize the use of them(coordinate framework with smooth transition between different performance objectives even if they are contradictory.

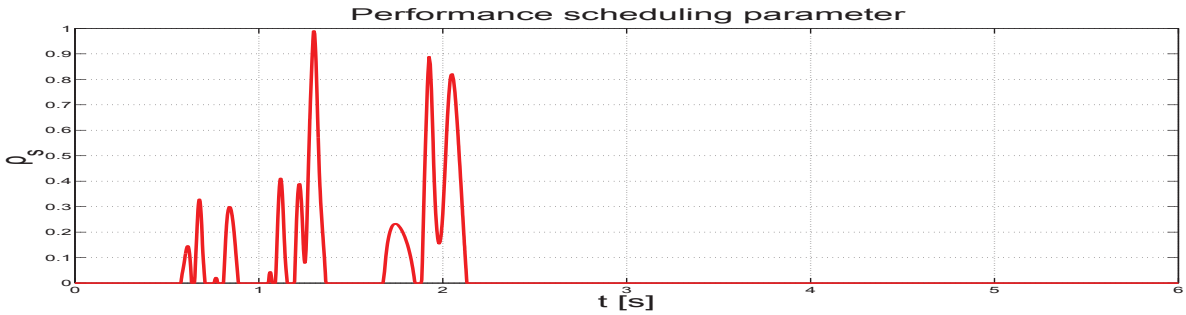

Figure 7.47: Steering/suspension scheduling parameter ρ_s

7.3.2.3 Simulation Results

To test the efficiency of the proposed strategy, the following driving scenario is considered, including a braking actuator fault and a damper fault:

- The vehicle runs at 100km/h on a wet road ($\mu = 0.5$) in straight line.
- 5cm Road bump from $t = 0.5$s to $t = 1.5$s and from $t = 4$s to $t = 5$s)
- A double line change manoeuvre is performed (from $t = 2$s to $t = 6$s) by the driver.
- A saturation of $75N$ on the left rear braking actuator is applied to simulate the fault on the braking system at the beginning of the line change.
- A fault on front left damper: force limitation of 70% occurs at $t = 4$s.
- Lateral wind occurs at vehicle's front generating an undesirable yaw moment (from $t = 2.5$s to $t = 3$s).

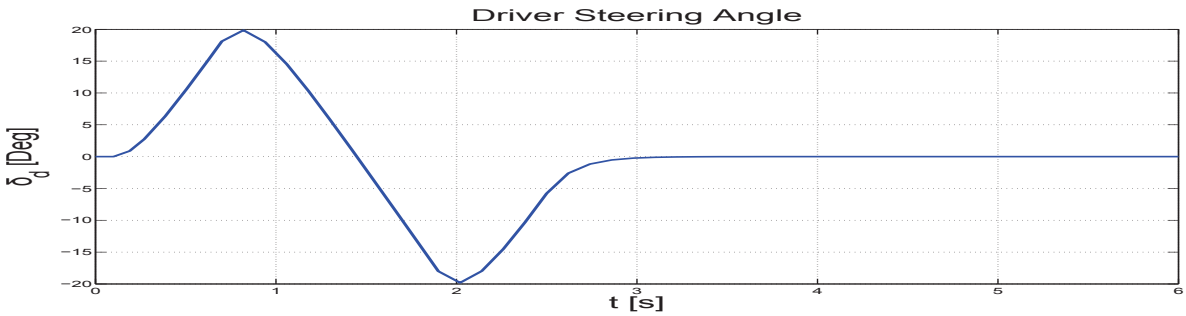

Figure 7.46: Driver angle input δ^0

The resulting monitoring signals ρ_b and ρ_s and ρ_l are obtained (see Fig. 7.49). This parameters allow to achieve the online adaptation of the proposed control structure to the performed driving scenarios and situations. These parameters allow to activate or deactivate the control actions, when required. Note that ρ_b monitors the braking efficiency (compared to an ABS system).

These parameters allow to activate or deactivate the control actions, when required. Note that ρ_b monitors the braking efficiency (compared to an ABS system).

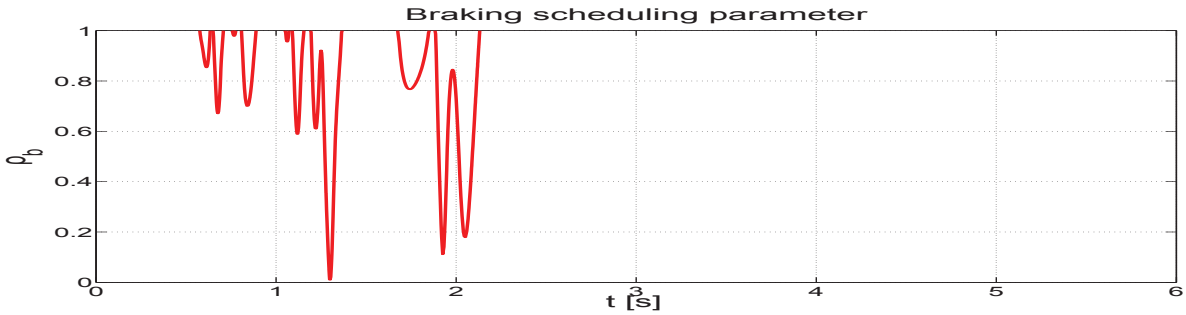

Figure 7.48: Braking monitoring parameter ρ_b

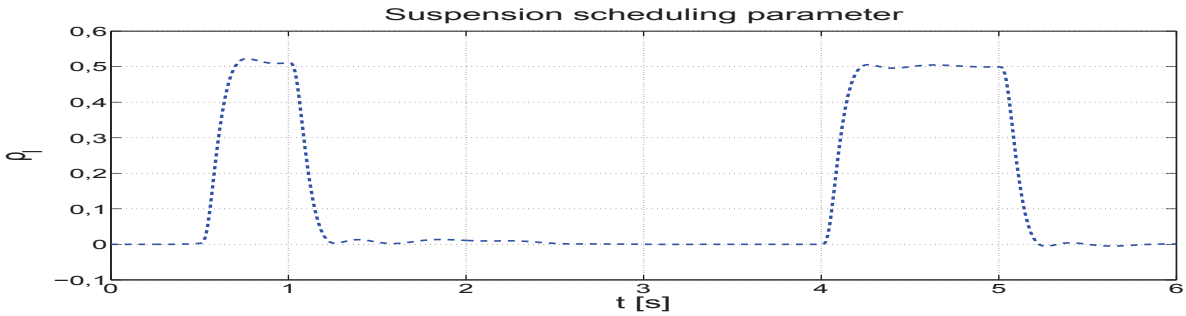

Figure 7.49: Control allocation scheduling parameter ρ_l

The ρ_s scheduling parameter, depends on the value of ρ_b. It also provides the necessary assistance to the driver by giving an additional steering δ^+ and setting the suspension dampers to ”hard” to enhance road handling in critical situations.

Also ρ_l allows to distribute the suspensions efforts depending on load transfer left/right to manage the overload on each corner of the vehicle by generating the adequate efforts.

It can be seen from Fig. 7.50 that the proposed strategy enhances the vehicle lateral stability. The vehicle yaw rate is considerably enhanced by the LPV approach, which improve very well car lateral dynamics.

Remark: For Fig. 7.50, a ”reference vehicle” yaw rate is given to have a better idea on the improvement brought by the proposed LPV strategy.

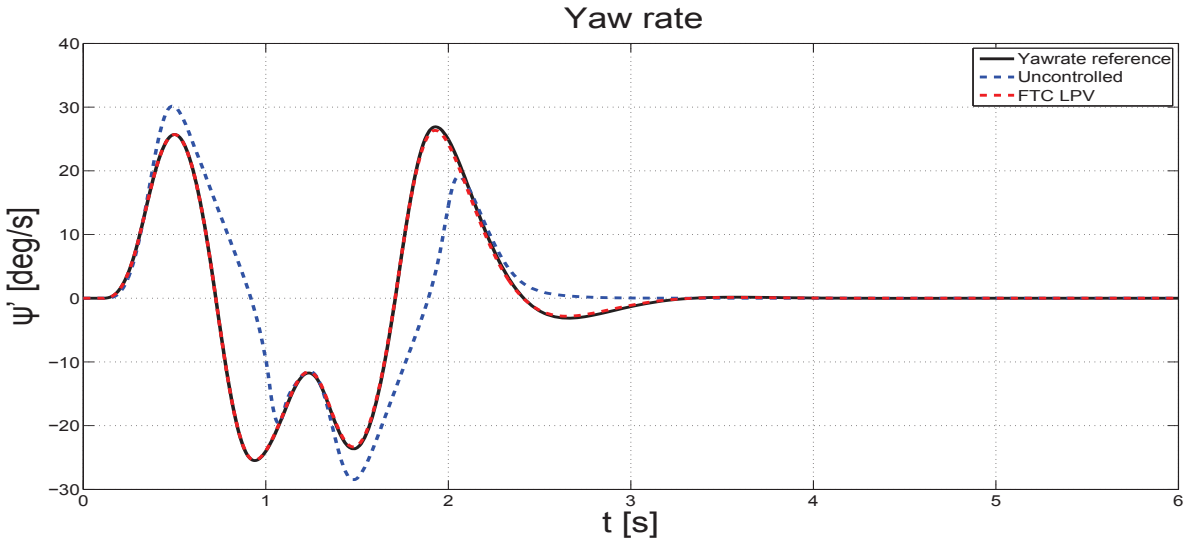

Figure 7.50: Yaw rate

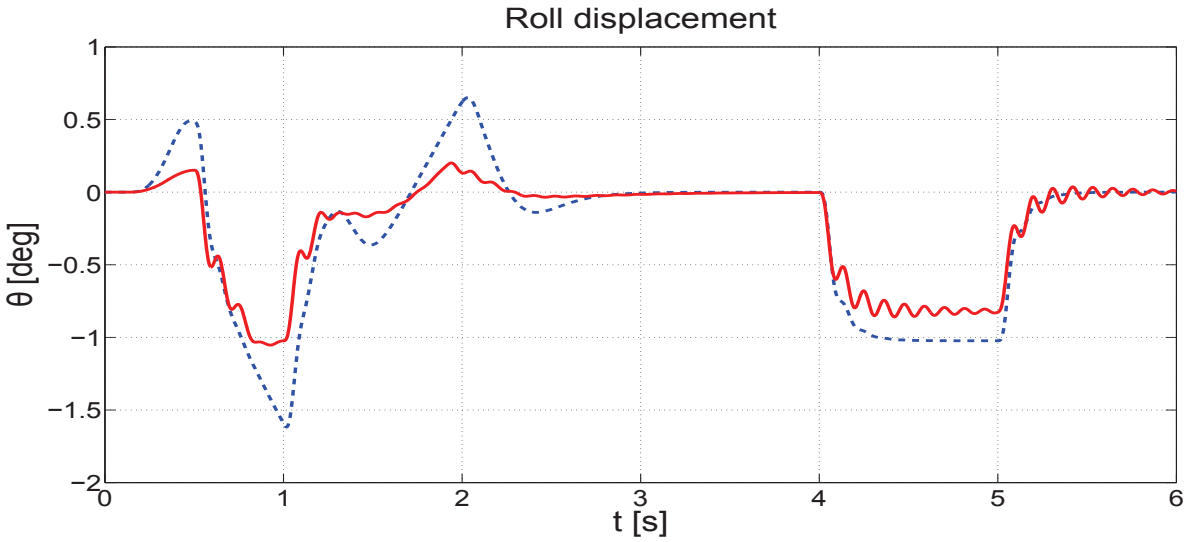

Figure 7.51: Roll motion of the chassis

Fig. 7.51 shows that the LPV design strategy, in addition of enhancing vehicle stability, improves the vertical dynamics. It can be seen that the roll dynamics are considerably attenuated which enhance the vehicle handling when facing critical driving situations.

Fig. 7.52 summarizes the braking/steering actuators actions and their effects on the vehicle stability. Indeed, it can be seen that the rear left braking actuators is faulty and its effort saturates quickly at low value (75 Nm) which simulate the actuator failure and generate a instability risk. Then, the remanning healthy braking actuators provides more effort to compensate the lack of the braking torque of the faulty actuator and also the steering control is activated to help keeping the vehicle stability. It is worth to note that the proposed LPV control design structure avoids the actuators saturation while coordinating hierarchically their work.

The last result in Fig. 7.52 shows the efficiency of the proposed strategy in term of vehicle stabiliza-

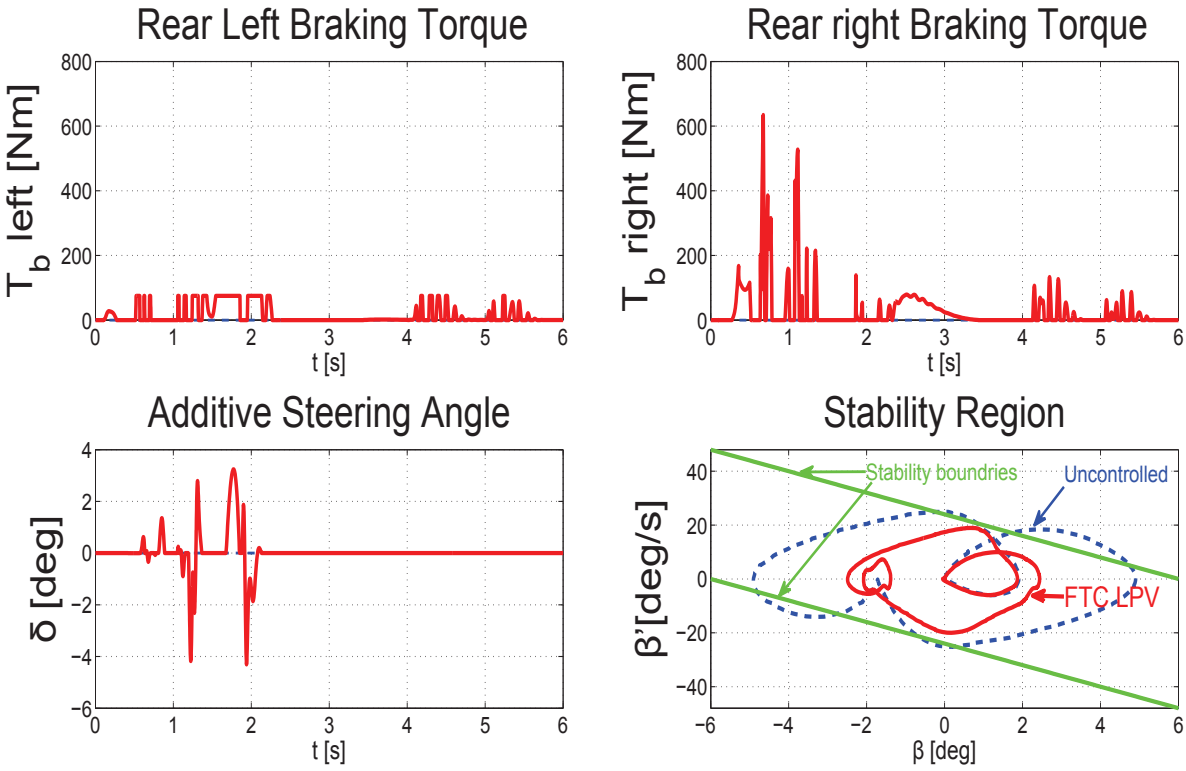

Figure 7.52: additive steering input, braking Actuators torques and the vehicle stability evaluation

tion. It can be clearly seen that the good coordination of the vehicle steering, braking and suspension improves very well the vehicle behaviour and enhance the various car dynamics (vertical, lateral...). The vehicle is kept, by the proposed LPV/$\mathcal{H}_\infty$, from going beyond the limits of the stability region (based on the sideslip stability observation of the vehicle) even when performing a dangerous driving situation.

Fig. 7.53 shows the result of the suspension control allocation strategy with the considered faulty dampers. Indeed, it can be seen that one of the dampers (the front left damper) provides a lower effort and is quickly saturated. The proposed LPV/$\mathcal{H}_\infty$ fault tolerant control strategy allows to manage this actuators failure by reconfiguration the suspension control to compensate the lack of the damping force in of the vehicle corners. This aims at ensuring the vehicle stability and avoiding critical driving situations.

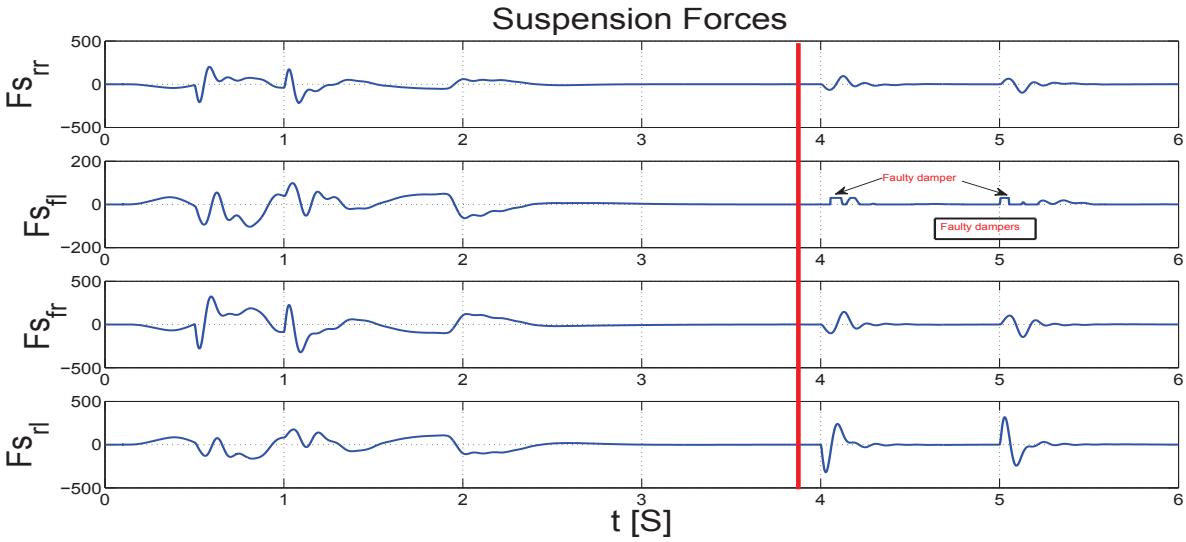

Figure 7.53: Suspension dampers efforts

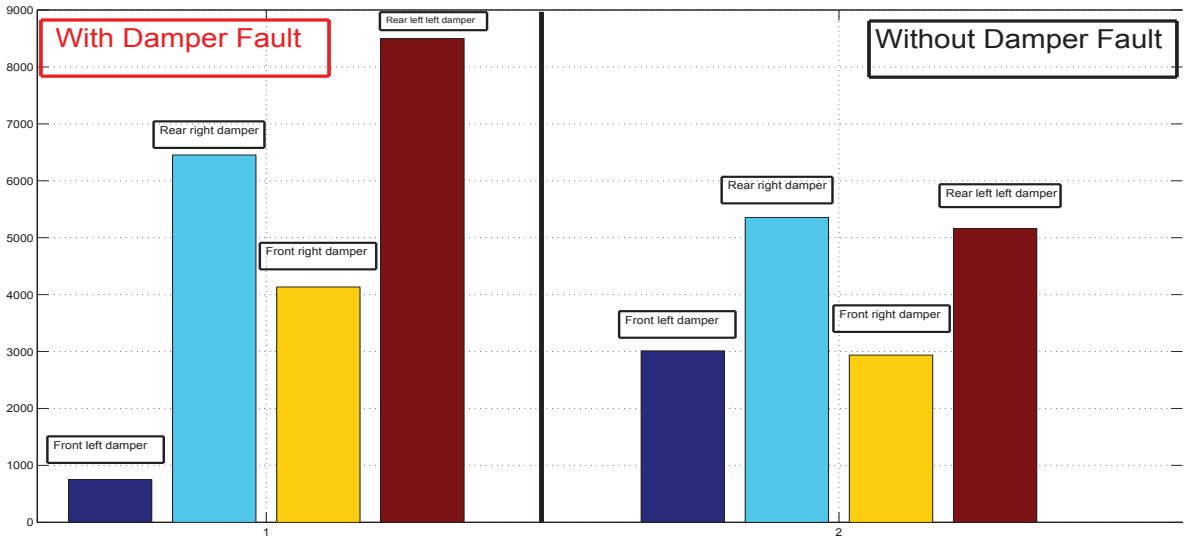

Figure 7.54: RMS value of the suspension dampers: Faulty and Healthy case

Also, Fig. 7.54 shows a comparison between the *RMS*of the suspensions dampers forces in the faulty and healthy case. The proposed LPV/$\mathcal{H}_\infty$ suspension allocation control strategy allows in the healthy case to provide the accurate damping forces on each one of the vehicle four corners. Conversely, in the faulty case as presented on the left figure where a failure on the front left damper occurs, the proposed strategy reconfigures the suspension control by providing more damping forces on the other healthy dampers. This reconfiguration compensates the lack of the damping in the faulty front left corner and ensures the vehicle stability in the critical driving situations.

7.3.3 Conclusion

In this study, the efficiency of the new proposed LPV/$\mathcal{H}_\infty$ control reconfiguration structure to manage different actuators failures has been proved. This have led to a reliable fault tolerant control strategy that allows to prevent the risk of loss of manoeuvrability and safety degradation in critical driving conditions by using one of the important advantage of the LPV/$\mathcal{H}_\infty$ control that coordinates hierarchically the use of different actuators.

7.4 Chapter conclusion

This chapter has presented an interesting LPV/$\mathcal{H}_\infty$ control structure. The efficiency of the proposed control strategy have been proven through two main contributions:

- A LPV/H_∞ suspension control with performance adaptation to roll behavior, embedded in a global vehicle dynamic control strategy using actuators coordination.
- LPV methods for fault-tolerant vehicle dynamic control to manage different actuators failures.

CHAPTER 8

A New Mixed vehicle Global Chassis Control based on LPV/$\mathcal{H}_\infty$ vertical and nonlinear Flatness lateral/longitudinal dynamics control

8.1 Introduction

As explained in chapter. 6, many works have tried to deals with the global chassis control involving several actuators. In (Németh and Gáspár, 2011), a new design method of actuator intervention for trajectory tracking is proposed. In (Chou and d'Andréa Novel, 2005*b*), an interesting nonlinear control law using suspension and braking actuators for commercial cars has been developed. Based on the LPV approaches, an integration of steering and braking controllers is proposed in (Doumiati *et al.*, March 2013*a*), and comments on this integration are given in (Boada *et al.*, March 2013). More recently, in (Gáspár *et al.*, August 2007), (Fergani *et al.*, 2012*a*), (Fergani *et al.*, 2012*b*), an LPV control structure that allows to coordinate several actuators and to improve different vehicle dynamics has been proposed. However, the suspension control depending the road profile coupled with longitudinal/lateral controller remains a challenging problem. Indeed, there are few studies that have already addressed such a problem.

The proposed control law is designed in hierarchical way to improve the overall dynamics of the vehicle. This global control strategy includes two controllers: The first one is the longitudinal/lateral nonlinear Flatness controller. It takes advantage of the flatness property (see (Fliess *et al.*, 1992), (Fliess *et al.*, 1995), (Fliess *et al.*, 1999)) to achieve a global linearization of the nonlinear system and the algebraic estimation techniques for numerical differentiation and filtering of noisy signals (Fliess *et al.*, 2008), (Mboup *et al.*, 2009), (Fliess, 2006*a*). Moreover, based on the adequate choice of the flat outputs, the flatness proof of a 3DoF two wheels nonlinear vehicle model is established. Thereafter, the combined longitudinal and lateral vehicle control is designed. The algebraic estimation techniques are used in order to have an accuracy estimation of the derivatives and filtering of the reference flat outputs. Such control strategy is developed in order to cope with coupled driving maneuvers like obstacle avoidance via steering control and stop-and-go control via braking or driving wheel torque.
The second part of the proposed strategy consists of the $LPV/\mathcal{H}_\infty$ suspension controller. This controller uses the lateral acceleration as a varying parameter to take into account the load transfers which affects directly the suspension systems and then to achieve the desired performance. Indeed, the lateral motion of the vehicle is highly correlated to the vertical one through the load transfers induced by the roll motions. This correlation is highlighted, in this study, and the $LPV/\mathcal{H}_\infty$ framework ensures the collaborative coordination between the vertical and the lateral dynamics performance objectives.

In the first part of this study, a new non linear flatness combined longitudinal and lateral vehicle controller is proposed. In order to enhance the passengers comfort and the vehicle stability and achieve a global chassis vehicle control, the suspension controller is integrated as a second part. The suspension controller uses the presented results in chapter. 7. Such an implementation can easily be achieved through the evaluation of the lateral dynamics. The evolution of the lateral acceleration is strongly related to the vehicle stability which affects the passengers comfort and vehicle safety.

8.2 Problem Statement of the integration of the Flatness and the LPV/H_∞ controllers

Based on the correlation between the vertical and the lateral vehicle dynamics, the coordination of these two controllers is established. The diagram of Fig. 8.1 describes the two advanced controllers and the interaction between them. In fact, the obtained longitudinal and lateral controlled motions with flatness controller are used to deduce the varying parameters that schedules the LPV/H_∞ suspension controller for the vertical dynamics.

The integration of these controllers allows to address a full vehicle dynamics control for the vehicle handling and safety improvement. More precisely, the control of longitudinal and lateral motion has a key role to cope with coupled driving maneuvers such as the obstacle avoidance via steering control, and simultaneously improve the passengers comfort and car roadholding by improving the vertical dynamics regarding the correlation with the lateral ones. In smart collaborative way, the LPV/H_∞ uses the relationship between the lateral and vertical motions to control the suspension systems, therefore, a coordination between the 3 main dynamics of the vehicle is established to achieve the desired performance objectives.

The relationship between the vertical and lateral dynamics of the vehicle is highlighted in this work thanks to the following equation:

$$\theta = \frac{z_{def_{fl}} - z_{def_{fr}} + z_{def_{rl}} - z_{def_{rr}}}{t_f} - \frac{m a_y h}{k_t} \tag{8.1}$$

where θ: is the roll motion of the vehicle, and a_y is the lateral acceleration (more details on the relationship between the vertical and the lateral dynamics are given in the following sections).
One can see clearly that the lateral acceleration affects directly the vertical dynamics of the car through the load transfer that increases considerably the role motion of the vehicle.

Also, an interesting point in this work is to turn the problem of conflicting dynamics performance objectives and their correlation and use it as a solution for the global chassis control.
The proposed strategy is summarized in the following diagram:

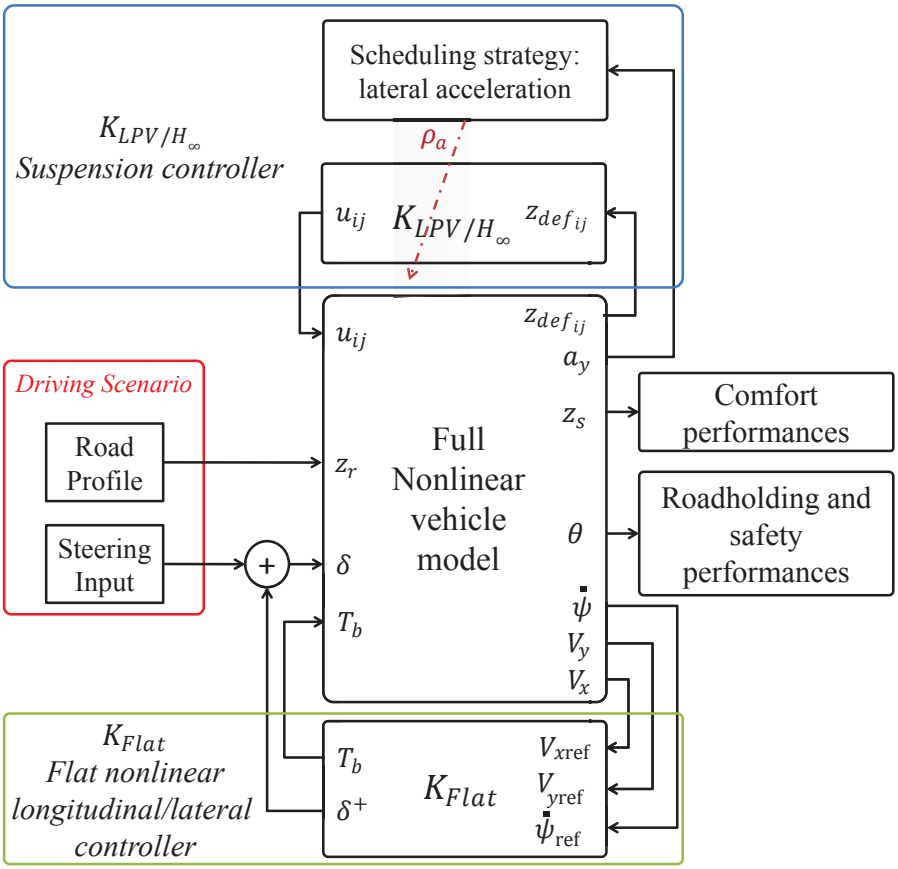

Figure 8.1: Diagram block of the integration strategy

It is based on full non linear model of the vehicle, with two kind of controllers acting simultaneously on the vertical dynamics (For the Linear Varying Parameters control) and the lateral/longitudinal dynamics (the non linear Flatness based control). An integration of these two control laws is achieved trough the existing correlations between the vehicle vertical, lateral and longitudinal dynamics.

8.3 Flatness-based nonlinear control

In this section, the design of the non linear longitudinal/lateral flatness control is described. The controller design structure is summarized in Fig. 8.2.

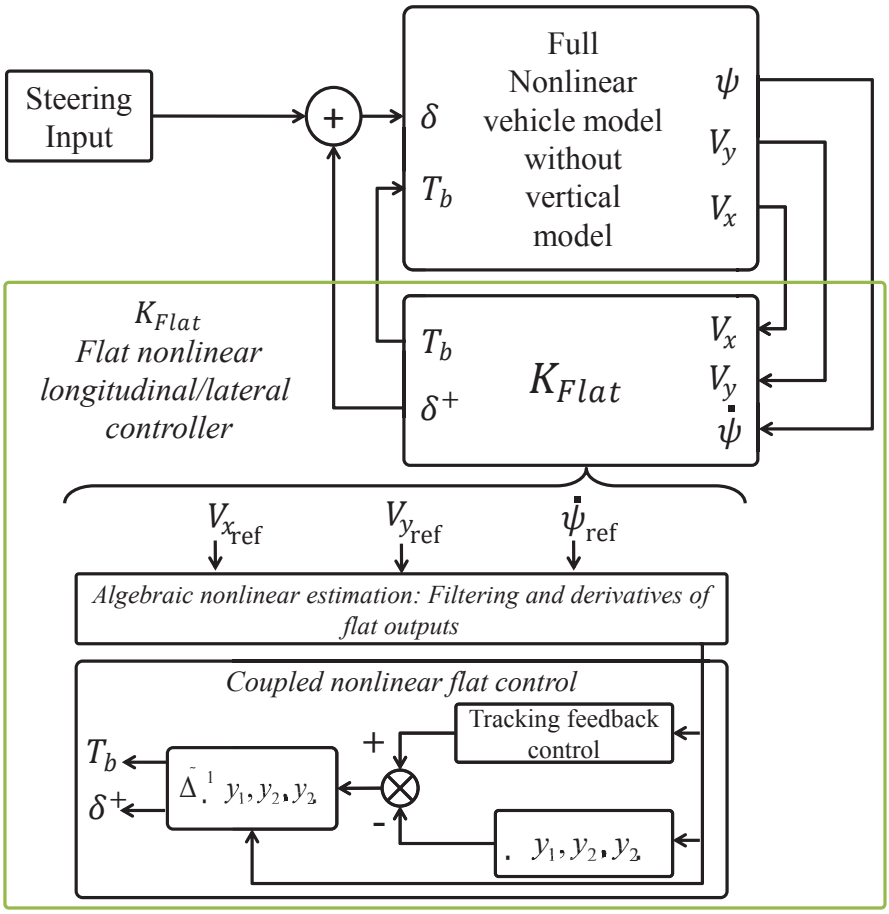

Figure 8.2: Diagram block of the nonlinear flat control

This scheme summarizes the flatness control design structure. The non linear Flatness controller K_{Flat} has as inputs the longitudinal velocity v_x, the lateral velocity v_y it provides the braking torques and the corrective steering angle that stabilize the vehicle in several driving situations.

8.3.1 Nonlinear Vehicle Models for control and simulations

The flatness-based longitudinal/lateral control design is achieved using the three degrees of freedom two wheels nonlinear model (*3DoF-NLTWVM*). The model equations are given as follows:

$$\begin{cases} m_s a_x = m_s(\dot{V}_x - \dot{\psi}V_y) = (F_{x1} + F_{x2}) \\ m_s a_y = m_s(\dot{V}_y + \dot{\psi}V_x) = (F_{y1} + F_{y2}) \\ I_z\ddot{\psi} = M_{z1} + M_{z2} \end{cases} \tag{8.2}$$

The 3DoF single-track nonlinear model (8.2) provides a good approximation of the longitudinal, lateral and yaw dynamics. Then, after some manipulations [1] of the equations in (8.2), the following nonlinear equations governing this model are obtained:

[1] See (Menhour and d' Andréa-Novel, Oct. 2011) for details on these models.

$$\dot{x} = f(x,t) + g(x)u + g_1 u_1 u_2 + g_2 u_2^2 \tag{8.3}$$

where

$$x = \begin{bmatrix} V_x \\ V_y \\ \dot{\psi} \end{bmatrix}, u = \begin{bmatrix} u_1 \\ u_2 \end{bmatrix}, f(x,t) = \begin{bmatrix} \dot{\psi} V_y - \frac{I_r}{m_s R}(\dot{\omega}_r + \dot{\omega}_f) \\ -\dot{\psi} V_x + \frac{1}{m_s}\left(-C_f\left(\frac{V_y + L_f\dot{\psi}}{V_x}\right) - C_r\left(\frac{V_y - L_r\dot{\psi}}{V_x}\right)\right) \\ \frac{1}{I_z}\left(-L_f C_f\left(\frac{V_y + L_f\dot{\psi}}{V_x}\right) + L_r C_r\left(\frac{V_y - L_r\dot{\psi}}{V_x}\right)\right) \end{bmatrix} \text{ and}$$

$$g(x,t) = \begin{bmatrix} \frac{1}{m_s R} & \frac{C_f}{m_s}\left(\frac{V_y + L_f\dot{\psi}}{V_x}\right) \\ 0 & (C_f R - I_r\dot{\omega}_f)/m_s R \\ 0 & (L_f C_f R - L_f I_r\dot{\omega}_f)/I_z R \end{bmatrix}.$$

where the longitudinal motion is controlled via the wheel torque $u_1 = T_\omega = T_m - T_b$, where $T_m = 0$ (no traction is considered here) and T_b the braking torque, and the lateral motion is controlled via the steering angle $u_2 = \delta$. The second order terms $u_1 u_2$ and u_2^2 are neglected because of their small magnitude. More details on the previously used model can be found in (Menhour and d' Andréa-Novel, Oct. 2011), (Menhour *et al.*, 2014).

8.4 Recall on flatness based algebraic theory

The idea of differentially flat systems appeared at the nineties. Flat systems are an important subclass of nonlinear control systems introduced via differential-algebraic methods, defined in a differential geometric framework.
The concept of differential algebra is used to define the flat systems, as introduced in (Fliess *et al.*, 1995) and later using Lie-Bäcklund transformations. Indeed, the system is said to be flat if one can find a set of variables, called the flat outputs, such that the system is (non-differentially) algebraic over the differential field generated by the set of flat outputs. It means that a system is flat if we can find a set of outputs, such that all states and inputs can be determined from these outputs without integration.
Differentially Flat systems are useful in situations where explicit trajectory generation is required. Since the behavior of Flat system is determined by the Flat outputs (as previously defined), we can plan trajectories in output space, and then map them to appropriate inputs. On the other hand, while this technique is quite powerful, the application differential algebraic results to systems with strong geometric structure while at the same time exploiting that structure remains a difficult issue without simplifications.
In the following, some theoretical recalls on the differential flatness control and estimation to better understand the collaborative work achieved with our colleagues from "Mines-Paritech".

8.4.1 Basic definitions

Definition 8.4.1 (*Flat system*)

For continuous-time systems, differential flatness is defined as follows. Let us Consider the system:

$$\dot{x} = f(x, u) \tag{8.4}$$

where $x = (x, \cdots, x_n) \in \mathbb{R}^n$ *and* $u = (u, \cdots, u_m) \in \mathbb{R}^m$. *It is said to be* differentially flat *(see (Fliess* et al., *1992), (Fliess* et al., *1995), (Fliess* et al., *1999) and (Lévine, 2009), (Sira-Ramírez and Agrawal, 1993)) if, and only if:*

- *there exists a vector-valued function* h *such that*

$$y = h(x, u, \dot{u}, \cdots, u^{(r)}) \tag{8.5}$$

  where $y = (y, \cdots, y_m) \in \mathbb{R}^m$, $r \in \mathbb{N}$;

- *the components of* $x = (x, \cdots, x_n)$ *and* $u = (u, \cdots, u_m)$ *may be expressed as*

$$x = A(y, \dot{y}, \cdots, y^{(r_x)}), \quad r_x \in \mathbb{N} \tag{8.6}$$

$$u = B(y, \dot{y}, \cdots, y^{(r_u)}), \quad r_u \in \mathbb{N} \tag{8.7}$$

Remember that y *in Eq. (8.12) is called a* flat output.

Remark: It is worth noticing that given a flat system, the number of components of a flat output is equal to the number of independent inputs. Also, let us recall some properties of the flat systems, that may be useful in the following work (proofs can be found easily in (Lévine, 2009)):

- A flat system is locally reachable.
- A linear system is flat if and only if it is controllable.
- Every flat system is endogenous dynamic feedback linearizable. Conversely, every endogenous dynamic feedback linearizable system is Flat.

In this study, the flatness property is used for both control and estimation purposes. Indeed, in the following thesis works, the algebraic estimation is used in this thesis study for the road profile estimation.

8.4.2 A short summary on the algebraic observer

The estimation method uses the algebraic framework devoted for the design of algebraic observers with unknown inputs (Barbot *et al.*, 2007), (Daafouz *et al.*, 2006), (Fliess and Join, 2008), (Ibrir, 2003), (Guerra *et al.*, 2007). The estimation approach uses also the algebraic identification methods

for the numerical differentiation of noisy signals (Fliess and Join, 2008), (Mboup *et al.*, 2009). The estimation with unknown input is based on the following properties:

Definition 8.4.2

(Barbot et al., *2007), (Daafouz* et al., *2006)*
Consider the following nonlinear model:

$$\begin{array}{l} \dot{x}(t) = f(x(t), u(t)) \\ y(t) = h(x(t)) \end{array} \tag{8.8}$$

where $x(t)$ is the state vector, $u(t)$ is the input, $y(t)$ is a smooth output and f is continuously differentiable and $f(0;0) = 0$. For the following, we assume that the input $u(t)$ and the output $y(t)$ are continuously differentiable for all $t \geq 0$.

The model (8.8) is said to be algebraically observable if there exist the integers $n_1 > 0$ and $n_2 > 0$ such that

$$x(t) = \Gamma\left(y,\, \dot{y}, \cdots, y^{(n_1)},\, u,\, \dot{u},\, \cdots, u^{(n_2)}\right)(t) \tag{8.9}$$

where $\Gamma(t)$ is a differentiable real-valued function of the outputs $y(t)$, the inputs $u(t)$, and their derivatives.

Definition 8.4.3

(Fliess and Join, 2008), (Ibrir, 2003)
An unknown input (or a fault) f_a is said to be diagnosable if it is possible to estimate the unknown input f_a from the measured outputs of the system. It means in other words that the unknown input f_a is diagnosable if it is algebraically observable, i.e, in general

$$P(f, u, \dot{u}, \cdots, y, \dot{y}, \cdots) = 0 \tag{8.10}$$

then, the reconstructor (8.10) can may be used to estimate the unknown input (or a fault) f.

Proposition 8.4.1

the algebraic observability of any nonlinear system with unknown inputs is equivalent to express the dynamical state and the unknown inputs as functions of the inputs, the measured outputs and their finite time derivatives.

Proposition 8.4.2

A system is said observable with unknown inputs if, any state variable or an input variable, can be formulated as a function of the output and their finite time derivatives. This function can be called as an input-free estimator. It means in other words that an input-output system is observable with unknown input if, and only if, its zero dynamics is trivial. In addition, if the system is square, then the system is called flat [2] *system with its flat output.*

Property 8.4.1

Consider the system

$$\dot{x} = f(x, u) \tag{8.11}$$

where $x = (x, \cdots, x_n) \in \mathbb{R}^n$ *and* $u = (u, \cdots, u_m) \in \mathbb{R}^m$. *It is said to be* differentially flat *(see (Fliess* et al., *1992), (Fliess* et al., *1995), (Fliess* et al., *1999) and (Lévine, 2009), (Sira-Ramírez and Agrawal, 1993)) if, and only if:*

- *there exists a vector-valued function* h *such that*

$$y = h(x, u, \dot{u}, \cdots, u^{(r)}) \tag{8.12}$$

  where $y = (y, \cdots, y_m) \in \mathbb{R}^m$, $r \in \mathbb{N}$;

- *the components of* $x = (x, \cdots, x_n)$ *and* $u = (u, \cdots, u_m)$ *may be expressed as*

$$x = A(y, \dot{y}, \cdots, y^{(r_x)}), \quad r_x \in \mathbb{N} \tag{8.13}$$

$$u = B(y, \dot{y}, \cdots, y^{(r_u)}), \quad r_u \in \mathbb{N} \tag{8.14}$$

Remember that y *in Eq. (8.12) is called a* flat output.

The above properties are equivalent to previously presented definitions .

8.4.3 A short definition of algebraic denoising and numerical differentiation

The numerical estimators [3] (8.28) are deduced from operational calculation and algebraic manipulations. For this, consider the following real-valued polynomial time function $x_N(t) \in \mathbb{R}[t]$ of degree N

$$x_N(t) = \sum_{\nu=0}^{N} x^{(\nu)}(0) \frac{t^\nu}{\nu!}, \ t \geq 0. \tag{8.15}$$

In the operational domain [4] (see e.g. (Yosida, 1984)), (8.15) becomes

$$X_N(s) = \sum_{\nu=0}^{N} \frac{x^{(\nu)}(0)}{s^{\nu+1}}. \tag{8.16}$$

Multiplying the left-side and the right-side of equation (8.16) on the left by $\frac{d^\alpha}{ds^\alpha} s^{N+1}$, $\alpha = 0, 1, \cdots, N$. The quantities $x^{(\nu)}(0)$, $\nu = 0, 1, \ldots, N$, which are linearly identifiable satisfy the following triangular system of linear equations:

$$\frac{d^\alpha s^{N+1} X_N}{ds^\alpha} = \frac{d^\alpha}{ds^\alpha} \left(\sum_{\nu=0}^{N} x^{(\nu)}(0) s^{N-\nu} \right), \ 0 \leq \alpha \leq N-1. \tag{8.17}$$

[3] For the details related to the developments used in this work, we refer the reader to (Fliess and Join, 2008), (Mboup *et al.*, 2009)

[4] $\frac{d}{ds}$ corresponds in time domain to the multiplication both sides by $-t$.

The time derivatives in (8.17) ($s^{\mu}\frac{d^{\iota}X_N}{ds^{\iota}}$, $\mu = 1, \ldots, N$, $0 \leq \iota \leq N$), are removed by the multiplying both sides of equation (8.17) by $s^{-\bar{N}}$, $\bar{N} > N$. Now, consider an analytic time function, defined by the power series $x(t) = \sum_{\nu=0}^{\infty} x^{(\nu)}(0)\frac{t^{\nu}}{\nu!}$, which is assumed to be convergent around $t = 0$. Approximate $x(t)$ by the truncated Taylor expansion $x_N(t) = \sum_{\nu=0}^{N} x^{(\nu)}(0)\frac{t^{\nu}}{\nu!}$ of order N. Good estimates of the derivatives are obtained by the same calculations as above.

Based on this development and after some simple mathematical manipulations, the following formulae may be obtained and used to estimate the 1^{st} order derivative of y:

$$\hat{\dot{y}}(t) = -\frac{3!}{h^3}\int_{t-h}^{t}(2h(t-\tau)-h)y(\tau)d\tau \tag{8.18}$$

Note that the sliding time window $[t-h,\ t]$ may be quite short.

Remark: The estimation methods (8.28) is not of asymptotic type and do not require any statistical knowledge of the corrupting noises (see (Fliess, 2006*a*) for details).

8.5 Flatness-based longitudinal/lateral control

In order to reduce the complexity of nonlinear model in Eq. (8.3), nonlinear terms such as u_1u_2 and u_2^2 are neglected.[5] Despite these simplifications some coupled behaviors are kept as shown by the functions $f(x,t)$ and $g(x,t)$. Eq. (8.3) becomes

$$\dot{x} = f(x,t) + g(x,t)u \tag{8.19}$$

In this study, the flatness property is used to design the controller. The differential flatness approach of nonlinear systems in a differential algebraic context was introduced in (Fliess *et al.*, 1992), (Fliess *et al.*, 1995), (Fliess *et al.*, 1999). The efficiency and the performance evaluation of this approach are demonstrated through a number of applications. Indeed, the necessary information to run the dynamic behavior of a real system are easily expressed by the appropriate flat outputs. Numerous engineering real applications using flat systems are already handled in the literature (see (Fliess *et al.*, 1995), (Fliess *et al.*, 1999), (Nieuwstadt and Murray, 1998), (Menhour *et al.*, 2011)). Such an approach is also used to manage the coupled nonlinear vehicle control (Fuchshumer *et al.*, 2005), (Menhour *et al.*, 2011), (Menhour *et al.*, 2012), (Menhour *et al.*, 2014) and underwater vehicles (Rathinam, 1996) (More application examples of the flatness approach can be found in (Lévine, 2009), (Sira-Ramírez and Agrawal, 1993)).
It is worth to recall that for this controller design, the braking and the wheels acceleration are controlled.
Here, the flatness approach is used to deal with a combined control of longitudinal and lateral vehicle motions. The following design problem and flatness property are used to establish the flatness of a 3DoF nonlinear vehicle model. Subsequently, the main objective of this section is presented.

[5] The results of Section 8.7 fully justify those approximations.

Problem 1

For the flatness proof of the model (8.19), we consider the following outputs:

$$\left\{ \begin{array}{l} y_1 = V_x \\ y_2 = L_f m_s V_y - I_z \dot{\psi} \end{array} \right. \tag{8.20}$$

where the first flat output y_1 is the longitudinal speed and the second one y_2 is the angular momentum of a point on the axis between the centers of the front and rear axles. The design problem addressed here concerns the flatness property of (8.19) with the outputs (8.20).

The flatness control is established thanks to the following flatness property (Fliess *et al.*, 1995), (Fliess *et al.*, 1999), (Lévine, 2009), (Sira-Ramírez and Agrawal, 1993).

The objective is to show the flatness of model (8.19) with outputs (8.20) according to the flatness property 8.12. Then, after some algebraic manipulations we obtain:

$$\left\{ \begin{array}{rcl} x & = & \left[\begin{array}{c} V_x \\ V_y \\ \dot{\psi} \end{array} \right] \\ & = & A(y_1, y_2, \dot{y}_2) \\ & = & \left[\begin{array}{c} y_1 \\ \frac{y_2}{L_1 m_s} - \left(\frac{I_z}{L_1 m_s} \right) \left(\frac{L_1 m_s y_1 \dot{y}_2 + C_r (L_1 + L_2) y_2}{C_r (L_1 + L_2)(I_z - L_2 L_1 m_s) + (L_1 m_s y_1)^2} \right) \\ - \left(\frac{L_1 m_s y_1 \dot{y}_2 + C_r (L_1 + L_2) y_2}{C_r (L_1 + L_2)(I_z - L_2 L_1 m_s) + (L_1 m_s y_1)^2} \right) \end{array} \right] \end{array} \right. \tag{8.21}$$

and

$$\left[\begin{array}{c} \dot{y}_1 \\ \ddot{y}_2 \end{array} \right] = \Delta(y_1, y_2, \dot{y}_2) \left(\begin{array}{c} u_1 \\ u_2 \end{array} \right) + \Phi(y_1, y_2, \dot{y}_2) \tag{8.22}$$

which is equivalent to

$$\left[\begin{array}{c} u_1 \\ u_2 \end{array} \right] = \Delta^{-1}(y_1, y_2, \dot{y}_2) \left(\left[\begin{array}{c} \dot{y}_1 \\ \ddot{y}_2 \end{array} \right] - \Phi(y_1, y_2, \dot{y}_2) \right) \tag{8.23}$$

where

$$\left\{ \begin{array}{rcl} \Delta_{11}(y_1, y_2, \dot{y}_2) & = & \frac{1}{m_s R} \\ \Delta_{12}(y_1, y_2, \dot{y}_2) & = & \frac{C_f}{m_s} \left(\frac{V_y + L_1 \dot{\psi}}{y_1} \right) \\ \Delta_{22}(y_1, y_2, \dot{y}_2) & = & \left(-L_1 m_s y_1 + \frac{L_2 C_r (L_1 + L_2)}{y_1} \right) \frac{(L_1 C_f R - L_1 I_\omega \dot{\omega}_f)}{I_z R} \\ & & + \frac{(C_r (L_1 + L_2)(V_y - L_2 \dot{\psi}) - L_1 m_s \dot{\psi} y_1^2)}{y_1^2} \frac{C_f (V_y + L_1 \dot{\psi})}{m_s y_1} - \frac{C_r (L_1 + L_2)}{y_1} \frac{R C_f - I_\omega \dot{\omega}_f}{m_s R} \\ \Delta_{21}(y_1, y_2, \dot{y}_2) & = & \frac{(C_r (L_1 + L_2)(V_y - L_2 \dot{\psi}) - L_1 m_s \dot{\psi} y_1^2)}{m_s R y_1^2} \end{array} \right.$$

and

$$\left\{ \begin{array}{rcl} \Phi_1(y_1, y_2, \dot{y}_2) & = & \dot{\psi} V_y - \frac{I_\omega}{m_s R} (\dot{\omega}_r + \dot{\omega}_f) \\ \Phi_2(y_1, y_2, \dot{y}_2) & = & -L_1 m_s y_1 f_3(x, t) - \frac{C_r (L_1 + L_2)}{y_1} f_2(x, t) \\ & & + \frac{C_r (L_1 + L_2)(V_y - L_2 \dot{\psi}) - L_1 m_s \dot{\psi} y_1^2}{y_1^2} f_1(x, t) + \frac{L_2 C_r (L_1 + L_2)}{y_1} f_3(x, t) \end{array} \right.$$

The flatness property holds therefore if the matrix $\Delta(y_1, y_2, \dot{y}_2)$ is invertible. It reads

$$\left\{ \begin{array}{rcl} \det(\Delta(y_1, y_2, \dot{y}_2)) & = & \Delta_{11}\Delta_{22} - \Delta_{21}\Delta_{12} \\ & = & \frac{\left(I_\omega \dot{\omega}_f - C_f R\right)\left(L_1^2 y_1^2 m_s^2 - Cr(L_1+L_2)L_2 L_1 m_s + C_r I_z L\right)}{I_z R^2 y_1 m_s^2} \neq 0 \end{array} \right. \tag{8.24}$$

This determinant, which depends only on the longitudinal speed $y_1 = V_x$, is indeed nonzero:

- The wheel rotation acceleration is less than RC_f/I_ω: RC_f/I_ω is around 10^4, then $I_\omega \dot{\omega}_f - C_f R \neq 0$.

- Notice that $I_z > L_1 m_s$, then: $C_r(L_2 + L_1)(I_z - L_1 m_s) + L_1^2 m_s^2 y_1^2 \neq 0$.

Thus

$$\left\{ \begin{array}{rcl} u & = & \left[\begin{array}{c} T_\omega \\ \delta \end{array} \right] \\ & = & B(y_1, \dot{y}_1, y_2, \dot{y}_2, \ddot{y}_2) \\ & = & \Delta^{-1}(y_1, y_2, \dot{y}_2) \left(\left[\begin{array}{c} \dot{y}_1 \\ \ddot{y}_2 \end{array} \right] - \Phi(y_1, y_2, \dot{y}_2) \right) \end{array} \right. \tag{8.25}$$

with $r_x = 1$ and $r_u = 2$. Finally, the system (8.3) is flat system with outputs (8.20), then, the outputs (8.20) are called flat outputs.

Then, in order to track the desired outputs y_1^{ref} and y_2^{ref}, we set the following output feedback

$$\left[\begin{array}{c} \dot{y}_1 \\ \ddot{y}_2 \end{array} \right] = \left[\begin{array}{c} \dot{y}_1^{ref} + K_1^1 e_{y_1} + K_1^2 \int e_{y_1} dt \\ \ddot{y}_2^{ref} + K_2^1 e_{y_2} + K_2^2 \int e_{y_2} dt + K_2^3 \dot{e}_{y_2} \end{array} \right] \tag{8.26}$$

where, $e_{y_1} = y_1^{ref} - y_1 = V_x^{ref} - V_x$ and $e_{y_2} = y_2^{ref} - y_2$. The choice of the gain parameters K_1^1, K_1^2, K_2^1, K_2^2 and K_2^3 is then straightforward.

8.5.1 Algebraic nonlinear estimation

It should be pointed out that this control law contains derivatives of reference signals which are estimated from measurements such as V_x^{ref}, V_y^{ref}, $\dot{\psi}^{ref}$ and the derivatives of the measured front and rear rotational speed wheels ω_f and ω_r. In order to minimize the effect of the noise on these derivatives, the numerical differentiation based on an algebraic nonlinear estimation [6] is proposed.

This estimation is performed using the recent advances in (Fliess *et al.*, 2008), (Mboup *et al.*, 2009), which yield efficient real-time filters [7]. The following formulae (see, e.g., (Collardo *et al.*, 2009)) may be used:

[6] See (Menhour *et al.*, 2011), (Villagra *et al.*, 2009), (Villagra *et al.*, 2011) for previous successful applications to intelligent transportation systems.

[7] The above estimation methods are not of asymptotic type and do not require any statistical knowledge of the corrupting noises (see (Fliess, 2006*a*) for details).

- Denoising:

$$\hat{y}(t) = \frac{2!}{T^2}\int_{t-T}^{t}(2T-3\tau)y(\tau)d\tau \tag{8.27}$$

- The numerical differentiation of a noisy signal:

$$\hat{\dot{y}}(t) = -\frac{3!}{T^3}\int_{t-T}^{t}(T-2\tau)y(\tau)d\tau \tag{8.28}$$

Note that the sliding time window $[t-T,\ t]$ may be quite short.

In this study, the algebraic nonlinear estimation method is applied to perform derivatives and filtering of some measured signals. The equations (8.29) and (8.30) illustrate the derivatives and filtering of longitudinal speed, lateral speed, yaw rate and wheels rotation speeds. The results of this application are used as reference signals in the different parts of the control strategy in (8.33).

- The estimated derivatives $\hat{\dot{V}}_x^{ref}$, $\hat{\dot{V}}_y^{ref}$, $\hat{\ddot{\psi}}^{ref}$, $\hat{\dot{\omega}}_f$ and $\hat{\dot{\omega}}_r$ are performed as follows:

$$\begin{bmatrix} \hat{\dot{V}}_x^{ref} \\ \hat{\dot{V}}_y^{ref} \\ \hat{\ddot{\psi}}^{ref} \\ \hat{\dot{\omega}}_f \\ \hat{\dot{\omega}}_r \end{bmatrix} = -\frac{3!}{T^3}\int_{t-T}^{t}(2T(t-\tau)-T)\begin{bmatrix} V_x^{ref} \\ V_y^{ref} \\ \dot{\psi}^{ref} \\ \omega_f \\ \omega_r \end{bmatrix} d\tau \tag{8.29}$$

- The filtering $\hat{V}_x^{ref}$, $\hat{V}_y^{ref}$ and $\hat{\dot{\psi}}^{ref}$ are performed as follows:

$$\begin{bmatrix} \hat{V}_x^{ref} \\ \hat{V}_y^{ref} \\ \hat{\dot{\psi}}^{ref} \end{bmatrix} = \frac{2!}{T^2}\int_{t-T}^{t}(3(t-\tau)-T)y(\tau)\begin{bmatrix} V_x^{ref} \\ V_y^{ref} \\ \dot{\psi}^{ref} \end{bmatrix} d\tau \tag{8.30}$$

Then, the flat outputs references are computed using equations (8.29) and (8.30) as follows:

$$\begin{cases} \hat{y}_1^{ref} &= \hat{V}_x^{ref} \text{ and } \hat{\dot{y}}_1^{ref} = \hat{\dot{V}}_x^{ref} \\ \hat{y}_2^{ref} &= L_1 m_s \hat{V}_y^{ref} - I_z \hat{\dot{\psi}}^{ref} \\ \hat{\dot{y}}_2^{ref} &= L_1 m_s \hat{\dot{V}}_y^{ref} - I_z \hat{\ddot{\psi}}^{ref} \\ \hat{\ddot{y}}_2^{ref} &= L_1 m_s \hat{\ddot{V}}_y^{ref} - I_z \hat{\dddot{\psi}}^{ref} \end{cases} \tag{8.31}$$

The tracking errors are then:

$$\begin{cases} \hat{e}_{y_1} &= \hat{y}_1^{ref} - y_1 \\ \hat{e}_{y_2} &= \hat{y}_2^{ref} - y_2 \\ \hat{\dot{e}}_{y_1} &= \hat{\dot{y}}_1^{ref} - \dot{y}_1 \\ \hat{\dot{e}}_{y_2} &= \hat{\dot{y}}_2^{ref} - \dot{y}_2 \end{cases} \tag{8.32}$$

Finally, the equation of the coupled nonlinear control obtained from equations (8.25), (8.26) and (8.31) is as follows:

$$\begin{aligned} u &= \begin{bmatrix} T_\omega \\ \delta \end{bmatrix} \\ &= \Delta^{-1}(y_1, y_2, \dot{y}_2)\left(-\Phi(y_1, y_2, \dot{y}_2) + \begin{bmatrix} \dot{\hat{y}}_1^{ref} + K_1^1 \hat{e}_{y_1} + K_1^2 \int \hat{e}_{y_1} dt \\ \dot{\hat{y}}_2^{ref} + K_2^1 \hat{e}_{y_2} + K_2^2 \int \hat{e}_{y_2} dt + K_2^3 \hat{\dot{e}}_{y_2} \end{bmatrix}\right) \end{aligned} \tag{8.33}$$

8.6 $LPV/\mathcal{H}_\infty$ based suspension control

The $LPV/\mathcal{H}_\infty$ suspension control shown on Fig. 8.3 is designed using a 7DoF vehicle model (8.34). It includes several vertical dynamics like:

- chassis acceleration $\ddot{z}_s$,
- four wheels accelerations $\ddot{z}_{us_{ij}}$,
- roll bounce acceleration $\ddot{\theta}$,
- pitch acceleration $\ddot{\phi}$.

The equations describing the vertical 7DOF model are giving as follows:

$$\begin{cases} \ddot{z}_s &= -\left(F_{sz_f} + F_{sz_r} + F_{dz}\right)/m_s \\ \ddot{z}_{us_{ij}} &= \left(F_{sz_{ij}} - F_{tz_{ij}}\right)/m_{us_{ij}} \\ \ddot{\theta} &= \left(\left(F_{sz_{rl}} - F_{sz_{rr}}\right) t_r + \left(F_{sz_{fl}} - F_{sz_{fr}}\right) t_f + m_s h \dot{V}_y\right)/I_x \\ \ddot{\phi} &= \left(F_{sz_f} l_f - F_{sz_r} l_r - m_s h \dot{V}_x\right)/I_y \end{cases} \tag{8.34}$$

Let us recall for the control design, linear models are considered for the stiffness k_{ij} and damping c_{ij} in the suspension force computation see chapter. 3.

8.6.1 About the scheduling parameter

It is now presented how the integration of both controllers for the longitudinal/lateral and vertical dynamics is provided. Such a task is achieved thanks to the scheduling parameter ρ_a dedicated to the $LPV/\mathcal{H}_\infty$ suspension control design as in Fig. 8.3. Indeed, the lateral and the vertical dynamics of the vehicle are correlated through the lateral and vertical tire forces as, (see (Brown *et al.*, December 2004) for more details):

$$F_{iy}(\beta_i) = Sign(\beta_i) F_{iz} \mu(\beta_i) \tag{8.35}$$

where i: is the index for front and rear wheels, F_{iy}: is the lateral force, β_i : is the sideslip, F_{iz}: is the vertical force and $\mu(\beta_i)$: is the road friction.

Furthermore, this relationship can be observed also in the load transfer and roll dynamic that depend on the lateral acceleration a_y (notice that $Fy = m_s a_y K$, where K: is a constant coefficient) as follows, see (Milliken and Milliken, 1995):

$$\begin{cases} \Delta Fz &= \left(F_{z_{fl}} + F_{z_{rl}} - F_{z_{fr}} - F_{z_{rr}}\right) \\ &= \left(m_{s_{fl}} + m_{s_{rl}} - m_{fr} - m_{s_{rr}}\right) 2S_1 g\theta + 2S_2 a_y m_s / l \end{cases} \tag{8.36}$$

where $S_1 = \frac{k_f}{t_f} + \frac{k_r}{t_r}$, $S2 = \frac{l_f h}{t_f} + \frac{l_r h}{t_r}$. It is clear that the load transfer generated by the vehicle bounce are largely influenced by the dynamics of the lateral acceleration, since the roll motion is also directly linked to a_y as follows (see (Brown *et al.*, December 2004)):

$$\theta = \frac{z_{def_{fl}} - z_{def_{fr}} + z_{def_{rl}} - z_{def_{rr}}}{t_f} - \frac{m_s a_y h}{k_t} \tag{8.37}$$

where $z_{def_{ij}}$: is the suspension deflections (i: front or rear, j: left or right), k_t : is the tire stiffness. Based on the lateral acceleration, the scheduling parameter is proposed as:

$$\rho_a = \left| \frac{a_y}{a_{y_{max}}} \right| \tag{8.38}$$

and will be used for performance adaptation.

8.6.2 LPV/H_∞ suspension controller design

The suspension control design with the performance adaptation (see (Savaresi *et al.*, 2010*a*)) presented in the framework of the $\mathcal{H}_\infty$ control approach including the parameter varying weighting functions:

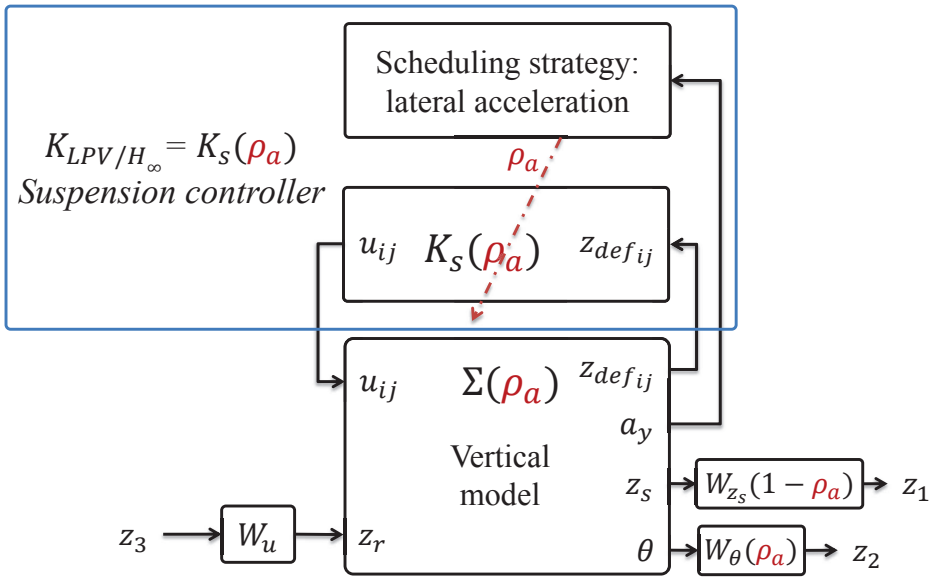

Figure 8.3: Diagram block of the LPV/H_∞ suspension control

Indeed, according to the control scheme proposed in Fig. 8.3, are chosen:

- $W_{z_s} = (1-\rho_a)\frac{s^2+2\xi_{11}\Omega_{11}s+\Omega_{11}^2}{s^2+2\xi_{12}\Omega_{12}s+\Omega_{12}^2}$ is selected to reduce the bounce amplification of the suspended mass motion (z_s) between $[0,\ 12]Hz$.

- $W_\theta = (\rho_a)\frac{s^2+2\xi_{21}\Omega_{21}s+\Omega_{21}^2}{s^2+2\xi_{22}\Omega_{22}s+\Omega_{22}^2}$ attenuates the roll bounce amplification in low frequencies.
- $W_u = 3.10^{-2}$ shapes the control signal.

Remark: It should be noticed that the parameters of these weighting functions are obtained using genetic algorithm optimization as in (Do *et al.*, 2012*a*).

According to Fig. 8.3, the following parameter dependent generalized system ($\Sigma(\rho_a)$) is obtained:

$$\Sigma(\rho_a) \;:\; \left\{ \begin{array}{rcl} \dot{\xi} & = & A(\rho_a)\xi + B_1(\rho_a)\tilde{w} + B_2 u \\ \tilde{z} & = & C_1(\rho_a)\xi + D_{11}\tilde{w} + D_{12}u \\ y & = & C_2\xi + D_{21}\tilde{w} + D_{22}u \end{array} \right. \tag{8.39}$$

where $\xi = [\mathcal{X}_{vert}\ \ \mathcal{X}_w]^T$, $\tilde{z} = [z_1\ \ z_2\ \ z_3]^T$, $\tilde{w} = [z_{r_{ij}}\ \ F_{dx,y,z}\ \ m_{dx,y}]^T$, $y = z_{def_{ij}}$, $u = u_{ij}^{H\infty}$ and $\mathcal{X}_w$ are the vertical weighting functions states.

Moreover, in the dangerous driving situations, the vehicle stability is weak and the lateral acceleration increases. According to this observation and in order to improve the handling of the vehicle, the parameter ρ_a is introduced to achieve the performance adaptation as follows:

- $\rho_a \longrightarrow 1$, the roll motion caused by high lateral accelerations is penalized to reduce the load transfer bounce and then enhance the roadholding, so the stability and safety of the vehicle.
- In normal driving situations, the lateral acceleration is low, consequently, the parameter ρ_a tends to 0. In this case, the LPV/H_∞ suspension control focuses on improving passengers comfort by reducing the chassis displacement and accelerations.

The proposed $LPV/\mathcal{H}_\infty$ robust controller is synthesized using the LMI framework for polytopic systems. The varying parameter ρ_a is considered bounded: $\rho_a \in [0,\ 1]$. Indeed, the LPV system (Eq. 8.39) includes a single scheduling parameter and can be described as a polytopic system, i.e, a convex combination of the systems defined at each vertex of a polytope defined by the bounds of the varying parameter. The synthesis of the two sub-system controllers is made in the framework of the H_∞ control of polytopic suspensions) as follow:s

Let assume that $x \in X \in \mathbb{R}^n$, $z \in Z \in \mathbb{R}^{n_z}$, $y \in Y \in \mathbb{R}^{n_y}$, $\tilde{w} \in W \in \mathbb{R}^{n_{\tilde{w}}}$ and $u \in U \in \mathbb{R}^{n_u}$ and $\rho_a \in \mathcal{P}_\rho$. After somme relaxation, the considered LPV generalized plant that copes to the polytopic approach is:

$$\left[\begin{array}{c} \dot{\xi} \\ \hline z \\ y \end{array}\right] = \left[\begin{array}{c|cc} A(\rho_a) & B_1(\rho_a) & B_2 \\ \hline C_1(\rho_a) & D_{11}(\rho_a) & D_{12} \\ C_2 & 0 & 0 \end{array}\right] \left[\begin{array}{c} \xi \\ \hline \tilde{w} \\ u \end{array}\right] \tag{8.40}$$

According to this general plant formulation, the LPV controller $K_s(\rho_a)$ designed is defined as,

$$\left[\begin{array}{c} \dot{x_c} \\ u \end{array}\right] = \left[\begin{array}{cc} A_c(\rho_a) & B_c(\rho_a) \\ C_c(\rho_a) & D_c(\rho_a) \end{array}\right] \left[\begin{array}{c} x_c \\ y \end{array}\right] \tag{8.41}$$

where $x_c \in X_c \in \mathbb{R}^n$ are the controller states, $u \in U \in \mathbb{R}^{n_u}$, $y \in Y \in \mathbb{R}^{n_y}$. Then, $\rho_a \in \mathcal{P}_\rho$, s.t.

$$\rho_a \in \left[\begin{array}{cc} \underline{\rho}_a & \overline{\rho}_a \end{array}\right],\ where, \underline{\rho}_a = \rho_{min} = 0\ and\ \overline{\rho}_a = \rho_{max} = 1 \tag{8.42}$$

According to the varying parameter $\rho_a \in \mathcal{P}_\rho \in \mathbb{R}^l$, the reconstruction of the LPV polytopic controller, composed by 2 vertices, can be expressed as:

$$K(\rho_a) = \sum_{i=1}^{2} \alpha_i(\alpha) \begin{bmatrix} A_{c_i} & B_{c_i} \\ C_{c_i} & D_{c_i} \end{bmatrix} \tag{8.43}$$

where c_i define the controller at each vertex of the parameter polytope and:
where,

$$\alpha_i(\rho_a) := \frac{\prod_{k=1}^{2} |\rho_k - \mathcal{C}(\omega_i)_k|}{\prod_{k=1}^{2} (\overline{\rho}_k - \underline{\rho}_k)} \, , i = 1, \ldots, N \tag{8.44}$$

$$\alpha_i(\rho_a) \geq 0 \text{ and } \sum_{i=1}^{2} \alpha_i(\rho_a) = 1 \tag{8.45}$$

The close loop system with the generalized plant ($\Sigma_{gv}(\rho_a)$) and the controller $K_s(\rho_a)$, represented in 8.3 , is given as follow:

$$\begin{bmatrix} \dot{\chi} \\ z \end{bmatrix} = \begin{bmatrix} \mathcal{A}(\rho_a) & \mathcal{B}(\rho_a) \\ \mathcal{C}(\rho_a) & \mathcal{D}(\rho_a) \end{bmatrix} \begin{bmatrix} \chi \\ w \end{bmatrix} \tag{8.46}$$

where

$$\begin{array}{rcl} \mathcal{A} & = & \begin{bmatrix} A(\rho_a) + B_2 D_c(\rho_a) C_2 & B_2 C_c(\rho_a) \\ B_c(\rho_a) C_2 & A_c(\rho_a) \end{bmatrix} \\ \mathcal{B} & = & \begin{bmatrix} B_1(\rho_a) + B_2 D_c(\rho_a) D_{21}(\rho_a) \\ B_c(\rho_a) D_{21}(\rho_a) \end{bmatrix} \\ \mathcal{C} & = & \begin{bmatrix} C_1(\rho_a) + D_{12} D_c(\rho_a) C_2(\rho_a) & D_{12} C_c(R_s) \end{bmatrix} \\ \mathcal{D} & = & D_{11}(\rho_a) + D_{12} D_c(\rho_a) D_{21}(\rho_a) \end{array} \tag{8.47}$$

where $\chi = [\xi \; x_c^T]^T \in \mathbb{R}^{2n}$, $z \in \mathbb{R}^{n_z}$, $\tilde{w} \in \mathbb{R}^{n_{\tilde{w}}}$.

More details see chapter. 2.

Remark: It is worth to stress that the use of only one varying parameter reduce the conservatism of the considered controller and the make it easy to implement the proposed.

8.7 Simulation results of the integrated strategy

In this section, we present the simulation results obtained with integrated[8] controller and considering a nonlinear vehicle model including vertical and suspension model (8.34).

The proposed simulation scenario is a line change maneuver applied to the block diagram of Fig. 8.1. This scenario is used to emphasize the efficiency of the integrated strategy to operate in critical driving situations. In the beginning of the scenario, the vehicle speed is $90\,km/h$ in straight line on

[8]The control law is obtained from the integrated of flat longitudinal/lateral control and LPV/H_∞ suspension control.

wet road ($\mu = 0.5$). The driver performs a line change maneuver between $t = 0.5s$ and $t = 2s$. First, a 5cm bump occurs on the left wheels (from $t = 0.5\,s$ to $t = 1s$) then another one between $t = 3\,s$ and $t = 4\,s$. Also, some lateral wind is considered generating an undesirable yaw moment (from $t = 2\,s$ to $t = 2.5s$).

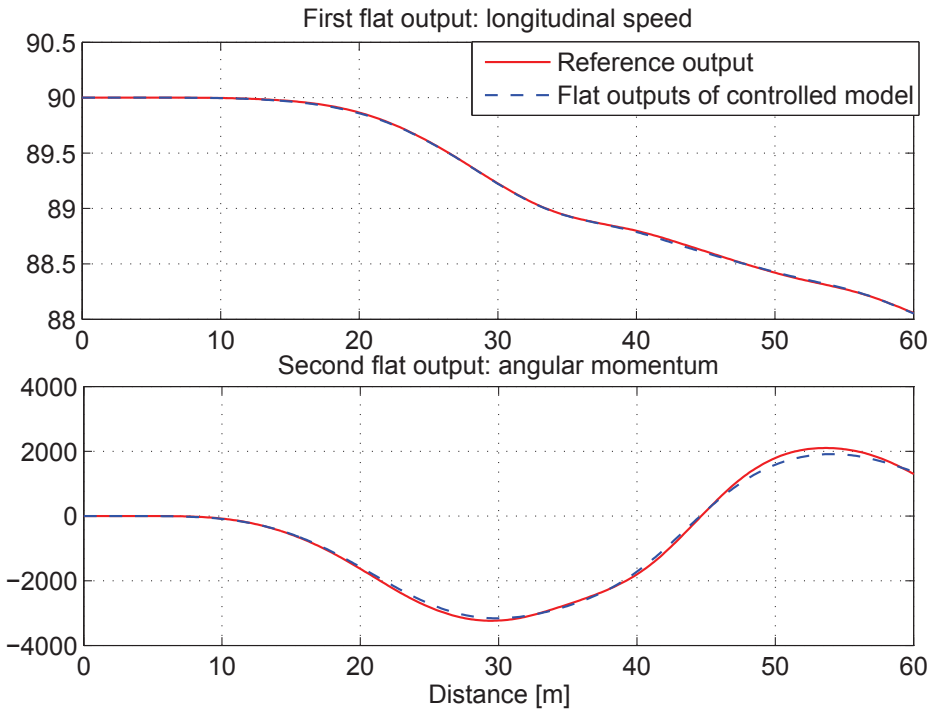

Figure 8.4: Flat outputs: reference and controlled model

Fig. 8.4 shows the performance results of the flat controller to track the desired flat outputs y_1 and y_2. Moreover, the steering angle and braking torque needed to track the flat outputs are presented in Fig. 8.5.

Figs. 8.6 and 8.7 show the lateral acceleration of the vehicle and the scheduling parameter used by the LPV/H_∞, respectively, while performing the proposed scenario. It can be seen that the lateral acceleration rises when performing the line change maneuver (lateral dynamics strongly excited), at the same time the considered varying parameter ρ_a value increases to achieve properly the performance scheduling task.

The chassis displacement (representing passengers comfort) and roll bounce motion of the vehicle (representing the vehicle roadholding) are given by Figs. 8.8 and 8.9.

Indeed, when the driver perform the line change and face the first bump, the driving situation is dangerous and the lateral acceleration increases (as in Fig. 8.6). Therefore, $\rho_a \longrightarrow 1$ (as shown in Fig. 8.7) and the suspension control is adapted to penalize the roll dynamics and reduce the load transfer and improve the vehicle safety and handling (see Section 8.6) and relax the weighting on the chassis displacement. Also, it can be clear seen in Fig. 8.8 that after the line change and when the vehicle face the bump in a straight road, the riving situation is normal, $\rho_a \longrightarrow 0$ and the suspension control focuses on improving passengers comfort by reducing the chassis displacement z_s.

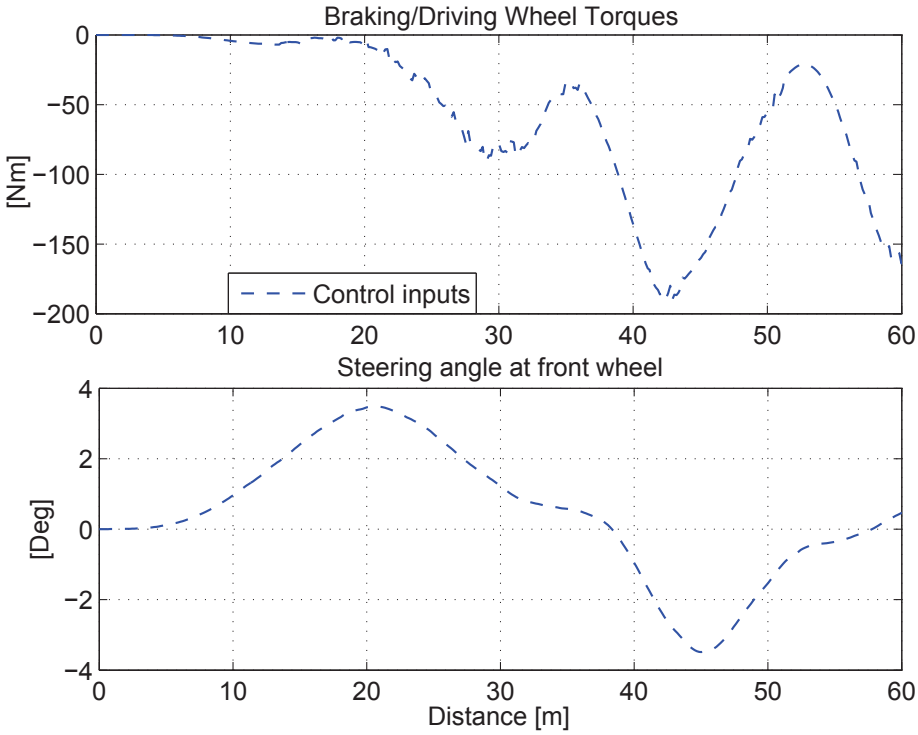

Figure 8.5: Coupled longitudinal/lateral flat control signals

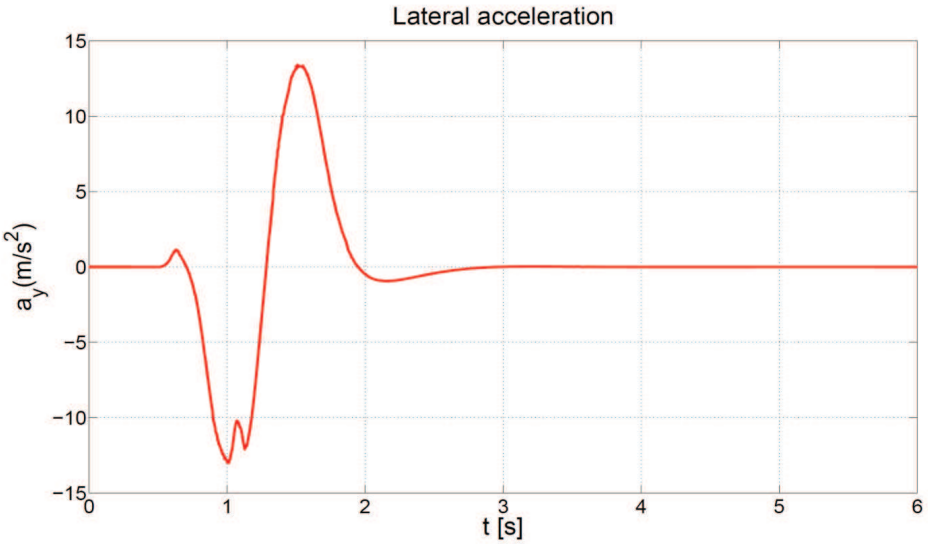

Figure 8.6: Lateral acceleration

Other results on the stability of the controlled vehicle are highlighted in Fig. 8.10. In fact, the controlled vehicle model remains inside of the stability region (defined sideslip dynamics of the car) even in the critical driving situations, however, the uncontrolled model operates outside the stability region. These results confirm the ability of the proposed integration strategy to keep the controlled

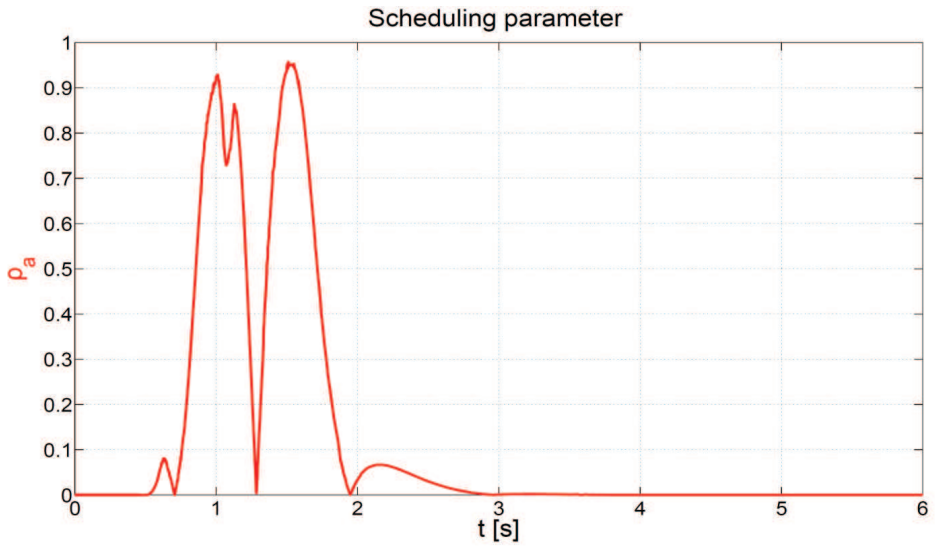

Figure 8.7: Scheduling parameter ρ_a

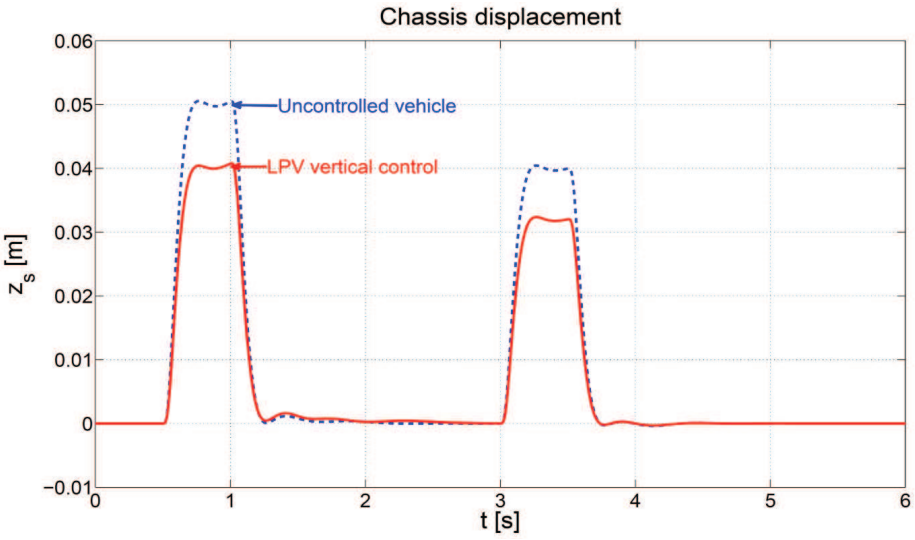

Figure 8.8: Chassis displacement z_s

vehicle model more stable.

The obtained results confirm the efficiency of this control strategy to enhance the vehicle dynamics and overcome the dangerous driving situations.

8.8 Conclusion

In this study, a novel integration strategy of two advanced vehicle controllers. Firstly, based on the flatness property of the nonlinear systems for the lateral/longitudinal flatness control and the

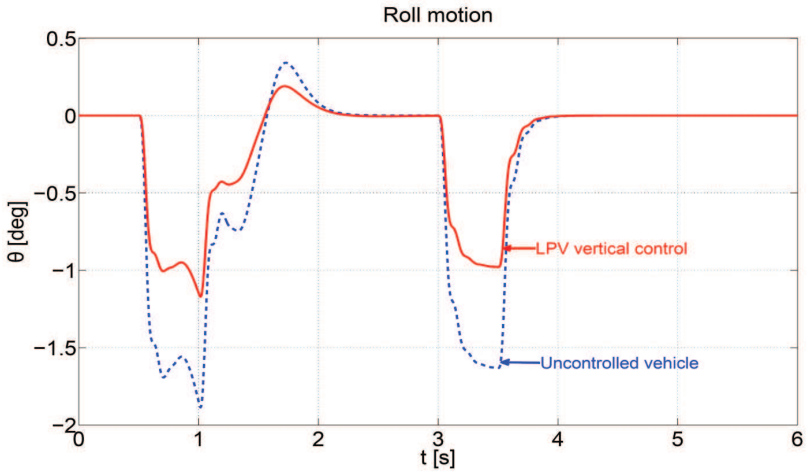

Figure 8.9: Roll angle θ

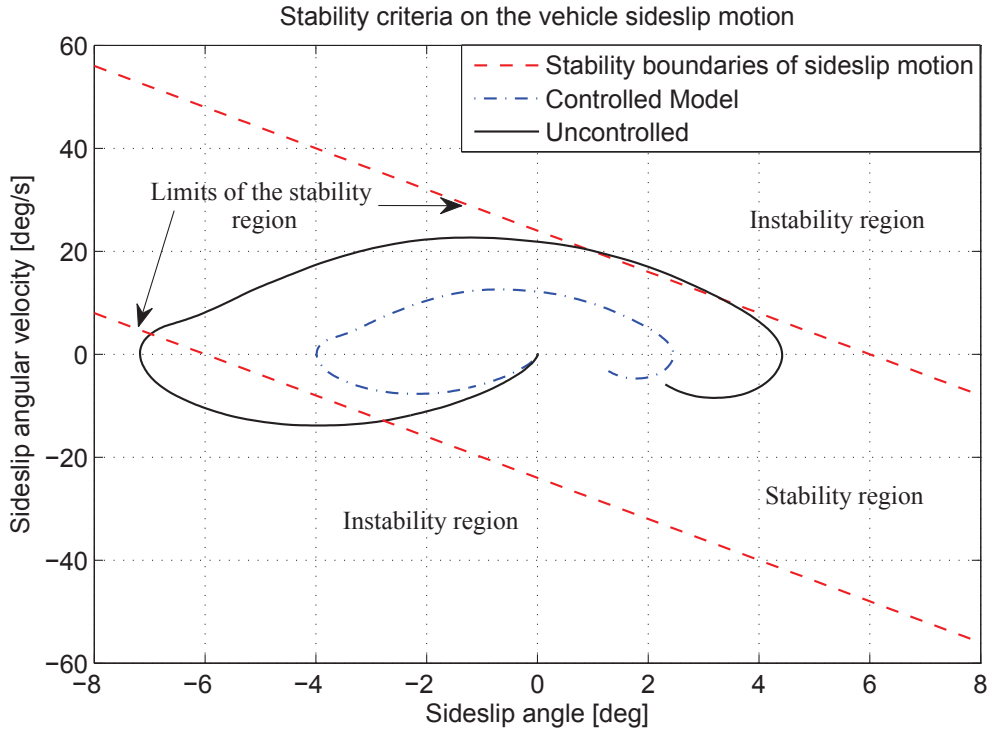

Figure 8.10: Stability criteria of sideslip motion: controlled and uncontrolled vehicle models

LPV/H_∞ vertical dynamics control have been designed respectively. Secondly an innovative coordination method between the two strategies has been introduced to ensure the communication and to establish the collaborative work of the two controllers. This integration aims to improve the handling and safety of the vehicle, and simultaneously ensures a control coordination of the several vehicle dynamics to perform combined maneuvers.
Simulation results emphasize the success of this collaborative strategy for enhancing the longitudinal, lateral and vertical dynamics and have shown the efficiency of the proposed approach. Also, using the

LPV coordination framework allows to simplify the implementation procedure.

CHAPTER 9

General conclusions and perspectives

Summary

This thesis has been concerned with the study and the analysis of the global chassis control through the use of the $LPV/\mathcal{H}_\infty$ robust control tools. The main issue is to work out new Global Chassis MIMO controllers that enhance the overall dynamics of the vehicle while preserving the vehicle stability in critical driving situations. This thesis is presented in 3 parts and 9 chapters as follows:

- In the first chapter, a presentation of the project in which the thesis is developed is given. Also, some historical facts concerning the vehicle dynamics studies are provided. Then, the general framework of the thesis, namely, the global chassis control for vehicle dynamics improvements.
- The second chapter recalls the theoretical tools used in the thesis. Thus, notions such as robustness, convexity, LMIs, LTI and LPV controller synthesis are given. This chapter aims at providing the reader with the necessary tools to understand the strategies developed in this thesis.
- The third chapter is concerned with the vehicle modeling. Indeed, the quarter and full vertical vehicle models and the extended bicycle model are presented for control design purposes. A semi-active magneto-rheological damper model has been validated in collaboration with colleagues from Tec Monterrey and used to develop semi-active suspensions control strategies. Also, a full non linear vehicle model (for simulation purposes) has been validated through an experimental procedure on a real vehicle in collaboration with colleagues from MIPS laboratory in Mulhouse.
- The fourth chapter presents the first important contributions of the thesis in the domain of road profile estimation. It includes 3 developed strategies using the commonly used sensors available on most of the commercial cars, as follows:
  - The first strategy is based on an $\mathcal{H}_\infty$ observer (work developed with colleagues from Tec Monterrey).
  - The second one is an algebraic observer with unknown input (work developed with colleagues from Mines ParisTech-CAOR).
  - The third one is based on a parametric adaptive observation of the road profile.

  Experimental results on a 1:5 scale vehicle have been used to evaluate the proposed road profile estimation method.
- The fifth chapter uses the results of the fourth one to develop road adaptive suspension control strategies. Two LPV/$\mathcal{H}_\infty$ controllers, based on the previously detailed estimation strategies, are developed:

  - The first one is a new road LPV adaptive semi-Active suspension controller for a quarter vehicle based on robust observer estimation of the road profile. This work was achieved in collaboration with colleagues from Tec Monterrey in Mexico (J.C. Tudon Matinez and Ruben Morales Mendez).
  - The second one is a new LPV/$\mathcal{H}_\infty$ semi-active suspension control strategy with performance adaptation to roll behavior for the full vehicle, based on a non linear algebraic road profile estimation. This work was achieved in collaboration with colleagues from Mines-ParisTech (Lghani Menhour and Brigitte D'Andréa Novel).

- Chapter six develops first the main contributions of the thesis in the global chassis control field. It proposes a hierarchical collaborative coordination between the various actuators of semi-active suspension, steering and braking subsystems to enhance the vehicle dynamics to prevent conflicts in terms of performance objectives. This GCC (Global Chassis Control) strategy combines the monitoring of the driving situation and the corresponding coordination of the actuators.

- Chapter seven presents a very interesting result concerning the global chassis control using LPV/$\mathcal{H}_\infty$ control allocation. It allows to achieve several performance objectives using a smart control structure that adapts the control to the considered vehicle dynamical behaviour. Indeed, two automotive based control objectives are achieved using the proposed LPV/H_∞ Global Chassis allocation strategy:

  - An LPV suspension control with performance adaptation to roll behavior, embedded in a global vehicle dynamic control strategy: it uses the control allocation approach to manage the load transfer distribution and suspensions efforts generation.

  - An LPV method for fault tolerant dynamics control: it uses the control allocation approach to manage the actuators failure: *e.g.* damper failure or braking actuators failure.

- Chapter eight concludes the dissertation with a new mixed global chassis control of the ground vehicles based on LPV/$\mathcal{H}_\infty$ vertical and nonlinear Flatness lateral/longitudinal dynamics control. It is based on a novel integration strategy of these two advanced vehicle controllers. This integration aims at improving the handling and safety of the vehicle, and it simultaneously ensuring a control coordination of the several vehicle dynamics to perform combined maneuvers.

Remark: Implementation of one of the developed LPV/$\mathcal{H}_\infty$ on a real "Renault Scenic" in collaboration with MIPS laboratory has been achieved lately ($04/07/2014$). The tests were performed by a professional race drive on a experimentally prepared driving circuit. The results were very satisfying.

9.1 Perspective

A lot of works have been initiated during the thesis and are in progress. Among others, the following seem to be of great interest:

- **Modeling & Identification**: Identification and modeling of the Electro-Rheological semi-active dampers. Also, achieve sensitivity analysis of the semi-active suspension.
  The main goal is to get the best model that allows to build controllers robust w.r.t. crucial non-linearities that affect the control performances.

- **Control design and analysis**: The LPV control strategies can be developed by considering various scheduling approaches and control structure. The coupled controllers that allow to enhance several vehicle dynamics within global chassis control strategies.
  Another, important issue is the use of allocation control approaches (easily implementable) to deal with actuators failure problems. One important feature is to reduce the conservatism induced by the use of the varying parameter and the polytopic approach and also use controllers order reduction tools to minimize the control implementation complexity.

- **Applications and Implementations**: First, an implementation of some developed algorithms have been already performed on a real vehicle within the collaboration with the MIPS laboratory of Mulhouse. The implementation was successful and the test of trajectory tracking was performed as expected. More implementation have to be performed after equipping the vehicle with semi-active dampers.
  Also, an implementation of the allocation control strategies is already scheduled on the Gipsa test bed vehicle for vertical dynamics enhancement. Also, scenarios of dampers failure are to be considered and results have to be analysed to develop more efficient strategy to manage critical situations.

- **Comparisons**: Comparisons with other approaches (predictive control, optimal control,...ect) can be developed to prove the efficiency of the developed strategies.

Also, a lot of results are in progress to be submitted to international journals.

Bibliography

(n.d.).

Acarman, T. (2009). Nonlinear optimal integrated vehicle control using individual braking torque and steering angle with on-line control allocation by using state-dependent riccati equation technique. *Vehicle Sys. Dyn* **47**, 155–177.

Airimitoaie, T-B and Ioan Doré Landau (2013). Indirect adaptive attenuation of multiple narrow-band disturbances applied to active vibration control. *Control Systems Technology, IEEE Transactions on* **22**(2), 761–769.

Alazard, Daniel (2003). Commande robuste des systèmes flexibles: synthèse des travaux de recherches.

Anh lam, Do (2011). Robust/LPV Control of vehicle dynamics for comfort and safety improvements. PhD thesis. PhD Thesis, Control System dpt of the GIPSA-lab - Grenoble INP.

Apkarian, P. and R.J. Adams (1998). Advanced gain-scheduling techniques for uncertain systems. *IEEE Transaction on Control System Technology* **6**(1), 21–32.

Aubouet, Sébastien (2010). Modeling and control of Soben semi-active suspension. PhD thesis. PhD Thesis, Control System dpt of the GIPSA-lab - Grenoble INP.

Barbot, J. P., M. Fliess and T. Floquet (2007). An algebraic framework for the design of nonlinear observers with unknown inputs. In: *46^{th} IEEE Conf. Decision Control, New Orleans*.

Bergounioux, M. (2001). *Optimisation et contrôle des systèmes linéaires (in French)*. DUNOD.

Boada, B. L., M. Jesús, L. Boada and V. Díaz (March 2013). Discussion on "integrated vehicle dynamics control via coordination of active front steering and rear braking". *European Journal of Control* **19(2)**, 144–145.

Bonnans, F. (2006). *Optimisation continue (in French)*. DUNOD.

Botero, Juan C, Massimiliano Gobbi, Giampiero Mastinu, Nicola Di Piazza and Rosario Martorana (2007). On the reformulation of the abs logic by sensing forces and moments at the wheels. In: *Advances in Automotive Control*. Vol. 5. pp. 265–272.

Boyd, S., L. El-Ghaoui, E. Feron and V. Balakrishnan (1994). *Linear Matrix Inequalities in System and Control Theory*. SIAM Studies in applied mathematics.

Brown, T., A. Hac and J. Martens (December 2004). Detection of vehicle rollover. In: *in SAE World Congress*. Michigan-Detroit.

Canale, Massimo, Lorenzo Fagiano, Mario Milanese and P Borodani (2007). Robust vehicle yaw control using an active differential and imc techniques. *Control Engineering Practice* **15**(8), 923–941.

Cartwright, K.V. (2007). Determining the Effective or RMS Voltage of Various Waveforms Without Calculus. *The Tech. Interface* **8**(1), 1–20.

Chou, H. and B. d'Andréa Novel (2005*a*). Global vehicle control using differential braking torques and active suspension forces. *Vehicle System Dynamics* **43**(4), 261–284.

Chou, H. and B. d'Andréa Novel (2005*b*). Global vehicle control using differential braking torques and active suspension forces. *Vehicle Syst. Dynamics* **43**, 261–284.

Ciarlet, P.G. (1998). *Introduction à l'analyse numérique matricielle et à l'optimisation*.

Collardo, F.A. Garcia, B. d'Andréa Novel, M. Fliess and H. Mounier (2009). Analyse fréquentielle des dérivateurs algébriques. In: *XXIIe Colloque GRETSI*.

Daafouz, J., M. Fliess and G. Millérioux (2006). Une approche intrinsèque des observateurs linéaires à entrées inconnues. In: *Conf. int. francoph. automatique, Bordeaux*.

Denny, M. (2005). The dynamics of antilock brake systems. *European Journal of Physics* **26**, 1007–1016.

Di Cairano, S., H.E. Tseng, D. Bernardini and A. Bemporad (2013). Vehicle yaw stability control by coordinated active front steering and differential braking in the tire sideslip angles domain. *Control Systems Technology, IEEE Transactions on* **21**(4), 1236–1248.

Do, A. L., O. Sename and L. Dugard (2010*a*). An LPV control approach for semi-active suspension control with actuator constraints. In: *Proceedings of the IEEE American Control Conference (ACC)*. Baltimore, Maryland, USA. pp. 4653 – 4658.

Do, A. L., O. Sename and L. Dugard (2012*a*). *Control of Linear Parameter Varying Systems with Applications*. Chap. LPV modeling and control of semi-active in automotive systems, pp. 381–411. Springer US.

Do, A.L., O. Sename and L. Dugard (2012*b*). LPV Modelling and Control of Semi-Active Dampers in Automotive Systems. In: *Control of Linear Parameter Varying Systems with Applications*. pp. Mohammadpour and Scherer, Springer, ch.15.

Do, Anh Lam, Cristiano Spelta, Sergio Savaresi, Olivier Sename, Luc Dugard and Diego Delvecchio (2010*b*). An LPV control approach for comfort and suspension travel improvements of semi-active suspension systems. In: *Proceedings of the 49th IEEE Conference on Decision and Control (CDC)*. Atlanta, GA. pp. 5660–5665.

Do, Anh Lam, J. M. Gomes da Silva Jr., Olivier Sename and Luc Dugard (2011). Control design for LPV systems with input saturation and state constraints: an application to a semi-active suspension. In: *the 50th IEEE Conference on Decision and Control (CDC)*. Orlando, Florida, USA.

Doumiati, M., A. Victorino, D. Lechner, G. Baffet and A. Charara (2010*a*). Observers for vehicle tyre/road forces estimations: experimental validation. *Vehicle Sys. Dyn* **48**, 1345–1378.

Doumiati, M., O. Sename, J. Martinez, L. Dugard and C. Poussot-Vassal (2010*b*). Gain-scheduled lpv/hinf controller based on direct yaw moment and active steering for vehicle handling improvements. In: *Proceedings of the 49th IEEE Conference on Decision and Control (CDC'10)*. Atlanta, Georgia.

Doumiati, M, O Sename, J Martinez, L Dugard and C Poussot-Vassal (2010*c*). Gain-scheduled lpv/hinf controller based on direct yaw moment and active steering for vehicle handling improvements. In: *Decision and Control (CDC), 2010 49th IEEE Conference on*. IEEE. pp. 6427–6432.

Doumiati, M., O. Sename, L. Dugard, J.-J. Martinez-Molina, P. Gaspar and Z. Szabo (March 2013*a*). Integrated vehicle dynamics control via coordination of active front steering and rear braking. *European Journal of Control* **19(2)**, 121–143.

Doumiati, Moustapha, Alessandro Correa Victorino, Ali Charara and Daniel Lechner (2011). Onboard real-time estimation of vehicle lateral tire–road forces and sideslip angle. *Mechatronics, IEEE/ASME Transactions on* **16**(4), 601–614.

Doumiati, Moustapha, Olivier Sename, Luc Dugard, John-Jairo Martinez-Molina, Peter Gaspar and Zoltan Szabo (2013*b*). Integrated vehicle dynamics control via coordination of active front steering and rear braking. *European Journal of Control* **19**(2), 121 – 143.

Doumiati, Moustapha, Olivier Sename, Luc Dugard, John-Jairo Martinez-Molina, Peter Gaspar and Zoltan Szabo (2013*c*). Integrated vehicle dynamics control via coordination of active front steering and rear braking. *European Journal of Control* **19**(2), 121 – 143.

El-Ghaoui, L. (1997). *Commande Robuste*. Ecole Nationale Supérieur des Techniques Avancées / Ecole Polytechnique.

Fergani, S., L. Menhour, O. Sename, L. Dugard and B.D. Novel (2013*a*). Study and comparison of non linear and lpv control approaches for vehicle stability control. In: *Control Automation (MED), 2013 21st Mediterranean Conference on*. pp. 303–310.

Fergani, S., L. Menhour, O. Sename, L. Dugard and B.D'Andrea Novel (2014*a*). Full vehicle dynamics control based on lpv/$\mathcal{H}_\infty$ and flatness approaches. In: *Control Conference (ECC), 2014 European*. pp. 2346–2351.

Fergani, S., O. Sename and L. Dugard (2012*a*). A LPV/$\mathcal{H}_\infty$ global chassis controller for performances improvement involving braking, suspension and steering systems. In: *Proceedings of the 7th IFAC Symposium on Robust Control Design*. Aalborg, Denmark. pp. 363–368.

Fergani, S., O. Sename and L. Dugard (2012*b*). Performances improvement through an lpv/$\mathcal{H}_\infty$; control coordination strategy involving braking, semi-active suspension and steering systems. In: *Decision and Control (CDC), 2012 IEEE 51st Annual Conference on*. pp. 4384–4389.

Fergani, S., O. Sename and L. Dugard (2013*b*). A lpv suspension control with performance adaptation to roll behavior, embedded in a global vehicle dynamic control strategy. In: *Control Conference (ECC), 2013 European*. pp. 1487–1492.

Fergani, S., O. Sename and L. Dugard (2013*c*). A new LPV/$\mathcal{H}_\infty$ global chassis control through load transfer distribution and vehicle stability monitoring. In: *Proceedings of IFAC Joint conference* 5*th Symposium on System Structure and Control,* 11*th Workshop on Time-Delay Systems* 6*th Workshop on Fractional Differentiation and Its Applications*. Grenoble, France.

Fergani, S., O. Sename and L. Dugard (2014*b*). A lpv/$\mathcal{H}_\infty$ fault tolerant control of vehicle roll dynamics under semi-active damper malfunction. In: *American Control Conference (ACC), 2014*. pp. 4482–4487.

Fialho, I. and G. Balas (2002). Road Adaptive Active Suspension Design Using Linear Parameter-Varying Gain-Scheduling. *IEEE Trans. on Control Syst. Tech.* **10**, 43–54.

Fliess, M. (2006*a*). Analyse non standard du bruit. *C.R. Acad. Sci. Paris* **I-342**, 797–802.

Fliess, M. and C. Join (2008). Commande sans modèle et commande à modèle restreint. *e-STA* **5**, 12–27.

Fliess, M., C. Join and H. Sira-Ramírez (2008). Non-linear estimation is easy. *Internat J. Modelling Identification Control* **4**, 12–27.

Fliess, M., J. Lévine, P. Martin and P. Rouchon (1992). Sur les systèmes non linéaires différentiellement plats. *Comptes rendus de l'Académie des sciences. Série 1, Mathématique* **315**, 619–624.

Fliess, M., J. Lévine, P. Martin and P. Rouchon (1995). Flatness and defect of nonlinear systems: introductory theory and examples. *Int. J. Control* **61**, 1327–1361.

Fliess, M., J. Lévine, P. Martin and P. Rouchon (1999). A lie-bäcklund approach to equivalence and flatness of nonlinear systems. *IEEE Trans. Automat. Control* **44**, 922–937.

Fliess, Michel (2006*b*). Analyse non standard du bruit. *Comptes-Rendus de l'Académie des Sciences, Série 1, Mathématiques* **342**, 797–802.

Fuchshumer, S., K. Schlacher and T. Rittenschober (2005). Nonlinear vehicle dynamics control - a flatness based approach. In: *44^{th} IEEE CDC & ECC, Sevilla*.

Gáspár, P., Z. Szabó and J. Bokor (2005). The design of an integrated control system in heavy vehicles based on an LPV method. In: *Proceedings of the 44th IEEE Conference on Decision and Control (CDC)*. Seville, Spain. pp. 6722–6727.

Gáspár, P., Z. Szabó, J. Bokor, C. Poussot-Vassal, O. Sename and L. Dugard (August 2007). Toward global chassis control by integrating the brake and suspension systems. In: *In Proceedings of the 5th IFAC Symposium on Advances in Automotive Control (AAC), Aptos, California, USA*.

Genta, G. and L. Morello (2009). *The Automotive Chassis: System Design*. Springer Science+Business Media.

Gillespie, T.D. (1992). *Fundamental of vehicle dynamics*. Society of Automotive Engineers, Inc.

Giua, A., M. Melas, C. Seatzu and G. Usai (2004). Design of a predictive semiactive suspension system. *Vehicle System Dynamics* **41**(4), 277–300.

González, A., E.J. Obrien, Y.Y. Li and K. Cashell (2008). The Use of Vehicle Acceleration Measurements to Estimate Road Roughness. *Vehicle System Dynamics* **46**(6), 483–499.

Guerra, R. M., A. Luviano-Juárez and J. Juan Rincón-Pasaye (2007). Fault estimation using algebraic observers. In: *the American Control Conference (ACC)*. New York City, USA.

Guo, Shuqi, Shaopu Yang and Cunzhi Pan (2006*a*). Dynamic modeling of magneto rheological damper behaviors. *Journal of Intelligent material systems and structures* **17**(1), 3–14.

Guo, Shuqi, Shaopu Yang and Cunzhi Pan (2006*b*). Dynamic modeling of magnetorheological damper behaviors. *Journal of Intelligent material systems and structures* **17**(1), 3–14.

Harris, Niall K, Arturo González, Eugene J OBrien and P McGetrick (2010). Characterisation of pavement profile heights using accelerometer readings and a combinatorial optimisation technique. *Journal of Sound and Vibration* **329**(5), 497–508.

He, J., DA. Crolla, MC. Levesley and WJ Manning (2006). Coordination of active steering, driveline, and braking for integrated vehicle dynamics control.. *Proc. Inst. Mech Engineers*.

Healy, A.J., E. Nathman and C.C. Smith (1977). An Analytical and Experimental Study of Automobile Dynamics with Random Roadway Inputs. *J. Dyn. Sys. Meas. and Control Trans. ASME* **99**(4), 284–292.

Hedrick, JK, D McMahon, V Narendran and D Swaroop (1991). Longitudinal vehicle controller design for ivhs systems. In: *American Control Conference, 1991*. IEEE. pp. 3107–3112.

Heyns, T., P.S. Heyns and J.P. Villiers (2012). A Method for Real-time Condition Monitoring of Haul Roads Based on Bayesian Parameter Estimation. *J. Terramech.* **49**, 103–113.

Hong, K.S., H.C. Sohn and J.K. Hedrick (2002). Modified Skyhook Control of Semi-Active Suspensions: A New Model, Gain Scheduling, and Hardware-in-the-Loop Tuning. *J. Dyn. Syst. Meas. and Control Trans. ASME* **124**, 158–167.

Ibrir, S. (2003). Online exact differentiation and notion of asymptotic algebraic observers. *IEEE Transactions on Automatic Control* **48(11)**, 922–937.

Iwasaki, T. and R.E. Skelton (1994). All controllers for the general $\mathcal{H}_\infty$ control problem: LMI existence conditions and state space formulas. *Automatica* **30**(8), 1307–1317.

Jonasson, M. and F. Roos (2008). Design and evaluation of an active electromechanical wheel suspension system. *to appear in Journal of Mechatronics*.

Jorge De-J, Lozoya-Santos, Ruben Morales-Menendez, Ricardo Ramirez-Mendoza, Juan C Tudón-Martinez, Olivier Sename and Luc Dugard (2012). Magnetorheological damper an experimental study. *Journal of Intelligent Material Systems and Structures* **23**(11), 1213–1232.

Kiencke, U. and L. Nielsen (2000). *Automotive Control Systems*.

Kim, H.J., H.S. Yang and Y.P. Park (2002). Improving the Vehicle Performance with Active Suspension using Road-Sensing Algorithm. *Computers & Structures* **80**, 1569–1577.

Landau, Ioan Doré, Aurelian Constantinescu and Daniel Rey (2005). Adaptive narrow band disturbance rejection applied to an active suspension, an internal model principle approach. *Automatica* **41**(4), 563–574.

Lévine, J. (2009). *Analysis and Control of Nonlinear Systems: A Flatness-based Approach*. Springer.

Li, Hongyi, Honghai Liu, Huijun Gao and Peng Shi (2012). Reliable fuzzy control for active suspension systems with actuator delay and fault. *Fuzzy Systems, IEEE Transactions on* **20**(2), 342–357.

Lim, Edward HM and J Karl Hedrick (1999). Lateral and longitudinal vehicle control coupling for automated vehicle operation. In: *American Control Conference, 1999. Proceedings of the 1999*. Vol. 5. IEEE. pp. 3676–3680.

Lin-Hui, Z., L. Zhi-Yuan and C. Hong (2010). Design of a nonlinear observer for vehicle velocity estimation and experiments.. *IEEE Transactions on Control Systems Technology*.

Lin, J.-S. (2007). Nonlinear control design of anti-lock braking systems with assistance of active suspension. *IET Control Theory and Applications* **1**, 343–348(5).

Lozoya-Santos, J.J., R. Morales-Menendez, J.C Tudón-Martínez, O. Sename, L. Dugard and R.A. Ramirez-Mendoza (2011). Control Strategies for an Automotive Suspension with a MR Damper. In: *18^{th} IFAC World Congress*. Italy. pp. 1820–1825.

Lu, J. (2004). A frequency-adaptive multi-objective suspension control strategy. *ASME Journal of Dynamic Systems, Measurement and Control* **126**(3), 700–707.

Martinez, John J and Marouane Alma (2012). Improving playability of blu-ray disc drives by using adaptive suppression of repetitive disturbances. *Automatica* **48**(4), 638–644.

Martinez, Juan .C. Tudon, soheib Fergani, Olivier Sename, John J.Martinez, Ruben Morales-Menendez, and Luc Dugard (2014). Adaptive road profile estimation in semi-active car suspensions. *Transactions on Control Systems Technology (IEEETCST), submitted*.

Mboup, M., C. Join and M. Fliess (2009). Numerical differentiation with annihilators in noisy environment. *Numer. Algorithm.* **50**, 439–467.

Menhour, L. and B. d' Andréa-Novel (Oct. 2011). Survey and contributions in vehicle modeling and estimation. Technical report. Rapport du projet INOVE.

Menhour, L., B. d'Andréa Novel, C. Boussard, M. Fliess and H. Mounier (2011). Algebraic nonlinear estimation and flatness-based lateral/longitudinal control for automotive vehicles. In: *14^{th} Int. IEEE Conf. ITS, Washington*.

Menhour, L., B. d'Andréa Novel, M. Fliess and H. Mounier (2012). Commande couplée longitudinale/latérale de véhicules par platitude et estimation algébrique. In: *CIFA , 7ème Conférence Internationale Francophone d'Automatique*. Grenoble, France.

Menhour, L., B. d'Andréa Novel, M. Fliess and H. Mounier (2014). Coupled nonlinear vehicle control: Flatness-based setting with algebraic estimation techniques. *Control Engineering Practice* **22**, 135–146.

Milliken, W. F. and D. L. Milliken (1995). *Race car vehicle dynamics*. Society of Automotive Engineers International.

Mohammadpour, Javad and Carsten Scherer (2012). *Control of linear parameter varying systems with applications*. Springer.

Moustapha, M., O. Sename, L. Dugard, J. Martinez-Molina, P. Gàspàr and Z. Szabo (2011). Nonlinear optimal integrated vehicle control using individual braking torque and steering angle with on-line control allocation by using state-dependent riccati equation technique. *Proc.Vehicle Sys. Dyn*.

Németh, B. and P. Gáspár (2011). Design of actuator interventions in the trajectory tracking for road vehicles. In: *In Proceedings of the 51th IEEE Conference on Decision and Control (CDC), Orlando, Florida, USA, December*.

Ngwangwa, H.M., P.S. Heyns, F.J.J. Labuschagne and G.K. Kululanga (2010). Reconstruction of Road Defects and Road Roughness Classification using Vehicle Responses with Artificial Neural Networks Simulation. *J. Terramech.* **47**, 97–111.

Nieuwstadt, M. J. Van and R. M. Murray (1998). Real time trajectory generation for differentially flat systems. *Int. J. Robust & Nonlinear Control* **8(11)**, 995–1020.

Pacejka, Hans (2005). *Tire and vehicle dynamics*. Elsevier.

Park, Jong Hyeon and Woo Sung Ahn (1999). H infin; yaw-moment control with brakes for improving driving performance and stability. In: *Advanced Intelligent Mechatronics, 1999. Proceedings. 1999 IEEE/ASME International Conference on*. pp. 747–752.

Poussot, C., O. Sename, S. Fergani, M. Doumiati and L. Dugard (2013). *"Global Chassis Control Using Coordinated Control of Braking/Steering Actuators", book chapiter of Robsut Control And Linear Parameter Approaches: Application to Vehicle Dynamics*. Springer.

Poussot-Vassal, C., C. Spelta, O. Sename, S.M. Savaresi and L. Dugard (2012). Survey and performance evaluation on some automotive semi-active suspension control methods: A comparative study on a single-corner model. *Annual Reviews in Control* **36**(1), 148 – 160.

Poussot-Vassal, C., O. Sename, L. Dugard and S. M. Savaresi (2011*a*). Vehicle dynamic stability improvements through gain-scheduled steering and braking control. *Vehicle System Dynamics* **49:10**, 1597–1621.

Poussot-Vassal, C., O. Sename, L. Dugard, P. Gáspár, Z. Szabó and J. Bokor (2011*b*). Attitude and handling improvements through gain-scheduled suspensions and brakes control. *Control Engineering Practice* **19**(3), 252 – 263.

Poussot-Vassal, C., O. Sename, L. Dugard, R. Ramirez-Mendoza and L. Flores (2006). Optimal Skyhook control for semi-active suspensions. In: *Proceedings of the 4th IFAC Symposium on Mechatronics Systems*. Heidelberg, Germany. pp. 608–613.

Poussot-Vassal, Charles (2008). Robust Linear Parameter Varying Multivariable Automotive Global Chassis Control. PhD thesis. Control System dpt of the GIPSA-lab - Grenoble INP.

Poussot-Vassal, Charles, Olivier Sename, Luc Dugard, Peter Gaspar, Zoltan Szabo and Jozsef Bokor (2011*c*). Attitude and handling improvements through gain-scheduled suspensions and brakes control. *Control Engineering Practice* **19**(3), 252–263.

Ramirez-Mendoza, R. (1997). Sur la modélisation et la commande de véhicules automobiles. PhD thesis (in french). INPG, Laboratoire d'Automatique de Grenoble (new GIPSA-lab), Grenoble, France.

Rathinam, M. (1996). Configuration flatness of lagrangian systems underactuated by one control. In: *Proceedings of the 35th IEEE Decision and Control, 11-13 Dec*.

Robson, J.D. (1979). Road Surface Description and Vehicle Response. *Int. J. Veh. Des.* **1**(1), 25–35.

Sammier, D. (2001). On modelling and control of the automotive suspensions. PhD thesis (in french). INPG, Laboratoire d'Automatique de Grenoble (new GIPSA-lab), Grenoble, France.

Savaresi, S., C. Poussot-Vassal, C. Spelta, O. Sename and L. Dugard (2010*a*). *Semi-Active Suspension Control for Vehicles*. Elsevier - Butterworth Heinemann.

Savaresi, Sergio M and Mara Tanelli (2010). *Active braking control systems design for vehicles*. Springer.

Savaresi, Sergio M, Charles Poussot-Vassal, Cristiano Spelta, Olivier Sename and Luc Dugard (2010*b*). *Semi-active suspension control design for vehicles*. Access Online via Elsevier.

Savaresi, S.M. and C. Spelta (2007). Mixed sky-hook and ADD: Approaching the filtering limits of a semi-active suspension. *ASME Transactions: Journal of Dynamic Systems, Measurement and Control* **129**(4), 382–392.

Scherer, C. (2004). Robust mixed control and LPV control with full block scaling. Technical report. Delft University of Technology. Mechanical Engineering Systems and Control Group.

Scherer, C., P. Gahinet and M. Chilali (1997). Multiobjective output-feedback control via LMI optimization. *IEEE Transaction on Automatic Control* **42**(7), 896–911.

Scherer, C.W. (1996). Mixed $\mathcal{H}_2/\mathcal{H}_\infty$ control for time-varying and linear parametrically-varying systems. *International Journal of Robust and Nonlinear Control* **6**(9-10), 929–952.

Scorletti, G. (2004). *An introduction to the LMI optimization in Automatic Control (in French)*.

Sename, O., J.C. Tudon-Martinez and S. Fergani (2013). Lpv methods for fault-tolerant vehicle dynamic control. In: *Control and Fault-Tolerant Systems (SysTol), 2013 Conference on*. pp. 116–130.

Shuqui, G., Y. Shaopu and P. Cunzgi (2006). Dynamic modeling of magnetorheological damper behaviors. *Journal of Intelligent Material Systems And Structures* **17**, 3–14.

Sira-Ramírez, H. and S. Agrawal (1993). *Differentially Flat Systems*. Marcel Dekker.

S.Mammar and D.Koenig (2002). Vehicle handling improvement by active steering. *Vehicle Sys. Dyn* **38**, 211–242.

Spangler, Elson B and William J Kelly (1966). Gmr road profilometer-a method for measuring road profile. *Highway Research Record*.

Stavens, D. and S. Thrun (2006). A Self-Supervised Terrain Roughness Estimator for Off-Road Autonomous Driving. In: *Proc. of the 22^{th} Conf. on UAI*. USA. pp. 469–476.

Sun, Weichao, Huijun Gao and Okyay Kaynak (2011). Finite frequency h_∞ control for vehicle active suspension systems. *IEEE Transactions on Control Systems Technology* **19**(2), 416.

Tanelli, M., R. Sartori and S.M. Savaresi (2007). Sliding mode slip-deceleration control for brake-by-wire control systems. In: *Proceedings of the 5th IFAC Symposium on Advances on Automotive Control (AAC)*. Aptos, California.

Tjonnas, J. and T.A. Johansen (2010). Stabilization of automotive vehicles using active steering and adaptive brake control allocation. *Control Systems Technology, IEEE Transactions on* **18**(3), 545–558.

Tudon-Martinez, J.C., S. Varrier, R. Morales-Menendez, R. Ramirez-Mendoza, D. Koenig, J.-J. Martinez and O. Sename (2013*a*). Fault tolerant control with additive compensation for faults in an automotive damper. In: *Networking, Sensing and Control (ICNSC), 2013 10th IEEE International Conference on*. pp. 810–814.

Tudon-Martinez, Juan, C., Soheib Fergani, Olivier Sename, Rubén Morales-Menéndez and Luc Dugard (2014). Online Road Profile Estimation in Automotive Vehicles. In: *Proceedings of the ECC 2014*. Strasbourg, France.

Tudon-Martinez, Juan Carlos, Soheib Fergani, Sébastien Varrier, Olivier Sename, Luc Dugard, Ruben Morales-Menendez, Ricardo A RamÃrez-Mendoza et al. (2013*b*). Road adaptive semi-active suspension in an automotive vehicle using an lpv controller. In: *Advances in Automotive Control*. Vol. 7. pp. 231–236.

Villagra, J., B. d' Andréa-Novel, S. Choi, M. Fliess and H. Mounier (2009). Robust stop-and-go control strategy: An algebraic approach for nonlinear estimation and control. *International Journal of Vehicle Autonomous Systems* **7**, 270–291.

Villagra, J., B. d' Andréa-Novel, M. Fliess and H. Mounier (2011). A diagnosis-based approach for tire-road forces and maximum friction estimation. *Control Engineering Practice* **19**, 174–184.

Wang, Wei-Yen, Ming-Chang Chen and Shun-Feng Su (2012). Hierarchical fuzzy-neural control of anti-lock braking system and active suspension in a vehicle. *Automatica* **48**(8), 1698 – 1706.

Wong, J.Y. (2001). *Theory of Ground Vehicles*. John Wiley and Sons, Inc.

Yosida, K. (1984). *Operational Calculus: A Theory of Hyperfunctions*. Springer, New York, translated from Japanese.

Yousefzadeh, Mahdi, Shahram Azadi and Abbas Soltani (2010). Road profile estimation using neural network algorithm. *Journal of mechanical science and technology* **24**(3), 743–754.

Yu, Wuhui, Xinjie Zhang, Konghui Guo, Hamid Reza Karimi, Fangwu Ma and Fumiao Zheng (2013). Adaptive real-time estimation on road disturbances properties considering load variation via vehicle vertical dynamics. *Mathematical Problems in Engineering*.

Zhou, K., J. Doyle and K. Glover (1996). *Robust and Optimal Control*. New Jersey.

Zin, A. (2005). Robust automotive suspension control toward global chassis control. PhD thesis (in french). INPG, Laboratoire d'Automatique de Grenoble (new GIPSA-lab), Grenoble, France.

Zin, A., O. Sename, P. Gaspar, L. Dugard and J.Bokor (2008). Robust LPV - $\mathcal{H}_\infty$ control for active suspensions with performance adaptation in view of global chassis control. *Vehicle System Dynamics* **46**(10), 889–912.

Zito, Gianluca and Ioan Doré Landau (2005). Narmax model identification of a variable geometry turbocharged diesel engine. In: *American Control Conference, 2005. Proceedings of the 2005*. IEEE. pp. 1021–1026.